
GLOBAL ASSESSMENT OF SPECIES-SPECIFIC
HABITATS OF PLANKTONIC FORAMINIFERA
– AN ECOSYSTEM MODELING APPROACH –

Kerstin Kretschmer

GLOBAL ASSESSMENT OF SPECIES-SPECIFIC
HABITATS OF PLANKTONIC FORAMINIFERA
– AN ECOSYSTEM MODELING APPROACH –

DISSERTATION

submitted in partial fulfillment of the requirements for the
Doctoral degree in Natural Sciences (Dr. rer. nat.) at the Department
of Geosciences at the University of Bremen

by

Kerstin Kretschmer

MARUM - Center for Marine Environmental Sciences
and Faculty of Geosciences, University of Bremen

October 2017

Reviewers

Prof. Dr. Michael Schulz
*MARUM and Faculty of Geosciences,
University of Bremen*

Prof. Dr. Dr. h.c. Gerold Wefer
*MARUM and Faculty of Geosciences,
University of Bremen*

Date of colloquium: December 19, 2017

*Es gibt nur zwei Tage im Leben, an denen man nichts tun kann.
Der Eine heißt Gestern, der Andere heißt Morgen.
Also ist Heute der richtige Tag um zu leben und zu lieben.*

Dalai Lama

Statutory Declaration

Kerstin Kretschmer
Department of Geosciences
Klagenfurter Strasse 2
28359 Bremen

I herewith declare that this thesis has been created without illicit assistance and by the use of no other than quoted sources and auxiliary means. All statements which are literally or analogously taken from other publications have been marked by quotations. This thesis has not been submitted for the conferral of a doctorate degree elsewhere.

Place, Date

Signature

Own contribution. The first study has been autonomously developed by the candidate with contributions from all co-authors. The candidate designed the model experiments and performed the three different model simulations. The analysis of the model output has been autonomously carried out by the candidate. Additionally, she produced a new compilation of planktonic foraminiferal abundances for Heinrich Stadial 1 considering the five species used in this study. The candidate produced all figures and prepared the manuscript from the first draft to the final version with contributions from all co-authors. For the second study the candidate developed the model code, which she subsequently added to the code trunk of the ocean component of the global earth system model. She designed and finalized the model experiment and carried out the analysis of the model data. The candidate prepared all figures and authored the manuscript from the first draft to the submitted version. All co-authors revised the manuscript, provided valuable contributions regarding the interpretation of the data, and helped to structure the manuscript in an appropriate manner. The third study has been autonomously designed by the candidate. She prepared the forcing data sets and performed the model simulations. The candidate carried out the analysis and interpretation of the produced model data and created all figures. The first draft of the manuscript has been prepared by the candidate with contributions from all co-authors.

Abstract

Over the last few million years, the Earth's climate system has changed continuously on decadal to millennial time scales. Past climate conditions have been reconstructed based on fossil evidence of marine microorganisms, such as planktonic foraminifera. Planktonic foraminifera exhibit species-specific seasonal production patterns and different preferred depth habitats. To precisely reconstruct past climate conditions these spatial and temporal variations within the individual species distribution have to be considered. In this regard, an ecosystem modeling approach can help to gain a better knowledge about species-specific habitat shifts under climate change. In this study, a planktonic foraminifera model is used to predict monthly concentrations of the colder-water species *Neogloboquadrina pachyderma*, *Neogloboquadrina incompta*, and *Globigerina bulloides*, and of the warm-water species *Globigerinoides ruber* (white) and *Trilobatus sacculifer* throughout the world ocean. In particular, the seasonal distribution of the polar species *N. pachyderma* in the surface mixed layer of the North Atlantic Ocean during the last glacial period was investigated. In response to changes in the sea ice cover and food supply, the peak timing of *N. pachyderma* is shifted from the last glacial period to modern conditions by several months. However, for a more realistic simulation of species-specific habitats, the planktonic foraminifera model PLAFOM was adapted to allow for resolving the vertical dimension. This new model version estimates the foraminiferal biomass of the colder- and warm-water species as a function of temperature, nutrition, competition, and in particular light. To predict the species concentration over different water depths the model code of the improved version of the planktonic foraminifera model was added to the code trunk of the ocean component of a global earth system model. This model produces seasonally and vertically coherent distribution patterns that are in good agreement with available observations without any explicit parameterization in the vertical dimension regarding their ontogeny. The colder-water species exhibit a seasonal cycle in their depth habitat in the polar and subpolar regions: during the warm season they occur at mid-depth, while during the cold season they ascend through the water column and are found in the near-surface layer. The warm-water species show a less variable depth habitat and occur almost consistently close to the sea surface throughout the year in the tropics and subtropics. This emergence of species-specific depth habitats in the model that are consistent with available observations indicates that the population dynamics of planktonic foraminifera species may be driven by the same factors. Here the impact of global warming on the species' spatial and seasonal distribution patterns has been investigated. In response to changes in the temperature and food supply, the habitat range as well as the peak timing of both the colder-water and warm-water species will likely shift. In general, planktonic foraminifera do not respond uniformly to climate change due to their different ecological pref-

erences. Their habitat is altered in time and space, and depending on the ambient conditions either warm-water or colder-water species benefit strongly from these changes. Knowing how individual planktonic foraminifera species adapt to changing environmental conditions can help to obtain more precise estimates of the geological past and can provide implications for future climate change.

Zusammenfassung

In den letzten Millionen Jahren war das Klimasystem der Erde ständigen Schwankungen auf Zeitskalen von Dekaden bis zu Jahrtausenden ausgesetzt. Anhand von fossilen Belegen mariner Mikroorganismen, wie z.B. planktischer Foraminiferen, wurden vergangene Klimabedingungen rekonstruiert. Planktische Foraminiferen weisen artspezifische saisonale Verteilungsmuster auf und bevorzugen unterschiedliche Lebensräume. Eine präzise Rekonstruktion vergangener klimatischer Bedingungen setzt eine Berücksichtigung dieser artspezifischen Variabilität in der jeweiligen räumlichen und zeitlichen Verteilung voraus. Die Anwendung eines Ökosystemmodells kann diesbezüglich helfen, die Kenntnisse über die durch einen Klimawandel verursachten Veränderungen artspezifischer Lebensräume zu verbessern. In der vorliegenden Arbeit wird ein planktisches Foraminiferen-Modell verwendet, um die monatlichen Konzentrationen der Kaltwasserarten *Neogloboquadrina pachyderma*, *Neogloboquadrina incompta* und *Globigerina bulloides* sowie der Warmwasserarten *Globigerinoides ruber* (weiß) und *Trilobatus sacculifer* im gesamten Ozean zu berechnen. Hier wurde insbesondere die saisonale Verteilung der polaren Art *N. pachyderma* in der oberflächennahen Vermischungsschicht des Nordatlantiks während des letzten Glazials untersucht. Aufgrund von Veränderungen in der Meereisbedeckung und der Nahrungszufuhr hat sich der Zeitpunkt der Maximalproduktion von *N. pachyderma* im Vergleich zur Moderne um mehrere Monate verschoben. Um allerdings artspezifische Lebensräume noch realistischer vorhersagen zu können, wurde das planktische Foraminiferen-Modell PLAFOM angepasst, um zusätzlich die Darstellung der vertikalen Dimension zu ermöglichen. Diese neue Modellversion berechnet die Biomasse der Kalt- und Warmwasserarten als Funktion von Temperatur, Nahrungsverfügbarkeit, Wettbewerb und insbesondere Licht. Um die artspezifischen Konzentrationen in verschiedenen Wassertiefen bestimmen zu können, wurde der Modellcode der verbesserten Modellversion des planktischen Foraminiferen-Modells zum Quellcode der Ozeankomponente eines globalen Erdsystemmodells hinzugefügt. Obwohl eine explizite Parametrisierung der Ontogenese der einzelnen Arten in Abhängigkeit der Tiefe in diesem Modell nicht vorgenommen wurde, ergeben sich kohärente saisonale und vertikale Verteilungsmuster, die mit den vorhandenen Beobachtungen gut übereinstimmen. Der Lebensraum der Kaltwasserarten weist in den polaren und subpolaren Regionen einen saisonalen Verlauf mit der Tiefe auf. In wärmeren Jahreszeiten finden sich diese Arten in einer größeren Tiefe wieder, während sie in kälteren Jahreszeiten in der Wassersäule aufsteigen und nahe der Oberfläche auftreten. Der Lebensraum der Warmwasserarten ist von geringerer Variabilität mit der Tiefe geprägt, sodass diese Arten das ganze Jahr über in den Tropen und Subtropen fast ausschließlich nahe der Meeresoberfläche anzufinden sind. Das Auftreten einer Tiefenabhängigkeit artspezifischer Lebensräume im Modell, die mit den verfügbaren Beobachtungen übereinstimmen, deutet darauf hin, dass die Populations-

dynamik planktischer Foraminiferen von den gleichen Faktoren abhängt. Diesbezüglich wurde der Einfluss der globalen Erwärmung auf die räumliche und saisonale Verteilung der Arten untersucht. Durch die Temperaturänderungen und die Änderungen in der Nahrungszufuhr könnte sich sowohl die Ausdehnung des Lebensraums als auch der Zeitpunkt der Maximalproduktion der Warm- und Kaltwasserarten verschieben. Aufgrund ihrer unterschiedlichen ökologischen Vorlieben reagieren planktische Foraminiferen nicht einheitlich auf einen Klimawandel, wobei sich ihr Lebensraum sowohl räumlich als auch zeitlich verändert. Abhängig von den spezifischen Umgebungsbedingungen profitieren entweder Warmwasser- oder Kaltwasserarten von diesen Veränderungen. Kenntnisse über das Verhalten planktischer Foraminiferen während sich verändernder Umweltbedingungen können dazu beitragen genauere Abschätzungen der geologischen Vergangenheit zu erhalten und sie können die Auswirkungen des zukünftigen Klimawandels verdeutlichen.

Contents

Abstract	i
1 Introduction	1
1.1 Planktonic Foraminifera	3
1.2 Modeling Approach	5
1.3 Thesis Objectives and Outline	8
2 Modeling the distribution and seasonality of <i>Neogloboquadrina pachyderma</i> in the North Atlantic Ocean during Heinrich Stadial 1	11
2.1 Introduction	12
2.2 Data and Methods	14
2.2.1 PLAFOM	14
2.2.2 Model Experiments	15
2.2.3 Sediment Samples	16
2.2.4 Scaling of PLAFOM Output to Observed Relative Abundances of Individuals	17
2.2.5 Model Validation: Modeled Seasonal Patterns Versus Observations	20
2.3 Results	21
2.3.1 Relative Abundances of <i>N. pachyderma</i>	21
2.3.2 Seasonality of <i>N. pachyderma</i>	22
2.4 Discussion	23
2.4.1 Glacial Range Expansion of <i>N. pachyderma</i>	23
2.4.2 The Seasonality of <i>N. pachyderma</i>	25
2.4.3 Quantifying the Effect of Shifting Phenology on Stable Isotope Signals in <i>N. pachyderma</i>	28
2.4.3.1 $\delta^{18}\text{O}_c$ Signature During Modern Conditions	30
2.4.3.2 $\delta^{18}\text{O}_c$ Signature During the Last Glacial Period	31
2.4.3.2.1 Changes in $\delta^{18}\text{O}_c$ Based on SST Estimates	31
2.4.3.2.2 Changes in $\delta^{18}\text{O}_c$ Based on MLD Temperatures	32
2.4.3.2.3 Changes in $\delta^{18}\text{O}_c$ Based on Thermocline Temperatures	33
2.5 Conclusion	36

3	Modeling seasonal and vertical habitats of planktonic foraminifera on a global scale	39
3.1	Introduction	40
3.2	Methods	41
3.2.1	Approach	41
3.2.2	CESM1.2(BGC) Configuration	42
3.2.3	PLAFOM2.0	43
3.2.3.1	Growth Rate	43
3.2.3.2	Mortality Rate	44
3.2.4	Model Setup	45
3.2.5	Comparison to Observations	46
3.2.5.1	Core-top Data	46
3.2.5.2	Sediment Trap Data	46
3.2.5.3	Plankton Tow Data	47
3.3	Results	48
3.3.1	Modeled Horizontal Distribution Patterns	48
3.3.2	Modeled Seasonal Distribution	50
3.3.3	Modeled Vertical Distribution	52
3.3.4	Modeled Seasonal Variability of Habitat Depth	54
3.4	Discussion	54
3.4.1	Large-scale Patterns	54
3.4.1.1	Geographical Range of Planktonic Foraminifera Species	54
3.4.1.2	Seasonality of Planktonic Foraminifera Species	57
3.4.1.3	Spatial and Temporal Variability of Depth Habitats of Planktonic Foraminifera Species	58
3.4.2	Comparison with Local Observations	61
3.5	Conclusion	66
4	Response of marine zooplankton to global warming: insights from modeling planktonic foraminifera species distribution	69
4.1	Introduction	70
4.2	Materials and Methods	71
4.2.1	PLAFOM2.0	71
4.2.2	Model Simulations	72
4.3	Results	73
4.3.1	Changes in Oceanic Environmental Conditions	73
4.3.2	Changes in Species Biomass Distribution	74
4.3.3	Changes in Phenology	78
4.3.4	Changes in Vertical Distribution	82
4.4	Discussion	83
5	Conclusion and Outlook	93
	References	97

Supplements	117
S1 Technical Model Description	117
S2 Supporting Information for Chapter 2	125
S3 Supporting Information for Chapter 3	129
S4 Supporting Information for Chapter 4	163
Acknowledgments	167

List of Figures

1.1	Schematic View of the Seasonality and Depth Habitat of Planktonic Foraminifera	3
1.2	Fossil Specimens of Planktonic Foraminifera	6
1.3	Model Structure	8
2.1	Locations of Sediment Samples	17
2.2	Scaling of PLAFOM Output to Observations	19
2.3	Modeled Seasonal Patterns Versus Observations	22
2.4	Relative Abundances of <i>N. pachyderma</i>	23
2.5	Seasonality of <i>N. pachyderma</i>	24
2.6	Shift in the Phenology of <i>N. pachyderma</i>	27
2.7	Spatial Distribution of $\delta^{18}\text{O}_c$ Values for Modern Conditions	31
2.8	Spatial Distribution of Changes in the Observed $\delta^{18}\text{O}$ Values During the Last Glacial Period	33
2.9	Spatial Distribution of Changes in $\delta^{18}\text{O}_c$ Values During the Last Glacial Period	34
3.1	Locations of Observational Records	47
3.2	Species Relative Abundances	48
3.3	Species Peak Timing and Peak Amplitudes	51
3.4	Depth Transects of Annual Mean Concentration	52
3.5	Habitat Depth Variability	55
3.6	Model Versus Observations	63
3.7	Direct Comparison with Local Observations	64
4.1	Change in Environmental Conditions	75
4.2	Change in Species Abundance	76
4.3	Change in Species Seasonality	79
4.4	Change in Peak Timing and Peak Amplitude	81
4.5	Change in Depth of Maximum Production	83
4.6	Change in Foraminiferal Depth Distribution	85
4.7	Change in Zonal Average of Foraminiferal Abundance	89
S1.1	Schematic of Active Passive Tracer Modules	118
S2.1	Relative Abundances of <i>N. pachyderma</i> and Sea Surface Temperature Estimates	126

S3.1 Time Series of Year-to-year Difference of Model Variables	131
S3.2 Species Peak Timing and Peak Amplitudes per Latitude	132
S3.3 Model Results Versus Sediment Trap Data	133
S3.4 Model Results Versus Plankton Tow Data	144
S4.1 Change in Food Concentration	164
S4.2 Change in Depth Distribution of Environmental Conditions	165
S4.3 Change in Sea Surface Temperature	166

List of Tables

2.1	Core Locations and Information on Source Data	18
2.2	Information on Sediment Trap Data	21
2.3	Locations and $\delta^{18}\text{O}$ Values of Sediment Samples	32
2.4	Comparison of $\delta^{18}\text{O}$ Values	35
2.A1	Modifications of Competition Term Parameters	37
3.1	Modifications to Previous Model Version	45
4.1	Correlation of Foraminiferal Species with Environmental Parameters	88
S1.1	Species-specific Model Parameters.	121
S2.1	Relative Abundances of Planktonic Foraminifera During Heinrich Stadial 1	127
S3.1	Information on Sediment Trap Data	156
S3.2	Information on Plankton Tow Data	157
S3.3	Peak Season and Peak Amplitude – Model-Data-Comparison	160
S3.4	Average Living Depth – Model-Data-Comparison	162

List of Abbreviations

<i>G. bulloides</i>	<i>Globigerina bulloides.</i>
<i>G. elongatus</i>	<i>Globigerinoides elongatus.</i>
<i>G. ruber (white)</i>	<i>Globigerinoides ruber (white).</i>
<i>G. sacculifer</i>	<i>Globigerinoides sacculifer.</i>
<i>N. incompta</i>	<i>Neogloboquadrina incompta.</i>
<i>N. pachyderma</i>	<i>Neogloboquadrina pachyderma.</i>
<i>T. sacculifer</i>	<i>Trilobatus sacculifer.</i>
2xCO₂	Two times CO ₂ scenario.
4xCO₂	Four times CO ₂ scenario.
ALD	Average Living Depth.
BEC	Biogeochemical Elemental Cycling model.
CCSM3	Community Climate System Model, version 3.
CESM1.2	Community Earth System Model, version 1.2.2.
CESM1.2(BGC)	CESM1.2 configuration with BEC enabled.
CICE4	Community Ice Code, version 4.
CO₂	Carbon dioxide.
CORE	Coordinated Ocean-ice Reference Experiment.
Ctrl	Control simulation.
DCM	Deep Chlorophyll Maximum.
FORAMCLIM	Foraminifera Model.
GLODAP	Global Ocean Data Analysis Project.
H1	Heinrich Stadial 1.
IPCC	Intergovernmental Panel on Climate Change.

IRD	Ice-Rafted Debris.
LGM	Last Glacial Maximum.
LIG	Last Interglacial.
MARGO	Multiproxy Approach for the Reconstruction of the Glacial Ocean surface.
MLD	Mixed Layer Depth.
MLD Temp	Temperature at the MLD.
MOD	Modern conditions.
MPWP	Mid-Pliocene Warm Period.
MWP-1A	Meltwater Pulse 1A.
NAC	North Atlantic Current.
NCAR	National Center for Atmospheric Research.
OCMIP	Ocean Carbon Model Intercomparison Project.
PANGAEA	Data Publisher for Earth & Environmental Science.
PLAFOM	Planktonic Foraminifera Model.
PLAFOM2.0	Planktonic Foraminifera Model, version 2.
POP2	Parallel Ocean Program, version 2.
RCP	Representative Concentration Pathway scenario.
RMSE	Root-Mean-Square Error.
SST	Sea Surface Temperature.
Therm Temp	Temperature along the thermocline.
VD	Vertical Dispersion.
WOA09	World Ocean Atlas 2009.

Introduction

The Earth's climate system is permanently subject to changes on shorter (decadal) to longer (millennial) time scales. Over the last century both the atmosphere and global ocean have experienced a significant warming. Although the long-term temperature trend is considerably masked by natural variability (on synoptic, inter-annual, and decadal time scales), it has clearly been attributed to anthropogenic influences (*Huber and Knutti, 2012; Santer et al., 2013*). According to the fifth Assessment Report of the Intergovernmental Panel on Climate Change (*IPCC, 2013*), the anthropogenic increase in greenhouse gas concentrations contributed to the very substantial warming in the Arctic since the mid-20th century resulting in the decrease of the Arctic sea ice extent. Climate projections of the 21st century reveal that it is very likely that the Arctic sea ice cover will continue to shrink and thin as global mean surface temperatures rise (*IPCC, 2013*). Furthermore, over the last century the Greenland ice sheet has lost ice and contributed substantially to a rise in the global mean sea level (*Ewert et al., 2012; Sasgen et al., 2012; Shepherd et al., 2012; Kjeldsen et al., 2015; van den Broeke et al., 2016*). Satellite and field observations indicate an increase in the contribution of the Greenland ice sheet to global mean sea level from 0.09 mm/yr for 1992-2001 to 0.59 mm/yr for 2002-2011 (see *IPCC, 2013*, and references therein), and it is expected that this trend will continue over the next decades (e.g., *Fettweis et al., 2013*). Climate simulations show a partial or near-complete ice-free Greenland if a threshold temperature (current estimates range between 0.8°C and 2.2°C warmer than preindustrial temperatures) is passed and maintained for several millennia (*Greve, 2000; Ridley et al., 2005, 2010; Driesschaert et al., 2007; Charbit et al., 2008; Robinson et al., 2012*). On a multi-millennial time scale, the melting of the Greenland ice sheet self-amplifies and might become irreversible beyond this threshold, resulting in a reduction of the ice sheet to around 10% of its present-day volume, which is equivalent to a sea level rise of about 7 m (*IPCC, 2013*, and references therein).

For a better understanding of the recent and projected future changes, paleoclimate reconstructions should be considered, which provide detailed prospects about long-term changes and the variability of the climate system on time scales much longer than the instrumental era. For instance, sedimentary, fossil, and archaeological archives have been used to estimate past sea level changes (e.g., *Lambeck et al., 2004, 2010; Deschamps et al., 2012; Leorri et al., 2012*). These proxies reflect both local and global conditions, but are limited in space and time. Climate reconstructions reveal that global mean sea level was more than 5 m higher than present, with considerable contributions from the Greenland and Antarctic ice sheets, during the warm periods of the past few million years when global mean temperatures were more than 1°C warmer than preindustrial (*IPCC, 2013; Dutton et al., 2015*). For instance, during the mid-Pliocene warm period (MPWP; 3.3 to 3.0 million years ago) atmospheric carbon dioxide (CO₂) concentrations ranged between

350 and 450 ppm (*Pagani et al.*, 2010; *Seki et al.*, 2010) and global mean surface air temperatures were 1.9° to 3.6°C higher than during the preindustrial era (*Dowsett et al.*, 2012; *Haywood et al.*, 2013). Based on geological records *Miller et al.* (2012) suggested that peak estimates of the global sea level were 20 ± 10 m higher than present sea levels during the MPWP due to mass loss from the Greenland and Antarctic ice sheets. During the last interglacial period (LIG; 129,000 to 116,000 years ago), however, when global annual mean surface temperatures were $\sim 1^\circ$ to 2°C warmer than preindustrial temperatures (*Turney and Jones*, 2010; *Otto-Bliesner et al.*, 2013), the global mean sea level was for several thousand years 5 m higher relative to present-day, but did not exceed 10 m (*Kopp et al.*, 2009, 2013; *Dutton and Lambeck*, 2012). Based on paleoclimate archives, such as ice cores (*NEEM community members*, 2013), and model studies (*Robinson et al.*, 2011; *Born and Nisancioglu*, 2012; *Quiquet et al.*, 2013; *Stone et al.*, 2013), it is likely that the Greenland ice sheet contributed no more than 4.3 m to the global mean sea level (*IPCC*, 2013). During the last deglaciation ($\sim 21,000$ to 7,000 years ago) global mean sea level rose by ~ 120 m due to ice-sheet melting (*Fairbanks*, 1989; *Lambeck et al.*, 2002; *Peltier*, 2005), whereby a rapid sea level rise of 14 to 18 m occurred within ~ 340 years, which has been indicated by fossil coral reef deposits (*Deschamps et al.*, 2012). This period of rapid sea level rise is known as meltwater pulse 1A (MWP-1A; 14,650 to 14,310 years ago). Global mean sea level has also been affected during past cold periods. The last glacial period has been characterized with episodes of abrupt cooling in the North Atlantic Ocean (*Bond et al.*, 1992; *Bard et al.*, 2000; *Sanchez Goñi and Harrison*, 2010), which have been associated with large discharges of icebergs originating from the northern hemispheric ice sheets. During these Heinrich stadials global sea level rose by several meters (*Chappell*, 2002; *Rohling et al.*, 2008; *Siddall et al.*, 2008; *González and Dupont*, 2009; *Yokoyama and Esat*, 2011) and surface ocean properties changed considerably (*Bond et al.*, 1992; *Labeyrie et al.*, 1995; *Maslin et al.*, 1995; *Sarnthein et al.*, 1995; *Cortijo et al.*, 1997; *Bard et al.*, 2000). The release of massive amounts of freshwater from the retreating ice sheets during the past warm periods (such as the MPWP, LIG, and MWP-1A) or from the melting of icebergs during Heinrich stadials alters not only sea level, but likewise the ocean circulation and the oceanic freshwater budget, which also affects marine ecosystems.

Past meltwater events have been reconstructed by using fossil evidence of marine microorganisms. In particular, planktonic foraminifera are most commonly used as a paleoceanographic proxy. Based on stable oxygen isotope analyses of their calcite shells past meltwater events were identified and characterized (*Bond et al.*, 1992; *Broecker*, 1994; *Lubinski et al.*, 2001; *Knies and Vogt*, 2003; *Hall and Chan*, 2004; *Spielhagen et al.*, 2004; *Thornalley et al.*, 2010; *Stanford et al.*, 2011). However, the reconstruction of surface water properties from planktonic foraminifera requires extensive knowledge about the signal's origin in the water column and the time when it was preserved in the fossil shells. Depending on the ambient climate conditions, the habitats of planktonic foraminifera vary seasonally and spatially (*Mix*, 1987; *Mulitza et al.*, 1998; *Ganssen and Kroon*, 2000; *Skinner and Elderfield*, 2005; *Jonkers and Kučera*, 2015), and their changes have to be considered when interpreting proxy records. The signal preserved in fossil foraminifera is biased toward the conditions of species' maximum production and is essentially a result of both habitat and climate change (e.g., *Skinner and Elderfield*, 2005; *Jonkers and Kučera*, 2015, 2017). However, accounting for these effects is difficult as it requires independent data. Therefore, a modeling approach could offer an alternative for reducing the bias in paleoceanographic reconstructions by simulating changes in species-specific habitats under climate change. Such a modeling approach can contribute to more meaningful interpretations of proxy records, eventually aiding to a better understanding of climate change and its mechanisms.

1.1 Planktonic Foraminifera

Planktonic foraminifera are unicellular marine microorganisms, which are found everywhere in the open ocean inhabiting the top 100s of meters of the water column. Species assemblages can be grouped into five major faunal provinces: polar, subpolar, transitional, subtropical, and tropical (Bradshaw, 1959; Bé and Tolderlund, 1971; Hemleben et al., 1989; Kucera, 2007). These biogeographical distribution patterns of planktonic foraminifera can be linked to different environmental conditions defining the species-specific habitats. In general, the growth and distribution of individual planktonic foraminifera species depend on temperature, food supply, light intensity, and the structure of the water column (e.g., Fairbanks and Wiebe, 1980; Fairbanks et al., 1980, 1982; Bijma et al., 1990a; Watkins et al., 1996; Schiebel et al., 2001; Simstich et al., 2003; Field, 2004; Kuroyanagi and Kawahata, 2004; Žarić et al., 2005; Salmon et al., 2015; Rebotim et al., 2017). Based on sediment trap and stratified plankton tow records, seasonal distribution patterns of planktonic foraminifera have been inferred (e.g., Bé, 1960; Fairbanks and Wiebe, 1980; Deuser et al., 1981; Kohfeld et al., 1996; Field, 2004; Wilke et al., 2009; Jonkers et al., 2013; Jonkers and Kučera, 2015). The seasonality of planktonic foraminifera features a latitudinal pattern (Figure 1.1): in the high latitudes peak abundances are reached during the short summer season, the midlatitudes are characterized by a bimodal pattern with one large peak in spring and a smaller one in fall, and in the low latitudes seasonality is low with no dominant peak season (e.g., Hemleben et al., 1989; Schiebel et al., 2001; Schiebel and Hemleben, 2005, 2017; Jonkers and Kučera, 2015). The depth habitat of individual planktonic foraminifera species varies also in time and space depending on the prevailing climate conditions (e.g., Fairbanks and Wiebe, 1980; Fairbanks et al., 1982; Schiebel et al., 2001; Simstich et al., 2003; Field, 2004; Schiebel and Hemleben, 2005, 2017; Salmon et al., 2015; Rebotim et al., 2017). In the low latitudes species' abundances are highest in surface waters year-round, whereas towards the higher latitudes most species are found at depth, but may occur close to the surface during the winter season (Figure 1.1). Several studies showed that temperature and/or temperature-related environmental factors are responsible for the observed changes in species-specific habitats (Morey et al., 2005; Schiebel and Hemleben, 2005, 2017; Žarić et al., 2005; Jonkers and Kučera, 2015, 2017; Rebotim et al., 2017).

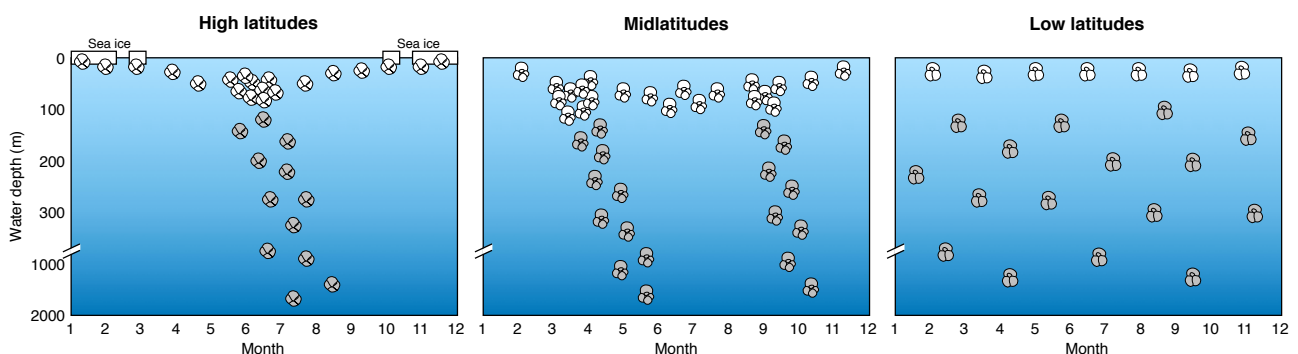


Figure 1.1: Schematic view of the seasonality and depth habitat of planktonic foraminifera (white tests). The species' seasonal succession is exemplified by the cold-water species *Neogloboquadrina pachyderma* for the high latitudes, by the temperate water species *Globigerina bulloides* for the midlatitudes, and by the warm-water species *Globigerinoides ruber* for the low latitudes. *Neogloboquadrina pachyderma* lives in the lower layers of the Antarctic sea ice during winter. Mass flux of empty tests (grey) follows the timing of the production peaks, during summer in the high latitudes and during spring/fall in the midlatitudes. In the low latitudes the production of surface-dwelling planktonic foraminifera is seasonally uniform and, thus, sedimentation of empty tests is less seasonally driven compared to the higher latitudes. Adapted from Schiebel and Hemleben (2005).

In the modern ocean more than 40 extant planktonic foraminifera morphospecies are known (*Hemleben et al.*, 1989; *Schiebel and Hemleben*, 2017), which are divided into spinose and non-spinose species (*Murray*, 1897). Most planktonic foraminifera are, to a varying degree, omnivorous, whereby spinose species are more adapted to a carnivorous diet preferring animal prey (i.e., zooplankton such as copepods) and non-spinose species tend to be more herbivorous preferring phytoplankton (mainly diatoms and dinoflagellates) (*Hemleben et al.*, 1989). The majority of the spinose species has been associated with photosynthesizing symbionts (primarily dinoflagellates) (e.g., *Anderson and Bé*, 1976; *Spindler and Hemleben*, 1980; *Erez*, 1983; *Jørgensen et al.*, 1985; *Spero and Parker*, 1985; *Spero*, 1987; *Gastrich*, 1987; *Gastrich and Bartha*, 1988; *Hemleben et al.*, 1989). Due to their light dependence symbiont-bearing species inhabit the photic zone of the world ocean, whereas symbiont-barren species are also found in deeper waters below the photic zone. However, the highest population density of planktonic foraminifera occurs in the mixed layer and/or thermocline. Based on culturing experiments and field studies it is evident that individual planktonic foraminifera species inhabit characteristic ecological niches, which are defined by each species' optimum temperature and temperature tolerance limits as well as by their food requirements (e.g., *Bé and Tolderlund*, 1971; *Fairbanks and Wiebe*, 1980; *Vincent and Berger*, 1981; *Hemleben et al.*, 1989; *Bijma et al.*, 1990a; *Žarić et al.*, 2005).

During their ontogenesis planktonic foraminifera build a multi-chambered calcite shell (*Hemleben et al.*, 1989). After reproduction the calcareous shells of dead specimens rapidly sink to the seafloor (Figure 1.1) (*Takahashi and Bé*, 1984) and become well preserved in the sediment. Indeed, it has been suggested that planktonic foraminifera may play an important role in the marine carbonate cycle (*Schiebel*, 2002). Planktonic foraminifera are a commonly used paleoceanographic proxy to reconstruct past climates. Their fossil shells preserve the physical and chemical properties of the species-specific habitats and can, therefore, provide information on environmental conditions of past oceans. However, to reconstruct past climate conditions detailed knowledge about the species' ecology is required. Since the species-specific habitats are strongly influenced by the prevailing ambient conditions, which control the growth as well as the spatial and temporal distribution of the individual planktonic foraminifera species, the signals recorded in the fossil shells most likely reflect only the hydrographic and biological states of a certain location at a specific point in time. Hence, the signal is biased toward the time and depth of maximum production excluding information from such conditions that are unfavorable for the survival of planktonic foraminifera species or for their calcification. However, the reconstruction of past meltwater fluxes (such as during the MPWP, LIG, MWP-1A, or Heinrich stadials) based on stable oxygen isotope measurements on fossil foraminifera requires information on their exact calcification depth. In paleoclimate reconstructions it is assumed that, for instance, the main polar species *Neogloboquadrina pachyderma* calcifies close to the surface, although present-day observations from the Nordic Seas show that this species attains its isotopic signal in deeper waters along the halocline (*Simstich et al.*, 2003). This vertical offset between actual and assumed calcification depth implies that the full extent of the surface water freshening due to (past) meltwater pulses is not fully reflected in the oxygen isotope signal of this species, which results in a systematic underestimation of the true salinity anomaly. The reduction of this bias is difficult and would require independent fossil evidence. Using a modeling approach could help to correct the offset. Furthermore, for a better understanding of the ecology of planktonic foraminifera (ecosystem or ecophysiological) modeling approaches can provide information on the control mechanisms influencing species-specific habitats and/or on spatial and temporal variations in the species' distribution in response to changes in the climate system on a global scale at almost any time. By combining observational records with model simulations our current understanding of the Earth's climate system can be improved and might, likewise, result in a comprehensive and more reliable interpretation of

proxy records.

1.2 Modeling Approach

At present, two modeling approaches simulating the global distribution of planktonic foraminifera exist. *Fraile et al.* (2008) used an ecosystem approach (PLAFOM) to determine dynamic changes in the foraminiferal biomass in the surface mixed layer, whereas *Lombard et al.* (2011) used an ecophysiological approach (FORAMCLIM) to capture the growth rate of different foraminiferal species. The FORAMCLIM model has been empirically based on observed physiological processes in live specimens during laboratory experiments or field observations, and, thus, simulates the growth of eight distinct foraminiferal species as a function of nutrition, respiration, and photosynthesis (*Lombard et al.*, 2011). Those physiological processes strongly depend on temperature, light availability, and food concentration. The model parameters have been calibrated against a compilation of plankton tow data and/or culturing experiments (*Lombard et al.*, 2011). FORAMCLIM successfully captured the spatial distribution pattern of different planktonic foraminifera species and is able to predict the season and depth of the maximum species-specific growth potential when using in situ observations or model output of a biogeochemical model as forcing (*Lombard et al.*, 2011). The planktonic foraminifera model PLAFOM, however, predicts the global monthly surface concentration of five distinct foraminiferal species (*Fraile et al.*, 2008). The change in the foraminifera carbon concentration is a function of total grazing and mass loss, and depends on temperature as well as food availability. PLAFOM has been run within an ecosystem model for the global surface ocean (*Moore et al.*, 2002a), which provides information on the species-specific food sources. The underlying model parameters have been empirically calibrated against a multitude of sediment trap data (*Fraile et al.*, 2008). PLAFOM successfully simulated the biogeographical and seasonal distribution patterns of several planktonic foraminifera in the global surface ocean, and has, additionally, been used to predict species-specific distributional patterns under changing environmental conditions at different geological time scales (*Fraile et al.*, 2008, 2009a,b; *Kretschmer et al.*, 2016).

Both modeling approaches produce spatially and temporally coherent large-scale patterns for different planktonic foraminifera species, but are, nevertheless, limited in their capability to reproduce species-specific habitats in their full extent for different reasons. Since FORAMCLIM is empirically based on parameters derived from laboratory experiments the growth rate relationships may not hold for the real ocean (*Lombard et al.*, 2011; *Roy et al.*, 2015). The laboratory-based relationships between the environmental conditions and the foraminiferal growth rates have been derived from specific specimens, whose physiological responses could be more related to stress rather than to environmental perturbations (*Roy et al.*, 2015). So far, it has not been possible to reproduce planktonic foraminifera under controlled laboratory conditions, indicating that foraminifera behave differently in the laboratory than in their natural habitat. Hence, FORAMCLIM is limited to the processes observed in the laboratory and might only to some extent hold for the species' behavior in their natural environment. Additionally, FORAMCLIM predicts only cytoplasm growth of individual species (i.e., the changes in the organic weight of the foraminifera) and does not consider variations in the shell size (*Lombard et al.*, 2011). PLAFOM, however, is based on parameterizations of many processes (such as predation, competition, and mortality) that are still not well known (*Hemleben et al.*, 1989; *Schiebel and Hemleben*, 2017). Furthermore, the parameter optimization is hampered due to the observational data currently available, which only represent snapshots of the population dynamics in time and space. In compar-

ison with FORAMCLIM, PLAFOM reproduces species' abundances only in the surface mixed layer without resolving the vertical dimension (Fraile *et al.*, 2008; Lombard *et al.*, 2011). Hence, vertical variations in the species-specific habitats due to changing environmental conditions cannot be captured in this 2D approach.

Paleoclimate reconstructions based on fossil foraminifera are potentially subject to biases due to the assumptions that are made, leading to erroneous estimates of past climate conditions. To provide a reliable tool that can help to reduce the biases, it is essential to realistically resolve species-specific habitats in time and space, including the vertical dimension. In this study, PLAFOM has been further developed to simulate more realistically the species' behavior under different environmental conditions and to assess population dynamics on a global scale. In this updated version of PLAFOM (hereafter referred to as PLAFOM2.0) the growth rate is apart from food concentration and temperature a function of light (for species with symbionts). To fully resolve the vertical dimension PLAFOM2.0 has been added to the code trunk of the ocean component of the Community Earth System Model, version 1.2.2 (CESM1.2; Hurrell *et al.*, 2013) as a separate module with the Biogeochemical Elemental Cycling model developed by Moore *et al.* (2004) being active. This model system is able to predict spatially and temporally varying global species-specific habitats of five planktonic foraminifera, which are among the most abundant species in the modern ocean and have been widely used in culturing experiments and/or paleoceanographic reconstructions. PLAFOM2.0 considers the cold-water species *Neogloboquadrina pachyderma*, the temperate water species *Neogloboquadrina incompta* and *Globigerina bulloides*, and the warm-water species *Globigerinoides ruber* (white) and *Trilobatus sacculifer* (Figure 1.2).

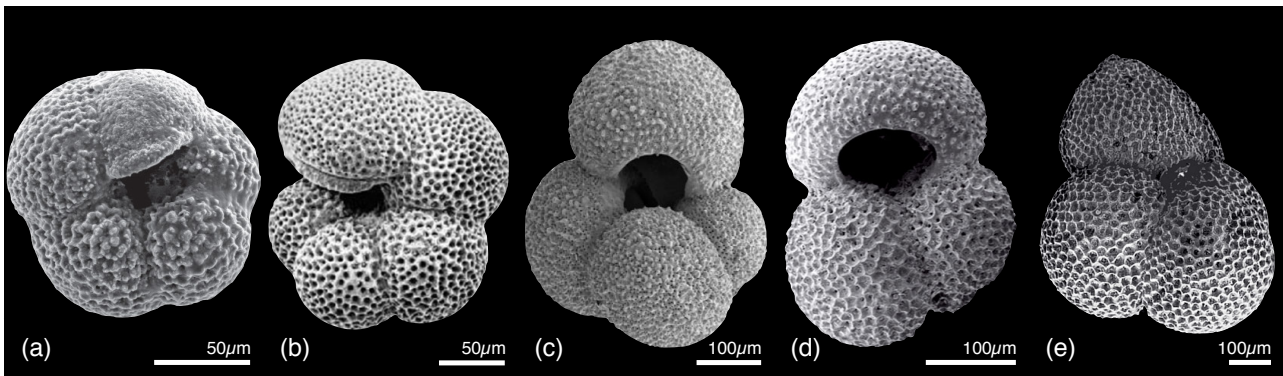


Figure 1.2: Fossil specimens of planktonic foraminifera: (a) *Neogloboquadrina pachyderma*, (b) *Neogloboquadrina incompta*, (c) *Globigerina bulloides*, (d) *Globigerinoides ruber* (white), and (e) *Trilobatus sacculifer*. Photo courtesy of <http://www.foraminifera.eu> and citations therein.

Planktonic foraminifera species

Neogloboquadrina pachyderma dominates the polar waters of both hemispheres (e.g., Bé, 1977) and can even survive within Antarctic sea ice (Spindler and Dieckmann, 1986; Dieckmann *et al.*, 1991). This species prefers living in areas, where sea surface temperatures (SSTs) remain below 10 °C (Bé, 1969; Bé and Tolderlund, 1971; Bé and Hutson, 1977). *Neogloboquadrina pachyderma* is a non-spinose species and feeds almost exclusively on diatoms (Hemleben *et al.*, 1989). Peak abundances of this species usually occur in the upper 100 m of the water column (Kohfeld *et al.*, 1996; Stangeew, 2001; Mortyn and Charles, 2003; Kuroyanagi and Kawahata, 2004; Bergami *et al.*, 2009; Pados and Spielhagen, 2014) and have been related to the timing in the primary productivity (Jonkers and Kučera, 2015). At present up to eight different genotypes of *N. pachyderma* have been identified (Darling *et al.*, 2003, 2004, 2006; Darling and Wade, 2008; André *et al.*, 2014), whereby the North Atlantic and Arctic Oceans are only inhabited by a single genetic type (Darling *et al.*, 2004, 2007). Note until the publication of Darling *et al.* (2006) this species was formerly assigned to *N. pachyderma* (sin.).

Neogloboquadrina incompta was until the publication of *Darling et al.* (2006) referred to as *N. pachyderma* (dex.). *Neogloboquadrina incompta* typically occurs in the subpolar and temperate waters of the world oceans and is also highly abundant in upwelling regions (e.g., Bé, 1969; Bé and Tolderlund, 1971; Bé and Hutson, 1977; Giraudeau, 1993; Boltovskoy et al., 1996; Darling et al., 2006). This species prefers living in warmer waters compared to *N. pachyderma* (e.g., Kuroyanagi and Kawahata, 2004; Iwasaki et al., 2017) and exhibits a broad optimum SST range ($\sim 8 - 22^\circ\text{C}$, Žarić et al., 2005). *Neogloboquadrina incompta* has been mostly found at mid-depth being associated with high chlorophyll *a* concentrations (Ortiz et al., 1995; Mortyn and Charles, 2003; Field, 2004; Kuroyanagi and Kawahata, 2004; Iwasaki et al., 2017; Rebotim et al., 2017). This non-spinose species has a preference to feed on phytoplankton (Hemleben et al., 1989) and encompasses of two genetic lineages (Darling et al., 2006).

Globigerina bulloides is associated with temperate to subpolar water masses and is also found in upwelling regions (e.g., Bé, 1969; Bé and Tolderlund, 1971; Bé and Hutson, 1977; Giraudeau, 1993; Boltovskoy et al., 1996; Naidu and Malmgren, 1996). *Globigerina bulloides* has been related to high productivity areas and is, thus, highly abundant at depths associated with a deep chlorophyll maximum (Fairbanks and Wiebe, 1980; Mortyn and Charles, 2003; Wilke et al., 2009; Iwasaki et al., 2017) or near-surface in the coastal and equatorial upwelling regions (Ortiz et al., 1995; Watkins et al., 1998; Peeters and Brummer, 2002; Field, 2004; Kuroyanagi and Kawahata, 2004). It is a spinose species and according to the latest findings possesses photosynthesizing cyanobacterial endobionts (Bird et al., 2017). Several genetic types of *G. bulloides* have been distinguished (e.g., Darling et al., 2000; Darling and Wade, 2008; Seears et al., 2012; Morard et al., 2013; André et al., 2013, 2014), which likely have different ecological preferences (Kucera and Darling, 2002; Darling and Wade, 2008).

***Globigerinoides ruber* (white)** is typically found in subtropical to tropical waters (e.g., Bé and Tolderlund, 1971; Bé, 1977; Bé and Hutson, 1977). It usually inhabits the upper 100 m of the water column and has been considered as a surface-dwelling species (e.g., Bé and Hamlin, 1967; Fairbanks et al., 1982; Kemle-von Mücke and Oberhänsli, 1999; Schiebel et al., 2002; Wilke et al., 2009; Rippert et al., 2016). *Globigerinoides ruber* (white) is most abundant in warm waters with optimum temperatures ranging between 25° and 30°C (Žarić et al., 2005) and exhibits year-round a rather uniform flux pattern with no prominent seasonal peak, which is strongly related to temperature (Jonkers and Kučera, 2015). It is a spinose species bearing algal symbionts and preferably feeds on zooplankton (Hemleben et al., 1989). This species consists of up to five genotypes belonging to two lineages, which might exhibit different habitats (Aurahs et al., 2009, 2011).

Trilobatus sacculifer was until the publication of Spezzaferri et al. (2015) generically assigned to *Globigerinoides sacculifer*. *Trilobatus sacculifer* is most abundant in the tropical regions (e.g., Bé and Hamlin, 1967; Bé, 1977; Fairbanks et al., 1982; Kemle-von Mücke and Oberhänsli, 1999; Schiebel et al., 2002; Rippert et al., 2016) and absent at low temperatures with an optimum temperature range exceeding 23°C (Žarić et al., 2005). This spinose species prefers living in the photic zone (i.e., close to the surface), bears dinoflagellate symbionts, and its diet consists mainly of zooplankton (primarily copepods) (Hemleben et al., 1989). *Trilobatus sacculifer* is genetically homogeneous worldwide, thus, only a single genotype exist (André et al., 2013).

The five considered planktonic foraminifera species have been added as optional passive tracers to the code trunk of the ocean component of CESM1.2. In general, PLAFOM2.0 is driven by temperature, food concentration, and light availability (which matters only for species with symbionts). The species-specific food concentrations are simulated by the ecosystem model at every time step and are subsequently used by PLAFOM2.0 to calculate the monthly carbon concentration of the five planktonic foraminifera species mentioned above (Figure 1.3). The species-specific temperature tolerance limits and food preferences have been derived from laboratory experiments or field observations (e.g., Hemleben et al., 1989; Bijma et al., 1990a; Watkins et al., 1996; Watkins and Mix, 1998; Arnold and Parker, 1999; Žarić et al., 2005).

This ecosystem modeling approach can help to better understand habitat dynamics of individual planktonic

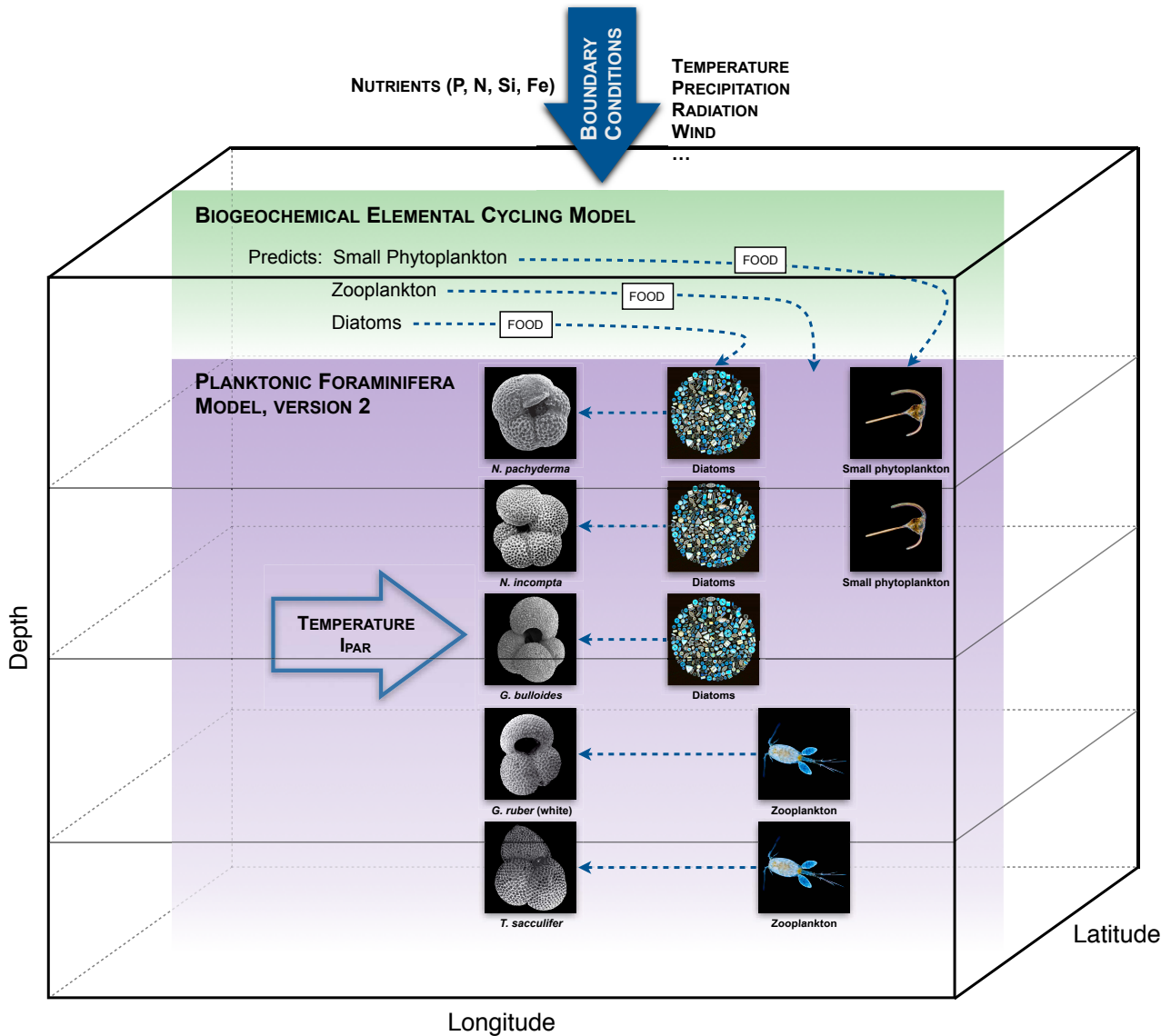


Figure 1.3: Schematic view of the global model structure. Note that the foraminifera concentration of each species is calculated for each depth layer respectively. Photo courtesies of <http://www.foraminifera.eu>, <https://www.nualgiaquarium.com>, <https://www.britannica.com>, and <http://www.todayifoundout.com>.

foraminifera not only on a regional, but also on a global scale. Additionally, information on the species' behavior during different time periods (i.e., the geological past or the future) and, thus, in response to varying climate/environmental conditions can be provided. In general, this approach can essentially contribute to a more accurate evaluation and interpretation of paleoceanographic records, potentially resulting in a better understanding of climate change.

1.3 Thesis Objectives and Outline

The aim of this thesis is to provide a better understanding of species-specific habitat dynamics of planktonic foraminifera on a regional and global scale by using an ecosystem modeling approach. Planktonic foraminifera respond to changing environmental conditions exhibiting variations in their habitats in time and space. The assumption of constant species-specific habitats in paleoceanographic reconstructions (based on fossil

evidence of planktonic foraminifera species) could result in biased estimates of past climate conditions. This ecosystem modeling approach could allow for reducing the bias. This study aims to assess and quantify the seasonally varying species-specific (depth) habitats of five planktonic foraminifera species in regard to different climate conditions. To allow for a better interpretation of paleoclimate reconstructions the following hypotheses are tested in this study:

- The peak abundance of planktonic foraminifera species shifts by several months when different climate conditions occur.
- Planktonic foraminifera species respond differently to changing environmental conditions by lowering or deepening their vertical habitat.

By applying an existing planktonic foraminifera model and by implementing an improved version of this model into an earth system model, the following scientific questions will be addressed to test these hypotheses:

- To what degree do seasonal variations in the production of the polar species *Neogloboquadrina pachyderma* affect paleoceanographic reconstructions during Heinrich Stadial 1 (~18,000 to 15,000 years ago) in the North Atlantic Ocean?
- How do species-specific depth habitats of individual planktonic foraminifera vary in time and space? Which mechanisms control these variations?
- What impact does global warming have on species-specific habitats of planktonic foraminifera?

Chapter 2 deals with the seasonal variations in the production of the Arctic planktonic foraminifera species *Neogloboquadrina pachyderma* and to what degree these variations may affect paleoceanographic reconstructions during glacial-interglacial times. Therefore, the distribution and seasonality of *N. pachyderma* has been simulated in the surface mixed layer at geological time scales in the North Atlantic Ocean north of 30°N. The model performance has been validated by comparing the predicted distribution of the species with observations from marine sediment core records and sediment trap data.

In chapter 3 the updated version of the existing planktonic foraminifera model, i.e., PLAFOM2.0, is introduced in detail. Here the vertical and seasonal distribution of individual planktonic foraminifera species and their sensitivity to potential driving factors on a global scale are analyzed. The predicted distribution patterns of the considered planktonic foraminifera species are compared to plankton tow and sediment trap data from different locations distributed over the world oceans. Additionally, the model performance is discussed extensively, including caveats in the model-data-comparison.

In chapter 4 the impact of global warming on the distribution of planktonic foraminifera is investigated. In particular, the response of each planktonic foraminifera species to changes in food availability and ocean temperature has been extensively analyzed. Therefore, the model system has been forced with climatologies based on a doubling or quadrupling of atmospheric CO₂.

Chapter 2 through chapter 4 of this thesis represent individual manuscripts. Chapter 2 is already peer-reviewed and published in *Paleoceanography*, chapter 3 has been submitted to *Biogeosciences*, and chapter 4 is in the early stage of preparation for submission to *Global Change Biology*. The thesis is complemented by concluding remarks and an outlook (chapter 5) as well as a supplement, which provides supporting information for the individual manuscripts and a detailed description of the model configuration.

Modeling the distribution and seasonality of *Neogloboquadrina pachyderma* in the North Atlantic Ocean during Heinrich Stadial 1

Kerstin Kretschmer^{1*}, Michal Kucera¹, and Michael Schulz¹

¹MARUM-Center for Marine Environmental Sciences and Faculty of Geosciences, University of Bremen, Bremen, Germany
Paleoceanography (2016), 31, 1–25

Contents

2.1	Introduction	12
2.2	Data and Methods	14
2.2.1	PLAFOM	14
2.2.2	Model Experiments	15
2.2.3	Sediment Samples	16
2.2.4	Scaling of PLAFOM Output to Observed Relative Abundances of Individuals	17
2.2.5	Model Validation: Modeled Seasonal Patterns Versus Observations	20
2.3	Results	21
2.3.1	Relative Abundances of <i>N. pachyderma</i>	21
2.3.2	Seasonality of <i>N. pachyderma</i>	22
2.4	Discussion	23
2.4.1	Glacial Range Expansion of <i>N. pachyderma</i>	23
2.4.2	The Seasonality of <i>N. pachyderma</i>	25
2.4.3	Quantifying the Effect of Shifting Phenology on Stable Isotope Signals in <i>N. pachyderma</i>	28
2.4.3.1	$\delta^{18}\text{O}_c$ Signature During Modern Conditions	30
2.4.3.2	$\delta^{18}\text{O}_c$ Signature During the Last Glacial Period	31
2.4.3.2.1	Changes in $\delta^{18}\text{O}_c$ Based on SST Estimates	31
2.4.3.2.2	Changes in $\delta^{18}\text{O}_c$ Based on MLD Temperatures	32
2.4.3.2.3	Changes in $\delta^{18}\text{O}_c$ Based on Thermocline Temperatures	33
2.5	Conclusion	36

*Fossil shells of planktonic foraminifera serve as the prime source of information on past changes in surface ocean conditions. Because the population size of planktonic foraminifera species changes throughout the year, the signal preserved in fossil shells is biased toward the conditions when species production was at its maximum. The amplitude of the potential seasonal bias is a function of the magnitude of the seasonal cycle in production. Here we use a planktonic foraminifera model coupled to an ecosystem model to investigate to what degree seasonal variations in production of the species *Neogloboquadrina pachyderma* may affect paleoceanographic reconstructions during Heinrich Stadial 1 (~ 18 – 15 cal. ka B.P.) in the North Atlantic Ocean. The model implies that during Heinrich Stadial 1 the maximum seasonal production occurred later in the year compared to the Last Glacial Maximum (~ 21 – 19 cal. ka B.P.) and the preindustrial era north of 30°N. A diagnosis of the model output indicates that this change reflects the sensitivity of the species to the seasonal cycle of sea ice cover and food supply, which collectively lead to shifts in the modeled maximum production from the Last Glacial Maximum to Heinrich Stadial 1 by up to 6 months. Assuming equilibrium oxygen isotopic incorporation in the shells of *N. pachyderma*, the modeled changes in seasonality would result in an underestimation of the actual magnitude of the meltwater isotopic signal recorded by fossil assemblages of *N. pachyderma* wherever calcification is likely to take place.*

2.1 Introduction

The last glacial period was characterized by rapid climate changes with episodes of abrupt cooling in the North Atlantic region (Bond et al., 1992; Bard et al., 2000; Sanchez Goñi and Harrison, 2010). During these Heinrich stadials (we refer here to a stadial containing a Heinrich event (cf. Rasmussen et al., 2014)—hence, a Heinrich stadial is longer (e.g., Stanford et al., 2011) than the associated Heinrich event) large discharges of icebergs from the northern hemispheric ice sheets entered the North Atlantic Ocean. Due to the melting of these icebergs and the subsequent release of freshwater it is hypothesized that the production of North Atlantic Deep Water was greatly reduced during those episodes (McManus et al., 1994, 1999, 2004; Sarnthein et al., 1995; Hemming, 2004; Stanford et al., 2006, 2011).

The climatic conditions of each Heinrich stadial were associated with profound changes in the surface ocean properties in the North Atlantic (e.g., Bond et al., 1992; Labeyrie et al., 1995; Maslin et al., 1995; Sarnthein et al., 1995; Cortijo et al., 1997; Bard et al., 2000), affecting marine plankton. As a result, each “Heinrich layer” is dominated by the polar planktonic foraminifera species *Neogloboquadrina pachyderma* (in the sense of Darling et al. (2006)). Today, this species thrives in polar waters, where it accounts for almost 100% of the total planktonic foraminiferal flux to marine sediments (Bé and Tolderlund, 1971). Studies of marine sediments and sediment trap records indicate that in the North Atlantic, the species dominates the planktonic foraminifera flux in areas where summer sea surface temperature (SST) remains below 10 °C (Tolderlund and Bé, 1971; Duplessy et al., 1991; Hilbrecht, 1996) and appears to be largely absent in regions with summer SST above 23.7 °C (Žarić et al., 2005). Observations from stratified plankton tows indicate that in the Arctic and North Atlantic Ocean maximum abundances of live specimens of *N. pachyderma* consistently occur in the top 100 m of the water column (e.g., Vilks, 1970, 1975; Stehman, 1972; Carstens and Wefer, 1992; Kohfeld et al., 1996; Volkmann, 2000; Pados and Spielhagen, 2014; Xiao et al., 2014). The exact position of the population maximum varies among the sampled regions and even between adjacent samples. In the North Atlantic, Pados and Spielhagen (2014) recorded maximum abundance mostly in their second

shallowest sampled interval (50–100 m), but they also found high abundances in their shallowest sampled interval (0–50 m) both in the ice-free Fram Strait and under ice cover off East Greenland. In the Northeast Water Polynya, *Kohfeld et al.* (1996) recorded the abundance maximum of the species mostly between 25 and 50 m. In contrast, the species calcification depth deduced from stable isotope composition of adult shells appears to range from the surface mixed layer to the subsurface at depth below 100 m (*Kohfeld et al.*, 1996; *Bauch et al.*, 1997; *Simstich et al.*, 2003).

The southward extension of this species during Heinrich stadials is well documented in marine sediments (e.g., *Bond et al.*, 1992; *Lebreiro et al.*, 1996; *Cacho et al.*, 1999; *Bard et al.*, 2000; *Eynaud et al.*, 2009), in particular during Heinrich Stadial 1 (H1, we refer here to the time span between 15 and 18 cal. ka B.P.). In these sediments, geochemical signals in shells of this species are used to reconstruct surface ocean conditions during H1, including the magnitude of the presumed meltwater discharge (*Hemming*, 2004). These reconstructions are critically dependent on the knowledge of the ecology of the species, including its calcification habitat and its phenology. During Heinrich stadials, the species expanded from polar to midlatitudes, which is unlikely not to have an effect on its phenology. Based on sediment trap data, the maximum productivity of *N. pachyderma* in the Nordic Seas occurs at present in the summer months (July–September) (*Kohfeld et al.*, 1996; *Jensen*, 1998; *Schröder-Ritzrau et al.*, 2001), whereas in the western North Atlantic and in the Irminger Sea the flux pattern of temperate/cold water planktonic foraminiferal species (including *Globigerina bulloides*, *Neogloboquadrina incompta*, and *N. pachyderma*) appears to be bimodal with two distinct pulses during the year: one in spring and one in fall (*Tolderlund and Bé*, 1971; *Jonkers et al.*, 2010, 2013; *Jonkers and Kučera*, 2015). Hence, the existing observational data indicate a shift in the phenology (from a unimodal to a bimodal pattern) with latitude for modern conditions. This effect in shifting phenology is not yet accounted for in the interpretation of proxy records, because it is difficult to constrain it by paleoecological data. However, phenology of planktonic foraminifera can be modeled as shown by *Žarić et al.* (2006), *Fraille et al.* (2008, 2009a,b), and *Lombard et al.* (2011).

In this study we investigate the distribution and seasonality of *N. pachyderma* in the North Atlantic Ocean (with the main focus on the area between 30°N and 80°N) during H1 and attempt to quantify the effect of shifting phenology in this species on proxy records. To this end, we modify the planktonic foraminifera model of *Fraille et al.* (2008) and drive it by H1 model simulations to obtain an estimate of monthly production of *N. pachyderma* during H1 throughout the whole North Atlantic and the resulting relative abundance of the species in the sediment. The fidelity of the model is tested by comparing the modeled distribution of the species with observations from marine sediment core records covering the time span of H1. The predicted phenology of the *N. pachyderma* flux during H1 is compared to modern (here referring to preindustrial) climate conditions and the Last Glacial Maximum (LGM, ~ 21 – 19 cal. ka B.P.), its sensitivity to the driving mechanisms is investigated and the consequences of the observed shifts in the phenology for the interpretation of proxies based on this species are discussed.

2.2 Data and Methods

2.2.1 PLAFOM

The planktonic foraminifera model PLAFOM developed by *Fraille et al.* (2008) predicts the global monthly surface concentration (in mmol C/m^3) of five planktonic foraminifera species, which are considered representative for a large portion of the foraminifera biomass in the surface ocean. The species have been selected on the basis of the traditional morphological taxonomy as an evaluation relies on the comparison with fossils, in which cryptic species cannot be detected. Therefore, the chosen species may represent artificial units, encompassing multiple genetically distinct species (*Kucera and Darling, 2002*). Also, the taxonomy of planktonic foraminifera is not always entirely consistent and the same species have been recorded under different names. It is therefore important to discuss the biological validity of the included species in the studied region and to clarify the taxonomy that was used to compare model output with fossil data.

Of the five species considered, the polar species *Neogloboquadrina pachyderma* is supplemented by the subpolar *N. incompta* (in the sense of *Darling et al.* (2006)) and *Globigerina bulloides* and the warm water species *Globigerinoides sacculifer* and *Globigerinoides ruber* (white). Among these, *G. sacculifer* is genetically homogeneous worldwide (*André et al., 2013*) and the empirical calibration of the model, which is based on global data, is therefore entirely appropriate. The species *G. ruber* (white) consists of up to five distinct genetic types belonging to two lineages (*Aurahs et al., 2009*). It has not yet been established to what degree the habitat of these genetic types differs, but they seem to occur globally and include a distinct morphotype corresponding to the concept of a different species (*G. elongatus; Aurahs et al.* (2011)). It is therefore possible that the calibration of this species is affected by the presence of different genetic types, which may lead to a poor fit between model and data. Fortunately, *G. ruber* (white) is rare in the focal area of this study in the North Atlantic (north of 30°N) and an accurate prediction of its abundance is only relevant at the northernmost edge of its distribution, which is more likely to be inhabited by fewer genetic types. *G. bulloides* in the North Atlantic includes at least three genetic types, which are very likely to possess different ecological preferences (*Kucera and Darling, 2002; Darling and Wade, 2008*), and the parameterization of the species in PLAFOM thus represents an artificial category. *N. incompta* is known to encompass only two genetic lineages, of which only one occurs throughout the Atlantic (*Darling et al., 2006*). This means that the parameterization of this species is more realistic, and any bias resulting from the lumping of these two lineages will affect the Atlantic results in the same way (i.e., it cannot account for spatial patterns in the model-data comparison). Most importantly, *Darling et al.* (2004, 2007) have shown that the entire North Atlantic and Arctic Ocean are inhabited by a single genetic type of *N. pachyderma*, which is thus likely to share the same ecological preferences throughout the region. This means that although the calibration of the model for this species may be biased by observations of other genetic types in the Southern Ocean, the model performance in the North Atlantic should be consistent and patterns in the data-model mismatch cannot be explained by the occurrence of different genetic lineages of the species.

The planktonic foraminifera model is mainly driven by sea surface temperature and food availability, including zooplankton, small phytoplankton, diatoms, and organic detritus. Species specific food preferences and temperature tolerance limits have been derived from both sediment trap data and culturing experiments (e.g., *Hemleben et al., 1989; Bijma et al., 1990a; Watkins et al., 1996; Watkins and Mix, 1998; Arnold and Parker, 1999; Žarić et al., 2005*). Variations in the foraminifera concentration are determined by the growth

and mortality rates of the population as follows:

$$\frac{dF}{dt} = (\text{GGE} \cdot \text{TG}) - \text{ML} \quad (2.1)$$

where F is the foraminifera carbon concentration, GGE (gross growth efficiency) is the portion of grazed matter that is incorporated into foraminiferal biomass, TG denotes total grazing, and ML represents mass loss. The total grazing is determined by food availability and temperature sensitivity of the foraminiferal species. The mass loss (mortality) depends on the natural death rate (respiration loss), predation by higher trophic levels, and competition. Compared to *Fraile et al.* (2008), we modified the parameterizations of the foraminiferal species concentration to optimize the agreement between model and species distribution from core tops and sediment trap data. We adjusted the free parameters in the competition terms of *G. ruber* (white) and *G. sacculifer* (for details see the Appendix). These modifications resulted in a reduction of the global root-mean-square error (RMSE) between the modeled annual mean and core-top relative abundances of the species under consideration by 2 to 5% compared to *Fraile et al.* (2008).

PLAFOM is run within an ecosystem model for the global surface ocean (*Moore et al.*, 2002a), which provides information on the food availability for the foraminiferal species. Initially, the model is spun-up for 2 years, to allow an equilibrium state to be reached (*Moore et al.*, 2002a). Afterward, the output from a third year is saved with monthly resolution. The longitudinal resolution amounts to 3.6° and the latitudinal resolution varies between 1° and 2° , with a higher resolution near the equator. A detailed description of the foraminiferal model and its behavior in the global domain is given in *Fraile et al.* (2008).

2.2.2 Model Experiments

To compare the behavior of *N. pachyderma* during glacial-interglacial periods, we performed three experiments with different environmental conditions: The control run was forced with modern (i.e., preindustrial) conditions, and the second and third runs with conditions concerning H1 and LGM, respectively. The ecosystem/foraminifera model is driven by global monthly estimates of a number of forcing parameters. Furthermore, the model equations are solved using a fifth-order Runge-Kutta method with an adaptive time step. The interpolation is performed in regular intervals resulting in monthly output.

In the control run, the model forcing includes sea surface temperature (from the World Ocean Atlas 1998) (*Conkright et al.*, 1999), surface shortwave radiation (*Bishop and Rossow*, 1991; *Rossow and Schiffer*, 1991), mixed layer depth (*Monterey and Levitus*, 1997), vertical velocity at the base of the mixed layer (from the NCAR-3D ocean model) (*Gent et al.*, 1998), constant turbulent mixing at the base of the mixed layer (0.15 m/d), percent sea ice cover (from the National Snow and Ice Data Center) (see *Moore et al.* (2002a) for details), and atmospheric iron flux (*Mahowald et al.*, 1999).

For the H1 and LGM runs we used climate simulations of *Merkel et al.* (2010) to force the foraminifera model with SST, mixed layer depth, surface shortwave radiation, sea ice fraction, and vertical velocity at the base of the mixed layer. *Merkel et al.* (2010) conducted a LGM simulation following the second phase of the Paleoclimate Modeling Intercomparison Project 2 (*Braconnot et al.*, 2007a,b) and an idealized Heinrich experiment initialized from the LGM boundary conditions with an additional freshwater anomaly of 0.2 Sv homogeneously distributed over the Nordic (Greenland, Iceland, and Norwegian) Seas (north of 65°N). The experiments have been performed with the global coupled Community Climate System Model

version 3 (CCSM3) (Collins *et al.*, 2006; Yeager *et al.*, 2006). Additionally, we used atmospheric iron fluxes of the LGM from Mahowald *et al.* (1999) as forcing for both our H1 and LGM simulations assuming that the dust deposition flux from the atmosphere has not changed considerably from the LGM to H1. In order to circumvent artificial effects caused by differences between modern boundary conditions used in the ecosystem model (largely observations) and the climate model, we used the same approach as Fraile *et al.* (2009b) and calculated anomalies of the modeled climatological forcing (i.e., for H1 and LGM with respect to preindustrial conditions). The respective anomalies were then added to the modern forcing of the ecosystem/foraminifera model.

2.2.3 Sediment Samples

To assess the ability of PLAFOM to reproduce the spatial pattern of variability of *N. pachyderma* in the North Atlantic during interglacial-glacial periods, model predictions (we refer here to the annual mean) were compared with fossil data. To this end, the five species modeled by PLAFOM have been aligned with the taxonomic concepts used for fossil planktonic foraminifera. Thus, until the publication of Darling *et al.* (2006), *N. pachyderma* has been referred to as *N. pachyderma* (sin.), whereas the species *N. incompta* corresponds to *N. pachyderma* (dex.). Following the arguments in Kucera *et al.* (2005), the fossil concept of *N. incompta* also includes specimens identified as the so called “pachyderma-dutertrei intergrade”. The concepts of *G. bulloides* and *G. ruber* (white) have typically been used consistently in the North Atlantic. In *G. sacculifer*, the form without a sac-like last chamber has often been referred to as *Globigerinoides trilobus*. In this study, both the model parameterization and the data-model comparison refer to the sum of specimens with and without the sac-like final chamber, consistent with the genetic results by André *et al.* (2013).

For modern conditions we used core-top data assembled by the MARGO project (Kucera *et al.*, 2005). For the LGM we used planktonic foraminiferal census data from the MARGO LGM data set (Kucera *et al.*, 2005). In order to compare our model data with observational records for H1, we produced a new compilation of planktonic foraminiferal abundances of the five species under consideration (see supporting information).

First, the PANGAEA database (www.pangaea.de) was searched to identify sediment cores from the MARGO LGM compilation with planktonic foraminiferal counts that appear to include samples from H1. The search was then extended by publications addressing the last glacial period with a particular focus on both the last 30,000 years (ka) and paleoceanographic reconstructions based on planktonic foraminifera (e.g., Mix and Ruddiman, 1985; Hayes *et al.*, 1999, 2005; Vogelsang *et al.*, 2001; Weinelt *et al.*, 2003; Eynaud *et al.*, 2009; Telford *et al.*, 2013). Finally, the PANGAEA database was searched for all sediment core records in the North Atlantic containing counts of *N. pachyderma*. Then, cores where the counts were based on an inappropriate size fraction (other than $> 150 \mu\text{m}$) were removed, as well as cores where not all species were counted (i.e., the relative abundance of *N. pachyderma* is available in these cores, but is related to all other species, not just the five species used in PLAFOM). The remaining cores were checked for their age models. Cores without accelerator mass spectrometry ^{14}C dating or conventional ^{14}C dating (based on the coarse-grained carbonate fraction) or cores with only one date in the top 30 ka have been removed. To be consistent with the majority of the included paleoceanographic studies in which a reservoir age of 400 years is assumed (e.g., Bard, 1988; Sarnthein *et al.*, 1995; Bauch *et al.*, 2001; Voelker *et al.*, 2009; Salgueiro *et al.*, 2010), all radiocarbon ages of the remaining cores have also been corrected for a marine reservoir

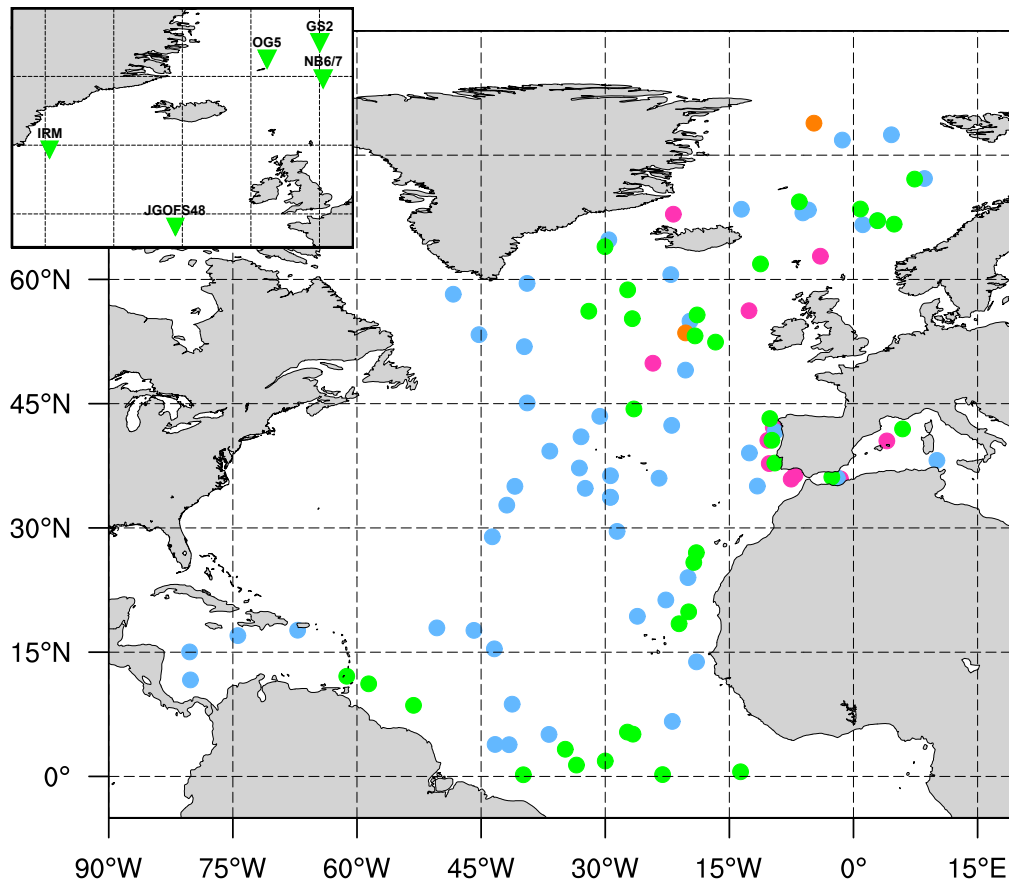


Figure 2.1: Locations of fossil data with planktonic foraminifera counts for Heinrich Stadial 1 (H1): Cores used for H1 compilation (solid green circles), cores with insufficient dating (solid light blue circles), cores with inconsistent counts (solid pink circles), and cores with smaller size fractions (solid orange circles). The insert shows the locations of the sediment traps (GS2, OG5, NB6/7, IRM, and JGOFS48) discussed in section 2.2.5. For more details see Tables 2.1 and 2.2 as well as the supporting information.

age of 400 years. However, we are aware that reservoir ages might have been considerably higher during H1, especially in the North Atlantic (*Waelbroeck et al., 2001; Sarnthein et al., 2007*) due to temporal and spatial variations in the atmospheric ^{14}C production and ocean circulation (*Franke et al., 2008*). Finally, the corrected ^{14}C ages have been converted to calendar ages by using INTCAL13 (*Reimer et al., 2013*). In total, we selected 34 sediment cores (Figure 2.1 and Table 2.1) to perform a comparative analysis of the distribution of *N. pachyderma* in the North Atlantic during H1.

To this end, we identified the interval of H1 in each core as the time slice between 15 and 18 cal. ka B.P. (cf. *Bard et al., 2000; Sarnthein et al., 2001; Kienast et al., 2013*), and determined the respective depth intervals (see supporting information) and collected and averaged the faunal records for this interval in each of the included cores.

2.2.4 Scaling of PLAFOM Output to Observed Relative Abundances of Individuals

To perform a comparative analysis, the relative abundances of the planktonic foraminifera species in fossil assemblages have been recalculated taking only those five foraminiferal species into consideration that are used by PLAFOM. Since PLAFOM calculates foraminiferal concentrations via carbon biomass ($\text{mmol C}/\text{m}^3$) modeled annual mean relative abundances (% biomass) were converted to annual mean relative abundances

Table 2.1: Core Locations and Information on Source Data^a

Core	Latitude (°N)	Longitude (°E)	Water Depth (m)	Faunal Data ^b	Age Model
GIK17730-4	72.11	7.39	2749	Schulz (1995)	Vogelsang et al. (2001) ^c
PS1243-1	69.40	-6.55	2711	related to Kandiano (2003)	Bauch et al. (2001); Kandiano (2003) ^d
GIK23065-2	68.50	0.83	2804	Schulz (1995)	Vogelsang (1990) ^c
GIK23071-3	67.09	2.91	1308	Schulz (1995)	Vogelsang (1990) ^c
GIK23074-1	66.67	4.91	1157	related to Dreger (1999); Voelker (1999)	Vogelsang (1990); Voelker (1999) ^c
L-348	63.95	-30.03	2262	Barash and Yushina (1999)	Barash and Yushina (1999) ^c
GIK16396-1	61.87	-11.24	1145	related to Dreger (1999); Voelker (1999)	Weinelt et al. (2003) ^c
MK-316	58.74	-27.29	2155	Barash and Yushina (1999)	Barash and Yushina (1999) ^c
GIK17051-3	56.16	-31.99	2295	Schulz (1995)	Vogelsang et al. (2001) ^c
L-198	55.71	-18.90	1265	Barash and Yushina (1999)	Barash and Yushina (1999) ^c
GIK17049-6	55.26	-26.73	3331	Schulz (1995)	Jung (1996); Vogelsang et al. (2001) ^c
GIK23415-9	53.18	-19.15	2472	related to Dreger (1999); Voelker (1999)	Weinelt et al. (2003) ^c
GIK17045-3	52.43	-16.67	3663	Schulz (1995)	Vogelsang et al. (2001) ^c
GIK15612-2	44.36	-26.54	3050	Kiefer (1998)	Kiefer (1998) ^c
SU92-03	43.20	-10.11	3005	Salgueiro et al. (2010)	Salgueiro et al. (2010) ^e
MD81-BC15	41.95	5.93	2500	related to Zachariasse et al. (1997)	Hayes et al. (1999) ^c
MD95-2040	40.58	-9.86	2465	de Abreu et al. (2003)	Schönfeld et al. (2003) ^c
MD95-2041	37.83	-9.51	1123	Voelker and de Abreu (2011)	Voelker et al. (2009) ^e
MD95-2043	36.14	-2.62	1841	Pérez-Folgado et al. (2003)	Cacho et al. (1999) ^c
GIK15637	27.01	-18.99	3849	Kiefer (1998)	Kiefer (1998) ^c
A180-39	25.83	-19.30	3470	related to CLIMAP Project Members (1981)	CLIMAP Project Members (1976) ^c
V30-51	19.87	-19.92	3409	related to Mix (1986)	Mix and Ruddiman (1985) ^c
V30-49	18.43	-21.08	3093	related to Mix (1986)	Mix and Ruddiman (1985) ^c
M35003-4	12.09	-61.24	1299	related to Hüls (2000)	Hüls and Zahn (2000) ^c
RC09-49	11.18	-58.59	1851	related to Mix (1986)	Mix and Ruddiman (1985) ^c
V25-75	8.58	-53.17	2743	related to Mix (1986)	Mix and Ruddiman (1985) ^c
V30-36	5.35	-27.32	4245	related to Mix (1986)	Mix and Ruddiman (1985) ^c
V27-178	5.10	-26.65	4327	related to CLIMAP Project Members (1981)	CLIMAP Project Members (1976) ^c
V25-60	3.28	-34.83	3749	related to Mix (1986)	Mix and Ruddiman (1985) ^c
RC13-189	1.86	-30.00	3233	related to Mix (1986)	Mix and Ruddiman (1985) ^c
V25-59	1.37	-33.48	3824	related to Mix (1986)	Mix and Ruddiman (1985) ^c
RC24-1	0.56	-13.65	3850	related to Mix (1986)	Mix and Ruddiman (1985) ^c
V30-41	0.22	-23.07	3874	related to Mix (1986)	Mix and Ruddiman (1985) ^c
V15-168	0.20	-39.90	4219	related to Mix (1986)	Mix and Ruddiman (1985) ^c

^a Sources of both used age models and planktonic foraminifera census data.

^b Data sets with distributions of planktonic foraminifera species in sediment cores are available online (www.pangaea.de).

^c Age calibration performed with INTCAL13 (Reimer et al., 2013).

^d Age calibration after Stuiver and Reimer (1993).

^e Age calibration performed with INTCAL04 (Reimer et al., 2004). The age difference to a calibration performed with INTCAL13 amounts to ~ 200 – 300 cal. years.

of the number of specimens (% individuals) accounting for the differences in weight and size and thus age (i.e., adults versus juveniles) of each species. For this conversion, the predicted mass flux-based annual mean relative abundance of *N. pachyderma* was scaled to the relative abundance of individuals using a logistic function. In total, we used 843 sediment cores (compiled by the MARGO project) (Kucera et al., 2005) distributed across the North Atlantic to perform a robust comparative analysis between modeled annual

mean relative abundances and core-top data.

Considering modern conditions in the North Atlantic a sinusoidal rather than linear relationship exists between the modeled (i.e., based on biomass) annual mean and core-top relative abundances of *N. pachyderma* (Figure 2.2a).

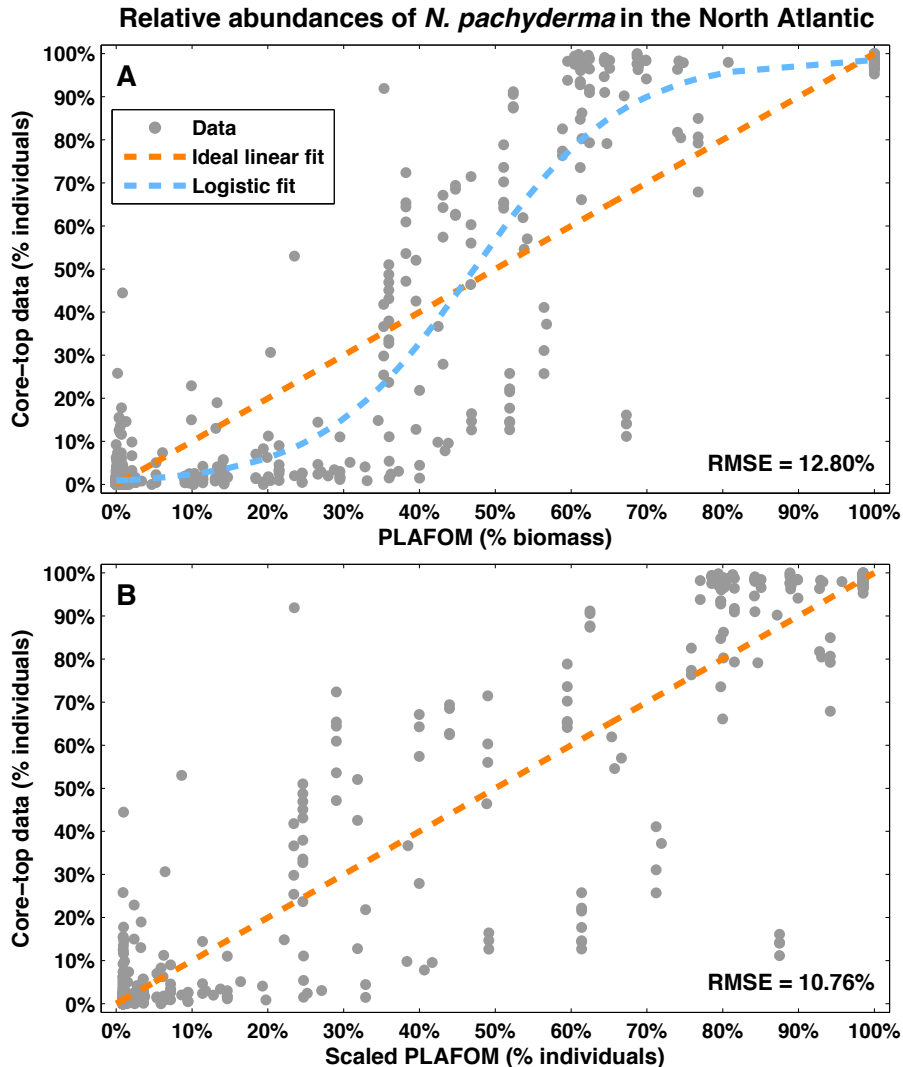


Figure 2.2: Relative abundances of *N. pachyderma* for (a) core-top data (% individuals) versus PLAFOM (% biomass) and (b) core-top data (% individuals) versus scaled PLAFOM (% individuals). For the comparison we used modeled annual mean relative abundances. The dashed orange lines in each panel indicate the ideal linear fit (line of equality) between core-top and model data. The light blue dashed line in Figure 2.2a represents the logistic fit given by equation (2.2). The respective root-mean-square errors between the core-top and modeled annual mean relative abundances are denoted by RMSE. For the underlying analysis we compared 843 sediment cores distributed over the entire North Atlantic with the equivalent model data for modern conditions.

For low relative abundances ($< 30\%$) in the observational records PLAFOM has the tendency to overestimate the relative abundance of *N. pachyderma*, whereas for high relative abundances ($> 70\%$) PLAFOM features an underestimation. This systematic bias arises from variations especially in size among the species being considered in PLAFOM. Additionally, PLAFOM predicts planktonic foraminiferal concentrations of only five species for the global domain, such that in the model parameterizations different genetic lineages of the species are considered, which are actually absent in the North Atlantic, whereas some North Atlantic species are ignored by the model (cf., Kucera, 2007; Fraile et al., 2008). These discrepancies collectively result in

an offset between modeled and observed relative abundances of *N. pachyderma*.

Here we corrected this offset by applying a logistic fit (equation 2.2):

$$f(x) = \frac{f_{\text{inf}}}{1 + \exp(-\alpha \cdot (x - x_{1/2}))} \quad (2.2)$$

with x being the annual mean relative abundance of *N. pachyderma*, $f_{\text{inf}} = 99\%$ (value as $x \rightarrow \infty$), $\alpha = 0.1$ (decay constant), and $x_{1/2} = 47\%$ (symmetric inflection point). Using equation (2.2) leads to a better agreement between PLAFOM and the observations from surface sediments for lower ($< 20\%$) and higher ($> 80\%$) relative abundances (Figure 2.2b). The deviations for intermediate relative abundances most likely arise due to the model parameterizations encompassing only five planktonic foraminifera species.

To perform intercomparison studies among different time slices we decided to use the same model parameterizations for the foraminiferal species concentration developed by *Fraile et al.* (2008) and further adjusted in this study (cf. section 2.2.1 and the Appendix) to predict the abundances of the five species considered in PLAFOM for H1 and the LGM. The foraminifera model has been calibrated based on global core-top planktonic foraminiferal counts (*Fraile et al.*, 2008). It was shown by *Fraile et al.* (2008) (refer to Figures 2–6 therein) that PLAFOM reproduces in the annual mean the global distributions of the five planktonic foraminiferal species under consideration for modern conditions relatively well with RMSEs $\leq 25\%$. To assess the deviation between the observed and predicted (we refer here to the annual mean) planktonic foraminiferal distributions, we calculated the root-mean-square error. For this, we applied the same approach as *Fraile et al.* (2008) and compared the data of each sediment sample with the nearest model grid point. This analysis was performed for each time slice separately.

2.2.5 Model Validation: Modeled Seasonal Patterns Versus Observations

To test whether our model matches the present-day seasonal production pattern in the North Atlantic, we compared the modeled distribution for modern conditions with observational data from five sites with sediment traps (Figure 2.3 and Table 2.2). Here we followed the same approach as *Jonkers and Kučera* (2015) and plotted fluxes for multiple years from each location on a \log_{10} scale against day of year, while replacing zero fluxes with half of the observed minimum flux (Figure 2.3). This conversion allows a direct comparison of the dominant timing of the observed maximum flux at a given site with the model, which is driven by long-term climatological means. Furthermore, we assume that the shell flux through the water column is proportional to the surface concentrations.

In the Nordic Seas (sites GS2, OG5, and NB6/7) the peak flux of *N. pachyderma* and *N. incompta* occurs in the second half of a year. The predicted seasonal flux is more focused, but the timing of the seasonal maximum is in good agreement with the observations (Figures 2.3a–2.3d). The flux patterns in the Irminger Sea and eastern North Atlantic (sites IRM and JGOFS48) show two flux maxima per year: one during late spring and a second smaller maximum during early fall. PLAFOM does not capture such a bimodal pattern, but the timing of the predicted productivity maximum corresponds with one of the two observed peak seasons (Figures 2.3e–2.3h). The reason why the modeled flux fails to reproduce the observed pattern with two seasonal peaks is likely to be sought in the climatological forcing. This long-term average in the forcing variables removes the interannual and multiannual variability which is still present in the observational data

Table 2.2: Information on Sediment Trap Data^a

Site ^b	Latitude (°N)	Longitude (°E)	Water Depth (m)	Trap Depth (m)	Deployment Time ^c	Duration (days)	Species ^d	Fraction (μm)	Source
GS2	75.0	0.0	3720	300	06/03/1994 to 05/11/1995	342	<i>N. pachyderma</i>	63-500	<i>Jensen (1998)</i>
OG5	72.4	-7.7	2624	500	08/06/1991 to 07/10/1992	339	<i>N. pachyderma</i>	63-500	<i>Jensen (1998)</i>
NB6/7	69.7	0.5	3273	500	08/06/1991 to 10/02/1993	780	<i>N. pachyderma</i> , <i>N. incompta</i>	63-500	<i>Jensen (1998)</i>
IRM	59.3	-39.4	2750	na ^e	08/31/2003 to 06/04/2007	988	<i>N. pachyderma</i> , <i>G. bulloides</i>	150-315	<i>Jonkers et al.</i> (2010, 2013)
JGOFS48	48.0	-21.0	na ^e	2000-3700	04/03/1989 to 04/16/1990	378	<i>N. incompta</i> , <i>G. bulloides</i>	>150	<i>Wolfteich (1994)</i>

^a Details of shell flux time series of settling planktonic foraminiferal assemblages. Data series are shown in Figure 2.3.

^b The location of each site is shown in Figure 2.1.

^c Dates are formatted as month/day/year.

^d Planktonic foraminiferal species considered in this study.

^e na, not available (i.e., not given in data set).

(although not shown in Figure 2.3). Furthermore, it is known that the timing of the peak season(s) of temperate and cold water species of planktonic foraminifera in the North Atlantic is linked to the timing of phytoplankton blooms and hence food supply (e.g., *Fairbanks and Wiebe, 1980; Wolfteich, 1994; Kohfeld et al., 1996; Jonkers and Kučera, 2015*). Phytoplankton phenology features a latitudinal pattern with a single spring bloom in the polar and subpolar Atlantic, a bimodal cycle (i.e., one large peak in spring and a smaller one in fall) in the temperate North Atlantic ($\sim 40 - 60^\circ\text{N}$), a single fall/winter bloom in the subtropical Atlantic, and no predominant seasonal peak in the tropical Atlantic (e.g., *Colebrook, 1979, 1982; Parsons et al., 1984; Taboada and Anadón, 2014*). Although the ecosystem model is able to capture the seasonal cycle of phytoplankton across most of the (North) Atlantic (cf. Figure 4 in *Moore et al., 2002a*) the bimodal pattern characteristic for the temperate North Atlantic is not fully resolved. This leads to a discrepancy between the modeled and observed seasonal patterns in planktonic foraminifera shown in Figure 2.3. It is nonetheless encouraging that the model appears to capture the timing of the peaks in the North Atlantic and also reproduces the general shift in peak season between the Nordic Seas and the more southerly locations (Figure 2.3).

2.3 Results

2.3.1 Relative Abundances of *N. pachyderma*

In general, the model results are in good agreement with the observational records. Among the three time slices the RMSE for the whole North Atlantic Ocean varies between ~ 11 and $\sim 17\%$. Although the error is larger for H1 ($\sim 14\%$) and LGM ($\sim 17\%$), it is of the same order of magnitude as the modern one ($\sim 11\%$).

During H1 the highest (up to 100%) modeled annual mean relative abundances (here given in % individuals after applying equation (2.2) for the conversion) of *N. pachyderma* in the North Atlantic Ocean are found in polar and subpolar surface waters (Figure 2.4a). Toward the south the occurrence of *N. pachyderma* reduces gradually. This species is, however, present as far south as $\sim 36^\circ\text{N}$ along the Iberian margin.

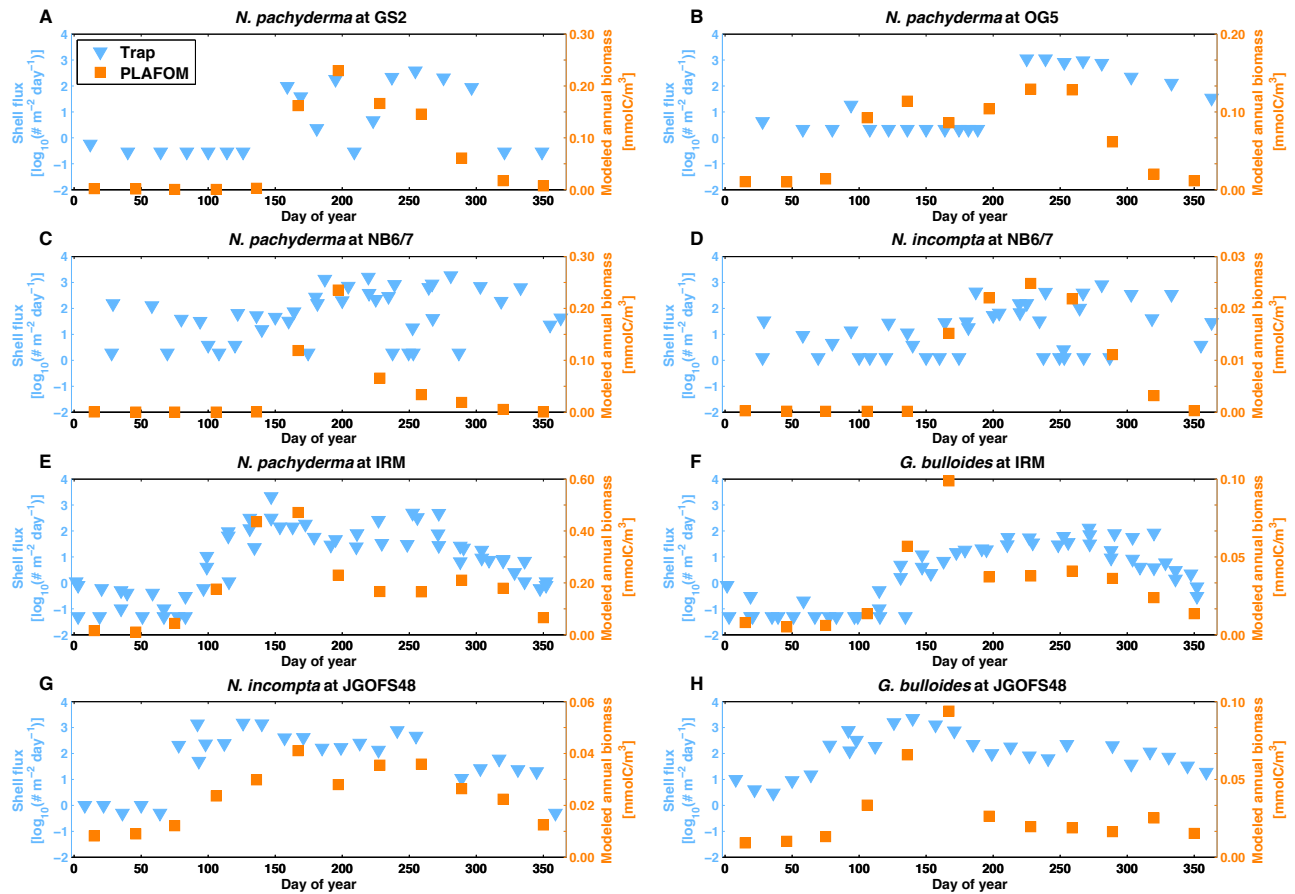


Figure 2.3: Comparison of export planktonic foraminiferal shell flux in sediment traps (light blue triangles) with modeled annual biomass for modern conditions (orange squares). Note that the difference in the units between sediment trap data [$\log_{10}(\# \text{ m}^{-2} \text{ day}^{-1})$] and model output (mmolC/m^3) does not affect the assessment of the peak timing. Data series of *N. pachyderma* at sites (a) GS2, (b) OG5, (c) NB6/7, and (e) IRM. Data series of *N. incompta* at sites (d) NB6/7 and (g) JGOFS48. Data series of *G. bulloides* at sites (f) IRM and (h) JGOFS48. The respective locations of each sediment trap are given in Table 2.2 and shown in Figure 2.1.

In comparison with modern (Figure 2.4b) and LGM (Figure 2.4c) conditions, the modeled mean annual range of *N. pachyderma* has expanded southward during H1. In particular, its annual mean distribution in the eastern North Atlantic reaches all the way along the Iberian margin. In the western basin of the North Atlantic the differences, especially between LGM and H1, are less pronounced.

2.3.2 Seasonality of *N. pachyderma*

During modern conditions the highest modeled flux of *N. pachyderma* throughout the North Atlantic occurs during spring from May to June (Figure 2.5a) which is supported by observations based on plankton tows and/or sediment traps (e.g., Tolderlund and Bé, 1971; Jonkers et al., 2010). In contrast, during H1 the modeled maximum production occurs more often throughout boreal summer (Figure 2.5b), whereas during the LGM maximum production is reached during late spring/early summer in PLAFOM (Figure 2.5c). As a result, the seasonal production maximum is shifted for H1 and LGM relative to modern conditions by 1–5 months in large parts of the North Atlantic (cf. Figures 2.5d and 2.5e). Here the maximum production occurs predominantly later in the year during the considered glacial times compared to modern conditions resulting in a seasonal shift.

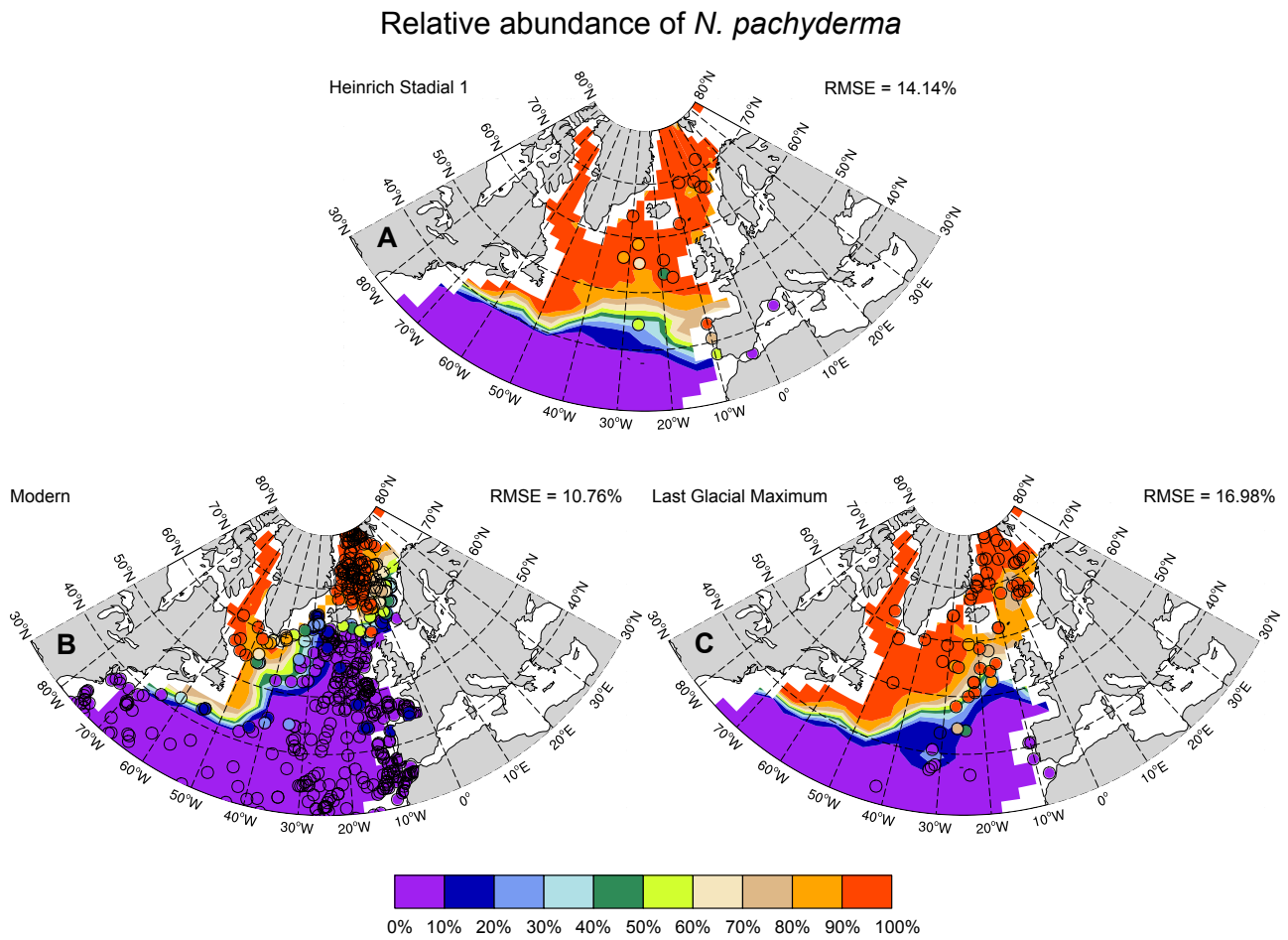


Figure 2.4: Relative abundances (% individuals) of *N. pachyderma* predicted by PLAFOM (contours) and from fossil data (circles) for (a) Heinrich Stadial 1, (b) modern conditions, and (c) the Last Glacial Maximum. The relative abundances consider only the five foraminiferal species included in PLAFOM. The contours represent annual mean values. The respective root-mean-square error is denoted by RMSE and calculated for the entire North Atlantic.

According to the model, maximum production is shifted by 1–2 months between H1 and the LGM for most of the North Atlantic (Figure 2.5f), leading to a clear seasonal bias. This bias is largest northeast of Newfoundland between 30° and 45°W, where the maximum in production occurs up to 6 months later during H1 relative to the LGM. Here H1 is characterized by a maximum flux in late summer/fall, whereas during the LGM the maximum production occurs as early as in March.

2.4 Discussion

2.4.1 Glacial Range Expansion of *N. pachyderma*

In line with the fossil record, the mean annual range of *N. pachyderma* predicted by PLAFOM expanded southward during the last glacial period. In response to cold water masses reaching up to 40°N (Sarnthein *et al.*, 1995, 2003; Pflaumann *et al.*, 2003; Kucera *et al.*, 2005; Eynaud *et al.*, 2009), *N. pachyderma* is predicted to dominate foraminifera assemblages during H1 and LGM as far south as the Iberian margin (Figure 2.4). Although the coverage of the validation data is less comprehensive than modern observations, the fossil data of both H1 and LGM compare favorably with the model predictions with RMSEs being in the

N. pachyderma (Figure 2.4b).

During glacial periods (here H1 and LGM) cold surface conditions (with SST < 10 °C) prevailed in the northeastern Atlantic (Sarnthein *et al.*, 1995; Pflaumann *et al.*, 2003), leading to a high relative abundance (> 80%) of *N. pachyderma* up to ~ 50 °N. However, during H1 this species is found as far south as ~ 36 °N and was even present to a small extent in sediment cores of the Mediterranean (cf. Figure 2.1) (Hayes *et al.*, 1999, 2005). The relatively high modeled and observed abundance of *N. pachyderma* (20–70%) along the Iberian margin indicates a penetration of polar surface waters at lower latitudes. This behavior is in agreement with previously published results of Eynaud *et al.* (2009). Based on the abundance of *N. pachyderma*, Eynaud *et al.* (2009) showed that during Heinrich Stadials 1 and 4 the Polar front shifted southward close to 42 °N and was present along the Iberian margin, suggesting a far southward penetration of polar surface waters.

Our results further support the findings of, e.g., Bard *et al.* (2000), de Abreu *et al.* (2003), and Eynaud *et al.* (2009) that the LGM was characterized by warmer surface waters along the Iberian margin as the modeled and observed percentages of *N. pachyderma* are less than 10% (Figure 2.4c). Previous studies provide evidence of warm, nearshore surface waters along the eastern North Atlantic during the LGM, indicating that the Polar front is absent along the Iberian margin and is located farther northward around 50 °N (cf., Eynaud *et al.*, 2009).

Based on the existing observational records it is evident that changes in the SST from LGM to H1 to modern conditions most likely led to the change in the distribution of *N. pachyderma*. This is also true for our model results. The shift in the modeled annual mean abundance pattern of *N. pachyderma* (Figure 2.4) is mainly controlled by the SST forcing (cf. Figure S2.1 in the supporting information). In the eastern subpolar North Atlantic the annual mean SST shows more distinct differences compared to the western North Atlantic between the investigated time slices (Figure S2.1). For instance, the +10 °C mean annual isotherm was shifted southward during the last glacial period (i.e., toward ~ 50 °N during the LGM and toward ~ 40 °N during H1) compared to modern conditions, where this isotherm is located around 60 °N in the eastern subpolar North Atlantic (Figure S2.1). This latitudinal shift in the annual mean SST is the main driving force for the simulated changes in the distributional pattern of *N. pachyderma*.

In summary, the change in the range seen in the paleoceanographic reconstructions is faithfully reproduced by our model (Figure 2.4). Hence, we can use PLAFOM to study the possible cause of the shift in maximum production of *N. pachyderma*.

2.4.2 The Seasonality of *N. pachyderma*

In general, it seems plausible that a shift by a few months in the phenology of *N. pachyderma* is caused by changing environmental conditions (e.g., SST and/or sea ice cover) from the LGM to H1.

To test the robustness of the model performance and to investigate in detail the cause(s) of the clear seasonal shift in phenology, we focus our analysis on the region with the largest magnitude of change. Therefore, we exemplarily chose three areas in the western North Atlantic enclosing the region where the most distinct difference in the modeled maximum production of *N. pachyderma* between H1 and LGM appeared (see Figure 2.5f).

Mackas et al. (2012) suggested that zooplankton phenology is primarily controlled by temperature. Several other studies (e.g., *Hemleben et al.*, 1989; *Wolfteich*, 1994; *Jonkers et al.*, 2010, 2013; *Jonkers and Kučera*, 2015), however, considered mixed layer depth, light, food, and nutrient availability as key parameters influencing the phenology of planktonic foraminifera. In high latitudes, seasonal changes in temperature are highly collinear with most of the other parameters, making it hard to resolve the direct forcing. Nevertheless, a meta-analysis by *Jonkers and Kučera* (2015) revealed that the trigger for annual peaks in temperate and cold water species of planktonic foraminifera is unlikely to be linked to temperature as such, because they occur at different locations irrespective of the ambient temperature. Instead, peak fluxes of *N. pachyderma* appear to be associated with the timing of the seasonal phytoplankton bloom events resulting in an increased food supply (e.g., *Fairbanks and Wiebe*, 1980; *Wolfteich*, 1994; *Kohfeld et al.*, 1996; *Jonkers and Kučera*, 2015). A relationship between the seasonal flux of this species and the seasonal distribution of phytoplankton is also implied in our model results. During H1 and LGM a unimodal pattern in the modeled flux of *N. pachyderma* can be observed in the western North Atlantic (Figure 2.6), which we will in the following mainly attribute to sea ice cover, food availability, and only in a broader sense to temperature, which indirectly affects primary production.

The farther south, the earlier the seasonal peak in *N. pachyderma* production occurs during H1. We attribute this effect to an earlier reduction in sea ice cover facilitating an earlier phytoplankton bloom. The large differences in sea ice cover between H1 and LGM (Figure 2.6b) are most likely the main cause for the clear shift in the modeled maximum production peak of *N. pachyderma* between H1 and LGM in the western North Atlantic (Figures 2.5f and 2.6a).

During the LGM the modeled sea ice cover remained relatively constant at rather low values (0 – 30%) for all the three chosen regions, whereas H1 is characterized by a strong seasonal cycle in sea ice fraction with higher values (up to 90%) in the winter months and a low sea ice cover during boreal summer (Figure 2.6b). The low persisting sea ice concentrations for the three exemplarily chosen areas during the LGM are consistent with the findings of *de Vernal et al.* (2000, 2005) and *Sarnthein et al.* (2003). Based on foraminiferal paleotemperature estimates (*Sarnthein et al.*, 2003) and/or dinocyst assemblages (*de Vernal et al.*, 2000, 2005), LGM sea ice extent has been reconstructed, showing that ice-free (sea ice cover < 50%) conditions prevailed throughout the year in the subpolar gyre south of 50°N and east of 45°W. In contrast, *Hillaire-Marcel and de Vernal* (2008) argue that during Heinrich stadials (especially H1) the sea ice cover was more extensive resulting in light $\delta^{18}\text{O}$ values recorded in *N. pachyderma* most likely due to the production of isotopically light brines during the sea ice formation. The simulated sea ice cover (used as forcing for our model) also shows a more extensive and widespread distribution over the North Atlantic during H1 compared to the LGM, which supports the findings of *Hillaire-Marcel and de Vernal* (2008). However, the resulting change in the $\delta^{18}\text{O}$ values of *N. pachyderma* would have the same sign when considering brine rejection from sea ice formation processes.

As primary productivity is decisively influenced by sea ice (e.g., *Arrigo et al.*, 2008; *Arrigo and van Dijken*, 2011; *Leu et al.*, 2011), the predicted diatom bloom occurs later during the year during H1 (Figure 2.6c) because of a higher, prolonged sea ice concentration and hence a lower assumed light transmittance compared to the LGM. This induces a shift in the modeled maximum production peak of *N. pachyderma* from LGM to H1 in Regions 1 and 2 (Figure 2.6a). Diatoms are most abundant in cold and nutrient-rich environments (*Smetacek*, 1985; *Crosta and Koç*, 2007), and their population increases with increasing light availability if sufficient amounts of nutrients are present (*Smetacek*, 1985; *Anderson*, 2000; *Arrigo et al.*, 2012). The

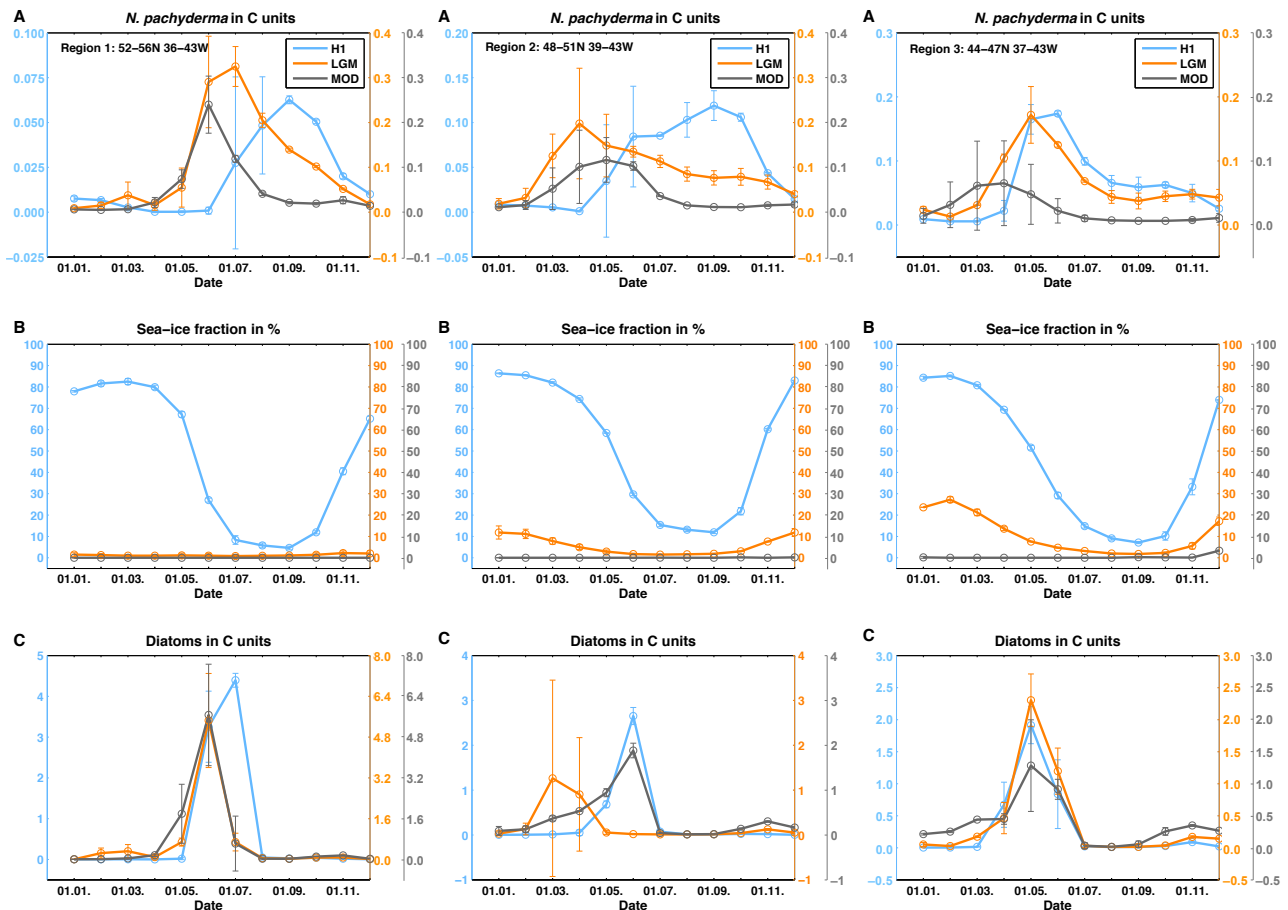


Figure 2.6: (a) Modeled annual biomass (mmol C/m^3) variation of *N. pachyderma*, (b) variation in modeled sea ice fraction (%), (c) modeled annual biomass (mmol C/m^3) variation of diatoms for modern conditions (MOD, grey), Heinrich Stadial 1 (H1, light blue), and the Last Glacial Maximum (LGM, orange). For comparison, we chose the following regions: 52 – 56°N, 36 – 43°W (left column); 48 – 51°N, 39 – 43°W (middle column); and 44 – 47°N, 37 – 43°W (right column) (see Figure 2.5f). The error bars indicate the standard deviations for the respective box averages. Note the partly different axis scaling.

rather late predicted peak in *N. pachyderma* in boreal summer during the LGM and H1 is due to the late (in comparison with present day) occurring diatom bloom (based on our model simulation) caused by the prevailing climate conditions influencing the nutrient concentrations. In general, a diatom peak is followed by a peak in the biomass of *N. pachyderma* which is also evident in our model results (see Figure 2.6). This is supported by the synthesis of *Jonkers and Kučera* (2015), in which they showed (based on sediment trap data) that the timing of primary productivity serves as a predictor of the peak flux timing of temperate/cold water foraminiferal species (including *N. pachyderma*).

The modeled biomass of *N. pachyderma* produced during the LGM is mainly considerably higher than during H1, which might be connected to a larger, less transparent sea ice fraction during H1 and also to a lower nutrient concentration and consequently a smaller diatom population predicted during H1 (cf. Figure 2.6). The reduction in foraminiferal biomass from the LGM to H1 can in part be associated with a decrease in the primary productivity and also reflects the dilution with ice-rafted debris (IRD) being deposited (*Bond et al.*, 1992; *Broecker*, 1994). *Bond et al.* (1992) further suggested that the reduction in *N. pachyderma* could also be related to changes in sea surface temperature and/or salinity making the surface layer inhospitable to the species. In marine sediment records light $\delta^{18}\text{O}$ values recorded in *N. pachyderma* are evident during H1 (e.g., *Bond et al.*, 1992; *Broecker*, 1994; *Sarnthein et al.*, 1995; *Hillaire-Marcel and de Vernal*, 2008;

Stanford et al., 2011). The light isotopic excursions might either be a signal for meltwater (i.e., low salinity pulses) (*Bond et al.*, 1992; *Broecker*, 1994; *Stanford et al.*, 2011) or might correspond to an enhanced sea ice formation producing isotopically light brines (*Hillaire-Marcel and de Vernal*, 2008; *Stanford et al.*, 2011; *Pearson*, 2012). In contrast, sediment deposited during the LGM is characterized with high $\delta^{18}\text{O}$ values of, for instance, *N. pachyderma* (e.g., *Sarnthein et al.*, 1995; *Hillaire-Marcel and de Vernal*, 2008) indicating a low rate in sea ice production in the North Atlantic. *Hillaire-Marcel and de Vernal* (2008) conclude that the shift in the $\delta^{18}\text{O}$ values from the LGM to H1 should not only be interpreted in terms of paleosalinity and/or paleotemperature changes but also in regard of the differences in the sea ice formation. This interpretation supports our findings that the modeled seasonal shift in the maximum production of *N. pachyderma* from LGM to H1 is likely caused by the differences in the sea ice concentration and consequently in the primary productivity (cf. Figure 2.6).

2.4.3 Quantifying the Effect of Shifting Phenology on Stable Isotope Signals in *N. pachyderma*

The change in the timing of the maximum production peak from the LGM to H1 (and likewise to present day) could lead to a bias in paleoceanographic reconstructions (based on, e.g., oxygen isotope signals recorded in *N. pachyderma*) of surface water properties. The isotopic signature of *N. pachyderma* in marine sediments is related to local temperature, local hydrography, and global ice volume. Hence, differences in the $\delta^{18}\text{O}$ values between H1 and the LGM (e.g., Figure 2.8 and Tables 2.3 and 2.4) arise in part from changes in those (surface water) properties (*Bond et al.*, 1992; *Ravelo and Hillaire-Marcel*, 2007; *Hillaire-Marcel and de Vernal*, 2008; *Pearson*, 2012). In order to assess to what extent the seasonal differences between H1 and LGM in the maximum production month of *N. pachyderma* (Figure 2.5f) affected the isotopic signal, we calculated the theoretical $\delta^{18}\text{O}$ values of inorganic calcite, $\delta^{18}\text{O}_c$, in per mil, after *O'Neil et al.* (1969) (cited in *Shackleton* (1974)):

$$\delta^{18}\text{O}_c = 21.9 - (310.61 + 10 \cdot T)^{0.5} + \delta_w \quad (2.3)$$

where T is the temperature (in $^{\circ}\text{C}$) and δ_w denotes the $\delta^{18}\text{O}$ values of the ambient seawater. We focus on the temperature effect, i.e., we assume $\delta_w = \text{const.}$ and neglect any freshwater effect. We are aware that the large freshwater input into the North Atlantic during H1, due to the melting of vast amounts of icebergs, resulted in a decrease of up to 2‰ in the $\delta^{18}\text{O}$ of polar foraminifera (*Cortijo et al.*, 1997; *Roche et al.*, 2004). However, a part of this signal could also be due to a changing seasonality, i.e., the signal preserved in the planktonic foraminifera shells reflects a different season as assumed when reconstructing surface water properties. Seasonal variations in planktonic foraminiferal fluxes are influenced by changes in phytoplankton productivity, the thermal structure of the water column, and SST (*Žarić et al.*, 2005, 2006), which likewise could affect their isotopic signature. Furthermore, the prevailing environmental conditions during glacial periods (here H1 and LGM) might have favored a different calcification depth and/or carbonate precipitation might have occurred at another time compared to present day due to a changing seasonality. The productivity/phenology of planktonic foraminifera can in part be linked to the seasonal cycle of temperature (*Žarić et al.*, 2005; *Jonkers and Kučera*, 2015). *Mackas et al.* (2012) found that temperature might serve as a timing cue for zooplankton (including planktonic foraminifera) to indicate suitable environmental conditions for their growth and reproduction. This is supported by *Jonkers and Kučera* (2015) who showed

that for tropical/subtropical species (e.g., *G. ruber* (white), *G. sacculifer*) the phenology is mainly driven by temperature. However, for temperate/cold water species primary productivity seems to serve as the timing cue (cf. section 2.4.2). Our model results also indicate that temperature has a rather indirect effect on the productivity of *N. pachyderma*. This is consistent with the review of observational data by Xiao *et al.* (2014) who also concluded that temperature is not the key factor controlling the $\delta^{18}\text{O}$ of *N. pachyderma* shells in Arctic Ocean sediments. This supports our approach to focus on productivity as the main factor affecting the shift in seasonality during climate transitions.

To estimate the extent of the seasonality effect regarding the modeled shift in phenology between H1 and the LGM, we consider two different cases: (1) the productivity of *N. pachyderma* varies seasonally and may affect sedimentary $\delta^{18}\text{O}$ and (2) the productivity of *N. pachyderma* is constant, thus independent from changes in the prevailing environmental conditions. To this end, we calculated the difference between either the weighted annual averages ($\overline{\Delta\delta^{18}\text{O}_{c_w}}$, first case) or the arithmetic annual means ($\overline{\Delta\delta^{18}\text{O}_c}$, second case) in the derived $\delta^{18}\text{O}_c$ for H1 and LGM based on equation (2.3) and different temperature estimates. Finally, the effect of seasonality can be determined by differentiation between a seasonality in the productivity and assuming a constant monthly productivity of *N. pachyderma*.

For case 1 (i.e., the production weighted case) we consider the temperature and seasonality effect by calculating the weighted annual average in $\delta^{18}\text{O}_c$ by using the productivity of *N. pachyderma*:

$$\overline{\delta^{18}\text{O}_{c_w}} = \frac{\sum_{i=1}^{12} w_i \cdot \delta^{18}\text{O}_{c_i}}{\sum_{i=1}^{12} w_i} \quad (2.4)$$

where $\overline{\delta^{18}\text{O}_{c_w}}$ is the weighted annual average of the theoretical $\delta^{18}\text{O}$ values of inorganic calcite (in ‰), w_i is the monthly productivity of *N. pachyderma* (in mmol C/m³), and $\delta^{18}\text{O}_{c_i}$ are the monthly theoretical $\delta^{18}\text{O}$ values of inorganic calcite based on equation (2.3) (in ‰). For case 2 (i.e., the unweighted case) we consider the temperature effect (as given by equation (2.3)) only by calculating the arithmetic mean as we assume that productivity has no impact. Therefore, the annual average of the theoretical $\delta^{18}\text{O}$ of inorganic calcite, $\overline{\delta^{18}\text{O}_c}$, is determined by using equation (2.4) with $w_i = 1$ for all i .

We calculated for modern, H1, and LGM conditions the theoretical $\delta^{18}\text{O}$ values of inorganic calcite (i.e., $\delta^{18}\text{O}_c$) for cases 1 and 2 and finally determined the effect of seasonality by comparing the two cases (i.e., $\overline{\delta^{18}\text{O}_{c_w}} - \overline{\delta^{18}\text{O}_c}$) (Figures 2.7 and 2.9). Since we are most interested in the effect of shifting phenology on the stable isotope signals in *N. pachyderma* during the last glacial period we focus our analysis on the difference in the simulated $\delta^{18}\text{O}_c$ values (calculated based on the different considered cases) between H1 and the LGM. Additionally, we assessed the potential effect of calcification depth by using three different temperature estimates to calculate the theoretical $\delta^{18}\text{O}$ values of inorganic calcite. Here we distinguish between carbonate precipitations occurring at the surface, at the mixed layer depth (MLD), and/or along the thermocline.

As described in section 2.2.2 we employ monthly temperature (covering the whole water column) and mixed layer depth estimates from Merkel *et al.* (2010) for H1 and the LGM. For modern conditions we used the temperature estimates of the World Ocean Atlas 1998 (Conkright *et al.*, 1999) as well as the MLD values of Monterey and Levitus (1997). For calculating the simulated $\delta^{18}\text{O}_c$ values at the surface we used the modeled monthly SST estimates as temperature input in equation (2.3). To obtain the monthly temperature at the MLD, we extracted those temperature values given at the depth closest and/or equal to the provided MLD

values for each grid point and every month. We note that for modern conditions the provided MLD differed between 25 and 999 m, for H1 between 25 and ~ 1022 m and for the LGM between 25 and ~ 1615 m in the region of interest (i.e., $30 - 80^\circ\text{N}$, $75^\circ\text{W} - 15^\circ\text{E}$). Monthly temperature at the thermocline in turn has been determined by extracting the temperature values at the depth where the vertical temperature gradient is maximum. This led to a thermocline depth differing between 20 and 1225 m for modern conditions, 20 and 1404 m for H1, and 20 and 760 m for the LGM in the region being examined. To smooth the data we additionally applied a boxcar running mean along the longitudinal and latitudinal axes with a window size of 9×9 grid points. Along the coastlines a fewer number of grid points are used for the averaging depending on the amount of missing (i.e., land) values present. For all three temperature estimates we used the monthly productivity of *N. pachyderma* as weights in equation (2.4). Since *N. pachyderma* thrives at the surface due to the plankton living there, it is not necessary to recalculate the monthly productivity of *N. pachyderma* considering the temperature along the MLD and/or thermocline even though *N. pachyderma* calcifies most likely at greater depths.

2.4.3.1 $\delta^{18}\text{O}_c$ Signature During Modern Conditions

Using the temperature estimates for three different depths yields similar spacial patterns in the simulated $\delta^{18}\text{O}_c$ distribution with higher values ($> 3\text{‰}$) in the North and lower values ($< 1\text{‰}$) in the South for considering both the seasonality/temperature as well as the temperature effect itself (Figure 2.7). This is consistent with the isotopic signals in the core-top data based on *N. pachyderma* shells for the North Atlantic (i.e., between 50°N and 80°N) (Waelbroeck *et al.*, 2005). We used in total the $\delta^{18}\text{O}$ values recorded in *N. pachyderma* shells of 129 core-top samples compiled by Waelbroeck *et al.* (2005) for a comparison with the derived estimates at the surface, the MLD, and the thermocline depth. The RMSE between the modeled nearest grid points and the core-top data is rather low with values between 0.62‰ (seasonality/temperature effect) and 0.68‰ (temperature effect) using SST, 0.60‰ (seasonality/temperature effect) and 0.68‰ (temperature effect) using MLD temperatures, and/or 0.52‰ (seasonality/temperature effect) and 0.62‰ (temperature effect) using thermocline temperatures as basis of calculation for the simulated $\delta^{18}\text{O}_c$ values (Figure 2.7).

Our results show that considering the productivity of *N. pachyderma* to determine the theoretical $\delta^{18}\text{O}$ values (i.e., the seasonality/temperature effect) leads to a smaller RMSE as only taken the temperature effect into account by itself. Hence, the seasonality effect, which causes to a large extent a negative isotopic signal in the North Atlantic, except for the North Sea and parts of the subtropical gyre (Figures 2.7c, 2.7f, and 2.7i), should not be neglected when reconstructing surface water properties.

Although the distributional patterns in the isotopic signature of the considered effects (seasonality/temperature, temperature, and seasonality) differ only slightly among the three different used temperature estimates, the simulated $\delta^{18}\text{O}_c$ values based on the temperature at the thermocline depth fit the observations best (Figures 2.7g and 2.7h). However, the RMSE is of the same order of magnitude when assuming that calcification occurs either at the surface or at depth, which indicates that the exact calcification depth of *N. pachyderma* is not well determined from observational records yet as it appears to range from the surface mixed layer to a depth below 100 m (Kohfeld *et al.*, 1996; Bauch *et al.*, 1997; Simstich *et al.*, 2003). This, however, gives us increased confidence to use our approach for the investigation of the seasonality effect on stable isotopes in *N. pachyderma* during the last glacial period.

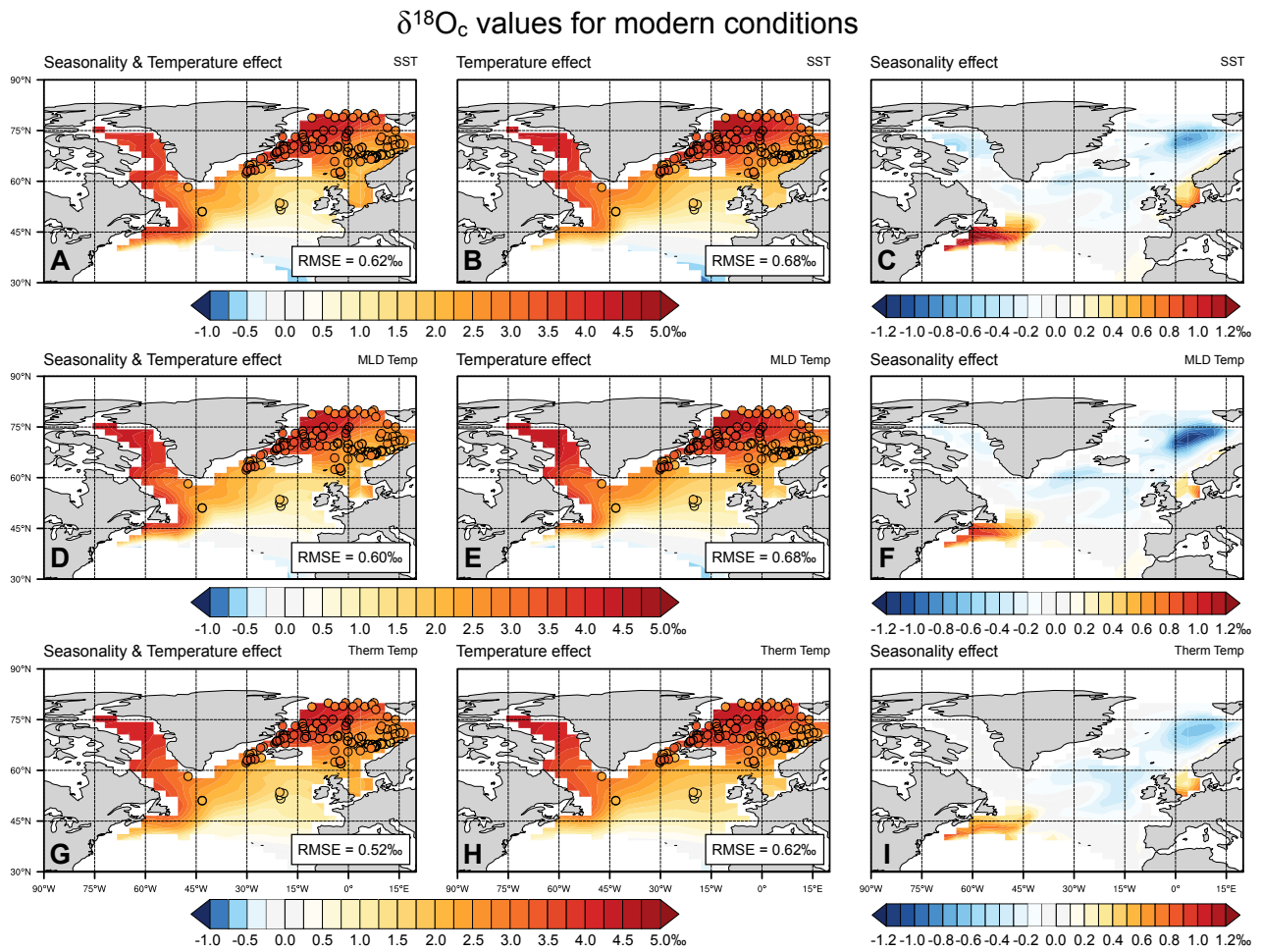


Figure 2.7: Spatial distribution of the theoretical annual mean $\delta^{18}\text{O}$ values of inorganic calcite ($\delta^{18}\text{O}_c$ in ‰) for modern conditions (contours) using (a–c) sea surface temperature (SST), (d–f) the temperature at the mixed layer depth (MLD Temp), and (g–i) the temperature along the thermocline (Therm Temp) as basis of calculation. Figures 2.7a, 2.7d, and 2.7g represent the joint seasonality and temperature effect (i.e., $\overline{\delta^{18}\text{O}_{c_w}}$); Figures 2.7b, 2.7e, and 2.7h the temperature effect (i.e., $\overline{\delta^{18}\text{O}_c}$); and Figures 2.7c, 2.7f, and 2.7i the seasonality effect (i.e., $\overline{\delta^{18}\text{O}_{c_w}} - \overline{\delta^{18}\text{O}_c}$), respectively. Figures 2.7a and 2.7b, Figures 2.7d and 2.7e, and Figures 2.7g and 2.7h additionally include the $\delta^{18}\text{O}$ core-top data (in ‰) of *N. pachyderma* (circles) given in *Waelbroeck et al.* (2005). The respective root-mean-square error is denoted by RMSE and has been calculated using 129 core-top samples when considering SST, MLD temperatures, or thermocline temperatures as input in equation (2.3).

2.4.3.2 $\delta^{18}\text{O}_c$ Signature During the Last Glacial Period

For reasons of comparability, we searched the PANGAEA database for sediment core records with $\delta^{18}\text{O}$ values based on *N. pachyderma* encompassing both the H1 and LGM time slice in the North Atlantic between 40° and 60°N (i.e., the area with the largest differences in the maximum production month between H1 and the LGM shown in Figure 2.5f) (Figure 2.8 and Table 2.3). Based on the six core locations we used the nearest model grid points for our analysis of the change in phenology (Figure 2.9 and Table 2.4).

2.4.3.2.1 Changes in $\delta^{18}\text{O}_c$ Based on SST Estimates

Differences between H1 and LGM in the simulated $\delta^{18}\text{O}_c$ at the surface that are estimated using both the productivity weighted and arithmetic annual means are, except for the south-western North Atlantic, positive

Table 2.3: Locations and $\delta^{18}\text{O}$ Values of Sediment Samples^a

Core	Latitude (°N)	Longitude (°E)	Water Depth (m)	$\delta^{18}\text{O}_{Np}$ (‰)		Source
				H1	LGM	
HU90-013-013	58.21	-48.37	3380	3.79	4.57	Hillaire-Marcel et al. (1994) ^b and Vogelsang et al. (2001) ^c
GIK17045-3	52.43	-16.67	3663	3.47	3.98	Sarnthein et al. (1994) ^b and Vogelsang et al. (2001) ^c
HU91-045-094	50.33	-45.69	3448	2.96	3.89	Hillaire-Marcel et al. (1994) ^b and Vogelsang et al. (2001) ^c
94-609	49.88	-24.24	3884	2.87	4.11	Bond et al. (1992) ^{b,c}
GIK15612-2	44.36	-26.54	3050	3.03	3.63	Kiefer (1998) ^{b,c}
V17-178	43.38	-54.87	4006	3.03	3.14	Keigwin and Jones (1995) ^{b,c}

^a $\delta^{18}\text{O}$ values of inorganic calcite (in ‰) recorded in *N. pachyderma* shells ($\delta^{18}\text{O}_{Np}$) for Heinrich Stadial 1 (H1) and the Last Glacial Maximum (LGM) time slice extracted with ISOMAP (courtesy of S. Mulitza).

^b Source of $\delta^{18}\text{O}_{Np}$ records.

^c Age model reference.

(Figures 2.9a and 2.9b) as SST is the only determining parameter to calculate the theoretical $\delta^{18}\text{O}$ values of inorganic calcite (cf. equation (2.3)). Based on the model, the positive values during H1 reflect the observation that the modeled surface ocean was colder in most areas of the North Atlantic Ocean compared to the LGM, which is consistent with reconstructions (e.g., Bard et al., 2000; Liu et al., 2009).

By comparing the differences (H1-LGM) in the simulated $\delta^{18}\text{O}_c$ values which have been determined by considering a seasonal cycle in productivity (case 1; Figure 2.9a) with those only being defined by the prevailing ambient sea surface temperature (case 2; Figure 2.9b) it is evident that the extent of primary productivity controlling the phenology differs between western and eastern North Atlantic (Figure 2.9c). In the western North Atlantic, where the strongest shift in the modeled maximum production month of *N. pachyderma* from LGM to H1 occurred (Figure 2.5f), the seasonality in the primary production (and thus food availability) has a positive effect on the productivity of *N. pachyderma* (as $\Delta\overline{\delta^{18}\text{O}_{c_w}} > \Delta\overline{\delta^{18}\text{O}_c}$), whereas in the eastern North Atlantic seasonality exerts a negative effect (as $\Delta\overline{\delta^{18}\text{O}_{c_w}} < \Delta\overline{\delta^{18}\text{O}_c}$). We note that the considered seasonality effect could also play a key role in determining the true $\delta^{18}\text{O}$ anomalies of inorganic calcite between H1 and LGM in the Greenland and Iceland Seas according to our model results (Figure 2.9c). However, in the Irminger and Norwegian Seas the effect of seasonality is small between H1 and LGM, so that a sedimentary signal (provided that calcification occurs at the surface) should reflect the true magnitude of the isotopic (or temperature) change.

2.4.3.2.2 Changes in $\delta^{18}\text{O}_c$ Based on MLD Temperatures

Using MLD temperatures to determine the differences in the simulated $\delta^{18}\text{O}_c$ (productivity weighted and arithmetic annual averages) between H1 and LGM yields similar spatial patterns compared to assuming a constant calcification depth at the surface (cf. Figures 2.9d and 2.9e). The dominating positive values of the simulated $\delta^{18}\text{O}_c$ values especially in the eastern North Atlantic (Figures 2.9d and 2.9e) indicate that even the subsurface ocean was colder during H1 compared to the LGM since the temperature at the MLD is the determining factor of the theoretical stable isotope values (cf. equation (2.3)).

For most of the North Atlantic ($> 45^\circ\text{N}$) the seasonality in the primary production exerts a stronger positive effect on the productivity of *N. pachyderma* (as $\Delta\overline{\delta^{18}\text{O}_{c_w}} > \Delta\overline{\delta^{18}\text{O}_c}$) using MLD temperature estimates

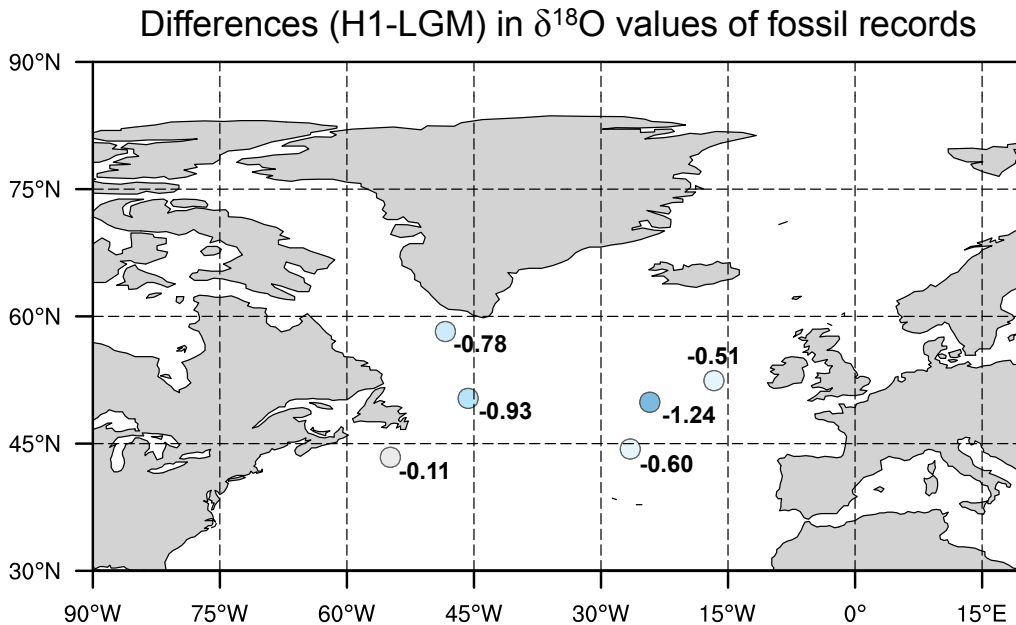


Figure 2.8: Spatial distribution of the changes (from the Last Glacial Maximum to Heinrich Stadial 1) in the $\delta^{18}\text{O}$ values (in ‰) recorded in *N. pachyderma* (see Table 2.4). The color code corresponds to the one used in Figure 2.9a.

instead of SST estimates (Figure 2.9f). This indicates that the seasonality effect is likely significant enough to play an important role in determining the magnitude of the isotopic change between H1 and LGM when assuming that calcification occurs at the MLD. The influence of the seasonality effect seems to be largest in the Nordic Seas with the simulated isotopic values exceeding 1.6 ‰ (Figure 2.9f).

2.4.3.2.3 Changes in $\delta^{18}\text{O}_c$ Based on Thermocline Temperatures

The differences in the simulated $\delta^{18}\text{O}_c$ values between H1 and LGM assuming that carbonate precipitation occurs along the thermocline are both less positive and negative but almost similarly distributed as those based on a calcification occurring at the MLD (Figure 2.9). Most of the North Atlantic, except for the central subtropical gyre, is characterized with positive values of the difference in the simulated $\delta^{18}\text{O}_c$ that have been estimated using either the productivity weighted or arithmetic annual means (Figures 2.9g and 2.9h) indicating that there the LGM was warmer along the thermocline depth compared to H1.

The productivity of *N. pachyderma* is also positively affected by the seasonality in the primary productivity in most parts of the region of interest providing a calcification depth along the thermocline (Figure 2.9i). However, the seasonality effect is less pronounced in comparison with the MLD estimates but nonetheless not negligible when reconstructing (surface) water properties.

At present it is assumed based on observational records that *N. pachyderma* calcifies between the surface mixed layer and a water depth of more than 200 m. This range in calcification depth supports our approach of using temperature estimates from different depths to analyze the effect of seasonality on stable isotope signals in *N. pachyderma*. Considering that carbonate precipitation occurs at the surface, at the mixed layer depth, or at the thermocline depth, our model results indicate that the seasonal cycle in the productivity of

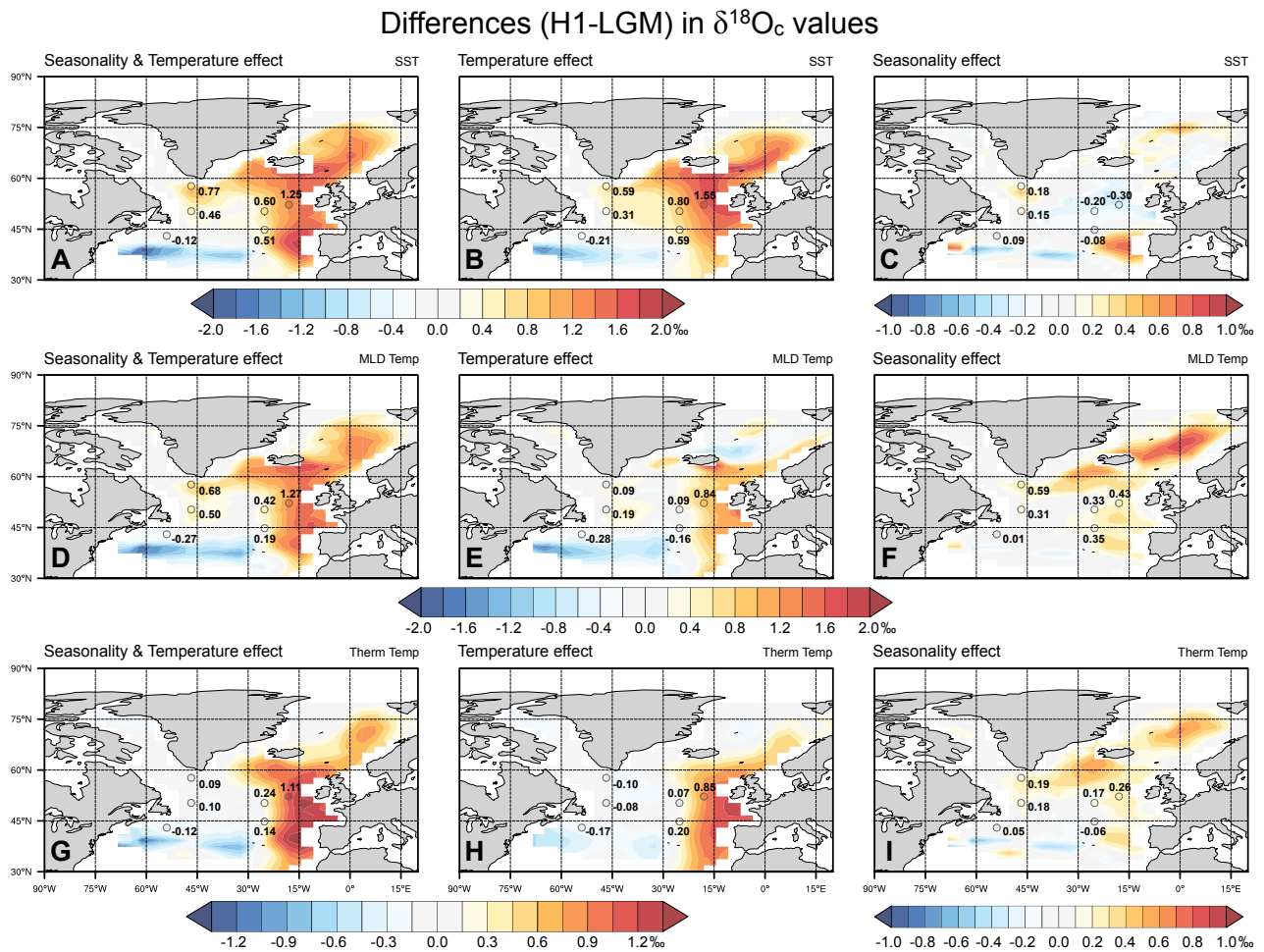


Figure 2.9: Spatial distribution of the changes in the theoretical annual mean $\delta^{18}\text{O}$ values of inorganic calcite ($\delta^{18}\text{O}_c$ in ‰) from the Last Glacial Maximum (LGM) to Heinrich Stadial 1 (H1) (contours) using (a–c) sea surface temperature (SST), (d–f) the temperature at the mixed layer depth (MLD Temp), and (g–i) the temperature along the thermocline (Therm Temp) as basis of calculation. Figures 2.9a, 2.9d, and 2.9g represent the joint seasonality and temperature effect (i.e., $\Delta\overline{\delta^{18}\text{O}_{c_w}}$); Figures 2.9b, 2.9e, and 2.9h the temperature effect (i.e., $\Delta\overline{\delta^{18}\text{O}_c}$); and Figures 2.9c, 2.9f, and 2.9i the seasonality effect (i.e., $\Delta\overline{\delta^{18}\text{O}_{c_w}} - \Delta\overline{\delta^{18}\text{O}_c}$), respectively. In each panel are for comparative reasons the derived $\delta^{18}\text{O}_c$ values given based on the six core locations using the nearest model grid points (cf. Tables 2.3 and 2.4).

N. pachyderma likely leads to an underestimation of the freshwater (meltwater) effect in paleoceanographic reconstructions in large parts of the North Atlantic including the IRD belt (40° – 50° N) (Ruddiman, 1977) and Nordic Seas. It is therefore necessary to consider not only the temperature (resulting in more positive $\delta^{18}\text{O}$ anomalies of inorganic calcite) and freshwater (resulting in more negative $\delta^{18}\text{O}$ anomalies of inorganic calcite) effects but also the seasonality effect to estimate the amplitude of the environmental changes from LGM to H1. However, the quantification of the exact calcification depth is also important to obtain the true magnitude of the isotopic change. To explain the observed negative anomalies in the $\delta^{18}\text{O}$ values of inorganic calcite (Figure 2.8) in the IRD belt region, a strong negative freshwater effect, resulting from lighter isotopic signals due to the large meltwater discharge during H1 compared to the LGM, is needed to counteract the positive temperature and seasonality effects (cf. Table 2.4). Hence, by neglecting the seasonality effect the freshwater effect will be underestimated when reconstructing past climate transitions.

Using a compilation of sediment trap data on fluxes of planktonic foraminifera, Jonkers and Kučera (2015) studied the determinants of the timing and strength of seasonal flux peaks. Based on the observed variability

Table 2.4: Comparison of $\delta^{18}\text{O}$ Values^a

Respective Core ^b	Latitude (°N)	Longitude (°E)	$\Delta\delta^{18}\text{O}_{Np}$	H1-LGM (‰)					
				based on SST		based on MLD Temp		based on Therm Temp	
				$\Delta\delta^{18}\text{O}_{c_w}$	$\Delta\delta^{18}\text{O}_c$	$\Delta\delta^{18}\text{O}_{c_w}$	$\Delta\delta^{18}\text{O}_c$	$\Delta\delta^{18}\text{O}_{c_w}$	$\Delta\delta^{18}\text{O}_c$
HU90-013-013	57.70	-46.80	-0.78	0.77	0.59	0.68	0.09	0.09	-0.10
GIK17045-3	52.20	-18.00	-0.51	1.25	1.55	1.27	0.84	1.11	0.85
HU91-045-094	50.30	-46.80	-0.93	0.46	0.31	0.50	0.19	0.10	-0.08
94-609	50.30	-25.20	-1.24	0.60	0.80	0.42	0.09	0.24	0.07
GIK15612-2	44.80	-25.20	-0.60	0.51	0.59	0.19	-0.16	0.14	0.20
V17-178	43.00	-54.00	-0.11	-0.12	-0.21	-0.27	-0.28	-0.12	-0.17

^a Difference in (theoretical) $\delta^{18}\text{O}$ values of inorganic calcite (in ‰) between Heinrich Stadial 1 (H1) and the Last Glacial Maximum (LGM) for the sediment samples given in Table 2.3 ($\Delta\delta^{18}\text{O}_{Np}$) as well as for cases 1 ($\Delta\delta^{18}\text{O}_{c_w}$) and 2 ($\Delta\delta^{18}\text{O}_c$) discussed in section 2.4.3 using sea surface temperature (SST), the temperature at the mixed layer depth (MLD Temp), and the temperature along the thermocline (Therm Temp) as calculation basis.

^b Respective cores of the nearest model grid points obtained at the core locations given in Table 2.3.

in flux seasonality, they concluded that changing seasonality during climate transitions should result in an underestimation of the actual magnitude of the environmental change recorded in fossil planktonic foraminifera. This conclusion is consistent with our findings. Our model successfully predicted the same kind of behavior in phenology as it is hypothesized from the observational data alone. Nevertheless, the potential existing bias in paleoceanographic reconstructions should further be assessed by combining changes in phenology with the inclusion of the depth dimension in the model.

Based on isotopic analyses from specimens in surface sediments, *Bé* (1960), *Boltovskoy* (1971), *Aksu and Vilks* (1988), and *Hemleben et al.* (1989) considered *N. pachyderma* to be a deep dwelling species as it was assumed to grow and calcify below 200 m water depth. In contrast, during life the species has a shallower depth habitat with maximum abundance in the upper 100 m of the water column (*Vilks*, 1970, 1975; *Stehman*, 1972; *Carstens and Wefer*, 1992; *Kohfeld et al.*, 1996; *Carstens et al.*, 1997; *Volkman*, 2000; *Pados and Spielhagen*, 2014; *Xiao et al.*, 2014). This discrepancy indicates that the bulk of the shell calcification in this species and hence the locking of the ambient seawater signal occur below the surface. This is supported by observations of peak abundances of encrusted forms of *N. pachyderma* between 100 and 200 m (*Kohfeld et al.*, 1996; *Bauch et al.*, 1997). This indicates that calcification more likely occurs at the MLD or thermocline depth than at the surface. Furthermore, this explains the better agreement of the distributional pattern between the simulated $\delta^{18}\text{O}_c$ values based on thermocline temperatures and the core-top data (cf. Figure 2.7). Even where the living (and calcification) depth varies, *N. pachyderma* is unlikely to record surface (mixed layer) conditions. For instance, in the sea ice covered regions of the Arctic Ocean *N. pachyderma* follows the chlorophyll maximum and is constrained to shallower depths (< 50 m) (*Simstich et al.*, 2003; *Pados and Spielhagen*, 2014; *Xiao et al.*, 2014), but because of stronger stratification, the species still records subsurface conditions. In consequence, the freshwater proportion in surface waters cannot be fully reflected in the $\delta^{18}\text{O}$ values of this species (*Simstich et al.*, 2003) and the $\delta^{18}\text{O}$ values of *N. pachyderma* likely provide an underestimation of the true meltwater signal of past climatic events (such as H1).

The apparently consistent subsurface calcification depth permits us to perform an analysis of the potential effects of changing seasonal production on isotopic signals in the region of interest. For this analysis we distinguish between a constant calcification depth at the surface, along the mixed layer, and/or along the

thermocline and only explore the effect of a changing flux pattern on the resulting sedimentary signal. Under the assumption that the modeled climatic fields are correct and PLAFOM has correctly captured the phenology and pattern of production of *N. pachyderma*, we conclude that changing phenology combined with cooling at either the surface or subsurface (i.e., at the MLD or along the thermocline) would induce an average isotopic signature between western and eastern North Atlantic of about -0.42‰ for the surface, -0.32‰ for the MLD and/or -0.47‰ for the thermocline estimates (see Figures 2.9a, 2.9d, and 2.9g), which amount, respectively, to 21%, 16% and/or $\sim 24\%$ of the presumed H1-LGM anomaly (Cortijo *et al.*, 1997; Roche *et al.*, 2004; Hemming, 2004) without any freshwater being added to the system. Because the sign of the respective signal is negative when added to the isotopic gradient measured on fossil shells of *N. pachyderma*, it would enhance the reconstructed isotopic gradient further. This implies that under a realistic modeling scenario and knowing the true calcification depth shifting phenology in planktonic foraminifera can have a considerable effect on proxy records.

2.5 Conclusion

Using the planktonic foraminifera model PLAFOM, the distribution of *N. pachyderma* at geological time scales in the North Atlantic Ocean north of 30°N was simulated. In comparison with modern climate conditions *N. pachyderma* spreads farther south during the Last Glacial Maximum and Heinrich Stadial 1, during which *N. pachyderma* is also found along the Iberian margin. Overall, the simulated distribution pattern of this foraminiferal species compares well with fossil records for all three time slices considered in this study.

Our model simulation further suggests a shift in the phenology from the LGM to H1. During H1 the maximum production of *N. pachyderma* usually occurred later during the year compared to the LGM. In the western North Atlantic the maximum production month is shifted by up to 6 months, which can primarily be related to changes in sea ice cover and food availability. The change in sea ice formation and, hence, its influence on the onset of primary production seem to play the crucial role in determining the seasonal shift from the LGM to H1.

Paleoceanographic reconstructions of sea surface properties based on oxygen isotopes recorded in *N. pachyderma* could be biased due to the change in timing of the maximum production peak. However, the influence of primary production on the shift in phenology varies spatially in the North Atlantic. Wherever *N. pachyderma* is likely to calcify (at the surface or at depth), we find that the simulated changes in the seasonality from LGM to H1 have similar effects on the isotopic signature in the North Atlantic north of 30°N with parts of the subtropical gyre being less affected, whereas in the IRD belt and Nordic Seas the amplitude of the meltwater effect recorded in fossil shells of *N. pachyderma* is likely to be underestimated. According to our model results up to 24% of the presumed H1-LGM anomaly in the IRD belt could be attributed to a shift in phenology and simultaneous cooling depending on the calcification depth of *N. pachyderma*.

Appendix 2.A1: Modifications of Competition Term

In PLAFOM the competition term of the mass loss equation is calculated as follows:

$$\text{competition} = \sum_i \left[F_p \cdot \frac{cl_{ij} \cdot F_i \cdot d}{F_i \cdot d + 0.1} \right] \quad (2.A1)$$

where F_p is the mortality term, F_i is the concentration of the foraminiferal species exerting competition, cl_{ij} represents the maximum competition pressure of the species i upon species j , and d is the e -folding constant, which controls the steepness of the Michaelis-Menton equation for competition. Compared to *Fraile et al.* (2008), we only modified equation (2.A1) for *G. ruber* (white) and *G. sacculifer* by adjusting the parameters d and cl_{ij} (Table 2.A1).

Table 2.A1: Modifications of Competition Term Parameters^a

Species Reference	<i>G. ruber</i> (white)		<i>G. sacculifer</i>	
	<i>Fraile et al.</i> (2008)	This Study	<i>Fraile et al.</i> (2008)	This Study
d	1	0.1	1	0.1
$cl_{N.pachyderma,j}$	0	0	0	0
$cl_{N.incompta,j}$	1	0.8	0	0
$cl_{G.bulloides,j}$	1	0.8	1	0.8
$cl_{G.ruber(white),j}$	-	-	0.8	0.2
$cl_{G.sacculifer,j}$	0.8	0.2	-	-

^a Adjustment of free parameters in competition term (equation (2.A1)) in comparison with original parameter settings of *Fraile et al.* (2008).

Acknowledgments

This paper has benefited from the constructive comments and suggestions of the three anonymous reviewers and the Editor, which greatly helped to improve our manuscript. We are grateful to X. Zhang and R. Rachmayani for providing the data of CCSM3 and to S. Mulitza for providing ISOMAP. We further like to thank J. Groeneveld for his helpful advice and the lively discussions. This project was supported by the DFG (Deutsche Forschungsgemeinschaft) through the International Research Training Group IRTG 1904 ArcTrain. All data can be obtained from the PANGAEA database ([doi.pangaea.de/10.1594/PANGAEA.861743](https://doi.org/10.1594/PANGAEA.861743)) or can be requested from the corresponding author (Kerstin Kretschmer, kkretschmer@marum.de).

Modeling seasonal and vertical habitats of planktonic foraminifera on a global scale

Kerstin Kretschmer^{1*}, Lukas Jonkers¹, Michal Kucera¹, and Michael Schulz¹

¹MARUM-Center for Marine Environmental Sciences and Faculty of Geosciences, University of Bremen, Bremen, Germany

Submitted to *Biogeosciences*

Contents

3.1	Introduction	40
3.2	Methods	41
3.2.1	Approach	41
3.2.2	CESM1.2(BGC) Configuration	42
3.2.3	PLAFOM2.0	43
3.2.3.1	Growth Rate	43
3.2.3.2	Mortality Rate	44
3.2.4	Model Setup	45
3.2.5	Comparison to Observations	46
3.2.5.1	Core-top Data	46
3.2.5.2	Sediment Trap Data	46
3.2.5.3	Plankton Tow Data	47
3.3	Results	48
3.3.1	Modeled Horizontal Distribution Patterns	48
3.3.2	Modeled Seasonal Distribution	50
3.3.3	Modeled Vertical Distribution	52
3.3.4	Modeled Seasonal Variability of Habitat Depth	54
3.4	Discussion	54
3.4.1	Large-scale Patterns	54
3.4.1.1	Geographical Range of Planktonic Foraminifera Species	54
3.4.1.2	Seasonality of Planktonic Foraminifera Species	57
3.4.1.3	Spatial and Temporal Variability of Depth Habitats of Planktonic Foraminifera Species	58
3.4.2	Comparison with Local Observations	61
3.5	Conclusion	66

*Species of planktonic foraminifera exhibit specific seasonal production patterns and different preferred vertical habitats. The seasonality and vertical habitats are not constant throughout the range of the species and changes therein must be considered when interpreting paleoceanographic reconstructions based on fossil foraminifera. Accounting for the effect of vertical and seasonal habitat tracking on foraminifera proxies at times of climate change is difficult because it requires independent fossil evidence. An alternative that could reduce the bias in paleoceanographic reconstructions is to predict species-specific habitat shifts under climate change using an ecosystem modeling approach. To this end, we present a new version of a planktonic foraminifera model, PLAFOM2.0, embedded into the ocean component of the Community Earth System Model, version 1.2.2. This model predicts monthly global concentrations of the planktonic foraminiferal species: *Neogloboquadrina pachyderma*, *N. incompta*, *Globigerina bulloides*, *Globigerinoides ruber* (white), and *Trilobatus sacculifer* throughout the world ocean, resolved in 24 vertical layers to 250 m depth. The resolution along the vertical dimension has been implemented by applying the previously used spatial parameterization of biomass as a function of temperature, light, nutrition, and competition on depth-resolved parameter fields. This approach alone results in the emergence of species-specific vertical habitats, which are spatially and temporally variable. Although an explicit parameterization of the vertical dimension has not been carried out, the seasonal and vertical distribution patterns predicted by the model are in good agreement with sediment trap data and plankton tow observations. In the simulation, the colder-water species *N. pachyderma*, *N. incompta*, and *G. bulloides* show a pronounced seasonal cycle in their depth habitat in the polar and subpolar regions, which appears to be controlled by food availability. During the warm season, these species preferably occur in the subsurface, while towards the cold season they ascend through the water column and are found closer to the sea surface. The warm-water species *G. ruber* (white) and *T. sacculifer* exhibit a less variable shallow depth habitat with highest biomass concentrations within the top 40 m of the water column. Nevertheless, even these species show vertical habitat variability and their seasonal occurrence outside the tropics is limited to the warm surface layer that develops at the end of the warm season. The emergence in PLAFOM2.0 of species-specific vertical habitats that are consistent with observations indicates that the population dynamics of planktonic foraminifera species may be driven by the same factors in time, space, and with depth, in which case the model can provide a reliable and robust tool to aid the interpretation of proxy records.*

3.1 Introduction

Planktonic foraminifera are found throughout the open ocean, where they inhabit roughly the top 500 m of the water column (Fairbanks *et al.*, 1980, 1982; Kohfeld *et al.*, 1996; Kemle-von Mücke and Oberhänsli, 1999; Mortyn and Charles, 2003; Field, 2004; Kuroyanagi and Kawahata, 2004; Bergami *et al.*, 2009; Wilke *et al.*, 2009; Pados and Spielhagen, 2014; Iwasaki *et al.*, 2017; Rebotim *et al.*, 2017). Their calcareous shells, preserved in ocean sediments, are widely used to reconstruct past climate conditions. To do so, information about their habitat including their horizontal and vertical distribution are needed. It is known from observational data that the prevailing environmental conditions, such as temperature, stratification, light intensity, and food availability, affect the growth and distribution of the individual planktonic foraminifera (Fairbanks *et al.*, 1980, 1982; Bijma *et al.*, 1990a; Watkins *et al.*, 1996; Schiebel *et al.*, 2001; Field, 2004; Kuroyanagi and Kawahata, 2004; Žarić *et al.*, 2005; Salmon *et al.*, 2015; Rebotim *et al.*, 2017).

Based on stratified plankton tow and sediment trap data, the seasonal succession of planktonic foraminifera

species has been assessed on a local/regional scale (e.g., *Fairbanks and Wiebe*, 1980; *Kohfeld et al.*, 1996; *Wilke et al.*, 2009; *Jonkers et al.*, 2013; *Jonkers and Kučera*, 2015), whereas for a broader regional/global perspective modeling approaches have been used to study the seasonal variations in the surface (mixed) layer of the ocean (*Žarić et al.*, 2006; *Fraile et al.*, 2008, 2009a,b; *Lombard et al.*, 2011; *Kretschmer et al.*, 2016). Comparatively less is known about the depth habitat of planktonic foraminifera species and how it varies seasonally. Although previous studies identified different environmental and ontogenetic factors (i.a., temperature, chlorophyll *a* concentration, the lunar cycle, and/or the structure of the water column), which influence the species-specific depth habitats including their mean living depth and vertical migration (e.g., *Fairbanks and Wiebe*, 1980; *Fairbanks et al.*, 1982; *Schiebel et al.*, 2001; *Simstich et al.*, 2003; *Field*, 2004; *Salmon et al.*, 2015; *Rebotim et al.*, 2017), the only attempt to model the vertical habitat is by *Lombard et al.* (2011).

It is well known that species-specific habitats vary seasonally and spatially depending on the prevailing climatic conditions (*Mix*, 1987; *Mulitza et al.*, 1998; *Ganssen and Kroon*, 2000; *Skinner and Elderfield*, 2005; *Jonkers and Kučera*, 2015). Yet, despite this evidence for a variable habitat, it is often assumed in paleoceanographic studies that the habitat of planktonic foraminifera is constant, i.e., it does not change in time and space, potentially leading to erroneous estimates of past climate conditions. *Jonkers and Kučera* (2017) recently highlighted how foraminifera proxies are affected by habitat tracking and showed that by not accounting for this behavior, spatial and temporal trends in proxy records may be underestimated. Given the habitat variability in planktonic foraminifera, it is more than likely that a climate-dependent offset from mean annual sea surface conditions results not only from a seasonal, but also from depth habitat variability due to changes in ambient conditions. Such vertical habitat variability was shown by *Rebotim et al.* (2017), who investigated parameters controlling the depth habitat of planktonic foraminifera in the subtropical eastern North Atlantic. In line with studies from other regions of the world ocean (e.g., *Fairbanks et al.*, 1982; *Bijma et al.*, 1990b; *Ortiz et al.*, 1995; *Schiebel et al.*, 2001; *Field*, 2004; *Salmon et al.*, 2015), *Rebotim et al.* (2017) identified distinct species-specific depth habitats, but they also showed that the habitats vary on lunar and seasonal time scales and in response to temperature, chlorophyll *a*, and other environmental factors. Evidence for variable depth habitats at least on a regional scale has emerged from studies in other regions (*Watkins et al.*, 1998; *Peeters and Brummer*, 2002; *Kuroyanagi and Kawahata*, 2004).

These observations underline the necessity to consider species-specific habitats and their variability on a global scale to increase the reliability of paleoceanographic reconstructions. However, a global assessment of species-specific depth habitat variability in time and space and the potential underlying control mechanisms is lacking. Since the observational data coverage of the global ocean is too sparse to provide in this regard a broad general estimate, we apply an ecosystem modeling approach to predict the vertical and seasonal distribution of planktonic foraminifera on a global scale.

3.2 Methods

3.2.1 Approach

To predict the seasonally varying global species-specific depth habitat of planktonic foraminifera, we modified the previously developed PLAFOM model (*Fraile et al.*, 2008; *Kretschmer et al.*, 2016), which is implemented

as an off-line planktonic foraminifera module into the ocean component of the Community Earth System Model, version 1.2.2 (CESM1.2; *Hurrell et al.*, 2013) with the biogeochemical model being enabled (i.e., the CESM1.2(BGC) configuration). This model system simulates the monthly concentrations of five modern planktonic foraminiferal species, which are widely used in paleoceanographic reconstructions. The original approach of *Fraile et al.* (2008) and *Kretschmer et al.* (2016) aimed to predict the distribution of planktonic foraminifera in the surface mixed layer on geological time scales. This model version has been successfully used to assess the effect of changing environmental conditions on species distributional patterns in time and space (*Fraile et al.*, 2009a,b; *Kretschmer et al.*, 2016) and to aid in interpreting paleoceanographic records regarding seasonal production shifts in the geological past (*Kretschmer et al.*, 2016), but could not provide any information about depth. To implement the vertical dimension, we used an approach, in which we first updated PLAFOM (hereafter referred to as PLAFOM2.0) by including light dependency for symbiont-bearing planktonic foraminifera and then applied the previously used spatial parameterization of biomass as a function of temperature, nutrition, and competition, together with light, on depth-resolved parameter fields. By combining PLAFOM2.0 with the CESM1.2(BGC) configuration, the vertical dimension can be resolved throughout the ocean, with 24 layers in the top 250 m.

3.2.2 CESM1.2(BGC) Configuration

We used the CESM1.2(BGC) configuration (*Moore et al.*, 2013; *Lindsay et al.*, 2014) as code base. This configuration includes the Biogeochemical Elemental Cycling (BEC) model (*Moore et al.*, 2004, 2006; *Krishnamurthy et al.*, 2007; *Moore and Braucher*, 2008), which is based on the upper ocean ecosystem model of *Moore et al.* (2002b,a) coupled to a biogeochemistry model based on the Ocean Carbon Model Intercomparison Project (OCMIP; *Doney et al.*, 2006).

The BEC model includes various potentially growth-limiting nutrients (nitrate, ammonium, phosphate, dissolved iron, and silicate), three explicit phytoplankton functional types (diatoms, diazotrophs, pico/nano phytoplankton), a partial calcifier class (representing coccolithophores), a single adaptive zooplankton class, dissolved organic matter, sinking particulate detritus, and full carbonate system thermodynamics (*Moore et al.*, 2004, 2013). Phytoplankton growth rates are controlled by temperature, light, and available nutrients (*Moore et al.*, 2002a, 2004). The single zooplankton pool grazes on all phytoplankton types, whereby the routing of grazed material varies depending on the type of prey (*Moore et al.*, 2004, 2013). For further details, we refer to *Moore et al.* (2002a, 2004, 2013).

The BEC model has been embedded into the ocean component of CESM, version 1.2.2. CESM1.2 is a fully coupled climate model consisting of several components including the atmosphere, ocean, land, and sea ice (*Hurrell et al.*, 2013), whereby the geophysical fluxes among the components are exchanged through a central coupler (*Craig et al.*, 2012). Here we performed simulations using the ocean model coupled to both the sea ice model and data models for the atmosphere, land, and river routing.

The CESM1.2 ocean component is the Parallel Ocean Program, version 2 (POP2; *Smith et al.*, 2010; *Danabasoglu et al.*, 2012), which is a z-level hydrostatic primitive equation model. Here we use the coarse-resolution configuration of POP2 (*Shields et al.*, 2012), where the longitudinal resolution amounts to 3.6° and the latitudinal resolution varies between 1° and 2°, with a finer resolution near the equator. POP2 employs a non-uniform dipolar grid with the North Pole being displaced into Greenland. With a total number

of 60 vertical levels, the grid spacing is fine near the surface (10 levels in the top 100 m) and increases with depth to 250 m near the bottom. The sea ice component of CESM1.2 is the Community Ice Code, version 4 (CICE4; *Hunke and Lipscomb, 2008; Holland et al., 2012*), which uses the same horizontal grid as the ocean model.

3.2.3 PLAFOM2.0

This new model version, PLAFOM2.0, considers the polar species *Neogloboquadrina pachyderma*, which is supplemented by the subpolar species *N. incompta* (sensu *Darling et al., 2006*) and *Globigerina bulloides* as well as by the warm-water algal symbiont-bearing species *Globigerinoides ruber* (white) and *Trilobatus sacculifer* (sensu *Spezzaferri et al., 2015*). Those species have been chosen as they can be considered to represent a large portion of the planktonic foraminiferal biomass in the surface ocean (for further details see *Kretschmer et al., 2016*). The different planktonic foraminifera species were added as optional passive tracers with the requirement that the BEC model is active.

PLAFOM2.0 is driven by temperature, the available food sources (including zooplankton, diatoms, small phytoplankton, and organic detritus), and also light availability, whereby the latter only matters with regard to the growth of the two algal symbiont-bearing species (*Erez, 1983; Jørgensen et al., 1985; Gastrich, 1987; Gastrich and Bartha, 1988*) and *G. bulloides*, which according to the latest findings hosts the picocyanobacterium *Synechococcus* as a photosynthesizing endobiont (*Bird et al., 2017*). *Synechococcus* is known to be important for cyanobacterial photosynthesis in marine and freshwater ecosystems (*Ting et al., 2002; Jodłowska and Śliwińska, 2014*).

The food preferences and temperature tolerance limits for each species have been derived from sediment trap data and culturing experiments (see *Fraile et al., 2008*, for details). Changes in the foraminifera carbon concentration for each species are determined as follows:

$$\frac{dF}{dt} = (GGE \cdot TG) - ML \quad (3.1)$$

where F is the foraminifera carbon concentration (in mmol C m^{-3}), GGE (gross growth efficiency) is the portion of grazed matter that is incorporated into foraminiferal biomass, TG represents total grazing (i.e., the growth rate in $\text{mmol C m}^{-3}\text{s}^{-1}$), and ML denotes mass loss (i.e., the mortality rate in $\text{mmol C m}^{-3}\text{s}^{-1}$). To properly simulate the vertical distribution of each considered planktonic foraminifera, we included light dependency and modified parts of the parameterizations of the foraminiferal species concentration. Therefore, we extended the growth rate equation by not only considering food availability and temperature sensitivity, but also light intensity to define growth. Additionally, we adjusted parts of the mortality rate equation to improve the model accuracy. In the following, the performed modifications are described in detail in regard to the growth and mortality rates. The modifications compared to the earlier model version are summarized in Table 3.1.

3.2.3.1 Growth Rate

The growth rate depends on the available food and temperature sensitivity of each foraminiferal species as well as on light for the species with algal symbionts and/or cyanobacterial endobionts. To account for

the light dependence with depth influencing the growth of *G. bulloides* and of the spinose species *G. ruber* (white) and *T. sacculifer*, we included a photosynthetic growth rate. We applied a similar approach as Doney *et al.* (1996) and Geider *et al.* (1998), who determined phytoplankton growth rates by available light and nutrients as used in the BEC model (Moore *et al.*, 2002a, 2004).

Photosynthesis depends on light availability and temperature. This co-dependency can be expressed as follows:

$$P_{F,photo} = P_{F,max} \cdot \left[1 - \exp\left(\frac{-\alpha_{PI} \cdot I_{PAR}}{P_{F,max}}\right) \right]$$

where $P_{F,photo}$ is the foraminiferal specific rate of photosynthesis (in s^{-1}) and $P_{F,max}$ is the maximum value of $P_{F,photo}$ at temperature T (in s^{-1}), calculated as:

$$P_{F,max} = P_{F,0} \cdot T_{func}$$

α_{PI} is the initial slope of the photosynthesis-light curve (in $m^2 W^{-1} s^{-1}$) (Table 3.1), I_{PAR} is the average irradiance over the mixed layer depth provided by the ecosystem model (in $W m^{-2}$), $P_{F,0}$ represents the maximum foraminiferal growth rate at a specific temperature T_0 (in s^{-1}) (Table 3.1), and T_{func} is the temperature response function (dimensionless). The temperature function is defined as:

$$T_{func} = q_{10}^{\frac{T-T_0}{10}} \quad (3.2)$$

with a q_{10} value of 1.5 (Sherman *et al.*, 2016) and T being the ambient ocean temperature (in K) and T_0 the reference temperature of 303.15 K.

The photosynthetic growth rate, P_F (in $mmol C m^{-3} s^{-1}$), can finally be determined as follows:

$$P_F = P_{F,photo} \cdot F \cdot p\%$$

where $p\%$ represents the fraction of photosynthesis contributing to growth (see Table 3.1).

3.2.3.2 Mortality Rate

The mortality rate is determined by respiration loss, predation by higher trophic levels, and competition among species. To improve the seasonal patterns in the foraminiferal biomass for low temperatures, we followed Moore *et al.* (2004) and adjusted the temperature dependence of the predation term (ML_{pred} in $mmol C m^{-3} s^{-1}$):

$$ML_{pred} = f_{mort2} \cdot T_{func} \cdot F_p^2$$

where f_{mort2} represents the quadratic mortality rate (in $s^{-1}(mmol C m^{-3})^{-1}$), T_{func} is the temperature response function (dimensionless) used for scaling, and F_p (in $mmol C m^{-3}$) is used to limit the planktonic foraminifera mortality at very low biomass levels. Compared to Fraile *et al.* (2008), here predation is scaled by Eq. (3.2), a temperature function using a q_{10} value of 1.5 (Sherman *et al.*, 2016).

Additionally, we included a stronger competitive behavior of *G. bulloides* by adjusting the free parameters

in the competition term. In PLAFOM2.0, competition (ML_{comp} in $\text{mmol C m}^{-3}\text{s}^{-1}$) is defined as follows:

$$ML_{comp} = \sum_i \left[F_p \cdot \frac{cl_{ij} \cdot F_i \cdot d}{F_i \cdot d + 0.1} \right]$$

with F_i being the concentration of the foraminiferal species exerting competition, cl_{ij} the maximum competition pressure of species i upon species j , and d the constant controlling the steepness of the Michaelis-Menten relationship for competition. In comparison with *Kretschmer et al.* (2016), we only modified the parameter cl_{ij} for *N. incompta*, *G. bulloides*, and *G. ruber* (white) (Table 3.1).

Table 3.1: Model Parameter and Their Modifications Relative to *Fraille et al.* (2008) and/or *Kretschmer et al.* (2016). The Original Value is Given in Parentheses.

Species	<i>N. pachyderma</i>	<i>N. incompta</i>	<i>G. bulloides</i>	<i>G. ruber</i> (white)	<i>T. sacculifer</i>
$P_{F,0}$	- (-)	- (-)	2.6 (-)	2.6 (-)	2.6 (-)
α_{PI}	- (-)	- (-)	0.012 (-)	0.01 (-)	0.07 (-)
$p\%$	- (-)	- (-)	0.3 (-)	0.3 (-)	0.4 (-)
T_{thres}	18.0 (24.0)	3.0 (-0.3)	3.0 (-0.3)	10.0 (5.0)	15.0 (15.0)
$cl_{N.pachyderma,j}$	- (-)	0.2 (0.2)	0 (0)	0 (0)	0 (0)
$cl_{N.incompta,j}$	- (-)	- (-)	0.1 (0.1)	0.2 (0.8)	0 (0)
$cl_{G.bulloides,j}$	- (-)	0.8 (0.5)	- (-)	0.8 (0.8)	0.8 (0.8)
$cl_{G.ruber(white),j}$	- (-)	0.2 (0.8)	0.1 (0.5)	- (-)	0.2 (0.2)
$cl_{T.sacculifer,j}$	- (-)	0 (0)	0.1 (0.5)	0.2 (0.2)	- (-)

$P_{F,0}$ – maximum foraminiferal growth rate (in day^{-1}) at 30 °C (derived from the maximum zooplankton growth rate at 20 °C given by *Doney et al.* (1996)).

α_{PI} – initial slope of the photosynthesis-light (PI) curve (in $\text{m}^2 \text{W}^{-1}\text{day}^{-1}$) (derived from PI-curve of *Synechococcus* given in *Jodłowska and Śliwińska* (2014) for *G. bulloides* and of endosymbiotic dinoflagellates given in *Jørgensen et al.* (1985) for *T. sacculifer*).

$p\%$ – fraction of photosynthesis contributing to foraminiferal growth rate.

T_{thres} – minimum (for *N. pachyderma*) or maximum (for all other species) threshold temperature at which foraminiferal species can thrive (in °C).

cl_{ij} – competition pressure of species i upon species j .

We added the present implementation of PLAFOM2.0 to the code trunk of POP2 as a separate module. Additionally, the food sources for the planktonic foraminifera species are computed in the ecosystem model and instantly passed to PLAFOM2.0 to calculate the foraminifera carbon concentration. For a more detailed description of the planktonic foraminifera model and its behavior on a regional/global scale in the surface mixed layer, we refer to *Fraille et al.* (2008) and *Kretschmer et al.* (2016).

3.2.4 Model Setup

To test the model, we performed a preindustrial-control experiment. Therefore, we derived the initial ocean and sea ice states from an ocean-ice-only simulation, which did not include the BEC ocean biogeochemistry. This model integration was spun-up from rest for 1250 years to approach a quasi steady state by using a climatological forcing (based on atmospheric observations and reanalysis data) as repeated normal year forcing. Heat, freshwater, and momentum fluxes at the sea surface are based on the atmospheric data sets developed by *Large and Yeager* (2004, 2009) and implemented following the CORE-II-protocol (Coordinated Ocean-ice Reference Experiment) suggested by *Griffies et al.* (2009).

The tracer fields resulting from the end of this spin-up run were used to initialize the CESM1.2(BGC) preindustrial-control simulation. The biogeochemical tracer fields were, i.a., initialized from data-based climatologies. For instance, initial nutrient (phosphate, nitrate, silicate) distributions were taken from

the World Ocean Atlas 2009 (WOA09; *Garcia et al.*, 2010), initial values for dissolved inorganic carbon and alkalinity are from the Global Ocean Data Analysis Project (GLODAP; *Key et al.*, 2004), whereas zooplankton, phytoplankton pools, and dissolved organic matter have been initialized uniformly at low values (*Moore et al.*, 2004). Additionally, each planktonic foraminiferal species was also initialized uniformly at low values assuming the same (vertical) distribution as the zooplankton component of the BEC model. Furthermore, the atmospheric deposition of iron and dust is based on the climatology of *Luo et al.* (2003).

The CESM1.2(BGC) preindustrial-control simulation was integrated for 200 years to reach stable conditions in the ocean biogeochemistry in the upper 500 m of the water column (see Figure S3.1 in the Supplement). Since this simulation has been forced and/or initialized based on climatologies, inter-annual variability and forcing trends can be excluded and, therefore, we focus our analysis on the model output of only one year, here of year 200.

3.2.5 Comparison to Observations

To validate the model performance, we compare the simulated spatial and temporal distributions of the considered planktonic foraminiferal species with data from core-tops, sediment traps, and plankton tows (Figure 3.1). Based on data availability, we focus our analysis on distinct regions distributed over the world ocean covering all climate zones from the poles to the tropics.

3.2.5.1 Core-top Data

To examine the spatial pattern of the five considered planktonic foraminiferal species, we compared the model predictions with fossil data by using in total 2844 core-top samples distributed over all oceans (Figure 3.1a). We combined the Brown University Foraminiferal Database (*Prell et al.*, 1999) with the data assembled by the MARGO project (*Kucera et al.*, 2005), and the data sets provided by *Pflaumann et al.* (1996, 2003). For the comparison, we recalculated the relative abundances of the faunal assemblages by only considering those five species used in PLAFOM2.0.

3.2.5.2 Sediment Trap Data

To compare modeled and observed seasonal production patterns, several sediment traps (Table S3.1 in the Supplement, Figure 3.1b) have been examined. Those can provide foraminiferal shell fluxes continuously collected over several months or even years. However, some sediment traps comprise only of a few months (i.e., less than a year) and might have just recorded local short-term processes of a particular season/year and can, thus, not provide a long-term/climatological mean.

Here we use the same approach as in *Jonkers and Kučera* (2015) and present the observed fluxes for multiple years from every location on a \log_{10} scale versus day of year, whereby the zero fluxes have been replaced by half of the observed minimum flux. In this way, we can directly compare the peak timings of the measured fluxes at each location with the model, whereby we assume that the flux through the water column (in $\# \text{ m}^{-2} \text{ day}^{-1}$) is proportional to the volume integrated model concentrations (in mmol C m^{-3}).

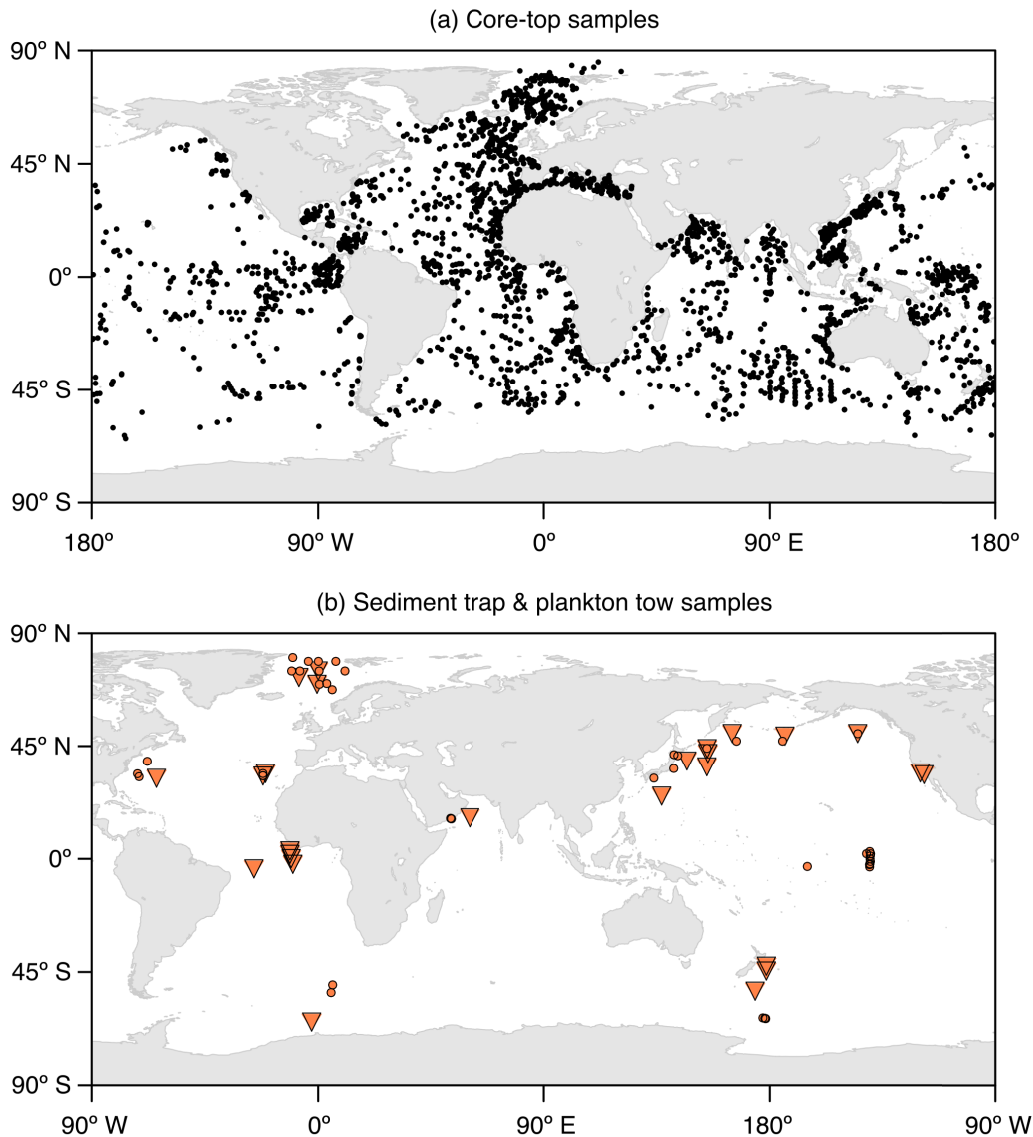


Figure 3.1: Locations of (a) the core-top samples with planktonic foraminifera counts and (b) the plankton tow (orange circles) and sediment trap (orange triangles) samples used for the model validation. The map in Figure 3.1a shows a combination of the data sets of *Prell et al.* (1999), *Pflaumann et al.* (1996, 2003), and *Kucera et al.* (2005). The respective information on the sediment trap and plankton tow data shown in Figure 3.1b is given in Tables S3.1 and S3.2 in the Supplement.

3.2.5.3 Plankton Tow Data

To analyze the vertical distribution, plankton net hauls from different sites distributed across the world ocean (Table S3.2 in the Supplement, Figure 3.1b) have been used for a comparison with the simulated vertical distributions. Plankton tow samples have been collected by means of a multiple opening-closing net with a vertical resolution differing between 5 depth levels (one haul) and up to 13 depth levels (two or more consecutive hauls) resolving the upper 100s of meters of the water column. Since the plankton tow data has been collected during a particular time (i.e., a specific day/month) (Table S3.2), the same month has been considered for the simulated vertical planktonic foraminifera profile for the model-data comparison.

Here we followed the same approach as *Rebotim et al.* (2017) and calculated an average living depth (ALD) and the vertical dispersion (VD) around the ALD to provide a direct comparison with the modeled depth

profile. The ALD (in m) is defined as follows:

$$ALD = \frac{\sum_i C_i \cdot D_i}{\sum_i C_i}$$

with C_i being the foraminiferal species concentration (in $\# \text{ m}^{-3}$) in the depth interval D_i and VD (in m) is calculated as:

$$VD = \frac{\sum_i (|ALD - D_i| \cdot C_i)}{\sum_i C_i}$$

For further information, we refer to *Rebotim et al.* (2017).

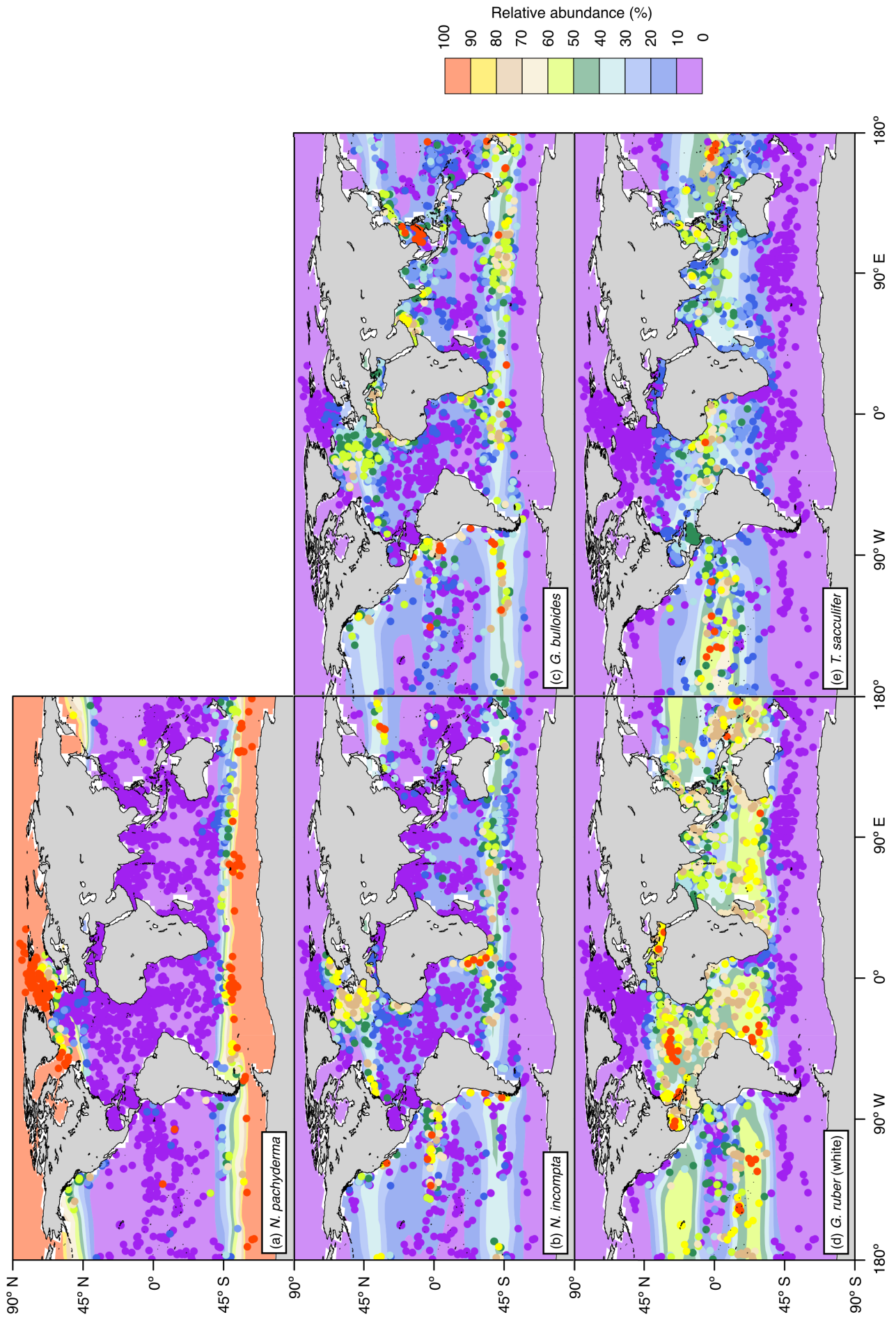
3.3 Results

3.3.1 Modeled Horizontal Distribution Patterns

The modeled global spatial distribution patterns based on the depth integrated annual mean relative abundances of the five considered foraminiferal species (Figure 3.2) correspond to the five major provinces of the modern ocean (i.e., polar, subpolar, transitional, subtropical, and tropical) known to be inhabited by those species (*Bradshaw*, 1959; *Bé and Tolderlund*, 1971; *Hemleben et al.*, 1989; *Kucera*, 2007). Note that since the core-top data used for comparison can neither provide any information about the depth habitat of the planktonic foraminiferal species nor about their life cycle, the modeled annual mean relative abundances have been obtained by integrating the individual foraminiferal concentrations over the whole water column and by subsequently calculating the percentage of each species relative to the total foraminiferal biomass.

The cold-water species *N. pachyderma* is confined to the high latitudes dominating the polar waters of both hemispheres. *Neogloboquadrina pachyderma* shows the highest annual mean relative abundances (> 90%) north of the Arctic Circle and south of the Antarctic Convergence, whereas toward the subtropics the species' occurrence reduces gradually (Figure 3.2a). *Neogloboquadrina incompta* is mainly found in the subpolar to transitional water masses of the world ocean. This species shows highest annual mean relative abundances (> 30%) in the subantarctic belt as well as in the upwelling region of the equatorial Pacific and in the coastal upwelling systems associated with the cold eastern boundary currents of the Atlantic and Pacific Oceans (Figure 3.2b). *Globigerina bulloides* exhibits a similar distribution pattern as *N. incompta*. It is present in the subpolar to transitional waters of the world oceans with the highest annual mean relative abundances (> 30%) occurring in the Southern Ocean, the upwelling areas of the Pacific Ocean, and in the subpolar gyres (Figure 3.2c). The warm-water species *G. ruber* (white) is mostly confined to the subtropical and tropical regions of both hemispheres, whereby the highest annual mean relative abundances of up to

Figure 3.2 (facing page): Relative abundances of the depth integrated modeled annual mean concentration (pale-colored contours; % biomass) and of the core-top samples (circles; % individuals) for (a) *N. pachyderma*, (b) *N. incompta*, (c) *G. bulloides*, (d) *G. ruber* (white), and (e) *T. sacculifer*. The relative abundances consider only the five foraminiferal species included in PLAFOM2.0. Note that we are aware that for a small number of core-top samples the relative abundances of the individual planktonic foraminiferal species are overestimated due to the recalculations by only considering *N. pachyderma*, *N. incompta*, *G. bulloides*, *G. ruber* (white), and *T. sacculifer* rather than the whole assemblage. However, the overall general pattern does not change and can, thus, be used for the model-data comparison.



60% are reached in the subtropical gyres (Figure 3.2d). Lowest annual mean relative abundances can be found in the ocean's upwelling areas, especially in the equatorial Pacific cold tongue, where *G. ruber* (white) appears to be almost absent. The distribution pattern of *T. sacculifer* is limited to the warm waters of the subtropics and tropics, and is similar to the one of *G. ruber* (white). *Trilobatus sacculifer* shows highest annual mean relative abundances (> 50%) in the equatorial Pacific between 15°N and 15°S and exhibits low annual mean relative abundances (< 20%) in the upwelling regions of the ocean basins (Figure 3.2e).

3.3.2 Modeled Seasonal Distribution

For each foraminiferal species the month of maximum production changes on average with temperature and consequently with latitude (Figure 3.3, Figure S3.2 in the Supplement). There is a general tendency for the maximum production peak of the cold-water species *N. pachyderma* to occur later in the year (i.e., during summer) for lower annual mean temperatures (Figures 3.3a and S3.2a). With increasing mean annual temperatures, however, the peak timing occurs earlier in the year (i.e., during spring) (Figure 3.3a). For *N. incompta* maximum production is reached during late summer in the midlatitudes at lower temperatures and is shifted towards spring/early summer when temperatures increase (Figure S3.2b). In the low latitudes at high temperatures, however, peak fluxes of *N. incompta* occur constantly throughout the year (Figure 3.3b). The peak timing of *G. bulloides* is similar to the peak timing of *N. incompta*, where the highest modeled fluxes are reached later (earlier) in the year in the midlatitudes at lower (higher) temperatures (Figure S3.2c). In the warm waters (of the tropics), the maximum production of *G. bulloides* occurs year-round (Figure 3.3c). Both *N. incompta* and *G. bulloides* show indications of a double peak in their timing that is shifted towards the first half of the year when temperatures rise (Figures 3.3b and 3.3c). This earlier-when-warmer pattern is also indicated in the peak timing of *N. pachyderma* (Figure 3.3a). The maximum in the modeled flux of *G. ruber* (white) occurs year-round in the warm waters of the world ocean in the subtropical/tropical regions (Figure S3.2d). In colder waters (e.g., towards higher latitudes), the maximum production of *G. ruber* (white) is reached in late summer/fall (Figure 3.3d). A similar seasonal pattern in the peak timing is evident for the tropical species *T. sacculifer* with peak fluxes occurring year-round at high temperatures in the low latitudes (Figure S3.2e) and in fall when the ambient temperatures are lower (Figure 3.3e). The peak timing of both *G. ruber* (white) and *T. sacculifer* is shifted to later in the year when the surroundings become colder (Figures 3.3d and 3.3e).

Although seasonal changes in the modeled foraminiferal peak fluxes with temperature are evident, all five species exhibit an almost constant peak amplitude (i.e., the maximum concentration divided by the annual mean) in their preferred habitat, which is, i.a., limited by temperature. Outside their preferred living conditions the peak amplitudes increase for most of the species considerably (Figure 3.3). For the warm-water species *G. ruber* (white) and *T. sacculifer*, peak amplitudes rise when the ambient temperatures fall below 20°C (Figures 3.3d and 3.3e). The peak amplitudes of both *N. incompta* and *G. bulloides* increase with temperatures falling below 5°C (Figures 3.3b and 3.3c). Additionally, with temperatures exceeding 25°C the peak amplitude of *N. incompta* increases (Figure 3.3b). For the cold-water species *N. pachyderma*, the relation between peak amplitudes and mean annual temperatures is more complex (Figure 3.3a).

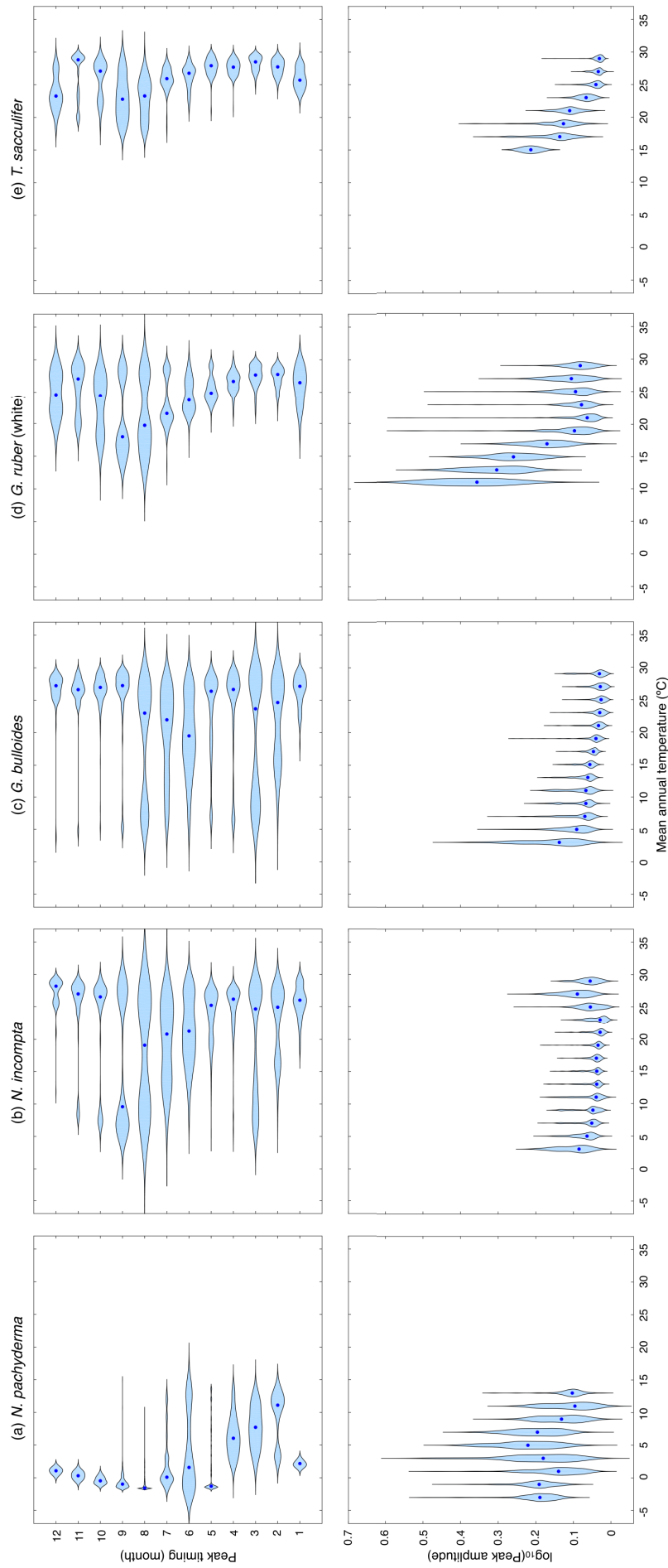


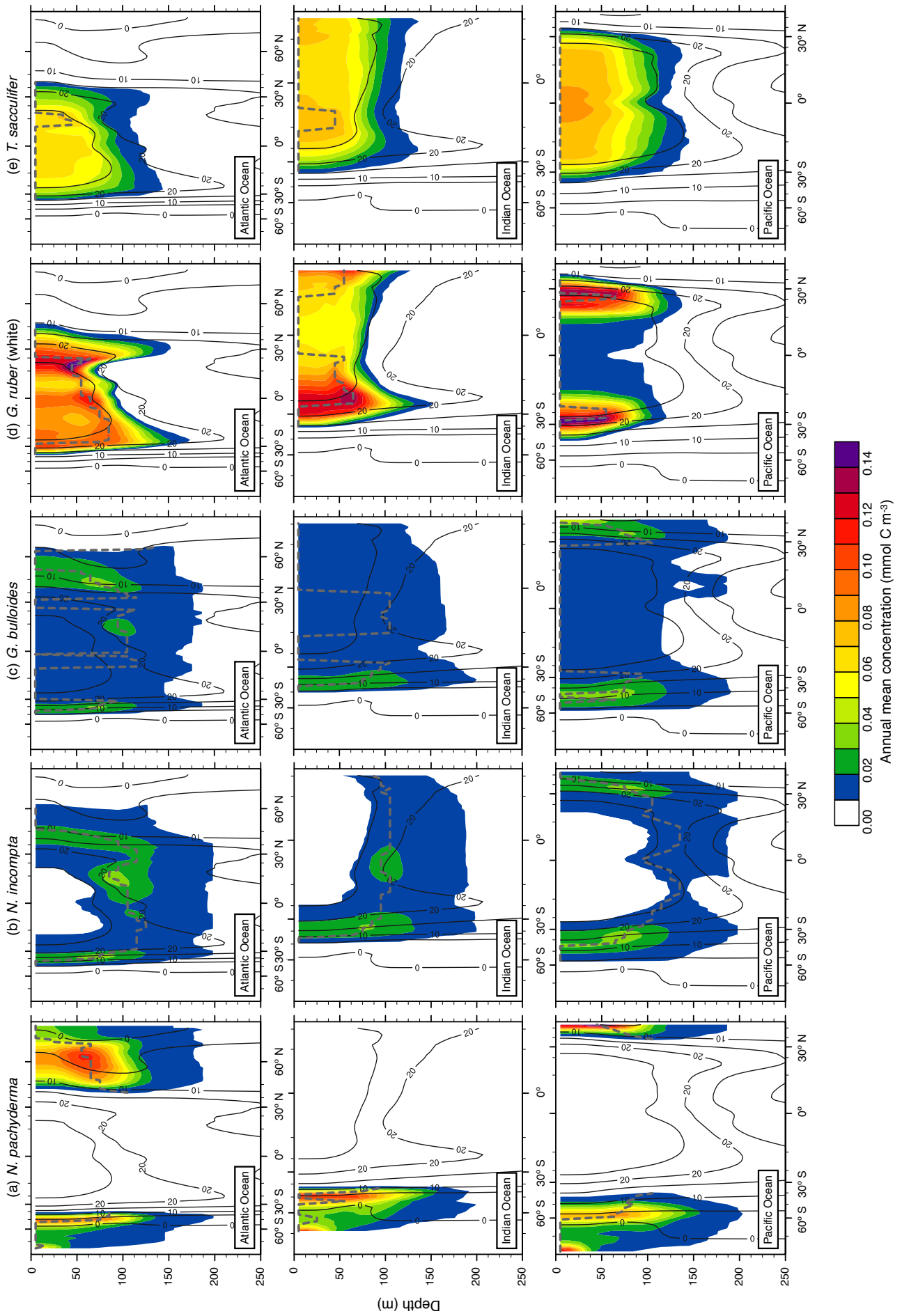
Figure 3.3: Violin plots showing the dependence of the modeled peak timing (top row) and/or the modeled peak amplitude (bottom row) on the annual mean temperature (in °C) averaged over the top 55 m of the water column for (a) *N. pachyderma*, (b) *N. incompta*, (c) *G. bulloides*, (d) *G. ruber* (white), and (e) *T. sacculifer*. The blue dots represent the respective median values. The modeled peak timing is given in months and the modeled peak amplitude has been log-transformed. Note that the peak timings of each species from the southern hemisphere have been transformed to northern hemisphere equivalents by adding or subtracting 6 months.

3.3.3 Modeled Vertical Distribution

Among the three major ocean basins the modeled vertical distribution of each considered planktonic foraminiferal species shows similar patterns in the annual mean (Figure 3.4). The temperate/cold-water species (i.e., *G. bulloides*, *N. incompta*, and *N. pachyderma*) occur in the surface to subsurface layers up to 200 m water depth (Figures 3.4a, 3.4b and 3.4c). *Neogloboquadrina pachyderma* is consistently present in the top few 100 m of the water column in the high latitudes and absent in the subtropical/tropical regions. In the polar waters of the three ocean basins, maximum annual mean concentrations are found close to the surface and subsequently descend with depth toward lower latitudes. The highest annual mean concentrations of *N. pachyderma* are, however, located in the subpolar gyres between 0 and 80 m water depth (Figure 3.4a). *Neogloboquadrina incompta* is in general present between 60°N and 60°S with the annual mean concentration reaching its maximum at around 100 m water depth. In the mid- to higher latitudes, *N. incompta* is found in the surface to subsurface of the Atlantic, Indian, and Pacific Oceans, but seems to be largely absent in the respective surface layers of the tropics. However, the annual mean concentration increases with depth especially from the subpolar regions toward the equator (Figure 3.4b). As for *N. incompta*, *G. bulloides* has been consistently found from the surface to ~ 200 m water depth between about 60°N and 60°S. Depending on the ocean basin, maximum annual mean concentrations of *G. bulloides* are either mainly reached at the surface (i.e., in the Indian and Pacific Oceans) or at depth (i.e., in the Atlantic Ocean), but also subsurface in the subpolar regions of the three chosen transects (Figure 3.4c).

The warm-water species, *G. ruber* (white) and *T. sacculifer*, are found between the surface of each ocean basin and 100 m water depth, thus occurring in a shallower depth range compared to *N. pachyderma*, *N. incompta*, and *G. bulloides* (Figures 3.4d and 3.4e). Among all five planktonic foraminiferal species, *G. ruber* (white) exhibits the highest annual mean concentrations along the transects (Figure 3.4). This species is confined to the subtropical/tropical regions of the ocean basins with the highest annual mean concentrations occurring between 20° and 30° latitude and the lowest around the equator. Along the transect of the Atlantic Ocean, maximum annual mean concentrations are almost consistently reached at depth between 50 and 80 m, whereas in the Indian and Pacific Oceans, the annual mean concentrations of *G. ruber* (white) reach their maximum at the surface in the low latitudes and at around 60 m water depth at those locations, where the highest abundance of this species is found (Figure 3.4d). *Trilobatus sacculifer* also occurs predominantly between 30°N and 30°S with annual mean concentrations gradually decreasing with depth. Compared to the other planktonic foraminiferal species, *T. sacculifer* exhibits a rather uniform distribution pattern along the different transects with the maximum annual mean concentrations being primarily located at the surface (Figure 3.4e).

Figure 3.4 (facing page): Depth transects of the modeled annual mean concentration (mmol C m^{-3}) along ~ 27°W in the Atlantic Ocean (top row), ~ 71°E in the Indian Ocean (middle row), and ~ 162°W in the Pacific Ocean (bottom row) over the top 250 m for (a) *N. pachyderma*, (b) *N. incompta*, (c) *G. bulloides*, (d) *G. ruber* (white), and (e) *T. sacculifer*. The dashed grey lines mark the depth of the maximum modeled annual mean production for each planktonic foraminiferal species, respectively. The black contour lines indicate the annual mean temperature estimates. The blank areas denote, where a species is absent.



3.3.4 Modeled Seasonal Variability of Habitat Depth

In the model, the depth of maximum production of each considered planktonic foraminifera changes over the course of a year (Figure 3.5). Towards higher latitudes, *N. incompta* and *N. pachyderma* show in general maximum abundances at lower depth levels compared to low and midlatitudes. In polar regions, *N. pachyderma* occurs close to the surface during winter and descends through the water column from spring to summer with maximum abundances being reached at mid-depth in summer. In the subpolar regions, *N. pachyderma* is generally found at deeper depths between 50 and 100 m for almost the entire year except for the winter season, where highest concentrations are reached close to the surface (Figure 3.5a). The depth habitat of *N. incompta* increases from spring to summer and is shallower in winter in the subpolar regions (Figure 3.5b). In the subtropics and tropics, however, *N. incompta* shows highest concentrations consistently below 90 m water depth year-round.

Globigerina bulloides exhibits a relatively shallow habitat along the equator throughout the year (Figure 3.5c). In the subpolar regions, the depth of maximum production of *G. bulloides* varies seasonally and, similar to *N. incompta*, is shallower during winter and deepest during summer. The depth habitat of *G. ruber* (white) is mostly confined to the top 60 m of the water column and seems to be less variable compared to the temperate and cold-water species (Figure 3.5). In the midlatitudes, highest concentrations of *G. ruber* (white) occur close to the surface during the entire year, whereas in the subtropical/tropical regions, this species is most abundant below 20 m and shows a weak seasonal cycle, occurring deeper in late summer/early fall (Figure 3.5d). *Trilobatus sacculifer* exhibits the least variable depth habitat among the five considered species and is consistently found close to the surface above 20 m water depth throughout the year (Figure 3.5e).

3.4 Discussion

3.4.1 Large-scale Patterns

3.4.1.1 Geographical Range of Planktonic Foraminifera Species

The predicted global distribution patterns of the five considered planktonic foraminiferal species are in good agreement with the core-top data (Figure 3.2). *Neogloboquadrina pachyderma* is most abundant in the polar-subpolar waters of the northern and southern hemispheres both in the model and in the core-top samples (Figure 3.2a). This cold-water species dominates the waters north of the Arctic Circle and south of the Antarctic Convergence with relative abundances exceeding 90% and is very rarely found in subtropical/tropical waters, which is also seen in the model output. Bé (1969), Bé and Tolderlund (1971), and Bé and Hutson (1977) showed that *N. pachyderma* mainly occurs in regions with sea surface temperatures (SSTs) below 10 °C, but is also present in the cold-temperate waters of, e.g., the subpolar gyres with relative abundances being reduced to 30-50%. Thus, in areas, which are influenced by warmer waters the abundance of this species decreases gradually. This is especially evident in the eastern North Atlantic Ocean, where the abundance of *N. pachyderma* is reduced to about 50% due to the influence of the warm Atlantic Water, which is transported northward by the North Atlantic Current (NAC) (Husum and Hald, 2012). In line with the observations, the modeled annual mean relative abundances of *N. pachyderma* also decrease

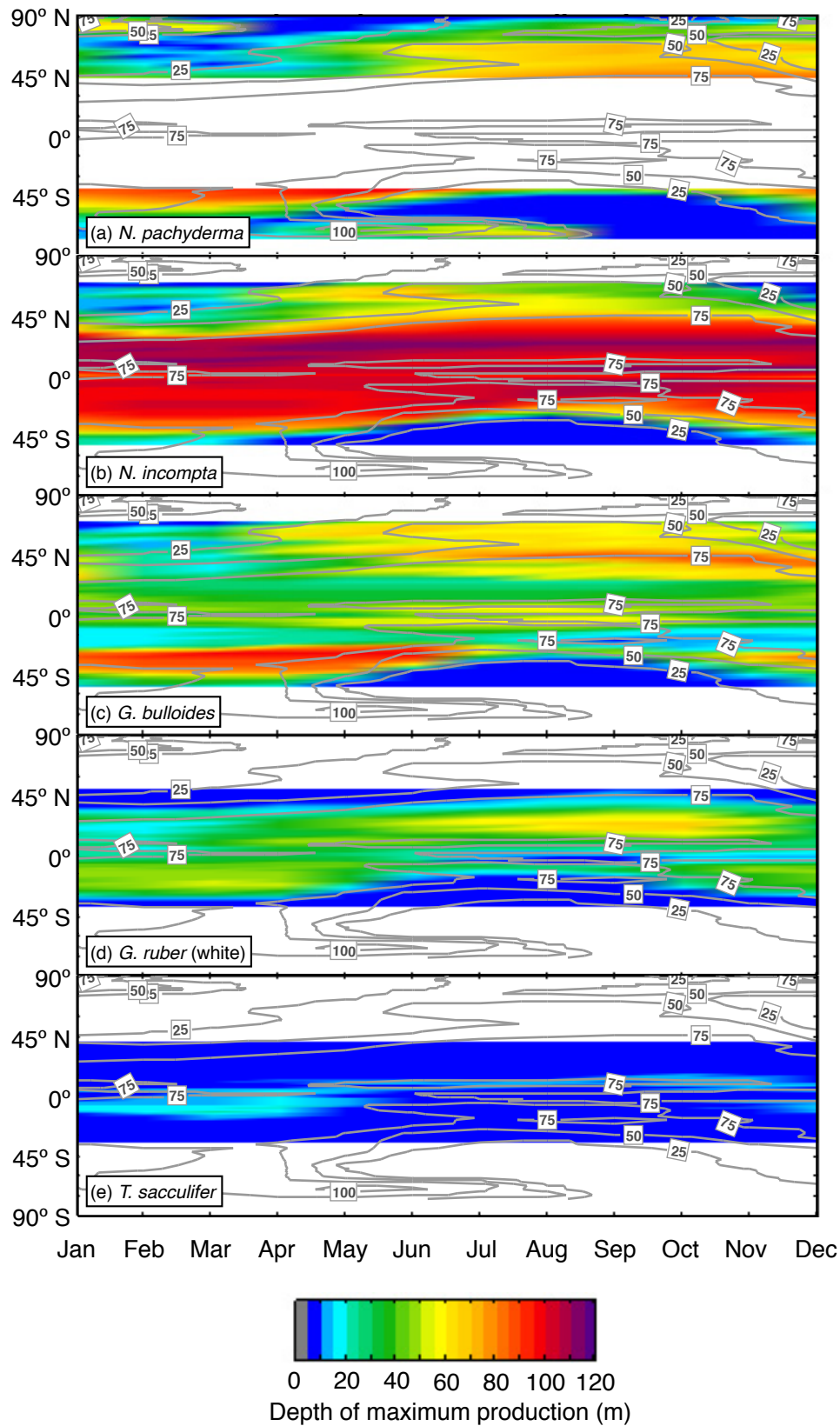


Figure 3.5: Zonal average of the depth (in m) at which the modeled maximum production of (a) *N. pachyderma*, (b) *N. incompta*, (c) *G. bulloides*, (d) *G. ruber* (white), and (e) *T. sacculifer* occurs over time. The grey contour lines indicate the zonal average of the (seasonally varying) depth of the chlorophyll maximum (in m). The blank areas denote, where a species is absent.

with decreasing latitude and, hence, get reduced towards warmer surface waters (Figure 3.2a). However, PLAFOM2.0 overestimates this species' abundance in the eastern North Atlantic (i.e., in the area, which is influenced by the NAC) compared to the core-top data. This model-data-mismatch might partly arise due to the underlying model parameterizations, which are mainly based on the environmental preferences (i.e., temperature tolerance limits) of the *N. pachyderma* genotype found in the Southern Ocean (for more details see *Frailé et al.*, 2008), which differs genetically from the single genotype in the North Atlantic (*Darling et al.*, 2004, 2006). It has been hypothesized that distinct genotypes seem to have different ecological preferences (*de Vargas et al.*, 1999; *Darling et al.*, 2000, 2006; *Stewart et al.*, 2001; *Bauch et al.*, 2003).

The modeled global distribution patterns of *N. incompta* and *G. bulloides* agree in general with the observations (Figures 3.2b and 3.2c). Both species predominantly occur in the subarctic/-antarctic and transitional waters of the world oceans (with relative abundances >50%), where the SST ranges between 10 ° and 18 °C (*Bé and Tolderlund*, 1971; *Bé and Hutson*, 1977). They are also highly abundant in the cool eastern boundary currents off Africa and South America (e.g., *Bé and Tolderlund*, 1971; *Giraudeau*, 1993; *Darling et al.*, 2006) as well as in the eastern North Atlantic and occur continuously in a subantarctic belt between 30 °S and the Antarctic Convergence (*Bé*, 1969; *Bé and Tolderlund*, 1971; *Boltovskoy et al.*, 1996). In addition, high abundances (>40%) of *N. incompta* are evident in the equatorial Pacific upwelling system and of *G. bulloides* in the Arabian Sea. The model predictions for both *N. incompta* and *G. bulloides* also show in accordance with the core-top samples higher abundances in the subantarctic belt (here both species account together for up to 90% of the modeled assemblage) and in the (coastal) upwelling regions of the Atlantic and Pacific Oceans. PLAFOM2.0, however, seems to constantly underestimate the relative abundances in those areas, where the assemblages are usually dominated by those two species according to the core-top data (Figures 3.2b and 3.2c). For instance, in the Benguela upwelling system, *N. incompta* and *G. bulloides* together account locally for >60% of the total planktonic foraminifera population (*Bé and Tolderlund*, 1971; *Giraudeau*, 1993), whereas in the model both species only account for ~ 40% of the assemblage, which is, however, still of the same order of magnitude. Furthermore, in the western Arabian Sea, the modeled annual mean relative abundance of *G. bulloides* ranges between 10 and 20%, which corresponds to the lower end of the observed range varying between 20 and ~ 50% (*Naidu and Malmgren*, 1996). Additionally, it is evident that the model slightly overestimates the species' abundance in the central subtropical/tropical waters of the ocean basins as they are infrequently (<10%) found in the faunal records (Figures 3.2b and 3.2c). These apparent discrepancies arise, on the one hand, due to an overestimation of the modeled annual mean abundances of *G. ruber* (white) especially in the upwelling regions. Secondly, since the model parameterizations are performed on a global scale, distinct genotypes (possibly having different environmental preferences) of *N. incompta* and especially *G. bulloides* (e.g., *Kucera and Darling*, 2002; *Darling and Wade*, 2008) cannot be included in detail in the model potentially resulting in the model-data-mismatch.

The simulated global distribution patterns of *G. ruber* (white) and *T. sacculifer* compare favorably with the core-top samples (Figures 3.2d and 3.2e). Both species dominate the subtropical and tropical waters of the global ocean, together accounting for 75-100% of the total planktonic foraminiferal fauna (*Bé and Tolderlund*, 1971; *Bé and Hutson*, 1977). *Globigerinoides ruber* (white) is the most abundant species in the subtropical areas, where SSTs range between 21 ° and 29 °C, whereas *T. sacculifer* shows highest relative abundances (>50%) in the tropics with SSTs between 24 ° and 30 °C (*Bé and Hutson*, 1977). Additionally, *G. ruber* (white) is also highly abundant (>50%) compared to *T. sacculifer* along the continental margins of the low latitudes (Figures 3.2d and 3.2e). However, in the coastal upwelling regions, *G. ruber* (white)

and *T. sacculifer* are rarely found as cooler water masses influence their usual habitat (e.g., Thiede, 1975). Since both species thrive in warmer waters, their (relative) abundance gradually diminishes when transported towards the higher latitudes, thus being absent in the subpolar/polar regions of the ocean basins. The model predictions for *G. ruber* (white) and *T. sacculifer* show in general similar patterns as the observations with higher loadings in the subtropical and tropical regions and a gradual decrease in the occurrence toward the poles (Figures 3.2d and 3.2e). PLAFOM2.0 is also able to reproduce the dominance of *G. ruber* (white) in the subtropics and of *T. sacculifer* around the equator; and together both species account for >70% of the modeled assemblage in the warm waters of the world ocean. Additionally, the reduction in the (relative) abundances in the upwelling regions (i.e., in the equatorial Pacific and along the coasts of South America and Africa) is likewise captured by the model. However, in those provinces dominated by *G. ruber* (white) and *T. sacculifer*, the relative abundances are underestimated in the model, whereas in the coastal upwelling regions the species' abundances are slightly overestimated compared to the observations. Such deviations may result from the over- and/or underestimation of *G. bulloides* and *N. incompta* in the tropical/subtropical or upwelling regions (Figures 3.2b and 3.2c) or from the coarse model resolution resulting in a misrepresentation of the coastal upwelling regions.

3.4.1.2 Seasonality of Planktonic Foraminifera Species

The meta-analysis of Jonkers and Kučera (2015), which is based on sediment trap data, revealed that the (spatially varying) seasonality of individual planktonic foraminifera is predominantly related to either temperature or the timing of primary productivity. For the temperate and cold-water species, such as *G. bulloides*, *N. incompta*, and *N. pachyderma*, one or two flux maxima have been observed, which occur earlier in the year at higher temperatures. This seasonal pattern is also to a large degree evident in the model results (Figures 3.3a-c and S3.2a-c). At lower temperatures (below 5 °C), the modeled season of maximum production for the cold-water species *N. pachyderma* is predominantly reached in (late) summer, whereas in the comparatively warmer subpolar and transitional waters, the modeled peak season is shifted towards spring (Figures 3.3a and S3.2a). A similar pattern can be observed for *N. incompta* and *G. bulloides*. In line with Jonkers and Kučera (2015), none of the three species shows a clear dependency of the peak amplitude with temperature (Figure 3.3a-c). The temperate and cold-water species exhibit a shift in their peak timing, but do not considerably change their peak amplitude. Hence, the observed and predicted earlier-when-warmer pattern can most likely be sought in the timing of the primary productivity rather than in a temperature dependence. Several studies showed that the seasonality of the temperate and cold-water planktonic foraminiferal species is closely tied to phytoplankton bloom events leading to an increased food supply (e.g., Fairbanks and Wiebe, 1980; Donner and Wefer, 1994; Wolfteich, 1994; Kohfeld et al., 1996; Mohiuddin et al., 2002, 2004, 2005; Northcote and Neil, 2005; Asahi and Takahashi, 2007; Storz et al., 2009; Wilke et al., 2009; Jonkers and Kučera, 2015). In particular, the flux of *G. bulloides* reaches highest values in response to an increased food supply to a large extent associated with open ocean and/or coastal upwelling (e.g., Thiede, 1975; Curry et al., 1992; Wolfteich, 1994; Naidu and Malmgren, 1996; Kincaid et al., 2000; Mohiuddin et al., 2004, 2005; Storz et al., 2009). The warm-water species *G. ruber* (white) and *T. sacculifer* exhibit relatively uniform annual flux patterns with almost no seasonal peak in the subtropical/tropical regions of the ocean basins (e.g., Deuser et al., 1981; Jonkers and Kučera, 2015). Similar to observations, the modeled timing of the low-amplitude peaks is random during the year in warm waters (Figures 3.3d-e and S3.2d-e). However, in colder waters, peak fluxes are concentrated towards fall

and peak amplitudes increase considerably both in the observations and in the model (Figures 3.3d-e and S3.2d-e). This shift in the seasonality can most likely be linked to temperature. In the low latitudes, optimum temperatures prevail all year round, whereas further north-/southward those optimum thermal conditions occur only during a short period later in the year. Thus, those species focus their flux into the warm season in colder waters (Figure 3.3d-e). This emerging behavior is consistent with observations from sediment traps (*Jonkers and Kučera*, 2015) and suggests that the seasonality of the warm-water species is driven by temperature rather than food availability, which is in agreement with observational studies (e.g., *Wolfteich*, 1994; *Eguchi et al.*, 1999, 2003; *Kincaid et al.*, 2000; *Kuroyanagi et al.*, 2002; *Mohiuddin et al.*, 2002, 2004; *Storz et al.*, 2009; *Jonkers and Kučera*, 2015).

3.4.1.3 Spatial and Temporal Variability of Depth Habitats of Planktonic Foraminifera Species

The modeled depth habitats of *N. pachyderma*, *N. incompta*, *G. bulloides*, *G. ruber* (white), and *T. sacculifer* differ among each other and show (distinct) spatial and temporal variability in response to different environmental conditions (Figures 3.4 and 3.5). Plankton tow studies have shown that the vertical distribution of planktonic foraminifera is mostly affected by temperature, primary productivity, light availability, and thermal/density stratification of the upper water column (e.g., *Fairbanks et al.*, 1982; *Ortiz et al.*, 1995; *Schiebel et al.*, 2001; *Field*, 2004; *Kuroyanagi and Kawahata*, 2004; *Salmon et al.*, 2015; *Rebotim et al.*, 2017).

In line with the observations, the modeled depth distribution patterns indicate that the warm-water species *G. ruber* (white) and *T. sacculifer* occur at shallower depths compared to the temperate and cold-water species *G. bulloides*, *N. incompta*, and *N. pachyderma* (see Figures 3.4 and 3.5). In the model, both *G. ruber* (white) and *T. sacculifer* have been consistently found from the surface to ~ 100 m water depth in the subtropical/tropical regions of the ocean basins (Figure 3.4d-e). In the tropics, they are most abundant close to the surface, which agrees well with the observations. In the Arabian Sea and in the central tropical Pacific Ocean, both species have been mostly found in the upper 60 m (*Peeters and Brummer*, 2002; *Watkins et al.*, 1996, 1998). In the transitional and subtropical waters, however, PLAFOM2.0 slightly underestimates the depth habitat of *G. ruber* (white) and *T. sacculifer* (Figures 3.4d-e and 3.5d-e) as they inhabit the upper 125 m in the western North Atlantic (*Fairbanks et al.*, 1980) and/or consistently occur from 0 to 200 m water depth in the subtropical eastern North Atlantic (*Rebotim et al.*, 2017) or in the seas surrounding Japan (*Kuroyanagi and Kawahata*, 2004). Nevertheless, both species typically live close to the surface (above 100 m) (e.g., *Bé and Hamlin*, 1967; *Fairbanks et al.*, 1982; *Kemle-von Mücke and Oberhänsli*, 1999; *Schiebel et al.*, 2002; *Wilke et al.*, 2009; *Rippert et al.*, 2016), thus being associated with a shallow depth habitat, which is reproduced by the model. Since *T. sacculifer* and *G. ruber* (white) are algal symbiont-bearing species, they are most abundant in the photic zone, where light intensities are highest, but also chlorophyll *a* concentrations and temperature control their habitat. Light intensity is especially important for the growth of *T. sacculifer* (*Caron et al.*, 1982, 1987; *Jørgensen et al.*, 1985; *Bijma et al.*, 1990a; *Watkins et al.*, 1998), whereas *G. ruber* (white) seems to be more affected by food availability (*Peeters and Brummer*, 2002; *Field*, 2004; *Kuroyanagi and Kawahata*, 2004; *Wilke et al.*, 2009) rather than light. This would explain why the highest modeled concentrations of *T. sacculifer* occur at shallower depths compared to *G. ruber* (white) (see Figures 3.4d-e and 3.5d-e). In comparison with the temperate and cold-water species, *G. ruber* (white) and *T. sacculifer* are most abundant in the model in waters with temperatures

above 22 °C and absent, where temperature values drop below 15 °C (see Figure 3.4), reflecting the different temperature tolerance limits of the two species.

Neogloboquadrina pachyderma, *N. incompta*, and *G. bulloides* generally thrive in cold to temperate waters. In the model, the depth habitat of those species decreases with increasing latitude (Figure 3.4a-c), indicating a preferred habitat in the subsurface (see Figure 3.5a-c). This is consistent with the observations from several locations, where the three species have typically been found between 50 and 200 m water depth (e.g., *Kohfeld et al.*, 1996; *Mortyn and Charles*, 2003; *Kuroyanagi and Kawahata*, 2004; *Bergami et al.*, 2009; *Wilke et al.*, 2009; *Pados and Spielhagen*, 2014; *Iwasaki et al.*, 2017; *Rebotim et al.*, 2017). In the subtropical to subpolar regions, the highest modeled concentrations of *G. bulloides* occur, however, between 60 and 100 m, whereas in the tropics, maxima are reached close to the surface (Figures 3.4c and 3.5c). This agrees well with the observations: *G. bulloides* has been found to be tightly linked to phytoplankton bloom events occurring either at deeper depth layers associated with a deep chlorophyll maximum (DCM) (*Fairbanks and Wiebe*, 1980; *Mortyn and Charles*, 2003; *Wilke et al.*, 2009; *Iwasaki et al.*, 2017) or in the coastal and equatorial upwelling regions, where a shoaling of the species' habitat towards the near-surface can also be related to high chlorophyll *a* concentrations (*Ortiz et al.*, 1995; *Watkins et al.*, 1998; *Peeters and Brummer*, 2002; *Field*, 2004; *Kuroyanagi and Kawahata*, 2004). *Neogloboquadrina incompta* is also highly abundant, where chlorophyll *a* concentrations are high, but, nevertheless has most often been observed at mid-depth (*Ortiz et al.*, 1995; *Mortyn and Charles*, 2003; *Field*, 2004; *Kuroyanagi and Kawahata*, 2004; *Iwasaki et al.*, 2017; *Rebotim et al.*, 2017). In the model, *N. incompta* shows also highest concentrations between 30 and 120 m (Figures 3.4b and 3.5b), clearly inhabiting the subsurface. This is especially evident in the tropics, where *N. incompta* is absent in the near-surface layers, but present, albeit in low numbers, around 100 m water depth. The predictions show, in general, that *N. incompta* prefers warmer waters compared to *N. pachyderma* and, where the species co-exist, *N. incompta* inhabits for this reason shallower depths (Figures 3.4a-b and 3.5a-b). This agrees with the observations from the subarctic Pacific and the seas around Japan (*Iwasaki et al.*, 2017; *Kuroyanagi and Kawahata*, 2004). *Neogloboquadrina pachyderma* is confined to the high latitudes with peak abundances occurring in the upper 100 m of the water column (*Kohfeld et al.*, 1996; *Stangeew*, 2001; *Mortyn and Charles*, 2003; *Kuroyanagi and Kawahata*, 2004; *Bergami et al.*, 2009; *Pados and Spielhagen*, 2014) (partly associated with high chlorophyll *a* concentrations), which agrees well with the model results. Although *N. pachyderma* has been classified as a “deep dweller” in different studies (*Bé*, 1960; *Boltovskoy*, 1971; *Hemleben et al.*, 1989; *Simstich et al.*, 2003), this species appears to be more surface-restricted at higher latitudes (*Carstens and Wefer*, 1992; *Kohfeld et al.*, 1996; *Mortyn and Charles*, 2003), which is also evident in the model results (Figures 3.4a and 3.5a).

Several studies showed that the depth habitat of planktonic foraminifera varies throughout the year in response to changing environmental conditions. *Rebotim et al.* (2017) identified an annual cycle in the habitat of *T. sacculifer* and *N. incompta* in the subtropical eastern North Atlantic. Both species appear to descend in the water column from winter to spring and reach their deepest habitat in spring to summer before ascending again to a shallower depth towards winter (*Rebotim et al.*, 2017). It has been associated that *N. incompta* is affected by chlorophyll *a* concentrations, hence, the seasonal shift in its habitat depth could be related to food availability as a DCM develops in the summer months. In the Canary Islands region, *G. ruber* (white) and *G. bulloides* have been found at lower depth levels during winter and, during summer/fall, shell concentrations were highest at deeper depths associated with the DCM (*Wilke et al.*, 2009). However, *G. ruber* (white) did occur at moderate abundance levels throughout the year, whereas *G.*

bulloides was only present in low numbers during wintertime in the study area of Wilke et al. (2009). Peeters and Brummer (2002) investigated the influence of a changing hydrography on the habitat of living planktonic foraminifera in the northwest Arabian Sea. During the southwest monsoon (occurring in summer), strong coastal upwelling associated with low SSTs and a near-surface chlorophyll maximum leads to high abundances of *G. bulloides* dominating the species assemblage in the uppermost part of the water column (Peeters and Brummer, 2002). In comparison, during the northeast monsoon (occurring in winter), a relatively warm nutrient-depleted surface mixed layer as well as a DCM develop resulting in high concentrations of *G. ruber* (white) and *T. sacculifer* near the surface, whereas the concentrations of *G. bulloides* are low and show a subsurface maximum between the DCM and the thermocline (Peeters and Brummer, 2002). Based on their findings, Peeters and Brummer (2002) conclude that the habitat depth of individual foraminifera strongly depends on the local hydrography controlling, i.a., the food availability. Watkins et al. (1998) also found high abundances of *G. bulloides* in the equatorial surface waters of the Pacific Ocean associated with higher primary productivity due to an intensified upwelling, but also with the zonal advection by the South Equatorial Current during La Niña conditions. In contrast, during El Niño conditions, *G. bulloides* has been absent in the central tropical Pacific (Watkins et al., 1996) due to unfavorable living conditions.

The change in the depth of modeled maximum production of each considered planktonic foraminifera throughout a year (Figure 3.5) agrees to a large extent with the observations. *Neogloboquadrina pachyderma* is almost constantly found in the subsurface (below 50 m) except during winter, where highest concentrations occur close to the surface (Figure 3.5a). The shift in the habitat depth most likely indicates that *N. pachyderma* is highly dependent on food availability (cf. Figure 3.5a) as this species has been extensively found at mid-depth during summer associated with the chlorophyll maximum (Kohfeld et al., 1996; Mortyn and Charles, 2003; Bergami et al., 2009; Pados and Spielhagen, 2014). The changes from a deeper to shallower depth habitat of *N. incompta* in the subpolar regions over the course of a year could be strongly affected by the food supply by potentially following the seasonal distribution of phytoplankton. In the low latitudes, maximum concentrations of *N. incompta* are constantly reached in the subsurface, which might be attributed to the presence of a permanent DCM (Figure 3.5b) being a characteristic feature throughout the low latitudes (Mann and Lazier, 1996). *Globigerina bulloides*, however, is found year-round close to the surface along the equator (Figure 3.5c), which, in line with the observations, can be associated with equatorial upwelling, but also the inclusion of the photosynthetic growth rate in the model could explain the occurrence of maximum concentration values at lower depth levels due to higher light requirements compared to *N. incompta*. In the subpolar regions, the depth habitat of *G. bulloides* varies seasonally, most likely following the chlorophyll maximum (Figure 3.5c). *Globigerinoides ruber* (white) constantly occurs close to the surface in the midlatitudes due to the prevailing temperature conditions, but in the low latitudes, this warm-water species exhibits a weak seasonal cycle in its depth habitat (Figure 3.5d), indicating its dependence on primary productivity, which agrees with the observations (Peeters and Brummer, 2002; Field, 2004; Kuroyanagi and Kawahata, 2004; Wilke et al., 2009). In line with Kuroyanagi and Kawahata (2004), our results suggest that *T. sacculifer* seems to prefer living in warmer waters than *G. ruber* (white) year-round (Figure 3.5e) and is most abundant at shallow depths, where the light intensity is highest.

3.4.2 Comparison with Local Observations

The emergence of seasonal and vertical habitat patterns consistent with observational data provides important support for our modeling approach, yet a more detailed comparison with observations is warranted to gain further insight into the model behavior. However, when comparing observational data and model output, one has to bear in mind several caveats. These can be broadly categorized into three groups: i) model resolution, ii) model parameterization, and iii) analytical constraints on the observations.

- i) The model resolution has limits on temporal and spatial scales when compared to sediment trap and plankton tow data. Most sediment trap time series span at most a few years and hence represent snapshots that are potentially aliased/biased by inter-annual, seasonal, and/or monthly variability, depending on the deployment time. The model, on the other hand, is forced using climatological data, thus representing a long-term average response that ignores such variability. Similarly, plankton tow samples represent even shorter (i.e., daily) snapshots, thus, not being able to reflect a long-term mean, such that the prevailing environmental conditions during their actual sampling time cannot be fully captured by the model. Additionally, because of the rather coarse resolution of the employed model configuration, only the nearest model grid points rather than the exact locations of the sediment traps and plankton tows (especially along the coast lines) can be considered. Thus, potentially resulting in different environmental conditions influencing the seasonality and depth habitat of planktonic foraminifera compared to the observations. The observational records are, additionally, affected by sub-grid phenomena (such as mesoscale eddies and/or steep gradients in particular near the coast). For instance, Gulf Stream cold core rings transport large planktonic foraminiferal assemblages into the generally nutrient-poor Sargasso Sea (*Fairbanks et al.*, 1980). In addition, *Beckmann et al.* (1987) found that an increase in zooplankton (including planktonic foraminifera) productivity coincided with an increase in phytoplankton biomass in a cold-core eddy in the eastern North Atlantic. Due to the coarse resolution of the underlying model configuration such sub-grid processes are not resolved and their impact cannot be reflected by PLAFOM2.0.
- ii) The underlying model parameterizations are limited in regard to taxonomic resolution and species' ontogeny. Different genotypes of one species could exhibit different habitat preferences (e.g., *Kuroyanagi and Kawahata*, 2004), which is not captured by PLAFOM2.0 since the model parameterizations do not resolve the different known genotypes of some of the considered planktonic foraminiferal species. Several studies from different areas also showed that the main habitat depth of some species increases from the surface to deeper water layers during shell growth (*Peeters and Brummer*, 2002; *Field*, 2004; *Iwasaki et al.*, 2017). This vertical migration of planktonic foraminifera during their ontogeny cannot be reproduced by PLAFOM2.0 as the model parameterizations do not include the individual species' life cycles.
- iii) The analytical constraints regarding the observational records include drift due to (sub-grid) ocean processes, distinction between live and dead specimens, collection depths, and taxonomic agreement among different studies. For instance, a few sediment trap samples might be compromised due to the collection of sinking particles derived from different regions of the surface ocean being transported through eddies and/or ocean currents (*Mohiuddin et al.*, 2004). Strong current velocities sometimes associated with eddies could lead to a tilt in the moored sediment trap resulting in fewer material

being collected by the trap (Yu *et al.*, 2001). The impact of eddies might, thus, hamper the observed season of maximum production of planktonic foraminifera as well as their average living depth. A further uncertainty in the plankton tow data arises from the identification of living cells, because dead cells with cytoplasm collected at depth still appear as living and lead to a shift in the average living depth to greater depth (Rebotim *et al.*, 2017). Uneven sampling intervals of the tows also result in a bias in the observed depth habitat (cf. Figure S3.4). Additionally, a taxonomic consistency within the observational data is assumed, which cannot be guaranteed as different researchers have been responsible for the data collection (see Tables S3.1 and S3.2).

With these caveats in mind, we compare the results of PLAFOM2.0 with 26 sediment trap records and 45 plankton tow samples from all oceans (Figure 3.1b, Tables S3.1 and S3.2). Note that the results of the point-by-point comparative analysis for each site and species are given in the Supplement (see Figures S3.3 and S3.4).

The peak season of the temperate and cold-water species is shifted from late summer in the higher latitudes towards spring at the more equatorward directed locations in the subpolar and transitional water masses both in the model and in the sediment trap records (Figure 3.6a, Table S3.3a). The modeled peak amplitudes of those species remain almost constant at rather low values independent of the considered region. In the sediment traps, however, the peak amplitude values are higher and more diverse and also no clear pattern is evident neither for the species nor for the provinces changing with latitude (Figure 3.6b, Table S3.3b). In line with the plankton tow samples, *N. pachyderma*, *N. incompta*, and *G. bulloides* occur to a large extent in the subsurface from the cold high latitudes to the warmer provinces. However, the modeled ALDs (ranging between 50 and 100 m) are considerably lower than the observed ALDs, which spread over 250 m (Figure 3.6c, Table S3.4). The warm-water species *G. ruber* (white) and *T. sacculifer* occur year-round in the subtropical/tropical regions with no distinct preference for a particular season both in the observations and in the model simulation (Figure 3.6a, Table S3.3a). In the transitional waters, however, their peak fluxes are consistently concentrated into fall, leading to higher peak amplitude values at least in the model (Figure 3.6b, Table S3.3b). Throughout the tropics and subtropics, the modeled peak amplitudes remain constant at low values. In the sediment trap records, however, the peak amplitudes are higher (compared with PLAFOM2.0) and vary within both species and within each province (Figure 3.6b). In the tropics, *G. ruber* (white) and *T. sacculifer* occur primarily close to the surface with ALDs below 50 m both in the model simulation and in the plankton tow records (Figure 3.6c, Table S3.4). In fact, the predicted ALD values (consistently ranging between the surface and 55 m) are lower in comparison with the observations in the transitional and subtropical waters and, accordingly, do not exhibit a similar value range as the plankton tow records.

In general, the point-by-point comparison between the observations and the model simulation reveals that the peak seasons are well predicted by PLAFOM2.0. The predicted peak amplitudes and average living depths also show realistic trends, but the model tends to underestimate the magnitude of these trends (cf. Figure 3.6). Additionally, some sediment trap flux time series of the temperate and cold-water planktonic foraminiferal species show two seasonal peaks a year (cf. Jonkers and Kučera, 2015) (see Figures S3.3 and 3.7a). PLAFOM2.0 is, however, not always able to faithfully reproduce this bimodal pattern (cf. Figures S3.3 and 3.7a). In the following, we try to identify the causes of discrepancies between the observations and predictions by comparing the model output with exemplarily chosen sediment trap records and/or plankton

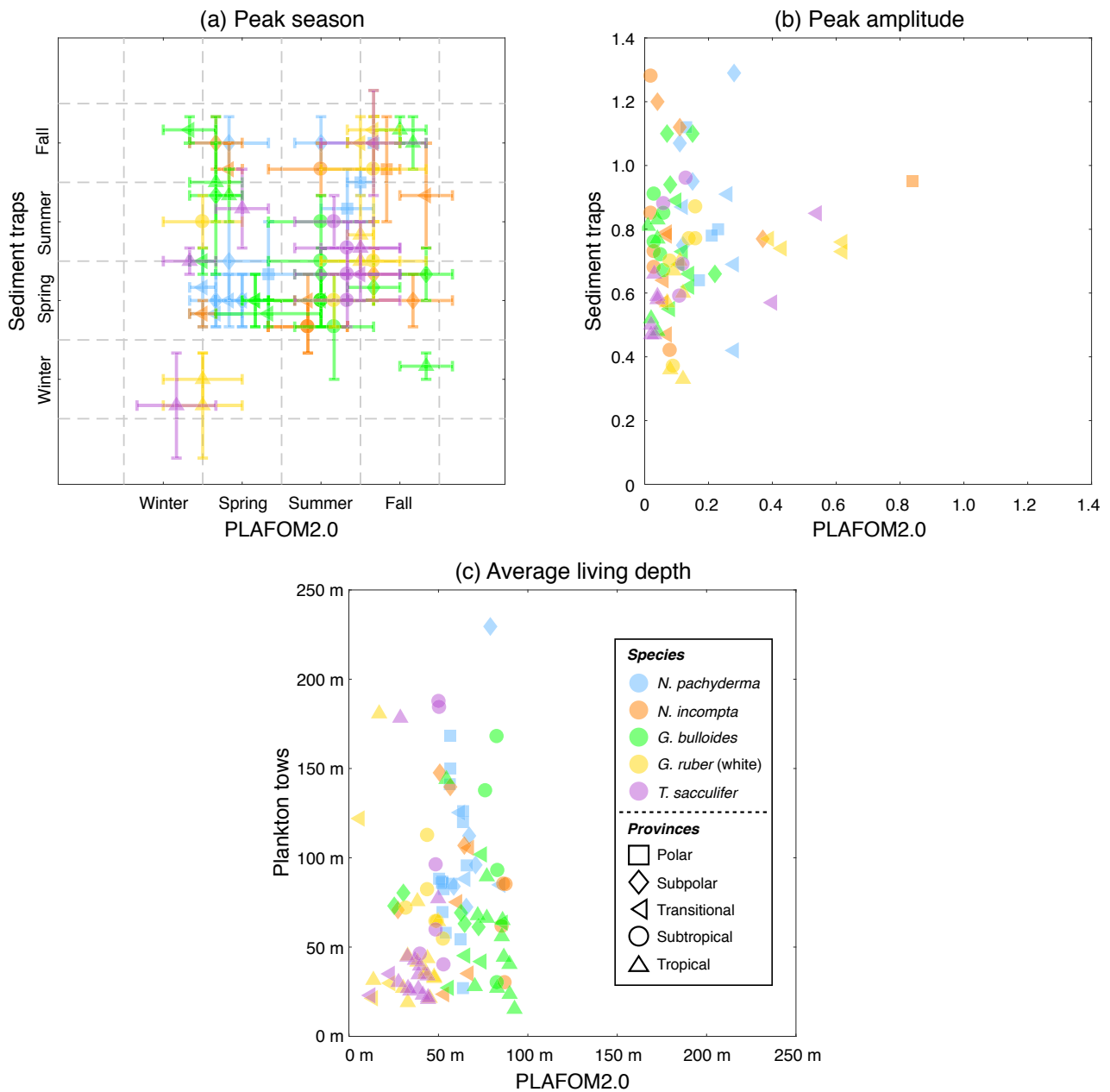


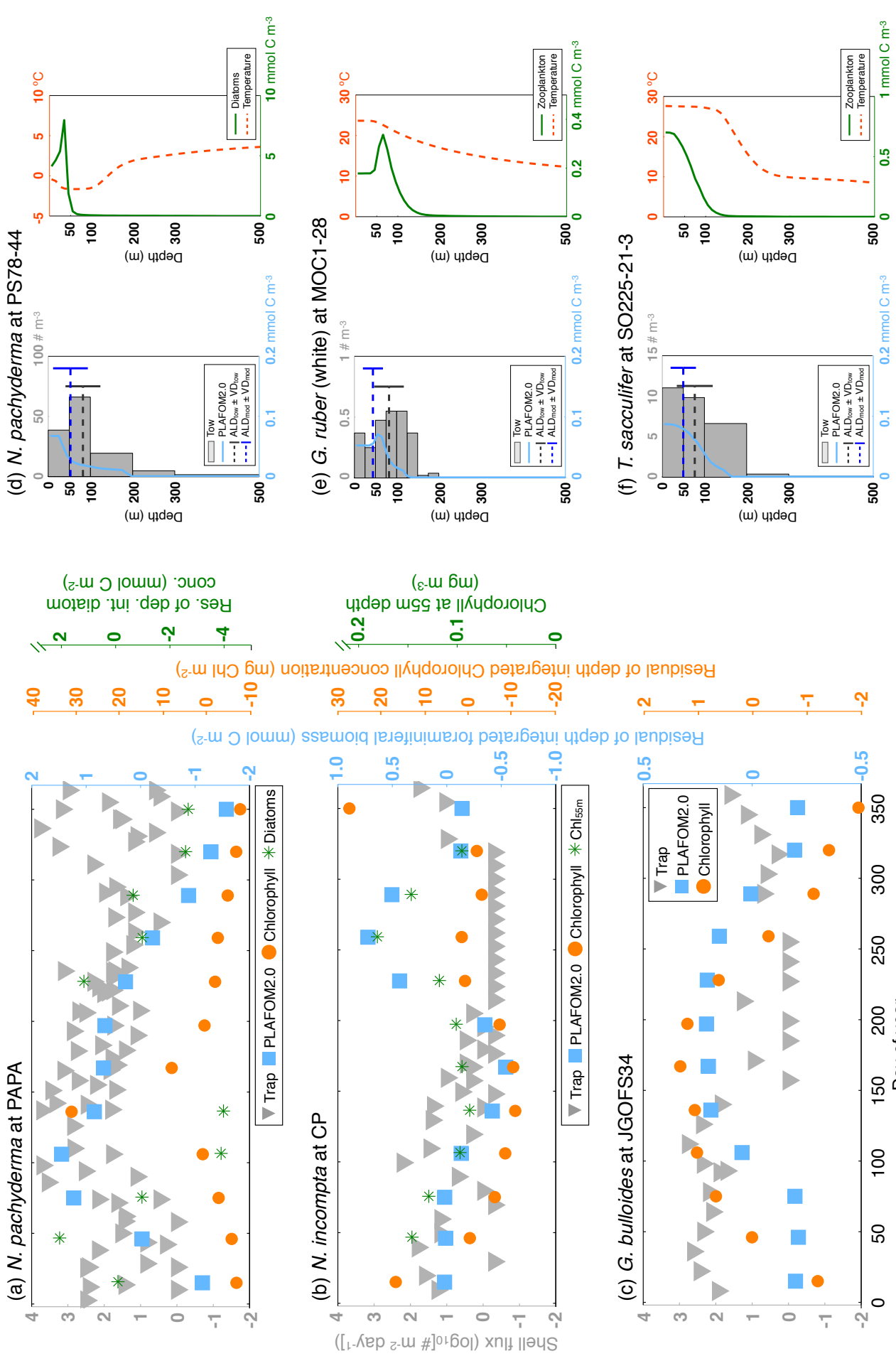
Figure 3.6: (a) Peak seasons (i.e., caloric season of the maximum production), (b) peak amplitudes (i.e., maximum production divided by the annual mean), and (c) average living depths (in m) for *N. pachyderma* (light blue), *N. incompta* (orange), *G. bulloides* (green), *G. ruber* (white) (gold), and *T. sacculifer* (orchid) based on either the sediment trap data (given in Table S3.3) or the plankton tow data (given in Table S3.4) vs. PLAFOM2.0. The symbols represent the polar (squares), subpolar (diamonds), transitional (left-pointing triangles), subtropical (circles), and tropical (upward-pointing triangles) provinces of the ocean, respectively. The symbols in (a) indicate the month corresponding to the mid-season and the error bars refer to the overall time frame given in Table S3.3a.

tow samples of three different locations in each case (Figure 3.7).

The timing of flux pulse(s) of the temperate and cold-water species has, in general, been linked to the timing of the peak in primary productivity (e.g., Fairbanks and Wiebe, 1980; Donner and Wefer, 1994; Wolfteich, 1994; Kohfeld et al., 1996; Mohiuddin et al., 2002, 2004, 2005; Northcote and Neil, 2005; Asahi and Takahashi, 2007; Storz et al., 2009; Wilke et al., 2009; Jonkers and Kučera, 2015). It is known from studies of the North Atlantic Ocean that phytoplankton seasonality changes with latitude, featuring a single spring bloom in the polar and subpolar Atlantic, a bimodal pattern (one large peak in spring, one smaller

peak in fall) in the temperate North Atlantic, a single fall/winter bloom in the subtropical Atlantic, and no prominent seasonal cycle in the tropical Atlantic (e.g., *Colebrook*, 1979, 1982; *Taboada and Anadón*, 2014; *Friedland et al.*, 2016). The ecosystem model (providing the food information for PLAFOM2.0), however, does not faithfully reproduce the observed seasonal cycle in the primary productivity (cf. Figure 4 in *Moore et al.*, 2002a). The simulated (depth integrated) chlorophyll concentration, used as an indicator for productivity, does not show two cycles per year (Figure 3.7a-c). Nevertheless, the peak timings of the (depth integrated) foraminifera concentration follow the maxima in the primary productivity. For instance, the modeled maximum production peak of *N. pachyderma* at site PAPA is preceded by a peak in the diatom concentration (Figure 3.7a), *N. incompta* reaches its maximum in the simulation more likely at depth at site CP following a DCM (Figure 3.7b), and *G. bulloides* predicted peak value at site JGOFS34 occurs slightly after the maximum in the chlorophyll concentration (Figure 3.7c). However, the ecosystem model seems to underestimate the seasonality in the primary productivity, which most likely leads to the model-data-mismatch in the seasonal pattern of the planktonic foraminifera concentration. Additionally, the variability of planktonic foraminifera biomass produced by PLAFOM2.0 is in general too low compared to the observations. This mismatch can either be explained by misrepresentations of the foraminiferal biomass or of the foraminifera response (to the environmental forcing) in the model parameterizations or by an underestimation of the driving factors (i.e., especially the main food sources as outlined above). The depth habitat of planktonic foraminifera depends on several environmental and ontogenetic factors (e.g., *Fairbanks and Wiebe*, 1980; *Fairbanks et al.*, 1982; *Schiebel et al.*, 2001; *Simstich et al.*, 2003; *Field*, 2004; *Salmon et al.*, 2015; *Rebotim et al.*, 2017). The simulated vertical distribution patterns can also be related to food availability and temperature (Figure 3.7d-f). For instance, at station PS78-44, peak abundances of *N. pachyderma* are reached in the top 50 m in the model corresponding to the highest diatom concentrations (Figure 3.7d). At station MOC1-28, the predicted depth profile of *G. ruber* (white) coincides with the vertical distribution pattern of zooplankton with both their maxima being reached at 55 m (Figure 3.7e). At station SO225-21-3, the modeled species' concentration of *T. sacculifer* decreases gradually with depth following the zooplankton distribution, but also temperature (Figure 3.7f). However, the simulated depth profiles differ from the observations, which is also indicated by the differences in the ALDs. In PLAFOM2.0, the foraminiferal species do not occur below 200 m water depth (cf. Figures 3.4 and 3.7d-f) most likely being restricted through food availability. Thus, depending on the vertical resolution of the sampling intervals of a plankton tow sample the predicted ALD is very likely lower by several meters than the observed ALD. In

Figure 3.7 (facing page): (a-c) Comparison of export planktonic foraminiferal shell fluxes in sediment traps (grey triangles) with the residuals (i.e., the deviation from the mean) of the depth integrated modeled foraminiferal biomass (light blue squares). Note that the difference in the units between sediment trap data ($\log_{10}[\# \text{ m}^{-2} \text{ day}^{-1}]$) and model output (mmol C m^{-2}) does not affect the assessment of peak timing. The orange circles denote the residuals of the depth integrated modeled chlorophyll concentration (in mg Chl m^{-2}), and the dark green asterisks indicate in (a) the residuals of the depth integrated modeled diatom concentration (in mmol C m^{-2}) and/or in (b) the modeled chlorophyll concentration (in mg m^{-3}) at 55 m water depth. (d-f) Comparison of the vertical distribution of live specimens in plankton tows (in $\# \text{ m}^{-3}$; grey bars) with the modeled foraminiferal concentration over depth (in mmol C m^{-3} ; light blue profiles). The dashed dark grey and blue lines indicate the average living depth (in m) and vertical dispersion calculated for the plankton tows ($\text{ALD}_{\text{tow}} \pm \text{VD}_{\text{tow}}$) and PLAFOM2.0 ($\text{ALD}_{\text{mod}} \pm \text{VD}_{\text{mod}}$), respectively. The dashed red lines denote the predicted temperature profiles (in $^{\circ}\text{C}$), whereas the dark green lines correspond to the modeled vertical distribution of (d) diatoms (in mmol C m^{-3}) and/or (e-f) zooplankton (in mmol C m^{-3}). Data series of (a) *N. pachyderma* at site PAPA, (b) *N. incompta* at site CP, and (c) *G. bulloides* at site JGOFS34. Depth profiles of (d) *N. pachyderma* at station PS78-44, (e) *G. ruber* (white) at station MOC1-28, and (f) *T. sacculifer* at station SO225-21-3. The respective locations of each sediment trap and plankton tow sample are given in Tables S3.1 and S3.2, respectively.



summary, PLAFOM2.0 is able to reproduce the observed species' behavior with regard to time and depth on a local scale, but is strongly dependent on the input variables (e.g., the food sources) provided by the ecosystem model and is, thus, limited in its capability to match the observations.

Keeping the caveats regarding the model resolution, model parameterizations, and analytical constraints on the observations in mind, the model-data-mismatch might, however, be reduced by a higher model resolution (in time and space), which would in turn increase the computational costs. A higher taxonomic resolution of the considered species (resulting in an increased number of passive tracers and likewise degrees of freedom) and by explicitly parameterizing the ontogeny of each individual planktonic foraminifera, thus, by considering the changes in the species' life cycles with depth, could considerably improve the model. The discrepancies between the model and the observations could, additionally, be minimized by including better ecological constraints on planktonic foraminifera species and their habitat, e.g., by introducing more phytoplankton and zooplankton functional groups in the ecosystem model to better resolve species' food preferences, which would, however, result in an increased computational cost. Nevertheless, additional knowledge about the factors controlling the habitat of planktonic foraminifera in time and space based on culturing experiments and field studies are needed for an optimization and better validation of the current model version. PLAFOM2.0, however, represents a major step forward from the previous model version and can be used to assess paleoclimate information in a better way.

3.5 Conclusion

A new version of the dynamic planktonic foraminifera model PLAFOM (PLAFOM2.0) has been developed and combined with the CESM1.2(BGC) model configuration to simulate species-specific seasonal and depth habitats for *N. pachyderma*, *N. incompta*, *G. bulloides*, *G. ruber* (white), and *T. sacculifer* on a global scale. In comparison with the original approach, where only species' concentrations in the surface mixed layer were predicted, PLAFOM2.0 includes a vertical component and, thus, predicts species' distribution patterns in space and time more realistically.

PLAFOM2.0 produces spatially and temporally coherent abundance patterns, which agree well with available observations. The model configuration faithfully reproduces the areal extent of the species. In line with core-top data, the modeled global distribution of each foraminifera changes with latitude. Additionally, PLAFOM2.0 successfully predicts the patterns in the timing of peak fluxes of planktonic foraminiferal species on a global scale. The earlier-when-warmer pattern for the temperate and cold-water species and the flux focusing at low temperatures of warm-water species, as inferred from observations by *Jonkers and Kučera* (2015), have emerged from the model.

Although an explicit parameterization of the vertical dimension is lacking, the model successfully predicts the preferred habitat depth of the individual planktonic foraminiferal species as well as the spatial and temporal variability in the vertical abundance. In accordance with the available observations, the warm-water species *G. ruber* (white) and *T. sacculifer* consistently occur close to the sea surface year-round in the tropics/subtropics, whereas the depth habitat of the colder-water species *N. pachyderma*, *N. incompta*, and *G. bulloides* changes seasonally in the polar/subpolar regions. During the cold season these species occur near-surface, while during the warmer season they descend in the water column to be found at mid-depth most likely following the chlorophyll maximum.

In general, paleoceanographic reconstructions based on planktonic foraminifera are hampered by the fact that the environmental signal preserved in their shells is the result of both habitat and climate change. The two effects are difficult to separate without independent data. PLAFOM2.0 presents a powerful tool to address this issue and can contribute to more meaningful comparisons of climate model results and paleoclimate reconstructions, ultimately aiding to the understanding of mechanisms of climate change.

Code and data availability. All model data can be obtained from the PANGAEA database (www.pangaea.de). The model code is available upon request from the corresponding author (Kerstin Kretschmer, kkretschmer@marum.de).

Competing interests. The authors declare that they have no conflict of interest.

Acknowledgements. We are grateful to Graham Mortyn for providing the plankton tow data from the Atlantic sector of the Southern Ocean. We would like to thank Gerlinde Jung and Jeroen Groeneveld for their helpful advice. This project was supported by the DFG (Deutsche Forschungsgemeinschaft) through the International Research Training Group IRTG 1904 ArcTrain.

Response of marine zooplankton to global warming: insights from modeling planktonic foraminifera species distribution

Kerstin Kretschmer^{1*}, Lukas Jonkers¹, Michal Kucera¹, Pepijn Bakker¹, and Michael Schulz¹

¹MARUM-Center for Marine Environmental Sciences and Faculty of Geosciences, University of Bremen, Bremen, Germany

In the early stage of preparation for submission to *Global Change Biology*²

Contents

4.1	Introduction	70
4.2	Materials and Methods	71
4.2.1	PLAFOM2.0	71
4.2.2	Model Simulations	72
4.3	Results	73
4.3.1	Changes in Oceanic Environmental Conditions	73
4.3.2	Changes in Species Biomass Distribution	74
4.3.3	Changes in Phenology	78
4.3.4	Changes in Vertical Distribution	82
4.4	Discussion	83

²For a Primary Research Article the journal requirements regarding the manuscript format are as follows: Abstract, Introduction, Materials and methods, Results, Discussion, Acknowledgements, and References.

The Earth's climate system is subject to continues change. Over the last century the atmosphere and ocean have warmed considerably, primarily due to anthropogenic influences. These changes have a strong impact on marine ecosystems, affecting the spatial and seasonal distribution of marine microorganisms. Paleoclimate reconstructions based on fossil evidence of marine microorganisms, such as planktonic foraminifera, have shown that individual species respond differently to climate change. Due to their ecological preferences the response is not uniform and, hence, an ecosystem modeling approach could be used to predict how marine zooplankton may respond to global warming. Here we use an ecosystem modeling approach to investigate exemplarily the impact of global warming on the spatial and temporal distribution of five different planktonic foraminifera species. In response to global warming, the total foraminiferal biomass will decrease on a global average. Additionally, the habitat range of individual planktonic foraminifera species is shifted poleward. Warm-water species will benefit most from this warming and will broaden their habitat, whereas the habitat of cold-water species will shrink and will be adjusted to deeper depth levels. The warming of the ocean leads also to a shift in the peak timing of maximum species production, which will occur in large parts of the ocean a few months earlier in the year compared to preindustrial climate conditions. These changes in the spatial and temporal distribution of marine zooplankton species are primarily caused by temperature variations; changes in food availability play only a minor role. The changes in the zooplankton distribution will become even more severe under a stronger global warming.

4.1 Introduction

Over the last century the Earth's climate system changed considerably. Observations reveal that the atmosphere and ocean have warmed significantly since the mid-19th century. This long-term temperature trend can be clearly attributed to anthropogenic influences, although it has been masked by natural climate variability (Huber and Knutti, 2012; Santer et al., 2013). According to the fifth Assessment Report of the Intergovernmental Panel on Climate Change (IPCC, 2013), the upper ocean (0 – 75 m) has warmed by 0.11 °C/decade from 1971 to 2010 due to increasing carbon dioxide (CO₂) concentrations in the atmosphere, influencing the oceanic carbon cycle and likewise marine ecosystems. Although the rapid warming of the climate system over the past century is unique for Earth's history, Earth's climate has been up to 2 °C warmer compared to the preindustrial era during several warm periods of the past few million years (IPCC, 2013, and references therein). Past climate conditions have been reconstructed by using fossil evidence of marine microorganisms. In particular, the marine zooplankton group of planktonic foraminifera has been extensively and most commonly used as paleoceanographic proxy. Their fossil shells have been well preserved in marine sediments, providing an excellent archive for past climate change based on the physical and chemical properties of the foraminiferal calcite shells (e.g., Kucera, 2007). It has been reported that planktonic foraminifera respond to changes in temperature, but also to variations in primary productivity (Fairbanks and Wiebe, 1980; Kohfeld et al., 1996; Watkins et al., 1996, 1998; Mulitza et al., 1998; Peeters and Brummer, 2002; Mortyn and Charles, 2003; Field, 2004; Morey et al., 2005; Žarić et al., 2005; Pados and Spielhagen, 2014; Xiao et al., 2014; Jonkers and Kučera, 2015; Rebotim et al., 2017). This is not surprising, as the growth and distribution of planktonic foraminifera strongly depend on temperature, light intensity, and food availability (Fairbanks et al., 1980, 1982; Hemleben et al., 1989; Bijma et al., 1990a; Watkins et al., 1996; Schiebel et al., 2001; Žarić et al., 2005; Rebotim et al., 2017), and their geographical extent is limited by the species-specific temperature tolerance range. In the past, planktonic foraminifera shifted their habitat due to changes in the ambient conditions (e.g., Bond et al., 1992; Sarnthein et al., 1995,

2003; *Lebreiro et al.*, 1996; *Bard et al.*, 2000; *Pflaumann et al.*, 2003; *Kucera et al.*, 2005; *Eynaud et al.*, 2009). The 20th-century warming trend of the upper ocean already affected the planktonic foraminifera population in parts of the world ocean (e.g., *Field et al.*, 2006; *Spielhagen et al.*, 2011). *Field et al.* (2006) found that in response to anthropogenic climate change the foraminiferal community in the Santa Barbara Basin was subject to a regime shift. Throughout the 20th century, an increase in abundance of tropical and subtropical species has been observed, whereas the abundance of temperate and cold-water species decreased due to ocean warming (*Field et al.*, 2006). Similar observations were made in the Arctic. Over the past ~ 100 years a steep increase of subpolar species, outnumbering polar specimens, has been observed in surface sediment samples of the Fram Strait, which has been related to an increased inflow of warm Atlantic Water advected from the Norwegian Sea (*Spielhagen et al.*, 2011).

Since planktonic foraminifera clearly respond to hydrographic changes, they can serve as a useful indicator for environmental change, aiding to the understanding of how global warming affects marine ecosystems. Climate projections show that the ocean will warm in the top one hundred meters by about 0.6°C to 2.0°C (depending on the Representative Concentration Pathway (RCP) scenario) by the end of the 21st century (*IPCC*, 2013). The response of primary productivity to climate change seems to be more complex and rather difficult to estimate. Depending on stratification, mixed layer depth, temperature, or light it has been projected that primary productivity will either decrease or increase (*Steinacher et al.*, 2010). *Roy et al.* (2015) recently showed that the distribution of foraminiferal abundance and diversity changes under future climate change due to variations in temperature and food availability. Here we use an ecosystem modeling approach to study the impact of global warming (induced by rising CO_2 concentrations in the atmosphere) on the spatial and temporal distribution of planktonic foraminifera. For this, the model has been run for preindustrial climate conditions and for two high CO_2 future emission scenarios, where we considered a doubling and a quadrupling of atmospheric CO_2 concentrations relative to the preindustrial era. Over the past decade atmospheric CO_2 concentrations increased on average by ~ 2.0 ppm/yr (*IPCC*, 2013), exceeding 400 ppm since 2013 (*Monastersky*, 2013), which is more than 40% greater than preindustrial values. Given that CO_2 concentrations continue to rise, potentially even at a higher rate than at present, a doubled preindustrial value will be reached well before year 2100, resulting in an increase of global mean surface air temperatures of more than 1.5°C (relative to preindustrial values) over the next century (*IPCC*, 2013). This indicates the relevance of studying future high CO_2 emission scenarios. Understanding the responses of planktonic foraminifera to future (anthropogenic) climate change can help to better interpret past climate variations recorded in marine sediments and could provide knowledge regarding adaptation strategies for marine microorganisms.

4.2 Materials and Methods

4.2.1 PLAFOM2.0

The planktonic foraminifera model PLAFOM2.0 is based on its predecessor, PLAFOM (developed by *Fraile et al.*, 2008), and predicts the global monthly carbon concentration (in mmol C/m^3) of the following five planktonic foraminifera species: *Neogloboquadrina pachyderma*, *N. incompta*, *Globigerina bulloides*, *Globigerinoides ruber* (white), and *Trilobatus sacculifer* in both the vertical and horizontal plane (*Kretschmer et al.*, 2017). These species belong to the most abundant species of the modern ocean and have additionally

been used in culturing experiments and paleoceanographic reconstructions. PLAFOM2.0 has been embedded into the ocean component of the Community Earth System Model, version 1.2.2 (CESM1.2; Hurrell *et al.*, 2013), with the Biogeochemical Elemental Cycling model developed by Moore *et al.* (2004) being active.

The planktonic foraminifera model is driven by temperature, food concentration (including zooplankton, small phytoplankton, diatoms, and organic detritus), and for the symbiont-bearing species (i.e., *G. bulloides*, *G. ruber* (white), and *T. sacculifer*) also by light availability. The species-specific food preferences and temperature tolerance limits have been derived from culturing experiments or field observations (for details see Fraile *et al.*, 2008). The food sources are computed in the ecosystem model and are instantly passed to PLAFOM2.0 to determine the variations in the foraminifera carbon concentration as follows:

$$\frac{dF}{dt} = (GGE \cdot TG) - ML$$

Here F is the foraminifera carbon concentration, GGE (gross growth efficiency) is the portion of grazed matter incorporated into foraminiferal biomass, TG denotes total grazing (i.e., the growth rate), and ML represents the mortality rate. The growth rate is apart from food concentration and temperature a function of light for the species with symbionts. The mortality rate depends on respiration loss, predation by higher trophic levels, and competition among species. A detailed description of the planktonic foraminifera model is given in Fraile *et al.* (2008) and Kretschmer *et al.* (2017).

4.2.2 Model Simulations

To assess the impact of global warming (induced by changes in the atmospheric CO₂ concentration) on the habitat of planktonic foraminifera, we performed three model simulations with different environmental conditions: The control run (abbreviated as Ctrl) was forced with preindustrial conditions (i.e., with atmospheric CO₂ values of 284.7 ppmv), and the second and third runs with climate conditions corresponding to atmospheric CO₂ concentrations of two (569.4 ppmv; abbreviated as 2xCO₂) or four (1138.8 ppmv; abbreviated as 4xCO₂) times the preindustrial value, which we refer to as global warming experiments. All simulations have been performed with CESM1.2, which is a state-of-the-art fully coupled climate model, consisting of four components representing the atmosphere, ocean, land, and sea ice (Hurrell *et al.*, 2013). Here we used a CESM1.2 configuration with the ocean model being coupled to both the sea ice model and data models for the atmosphere, land, and river routing.

As already mentioned, PLAFOM2.0 has been added as a separate module to the code trunk of the ocean component of CESM1.2, which is the Parallel Ocean Program, version 2 (POP2; Smith *et al.*, 2010; Danabasoglu *et al.*, 2012). Here we used the coarse-resolution configuration of POP2 with a longitudinal resolution amounting to 3.6° and a latitudinal resolution varying between 1° and 2° (Shields *et al.*, 2012). This configuration uses 60 levels in the vertical, whereby the grid spacing is finer near the surface with ten levels in the upper 100 m and increases with depth to 250 m at the bottom. The sea ice component is the Community Ice Code, version 4 (CICE4; Hunke and Lipscomb, 2008; Holland *et al.*, 2012), which uses the same horizontal resolution as POP2.

The preindustrial-control simulation has been initialized from the end of a 1250-year-long ocean-ice-only simulation, which did not include the ecosystem model. This control simulation has in turn been integrated

for 200 years and used a climatological forcing as repeated normal year forcing, whereby heat, freshwater, and momentum fluxes at the sea surface are based on the atmospheric data sets developed by *Large and Yeager* (2004, 2009) and implemented according to the CORE-II-protocol (Coordinated Ocean-ice Reference Experiment) after *Griffies et al.* (2009). The biogeochemical tracer fields have been initialized from the same data-based climatologies as described by *Kretschmer et al.* (2017). A detailed analysis of the control simulation including a thorough comparison with observations is given in *Kretschmer et al.* (2017).

The climatological boundary conditions for the two global warming experiments were derived independently from experiments for preindustrial and doubled/quadrupled atmospheric CO₂ content. Here each of the two global warming experiments (2xCO₂/4xCO₂) was initialized from the end of a 150-year-long fully coupled (but without the ecosystem dynamics included) equilibrium simulation with either an instantaneous doubling or quadrupling of atmospheric CO₂. We note that the control climate of these equilibrium simulations differs from the climate of the 1250-year-long ocean-ice-only simulation, which was used as a spin-up for PLAFOM2.0 embedded in CESM1.2. Specifically the global warming experiments are based on a spin-up without a significant meridional overturning circulation in the Atlantic Ocean. Based on the two equilibrium simulations climatologies for the heat, freshwater, and momentum fluxes at the sea surface have been generated to be used as repeated normal year forcing for the experiments abbreviated as 2xCO₂ and/or 4xCO₂. For both experiments, the biogeochemical tracer fields have been initialized from the same data-based climatologies as for the control run, since no equivalent data corresponding to a doubling or quadrupling of atmospheric CO₂ relative to the preindustrial era are available. Both global warming simulations have been integrated for 200 years to be consistent with the control run.

Since all three simulations are forced and/or initialized based on climatologies, inter-annual variability can be excluded from those experiments. Therefore, it is justified to examine the model output of only one year, in this case of year 200 for all three performed experiments, respectively.

4.3 Results

4.3.1 Changes in Oceanic Environmental Conditions

Planktonic foraminifera species distribution depends to a first order on temperature and food availability. Hence, to understand potential changes in species-specific seasonal and vertical habitats, changes in the environmental conditions should be considered. Here we focus on ocean temperature and the total food concentration (i.e., a combination of zooplankton, diatom, small phytoplankton, and large detrital concentration) averaged over the top 250 m of the water column (i.e., the habitat range of planktonic foraminifera).

In the preindustrial control run, the highest ocean temperatures (> 22 °C) averaged over the top 250 m occur in the subtropical gyres. Towards the poles ocean temperatures gradually decrease and reach values below the freezing point (Figure 4.1a). Under global warming, most parts of the global upper ocean (0 – 250 m) experience a significant warming of more than 2 °C in the 2xCO₂ experiment and of more than 4 °C in the 4xCO₂ experiment (Figure 4.1a). In particular, the subpolar gyres and the Southern Ocean are subject to a large temperature increase. However, in the tropics as well as in the northeastern North Atlantic, a cooling of a few degrees (up to –4 °C) of the upper 250 m of the water column is evident. This cooling is most pronounced in the 2xCO₂ simulation, whereas the strongest warming occurs when a quadrupling of

atmospheric CO₂ is considered (Figure 4.1a).

The total food concentration of the upper 250 m exhibits a rather uniform global distribution pattern in the control run, with lowest values in the Arctic Ocean and highest values in the shallow shelf regions (Figure 4.1b). There is a general tendency of an increase in total food concentration from lower latitudes towards midlatitudes. In the global warming simulations, the total food concentration decreases by up to 50% in the high latitudes. In particular, the Arctic Ocean features a considerable reduction in the total food concentration (Figure 4.1b). The lower and midlatitudes, however, experience almost no change, except for the subtropical and northeastern subpolar North Atlantic, where the total food concentration increases (by up to 50%) in both global warming scenarios relative to preindustrial conditions (Figure 4.1b).

In the control simulation, the peak timing in the total food concentration features a latitudinal pattern. In the polar regions, highest concentrations occur during the warm season (i.e., summer), whereas in the midlatitudes the peak timing is shifted toward earlier in the year and occurs during spring (Figure 4.1c). In the tropics, no clear seasonality is evident. In both global warming experiments, the peak season is shifted by up to 4 months toward later in the year in the subpolar gyre of the North Atlantic and in the Southern Ocean. In the Arctic Ocean and in the subtropical North Atlantic, peak concentrations are reached 2 to 4 months earlier in the year relative to the preindustrial era (Figure 4.1c). In the low latitudes, the peak timing is on average shifted by ± 2 months.

4.3.2 Changes in Species Biomass Distribution

The global annual mean abundance averaged over the top 250 m of the water column of all five planktonic foraminifera species considered in PLAFOM2.0 shows highest values in the subtropical regions. Towards higher latitudes the total species abundance decreases gradually, reaching lowest concentrations in the polar regions (Figure 4.2a). On a global average, the foraminiferal biomass decreases by $\sim 7\%$ during the global warming scenarios compared to the preindustrial era. In both global warming simulations, the species' total abundance decreases by up to 50% in the tropics and, in particular, in the subtropical gyres. A considerable reduction relative to the control run is also evident in the northern North Atlantic and along the Antarctic Convergence, which is more pronounced in the 2xCO₂ experiment compared to the 4xCO₂ simulation (Figure 4.2a). The Southern Ocean experiences a substantial increase in the annual mean biomass, in particular, in the Atlantic and Indian sectors in both global warming experiments. Additionally, the species' total abundance increases between 30° and 45°S as well as in the western subtropical North Atlantic by up to 50% (on average) (Figure 4.2a). In general, the changes in the total annual mean biomass concentration over the top 250 m relative to preindustrial conditions appear to be more pronounced under the 4xCO₂ scenario (Figure 4.2a).

Due to different ecological preferences, each species exhibits specific distribution patterns and responses differently to global warming. In the control simulation, the global modeled abundance pattern of the cold-water species *N. pachyderma* yields highest annual mean absolute abundances in the subpolar regions (Figure 4.2b). Towards the poles and lower latitudes the species' annual mean biomass concentration reduces gradually. In comparison with preindustrial climate conditions, the annual mean absolute abundance of *N. pachyderma* increases by up to 50% in the Southern Ocean and decreases by up to 50% along the Antarctic Convergence and south of the Arctic Circle when a doubling of atmospheric CO₂ (relative

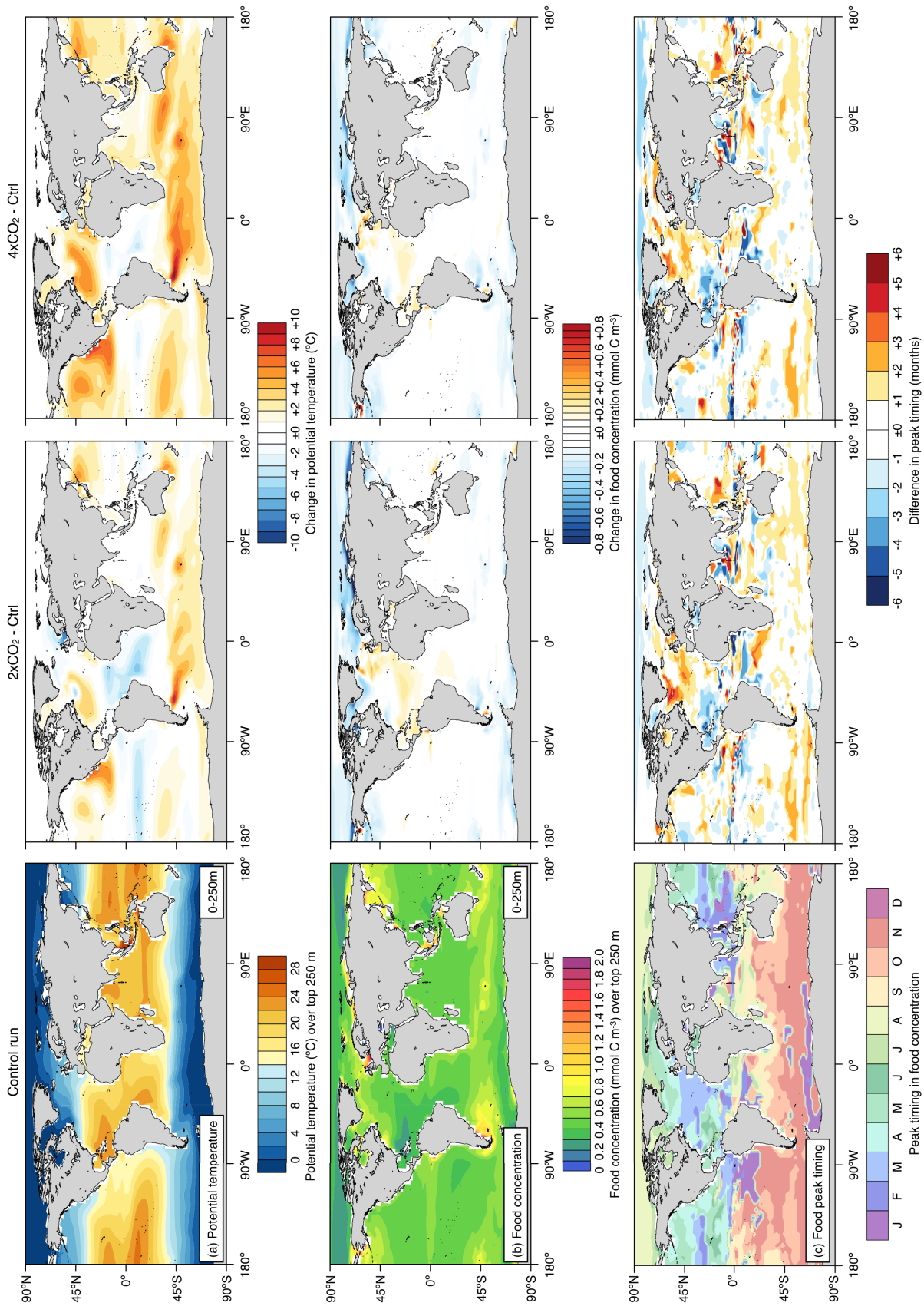


Figure 4.1: (a) Potential temperature (in °C), (b) total food concentration (in mmol C/m³) both averaged over the top 250 m, and (c) the peak timing of the total food concentration for the control run (left column) and the change (i.e., future CO₂ scenario - preindustrial control run) in (a) potential temperature, (b) total food concentration, and (c) the peak timing (in months) (middle column: 2xCO₂-Control; right column: 4xCO₂-Control).

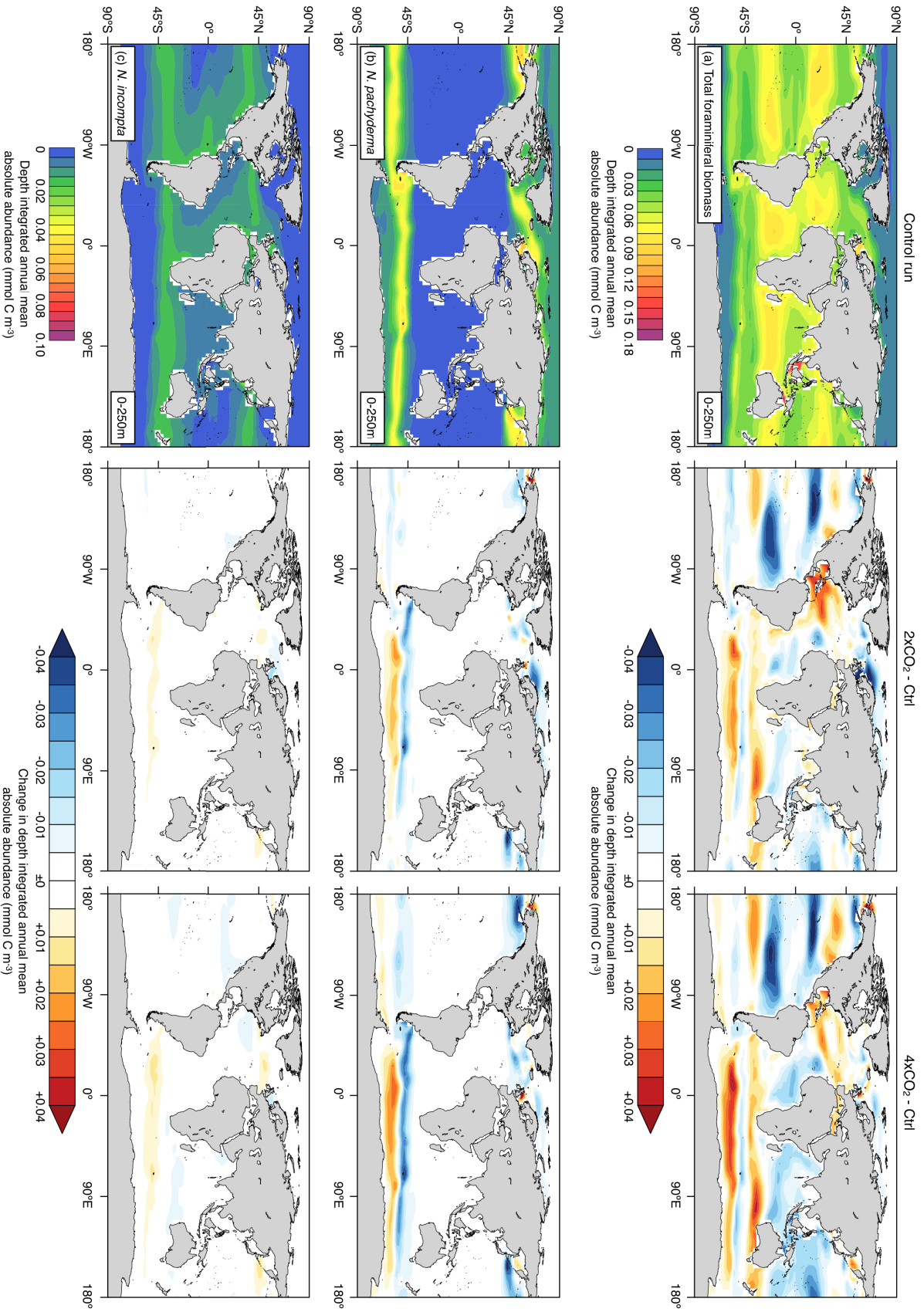


Figure 4.2 (cont. on next page): Abundances of the depth integrated (from the surface to 250 m water depth) modeled annual mean concentration (in mmol C/m^3) for the control run (left column) and the change (i.e., future CO_2 scenario - preindustrial control run) in the depth integrated annual mean abundance (middle column: $2\times\text{CO}_2$ -Control; right column: $4\times\text{CO}_2$ -Control) for (a) the total foraminiferal biomass, (b) *N. pachyderma*, and (c) *N. incompta*.

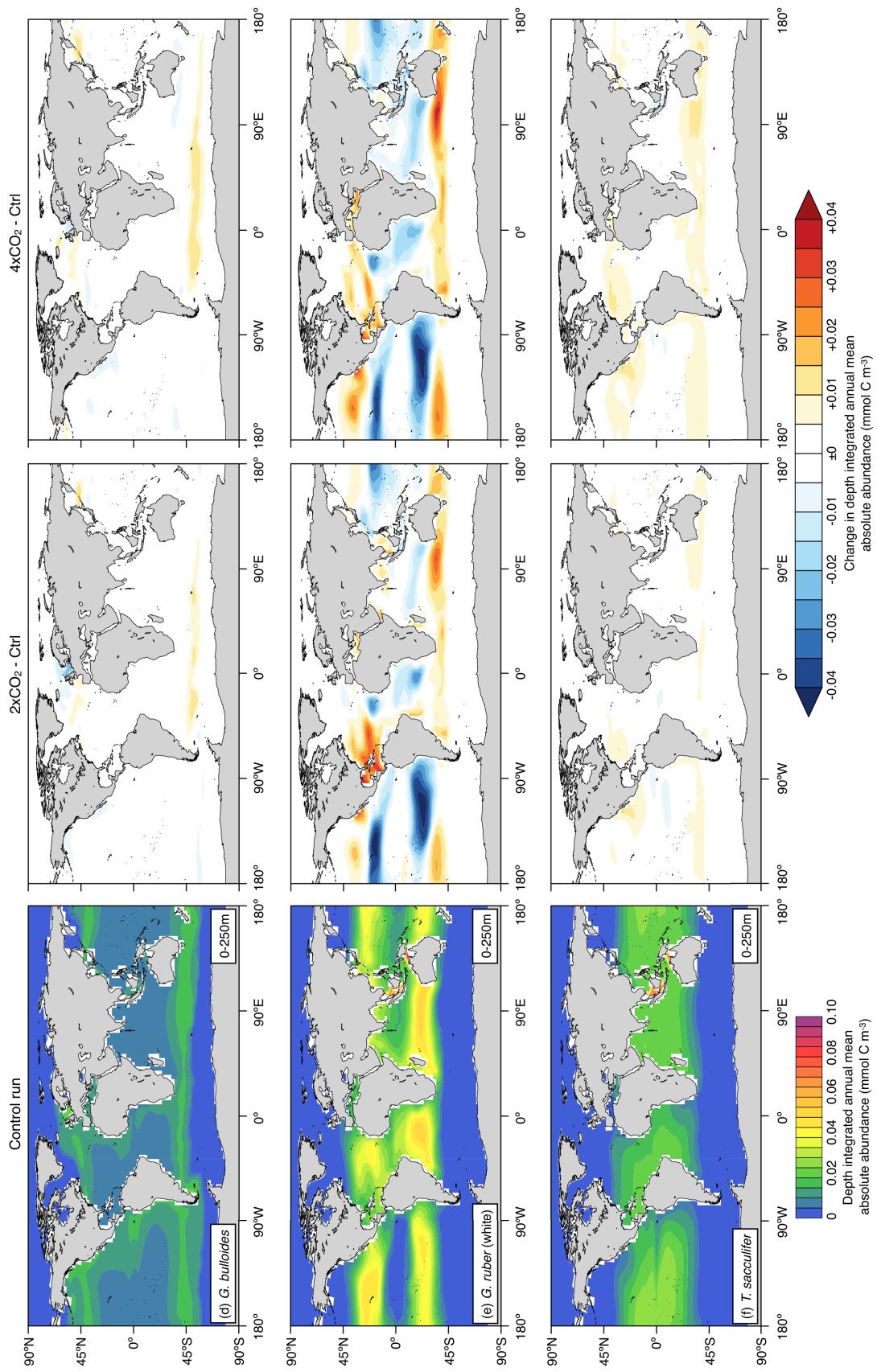


Figure 4.2 (cont.): Same as before for (d) *G. bulloides*, (e) *G. ruber* (white), and (f) *T. sacculifer*.

to preindustrial conditions) is considered. A quadrupling in atmospheric CO₂ leads to an even stronger decrease in this species' annual mean biomass of more than 60% in the midlatitudes and also to a more pronounced increase in the Southern Ocean (Figure 4.2b). The temperate water species *N. incompta* and *G. bulloides* predominantly occur in the subarctic/-antarctic and transitional waters as well as in the coastal and equatorial upwelling regions of the ocean basins in the control run (Figures 4.2c and 4.2d). In the two global warming scenarios, both species' annual mean absolute abundances almost double along the Antarctic Convergence, whereby a quadrupling in atmospheric CO₂ leads to an even higher increase. Both species' annual mean biomass concentrations reduce by up to 60% in few parts of the global ocean with again a higher reduction seen in the 4xCO₂ experiment (Figures 4.2c and 4.2d). The warm-water species, *G. ruber* (white) and *T. sacculifer*, dominate the subtropical and tropical regions of the ocean basins in the control simulation (Figures 4.2e and 4.2f). Both species are less abundant in the oceans' upwelling regions, whereby *G. ruber* (white) seems to be almost absent along the equatorial Pacific cold tongue. In both global warming experiments, *G. ruber* (white) exhibits a considerable loss in its annual mean absolute abundance of up to 80% in the subtropics/tropics, but shows an increase of more than 50% towards the midlatitudes (Figure 4.2e). The annual mean absolute abundance of *T. sacculifer*, however, increases in general in the subtropical and coastal upwelling regions in both scenarios, whereby this species becomes especially more abundant (+50% and more) in the subtropical gyres (Figure 4.2f).

4.3.3 Changes in Phenology

In the control simulation, the highest modeled flux of *N. pachyderma* occurs in spring between 40° and 60° latitude and/or during summer poleward of 60° latitude (Figure 4.3a). During the global warming scenarios, the maximum production occurs a few months earlier in the year in the polar regions, but later in the year in the subpolar gyres and the northeastern North Atlantic (Figure 4.3a). In general, the month of maximum production of *N. pachyderma* is shifted by 3-5 months relative to preindustrial conditions. For *N. incompta* and *G. bulloides* the maximum production is reached during summer in midlatitudes and during spring towards lower latitudes in the control experiment (Figures 4.3b and 4.3c). In the tropics, both species seem to occur year-round with no preference for a particular season. Global warming (due to a doubling or quadrupling of atmospheric CO₂ relative to the preindustrial era) leads to a shift in the maximum production month of *N. incompta* and *G. bulloides*. In the subtropical gyres, both species reach their maximum earlier in the year compared to the control run. In parts of the tropics and in the southern Indian Ocean, the maximum production is shifted towards later in the year when a doubling or quadrupling of atmospheric CO₂ is considered (Figures 4.3b and 4.3c). *Globigerinoides ruber* (white) and *T. sacculifer* occur year-round in the warm waters of the tropics during preindustrial conditions, but towards higher latitudes both species reach their maximum in production in late summer/early fall (Figures 4.3d and 4.3e). Compared to the control simulation, *G. ruber* (white) and *T. sacculifer* both experience a maximum shift in the maximum production of up to 6 months in the tropical regions in the two global warming experiments. For most of the other regions the change in seasonality amounts to ±1 month (Figures 4.3d and 4.3e).

Assessing the zonal averages in the peak timing (i.e., the timing of maximum production) and peak amplitude (i.e., the maximum concentration divided by the annual mean) of each species for each simulation yields first of all that global warming has a stronger effect on the peak timing than on the peak amplitudes (Figure 4.4). Overall, the zonal mean in the peak timing reflects the results of the global seasonality patterns (cf.

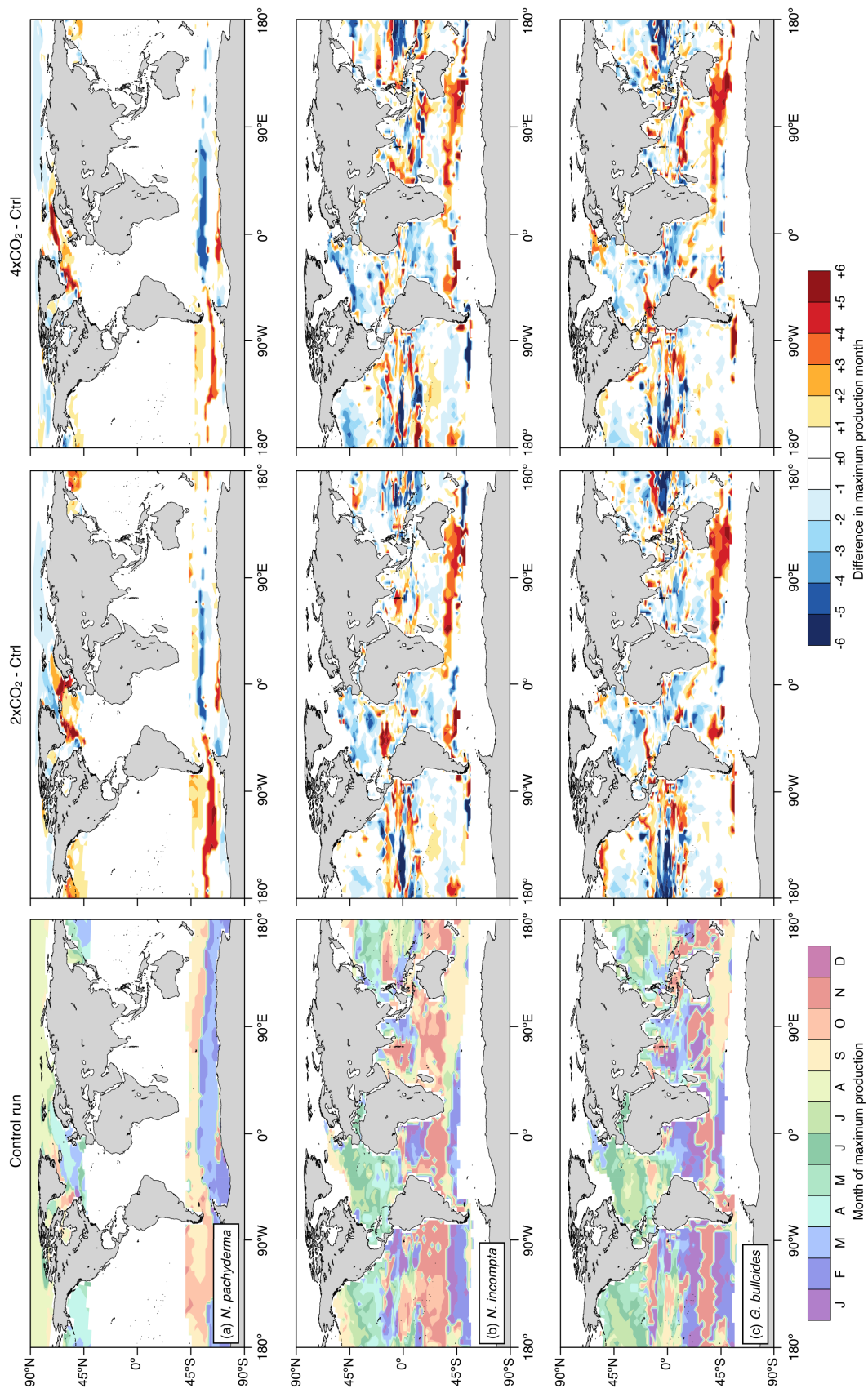
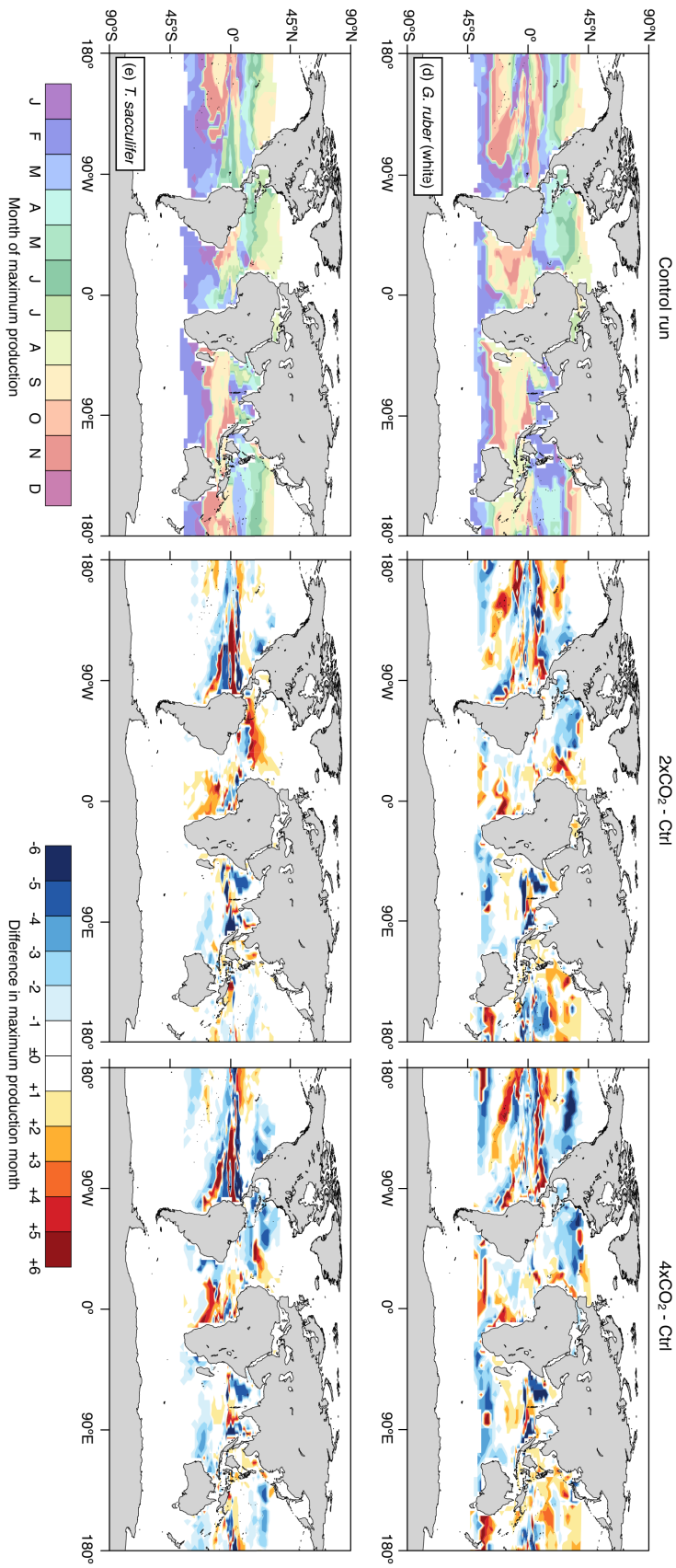


Figure 4.3 (cont. on next page): Maximum production month during the control simulation (left column), and the difference (in months) between the 2xCO₂ experiment and the control run (middle column), and/or the 4xCO₂ experiment and the control run (right column) for (a) *N. pachyderma*, (b) *N. incompta*, and (c) *G. bulloides*. Positive values indicate that maximum production occurs later in the year when a doubling or quadrupling of atmospheric CO₂ is considered relative to preindustrial conditions.



Figures 4.3 and 4.4). For the colder-water species *N. pachyderma*, *N. incompta*, and *G. bulloides* the peak timing occurs during the warm season in higher latitudes and earlier in the year (i.e., during spring) in lower latitudes in the control run (Figure 4.4a-c). In both global warming experiments, the species' peak timing is also shifted by a few months in the zonal average: in colder waters, the maximum production of these species is reached earlier in the year and in warmer waters, partly later in the year relative to preindustrial conditions (Figure 4.4a-c). The warm-water species *G. ruber* (white) and *T. sacculifer* occur year-round in the tropics and focus their peak fluxes into the warm season in colder waters (towards higher latitudes) both in the control simulation and the global warming experiments (Figure 4.4d-e).

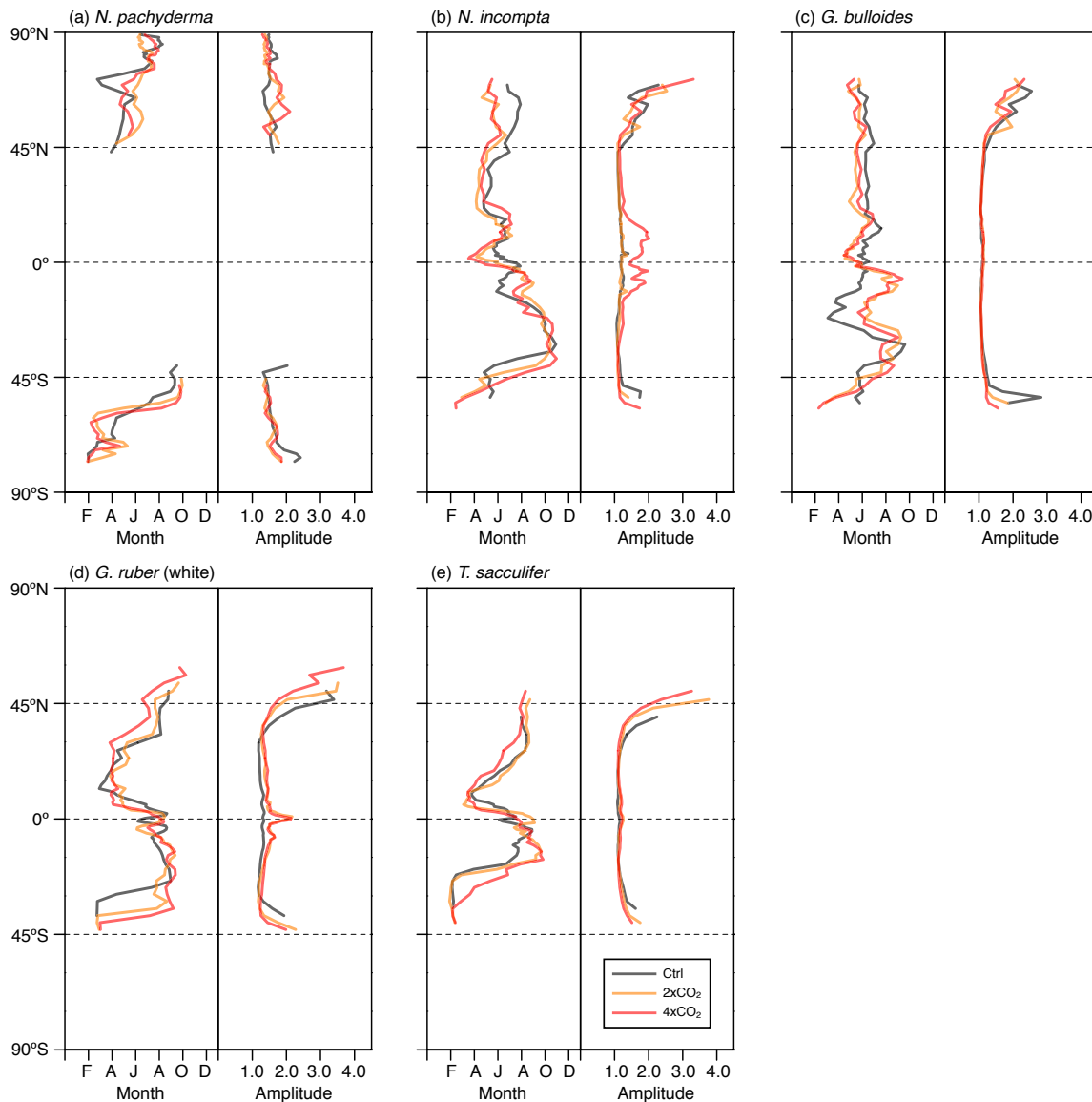


Figure 4.4: Zonal average of the peak timing (i.e., the month of maximum production) and the peak amplitude (i.e., the maximum concentration divided by the annual mean) for the control run (black lines) and the 2xCO₂ (orange lines) and 4xCO₂ (red lines) scenarios for (a) *N. pachyderma*, (b) *N. incompta*, (c) *G. bulloides*, (d) *G. ruber* (white), and (e) *T. sacculifer*.

The zonal average of the peak amplitudes yields relatively low values for the colder-water species, which do not change considerably with temperature and/or latitude in the control run (Figure 4.4a-c). This indicates a rather low seasonal variability in the species abundances. In the control simulation, the warm-water species show low amplitude values in the tropics and subtropics. Outside the low latitudes, the peak amplitude

values increase considerably (Figure 4.4d-e). In general, the variability as well as the zonal distribution of the peak amplitudes of each species are similar to preindustrial conditions under the global warming scenarios (Figure 4.4).

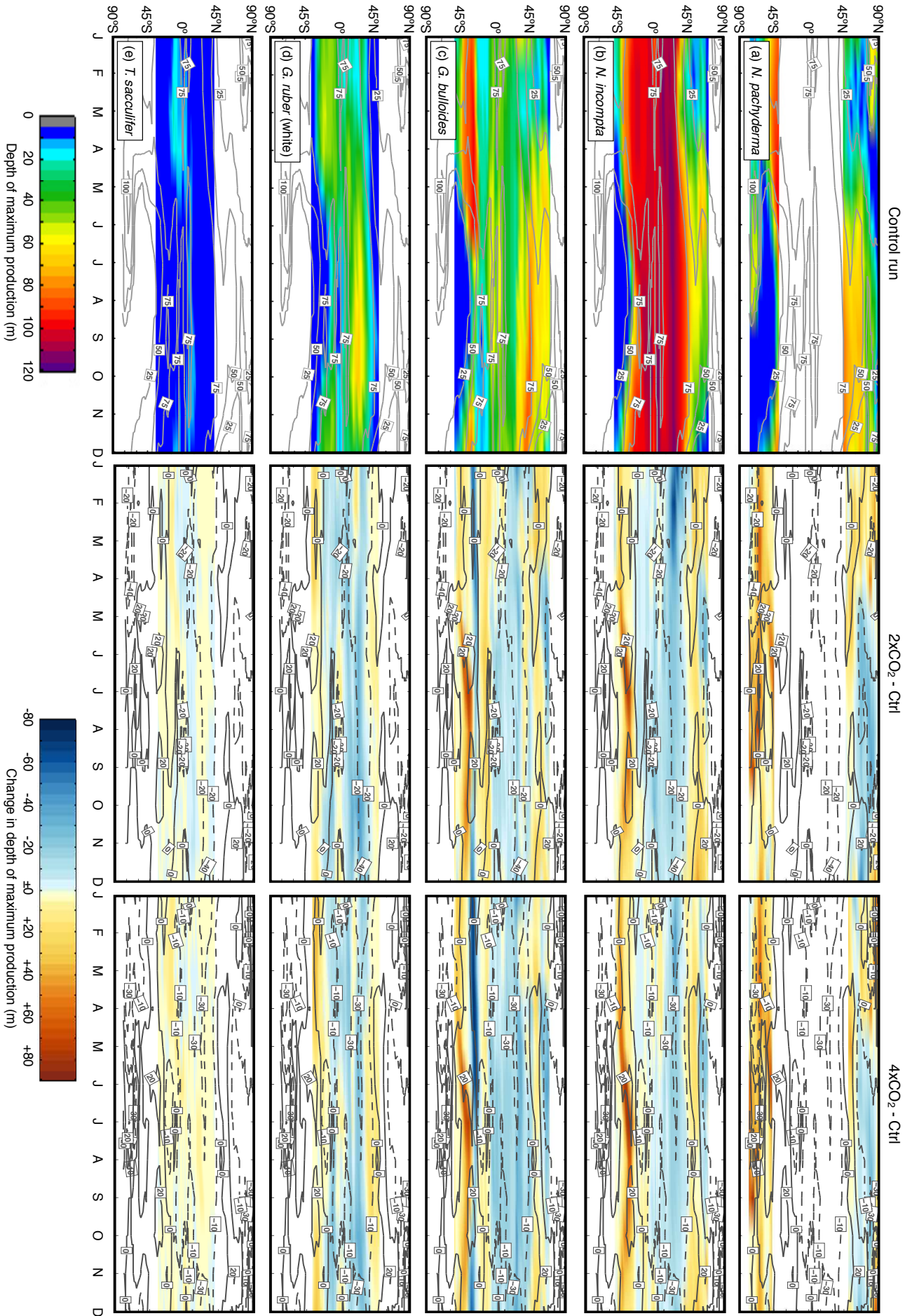
4.3.4 Changes in Vertical Distribution

The cold-water and temperate water species, i.e., *N. pachyderma*, *N. incompta*, and *G. bulloides*, exhibit a seasonal cycle in their depth habitat in the control simulation. *Neogloboquadrina pachyderma* is found close to the surface during winter and at mid-depth in summer in the polar regions (Figure 4.5a). Towards the midlatitudes, *N. pachyderma* reaches its maximum in abundance between 50 and 100 m water depth almost year-round. In both the 2xCO₂ and 4xCO₂ experiments, *N. pachyderma* will descend through the water column to even deeper depths over the course of a year especially in the southern hemisphere. In the northern hemisphere, however, *N. pachyderma* will occur at shallower depth levels, in particular, during summer compared to the control simulation (Figure 4.5a). *Neogloboquadrina incompta* is primarily found at shallower depths during winter and at deeper depths from spring to summer in the subpolar regions during preindustrial conditions (Figure 4.5b). At lower latitudes, *N. incompta* is year-round most abundant below 90 m water depth. In both global warming scenarios, the depth habitat of this species increases in the subpolar regions with the highest increase of up to 90 m occurring between 30° and 45°S, but decreases by on average 20 m in the subtropical/tropical regions relative to the control run (Figure 4.5b). This change is almost consistently evident over the entire year. The depth habitat of *G. bulloides* is in general shallower during winter and deepest during summer in the subpolar regions in the control run (Figure 4.5c). Along the equator, *G. bulloides* is most abundant closer to the sea surface during preindustrial conditions and its habitat will become even shallower during global warming (cf. Figure 4.5c). In the subpolar regions, maximum concentrations of *G. bulloides* will occur at deeper depth levels, in particular, in the southern hemisphere compared to the control run. In the northern hemisphere, the changes are less pronounced and the depth habitat varies on average by ± 10 m. Along 30°S, *G. bulloides* will experience the highest reduction in its depth habitat of about 80 m, in particular, under the 4xCO₂ global warming scenario, thus becoming most abundant close to the sea surface (cf. Figure 4.5c). The warm-water species *G. ruber* (white) shows highest concentration values near the surface year-round in the midlatitudes and exhibits a weak seasonal cycle with a preferred depth habitat below 20 m towards the tropics in the control simulation (Figure 4.5d). Under global warming conditions, the depth habitat of this species becomes slightly deeper in the midlatitudes and shallower in the low latitudes, whereby the changes amount to less than 20 m in both directions (Figure 4.5d). *Trilobatus sacculifer* exhibits almost no seasonal cycle in its depth habitat and occurs year-round close to the sea surface above 20 m during preindustrial conditions (Figure 4.5e). In both global warming experiments, the depth habitat of *T. sacculifer* will not change considerably, only up to a maximum of ± 15 m relative to the control simulation (cf. Figure 4.5e). Even under the global warming scenarios, including the predicted changes in the species-specific depth habitats, *G. ruber* (white) and *T. sacculifer* will still be confined to shallow depth levels, whereas *N. pachyderma*, *N. incompta*, and *G. bulloides* will still preferably occur in the subsurface for most of the year (cf. Figure 4.5).

4.4 Discussion

It is known from present-day observations that planktonic foraminifera highly depend on temperature, food availability, and to a lesser degree on light availability, which is only relevant for symbiont-bearing species (e.g., *Fairbanks et al.*, 1980, 1982; *Bijma et al.*, 1990a; *Watkins et al.*, 1996; *Schiebel et al.*, 2001; *Žarić et al.*, 2005; *Jonkers and Kučera*, 2015; *Rebotim et al.*, 2017). From paleoclimate reconstructions it is known that planktonic foraminifera respond to climate change on spatial and temporal scales (e.g., *Sarnthein et al.*, 1988; *Bond et al.*, 1992; *Broecker*, 1994; *Field et al.*, 2006; *Spielhagen et al.*, 2011; *Stanford et al.*, 2011). It is very likely that planktonic foraminifera will behave similarly in the future. The environmental conditions affecting and/or defining the habitat of individual planktonic foraminifera are subject to continuous change – whether due to natural climate variability or anthropogenic climate change. The increase in ocean temperatures over the last century had a strong impact on marine zooplankton (which includes planktonic foraminifera). Due to global warming individual zooplankton species experienced a poleward shift in their abundance pattern and peak timings occurred earlier in the year (*Richardson*, 2008; *Ji et al.*, 2010; *Mackas et al.*, 2012; *Steinberg and Landry*, 2017). Additionally, community structures/compositions were subject to substantial changes, resulting in changes in the total biomass, whereby some species benefit strongly from the warming and others show a drastic decline up to a total disappearance on a regional scale (*Mackas et al.*, 2012; *Steinberg and Landry*, 2017, and references therein). *Mackas et al.* (2012) suggested that temperature serves as a timing cue for zooplankton and showed that changes in the zooplankton seasonality can be linked to the recent warming trends. It has been projected that some phytoplankton species will decline considerably by the end of the 21st century both in their horizontal and vertical extent (*Jensen et al.*, 2017), which could influence the distribution of planktonic foraminifera substantially. Nevertheless, future climate projections indicate that ocean temperatures will increase in most regions, but primary productivity might either decrease in parts of the ocean or increase depending on stratification, mixed layer depth, light, and/or temperature limitation (*Steinacher et al.*, 2010). Additionally, a temperature increase in the (upper) ocean, as expected for the future, might result in a shift in the timing of phytoplankton bloom events (*Lassen et al.*, 2010) and could likewise alter the abundance and/or occurrence of individual planktonic foraminiferal species. Likewise, in our high CO₂ future emission scenarios, temperatures will rise in large parts of the global ocean (Figure 4.1a). Additionally, the total food concentration (consisting of zooplankton, diatoms, small phytoplankton, and large detritus) might exhibit both a decrease and an increase in response to global warming (Figure 4.1b), which will also induce a shift in the peak timing of several months (Figure 4.1c). Our model results also suggest that in response to a warming ocean (Figure 4.1a), the temperate and warm-water species (i.e., *N. incompta*, *G. bulloides*, *G. ruber* (white), and *T. sacculifer*) extend their habitat polewards, while the habitat of the cold-water species *N. pachyderma* shrinks (cf. Figure 4.2), which is in line with *Roy et al.* (2015). Overall, the total foraminiferal biomass will feature a reduction under global warming on a global

Figure 4.5 (facing page): Zonal average of the depth (in m) at which the modeled maximum production of (a) *N. pachyderma*, (b) *N. incompta*, (c) *G. bulloides*, (d) *G. ruber* (white), and (e) *T. sacculifer* occurs over time during the control simulation (left column) and of the change (i.e., future CO₂ scenario - preindustrial control run) in the depth of maximum production (middle column: 2xCO₂-Control; right column: 4xCO₂-Control). The grey contour lines indicate the zonal average of the (seasonally varying) depth of the chlorophyll maximum for the control run (left column) and/or the future change in the depth of the chlorophyll maximum (middle column: 2xCO₂-Control; right column: 4xCO₂-Control), whereby the solid (dashed) lines denote an increase (decrease) in the depth of the chlorophyll maximum. The blank areas indicate, where a species is absent.



average (cf. Figure 4.2a).

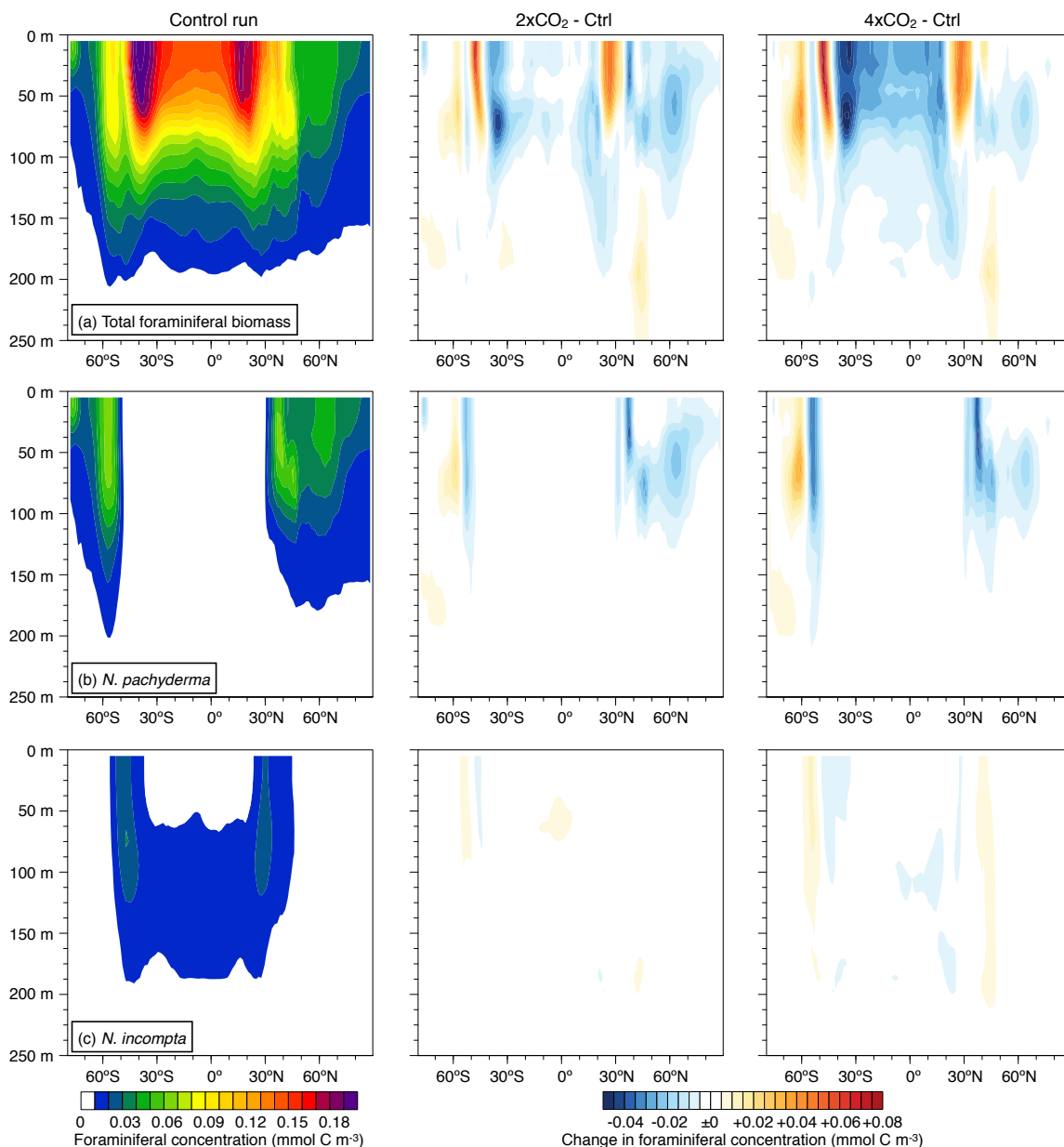


Figure 4.6 (cont. on next page): Zonal average of the modeled annual mean concentration over the top 250 m (in mmol C/m³) of the control simulation (left column) as well as of the change in the annual mean concentration (middle column: 2xCO₂-Control; right column: 4xCO₂-Control) for (a) the total foraminiferal biomass, (b) *N. pachyderma*, and (c) *N. incompta*.

The latitudinal shifts are also reflected in the zonally averaged species depth distribution (Figure 4.6). The total foraminiferal biomass exhibits a broadening in its habitat toward the Southern Ocean, while in the high latitudes of the northern hemisphere a slight decrease is evident (Figure 4.6a). Throughout the tropics and subtropics, the total foraminiferal biomass decreases from the surface to mid-depth, but features a strong increase in the midlatitudes in response to a strong warming (i.e., between 40–60°S and 20–40°N; Figure S4.2a in the supporting information). In those regions, where the strongest warming is predicted (Figure S4.2a), *G. ruber* (white) and *T. sacculifer* exhibit the strongest increase in their abundance throughout the water column (Figures 4.6e and 4.6f), whereas the abundance of *N. pachyderma* decreases (also at depth; Figure 4.6b). In particular, *G. ruber* (white) clearly features a shift in its habitat regime, whereby

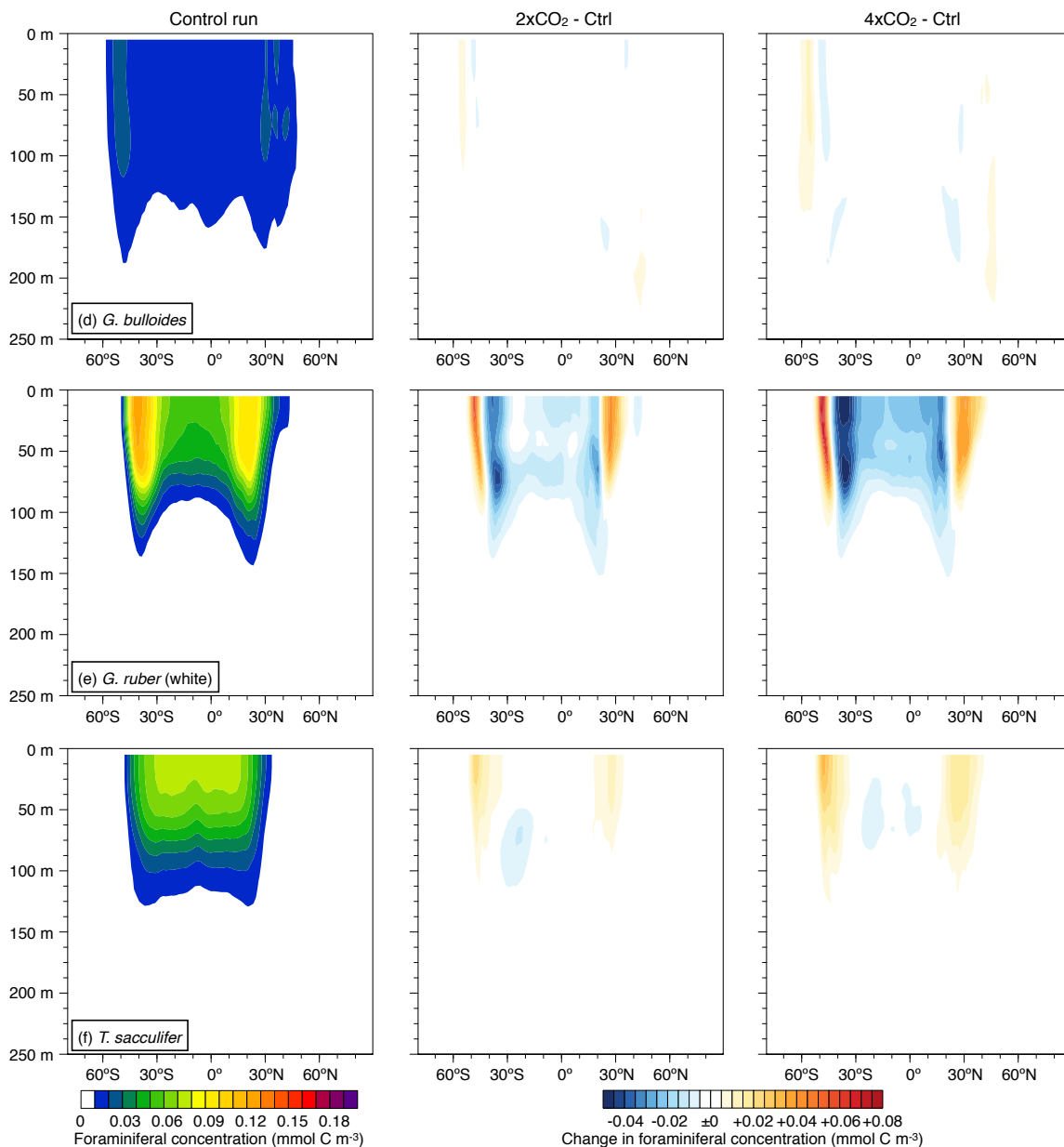


Figure 4.6 (cont.): Same as before for (d) *G. bulloides*, (e) *G. ruber* (white), and (f) *T. sacculifer*.

this species becomes slightly less abundant in the tropics/subtropics, but more abundant in the midlatitudes (Figure 4.6e). *Neogloboquadrina incompta* and *G. bulloides* also show a latitudinal broadening in their habitat throughout the water column along with a slight increase in their abundance (where the highest temperature increase is expected), which is much less pronounced compared to *G. ruber* (white) and *T. sacculifer* (cf. Figures 4.6c and 4.6d). In line with Roy *et al.* (2015), temperature seems to dominate the latitudinal shifts in the foraminiferal abundance (cf. Figures 4.1a, S4.2a, 4.2, and 4.6), whereas food availability does not seem to contribute to a large extent to these shifts as it does not change under the global warming scenarios in such a manner to alter the individual species habitat range (cf. Figures 4.1b, S4.1, and S4.2).

The zonal averages of foraminiferal abundance, temperature, and food availability over the top 250 m of the water column reveal similar results. The warm-water species respond strongly to changes in temperature, while the temperate and cold-water species are also slightly affected by alterations in the food availability

(cf. Figure 4.7, Table 4.1). In the zonal mean, *T. sacculifer* becomes less abundant in the tropics, but its annual mean relative abundance increases by up to 10%, because the annual mean relative as well as absolute abundances of *G. ruber* (white) decrease in the global warming scenarios (cf. Figures 4.7d and 4.7e). In the midlatitudes (between 30° and 45° latitude), the annual mean relative and absolute abundances of *G. bulloides* and *N. incompta* decrease, while *G. ruber* (white) and *T. sacculifer* increase (Figure 4.7b-e). Towards the higher latitudes, the dominance of *N. pachyderma* decreases, whereby *N. incompta* and *G. bulloides* become more abundant especially poleward of 45° latitude (Figure 4.7a-c). In comparison with the other species, *N. pachyderma* experiences the most pronounced changes, whereby its annual mean relative abundance reduces for example by up to 30% (Figure 4.7a). The zonal changes in the species' annual mean (relative/absolute) abundances due to global warming differ only slightly among the two future high CO₂ emission scenarios. However, in the 4xCO₂ experiment the deviations from the control simulation are unsurprisingly somewhat higher (cf. Figure 4.7). For the warm-water species (*G. ruber* (white) and *T. sacculifer*) the changes in the zonal mean are driven by the ocean temperature variations induced by the increase in atmospheric CO₂ (cf. Table 4.1). In the midlatitudes, the increase in abundance of *T. sacculifer* and *G. ruber* (white) follows, in particular, rising temperatures. The projected changes in food availability (we refer here to the main food source, i.e., zooplankton) and/or primary productivity (here indicated by chlorophyll concentration), which are most pronounced in the northern high latitudes, do not contribute to the projected variations of *T. sacculifer* and/or *G. ruber* (white) (cf. Figure 4.7d-e). However, regarding its depth habitat *G. ruber* (white) seems to respond to changes in the primary productivity at least in the tropical regions (Figure 4.5d). Based on plankton tow samples, it was shown that *G. ruber* (white) depends in parts on primary productivity (Peeters and Brummer, 2002; Field, 2004; Kuroyanagi and Kawahata, 2004; Wilke et al., 2009). Hence, a shift in the chlorophyll maximum towards the sea surface in the low latitudes due to global warming could lead to a shallower depth habitat of *G. ruber* (white) (Figure 4.5d). The warming of the upper ocean in the subtropical and temperate climate zones (Figures 4.1a and S4.2a) results, however, in a deepening of the depth habitat of *G. ruber* (white) as well as of *T. sacculifer* (Figures 4.5d and 4.5e). *Trilobatus sacculifer* exhibits also a slight increase in its depth of maximum production in the tropics in response to rising ocean temperatures. In line with Roy et al. (2015), the warm-water species feature a strong dependence on the ambient temperature, which drives the poleward shift in the species' abundances, but also their vertical shift, in particular, in the subtropics. The predicted zonal change in foraminiferal abundance of the temperate and cold-water species (*G. bulloides*, *N. incompta*, and *N. pachyderma*), however, seems to be mainly driven by temperature and to a lesser extent by food availability (cf. Figure 4.7a-c). The expected temperature increase between 45° and 60° latitude results in a decrease in abundance of *N. pachyderma* and a concurrent increase of *G. bulloides* and *N. incompta*. North of 60°N, the projected changes in the primary productivity and/or in the diatom concentration partly trigger the zonal changes of *N. pachyderma*, *N. incompta*, and *G. bulloides* (Table 4.1). This is also true for the projected changes in the species-specific depth habitats (cf. Figure 4.5a-c). It has been associated that the vertical distribution of the three above mentioned species is affected by chlorophyll a concentrations (Kohfeld et al., 1996; Watkins et al., 1998; Peeters and Brummer, 2002; Mortyn and Charles, 2003; Bergami et al., 2009; Wilke et al., 2009; Pados and Spielhagen, 2014; Rebotim et al., 2017). In line with the projected deepening (shallowing) of the chlorophyll maximum, the depth of maximum production of *N. pachyderma*, *N. incompta*, and *G. bulloides* increases (decreases) (Figure 4.5a-c). However, in parts of the Southern Ocean, *N. pachyderma* deepens its depth habitat during austral summer although the depth of the chlorophyll maximum becomes shallower. This indicates that the warming of the

Southern Ocean (Figures 4.1a and S4.2a) leads to a downward shift in the vertical distribution of this polar species (Figure 4.5a). Likewise, where no change in the chlorophyll maximum is projected, the predicted rise in ocean temperatures results in a deeper depth habitat for the temperate and cold-water species compared to preindustrial climate conditions (Figure 4.5a-c), suggesting more favorable living conditions at depth. Overall, our results suggest that both the colder- and warm-water species respond more likely to changes in temperature rather than in food availability. However, *G. ruber* (white) and *T. sacculifer* show a stronger correlation with temperature than *N. pachyderma*, *N. incompta*, and *G. bulloides* (cf. Table 4.1).

Table 4.1: Correlation of Changes in Foraminiferal Species with Changes in Environmental Parameters^a

	Temperature		Total Food Concentration		Main Food Source ^b	
	Ctrl - 2xCO ₂	Ctrl - 4xCO ₂	Ctrl - 2xCO ₂	Ctrl - 4xCO ₂	Ctrl - 2xCO ₂	Ctrl - 4xCO ₂
<i>N. pachyderma</i>	-0.09	-0.29	0.27	0.14	0.02	0.12
<i>N. incompta</i>	-0.14	0.21	0.33	-0.09	0.19	0.11
<i>G. bulloides</i>	-0.34	-0.13	0.33	0.05	0.29	0.22
<i>G. ruber</i> (white)	0.64	0.68	-0.26	-0.34	-0.27	-0.45
<i>T. sacculifer</i>	0.84	0.78	-0.26	-0.28	-0.15	-0.19

^a Change between future high CO₂ emission scenarios (2xCO₂, 4xCO₂) and the preindustrial control simulation (Ctrl) over the top 250 m. Note that for the calculation of the correlation only those points have been considered, where the foraminiferal concentration changes over the top 250 m due to global warming.

^b For *N. pachyderma*, *N. incompta*, and *G. bulloides* diatoms are the main food source and for *G. ruber* (white) and *T. sacculifer* zooplankton.

The projected changes in the environmental conditions also influence the seasonality of the individual planktonic foraminiferal species. The warming of the ocean leads to considerable shifts in phytoplankton bloom events. For instance the spring bloom occurs earlier in the year in the northern high latitudes in response to increasing temperatures (e.g., *Lassen et al.*, 2010). This, in turn, will most likely result in seasonal shifts of the foraminiferal production. All five considered species reach their maximum in production in large parts of their individual habitats earlier during the high CO₂ emission scenarios compared to the preindustrial era (Figure 4.3) due to a warming of the ocean, which reflects the present-day observations of *Mackas et al.* (2012). In the Arctic Ocean, the peak season of *N. pachyderma* is shifted by a few months towards earlier in the year, which is likely due to an earlier phytoplankton bloom (cf. Figure 4.1c). In the northern North Atlantic (north of 45°N), however, *N. pachyderma* exhibits peak fluxes later in the year in the high CO₂ emission scenarios (Figure 4.3a). This can likely be linked to the cooling of the surface ocean in this region (Figure S4.3), which, in turn, facilitates a late phytoplankton bloom (cf. Figure 4.1c). *Kretschmer et al.* (2016) showed that during cold climate conditions (such as during the last glacial period), the seasonal peak in the production of *N. pachyderma* occurs up to 4 months later in the year north of 45°N relative to preindustrial conditions due to a late occurring diatom bloom caused by the prevailing environmental conditions, which supports our findings. The seasonality of the temperate and cold-water species depends primarily on the timing of the primary productivity controlling the food supply (e.g., *Fairbanks and Wiebe*, 1980; *Donner and Wefer*, 1994; *Kohfeld et al.*, 1996; *Asahi and Takahashi*, 2007; *Storz et al.*, 2009; *Wilke et al.*, 2009; *Jonkers and Kučera*, 2015) and, thus, only indirectly on temperature. Hence, the shift in the phenology of those species is closely tied to food availability. *Neogloboquadrina incompta* and *G. bulloides* expand their habitat range in response to a warming ocean; this warming leads to earlier phytoplankton blooms in the subpolar regions and subsequently to earlier seasonal peaks in the foraminiferal production (Figure 4.3b-c). The seasonality of the warm-water species is, however, primarily driven by ambient temperatures (e.g., *Wolfteich*, 1994; *Kuroyanagi et al.*, 2002; *Mohiuddin et al.*, 2002, 2004; *Storz et al.*, 2009; *Jonkers and Kučera*, 2015). In response to rising ocean temperatures, *G. ruber* (white) and *T. sacculifer* shift their

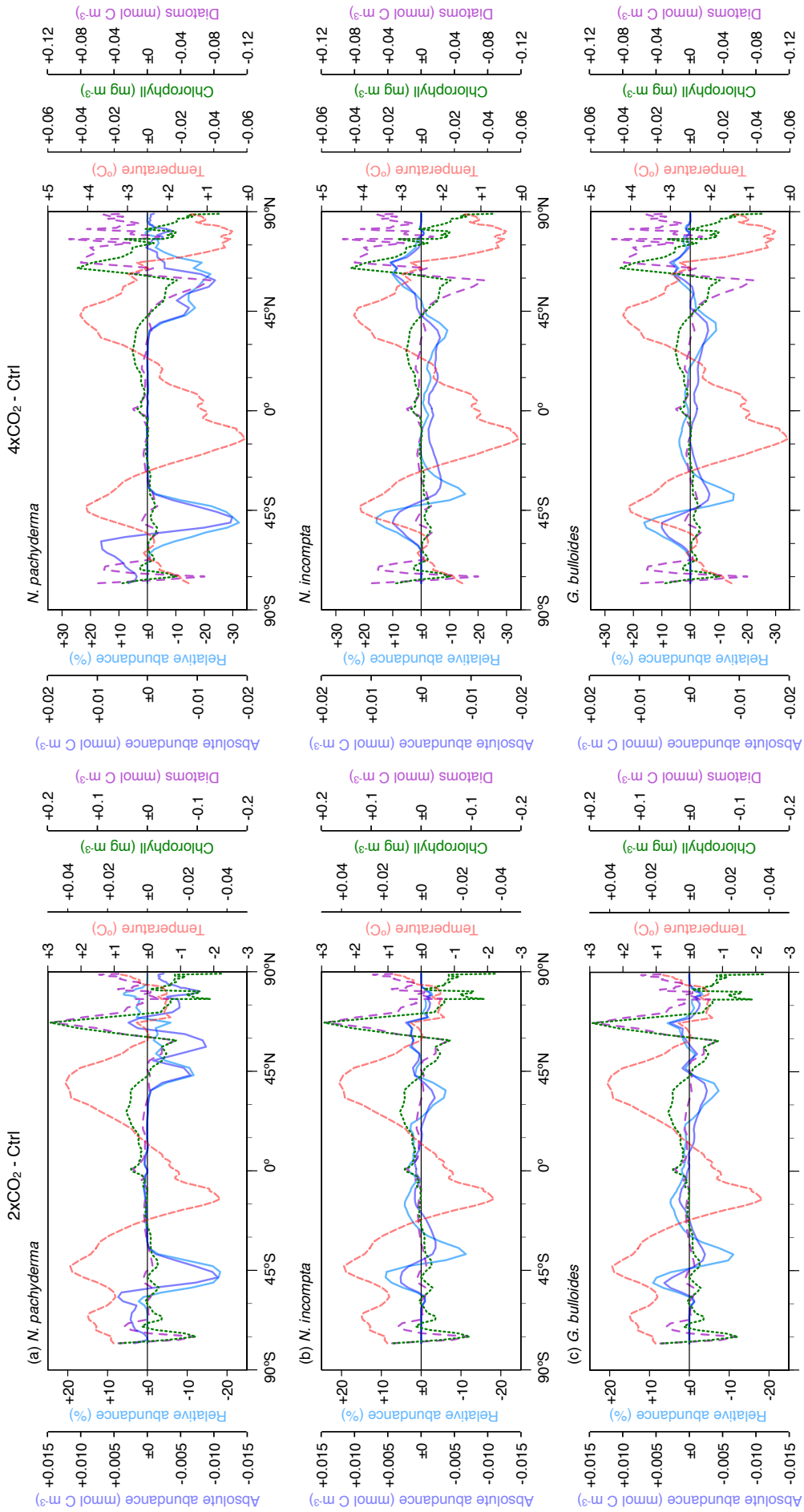


Figure 4.7 (cont. on next page): Change (i.e., future CO_2 scenario - preindustrial control run) in the zonal average of the depth integrated ($0 - 250 \text{ m}$) absolute (solid blue line; in mmol C/m^3) and relative abundances (solid light blue line; in %) of (a) *N. pachyderma*, (b) *N. incompta*, and (c) *G. bullioides*. Here the left column shows the difference between the $2\times\text{CO}_2$ and control simulations, and the right column the difference between the $4\times\text{CO}_2$ and control simulations. The dashed red and green lines in each panel denote the changes in the zonal averages of the depth integrated potential temperature (in $^{\circ}\text{C}$) and chlorophyll concentration (in mg/m^3) over the top 250 m , respectively. The dashed purple lines indicate the changes in the zonal averages of the depth integrated diatom concentration (in mmol/m^3) over the top 250 m .

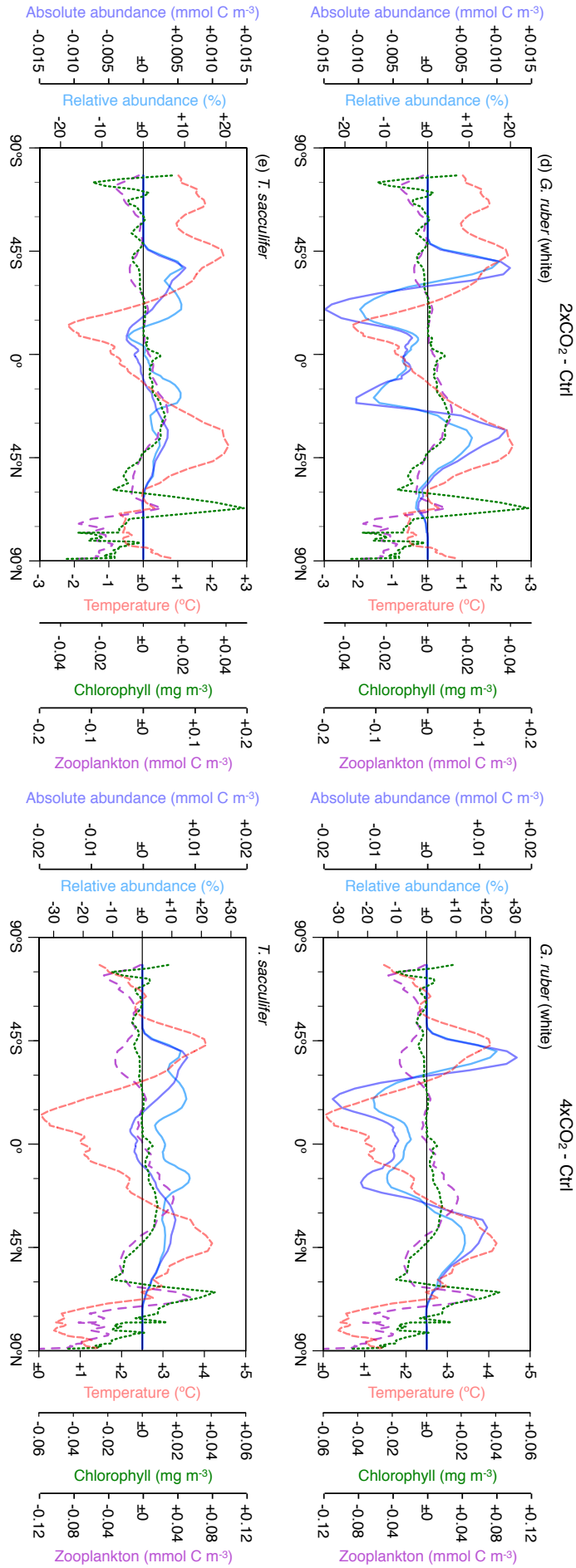


Figure 4.7 (cont.): Same as before for (d) *G. ruber* (white), and (e) *T. sacculifer*. The dashed red and green lines in each panel denote the changes in the zonal averages of the depth integrated potential temperature (in °C) and chlorophyll concentration (in mg/m³) over the top 250 m, respectively. The dashed purple lines indicate the changes in the zonal averages of the depth integrated zooplankton concentration (in mmol/m³) over the top 250 m.

habitat poleward from the tropics. This temperature increase leads, likewise, to an earlier onset of optimum living conditions for the warm-water species in the temperate climate zones resulting in production maxima, which occur earlier in the year compared to the preindustrial era (Figure 4.3d-e).

In summary, global warming could result in shifts in the foraminiferal habitat range, in species-specific depth habitats, and in the species phenology, which are primarily driven by temperature and to some degree by food supply. In response to a warming ocean, the habitat range of the individual planktonic foraminifera is shifted poleward, resulting in a narrower habitat range for *N. pachyderma* and a broader habitat range for the remaining species. However, increasing ocean temperatures will cause a decrease in species abundance in the species' formerly preferred and/or respected habitat, i.e., in the tropics for *T. sacculifer*, in the subtropics for *G. ruber* (white), in the temperate regions of the ocean for *G. bulloides* and *N. incompta*, and in the subpolar regions for *N. pachyderma* (cf. Figures 4.2 and 4.7). Due to the warmer climate the boundaries of each species' preferred environment are shifted in regard to the species' individual temperature tolerance limits. Therefore, *N. pachyderma* is retreating polewards and simultaneously deepens its habitat, whereas *G. ruber* (white) and *T. sacculifer* expand their habitat in width, but still occur close to the surface during the high CO₂ emission scenarios. Additionally, the peak in the maximum foraminiferal production is shifted in response to the environmental changes and occurs in large parts of the ocean a few months earlier in the year compared to preindustrial climate conditions. The changes in ocean temperature influence the primary productivity and both trigger the changes in the species-specific habitats and the seasonality of planktonic foraminifera. However, temperature variations have most likely a greater effect than changes in food availability on planktonic foraminifera species. The simulated responses of the individual foraminiferal species to the projected environmental changes can help to understand climate variability of the past and provide information of how marine microorganisms adapt to (anthropogenic) climate change. Based on our results, it is most likely that the already observed changes in the community composition of marine microorganisms (e.g., Mackas *et al.*, 2012; Steinberg and Landry, 2017) will become more severe in the future due to the ongoing climate change. Warm-water species will benefit most from global warming, whereas cold-water species will adjust their habitat to deeper depth layers or could become extinct if ocean temperatures continue to increase. Overall, the total biomass will decrease on a global average. A stronger (or accelerated) global warming could result in even greater changes, which could occur earlier than expected. However, we caution that our findings result from initial conditions of climatologies that are not fully representative of modern conditions.

Acknowledgements

This project was supported by the DFG (Deutsche Forschungsgemeinschaft) through the International Research Training Group IRTG 1904 ArcTrain. All data can be obtained from the PANGAEA database (www.pangaea.de) or upon request from the corresponding author (Kerstin Kretschmer, kkretschmer@marum.de).

Conclusion and Outlook

Paleoclimate reconstructions, based on fossil evidence of planktonic foraminifera, are subject to biases as the environmental signal preserved in the shells is a result of both habitat and climate change. It is difficult to distinguish between these effects without using independent data. In this study, an ecosystem modeling approach was used to predict species-specific seasonal and vertical habitats of planktonic foraminifera under climate change. The planktonic foraminifera model PLAFOM and in particular its successor, PLAFOM2.0, present robust tools, which can contribute to a more meaningful interpretation of proxy records, eventually aiding to a better understanding of climate change.

Both model versions produce spatially and temporally coherent abundance patterns for *Neogloboquadrina pachyderma*, *Neogloboquadrina incompta*, *Globigerina bulloides*, *Globigerinoides ruber* (white), and *Trilobatus sacculifer* on a global scale, which agree well with available observations. PLAFOM predicts species' concentrations in the surface mixed layer, whereas PLAFOM2.0 includes a vertical component and, thus, predicts species' distribution patterns in space and time more realistically.

Here, PLAFOM was essentially used to predict the distribution of the polar species *N. pachyderma* at different geological time scales in the North Atlantic Ocean north of 30°N. In line with the fossil record, PLAFOM faithfully captured the southward expansion of this species during the Last Glacial Maximum and Heinrich Stadial 1. The peak timing of *N. pachyderma* is shifted by up to 6 months and occurs later in the year during Heinrich Stadial 1 compared to the Last Glacial Maximum. This shift can primarily be related to changes in the sea ice cover and food supply. The change in the timing of the maximum production peak from the Last Glacial Maximum to Heinrich Stadial 1 could result in an underestimation of the actual magnitude of the meltwater isotopic signal recorded in fossil shells of *N. pachyderma*, wherever calcification is likely to take place (i.e., at the surface or at depth). This indicates that the surface water freshening during past meltwater events is not fully reflected in the stable isotope values of, e.g., *N. pachyderma*, resulting in an overestimation of sea surface salinities. It has been hypothesized that the formation of North Atlantic Deep Water was greatly reduced due to the freshwater input of past meltwater pulses (e.g., Maslin *et al.*, 1995; Hemming, 2004; McManus *et al.*, 2004). Accounting for the effect of changing seasonality on proxy records could result in an even stronger reduction of the North Atlantic Deep Water formation and likewise in a more substantial weakening of the Atlantic meridional overturning circulation during these events. This implies that current estimates of the strength of the Atlantic meridional overturning circulation during past meltwater events might be overestimated. Hence, the effect of changing seasonality on proxy records cannot be neglected when reconstructing past climate conditions.

For a more realistic simulation of species-specific habitats of planktonic foraminifera, PLAFOM was customized and extended to resolve the vertical dimension. The new model version, PLAFOM2.0, predicts spatially and temporally variable species-specific depth habitats that are consistent with available sediment trap data and plankton tow samples, although an explicit parameterization of the vertical dimension was not carried out. The depth habitat of the colder-water species, *N. pachyderma*, *N. incompta*, and *G. bulloides*, changes seasonally in the polar and subpolar regions, which appears to be controlled by food availability. During the cold season, these species are found close to the sea surface, while towards the warm season, they descend through the water column and occur at mid-depth. The warm-water species, *G. ruber* (white) and *T. sacculifer*, show a less variable depth habitat and occur year-round close to the sea surface in the tropical and subtropical regions. Outside their preferred habitat, their seasonal occurrence is limited to the warm surface layer that develops at the end of the warm season. The emergence of species-specific depth habitats that are consistent with observations indicates that PLAFOM2.0 provides a robust tool to aid both the interpretation of paleoceanographic records and the understanding of climate change.

Under global warming, the habitat range of individual planktonic foraminifera species will likely shift in response to changes in temperature and food availability. The warm-water species might expand their habitat, whereas the cold-water species might retreat from their former habitat. In response to global warming, individual species might have to adjust their depth habitat to deeper layers. It is likely that increasing ocean temperatures result in a shift in the timing of the maximum production peak of planktonic foraminifera. The changes in ocean temperatures and food supply due to global warming could substantially alter the community composition and structure of planktonic foraminifera on temporal and spatial scales. The response of each individual foraminiferal species to future climate change can aid to a better understanding of past climate variations.

In this study, the planktonic foraminifera model PLAFOM has been improved considerably. However, PLAFOM2.0 is still limited in predicting planktonic foraminifera species distributions in their full extent for the real ocean and, thus, requires further adjustments. The present model version only considers the five most abundant planktonic foraminifera species of the modern ocean, which are also most commonly used in paleoceanographic reconstructions. Considering more species could, however, result in more realistic abundance patterns. An improvement could also be achieved by including different genotypes of the considered species, as distinct genotypes exhibit most likely different ecological preferences. Some genotypes, however, are restricted to specific regions, thus, no globally uniform parameterization can be applied. Furthermore, PLAFOM2.0 would essentially be improved by considering the vertical migration through the water column during the species' life cycle by explicitly parameterizing the ontogeny of each species.

However, the above mentioned modifications would essentially increase the computational costs and likewise the degrees of freedom, and could also add more uncertainty concerning the prediction of species-specific habitats. Additionally, a proper implementation of these adjustments would require extensive knowledge about the species' ecological preferences, their competitive behavior as well as their adaptation strategies to seasonally varying environmental conditions. More culturing experiments and field studies are needed to obtain a better understanding of the factors controlling species-specific habitat variability, ultimately aiding to the optimization of the current model version. PLAFOM2.0, however, represents at present a robust tool that can essentially help to improve the interpretation of paleoceanographic reconstructions.

Nevertheless, for a better assessment of the potential bias in paleoceanographic reconstructions based on

stable isotopes recorded in planktonic foraminifera, PLAFOM2.0 should be combined with a module that calculates for instance species-specific oxygen and carbon isotope compositions of the modeled foraminiferal shells. This geochemical planktonic foraminifera model could provide a more realistic assessment of the impact of past meltwater injections into the ocean, such as during Heinrich Stadials, the mid-Pliocene warm period, the last interglacial period or meltwater pulse 1A, on foraminiferal-based proxy records. Additionally, this approach could provide more robust estimates of past meltwater pulses and could potentially allow for correcting the bias in paleoclimate reconstructions. Furthermore, the impact of ocean acidification due to global warming on the carbonate production of planktonic foraminifera could be assessed in more detail, providing implications for the global carbon cycle.

References

- Aksu, A. E., and G. Vilks (1988), Stable isotopes in planktonic and benthic foraminifera from Arctic Ocean surface sediments, *Can. J. Earth Sci.*, *25*, 701–109.
- Anderson, N. J. (2000), Miniview: Diatoms, temperature and climatic change, *European Journal of Phycology*, *35*, 307–314, doi:10.1080/09670260010001735911.
- Anderson, O. R., and A. W. H. Bé (1976), The ultrastructure of a planktonic foraminifer, *Globigerinoides sacculifer* (Brady), and its symbiotic dinoflagellates, *Journal of Foraminiferal Research*, *6*(1), 1–21.
- André, A., A. Weiner, F. Quillévéré, R. Aurahs, R. Morard, C. J. Douady, T. de Garidel-Thoron, G. Escarguel, C. de Vargas, and M. Kucera (2013), The cryptic and the apparent reversed: lack of genetic differentiation within the morphologically diverse plexus of the planktonic foraminifer *Globigerinoides sacculifer*, *Paleobiology*, *39*(1), 21–39, doi:10.5061/dryad.rb06j.
- André, A., F. Quillévéré, R. Morard, Y. Ujiie, G. Escarguel, C. de Vargas, T. de Garidel-Thoron, and C. J. Douady (2014), SSU rDNA Divergence in Planktonic Foraminifera: Molecular Taxonomy and Biogeographic Implications, *PLoS ONE*, *9*(8), e104641, doi:10.1371/journal.pone.0104641.
- Arnold, A. J., and W. C. Parker (1999), Biogeography of Planktonic Foraminifera, in *Modern Foraminifera*, edited by B. K. S. Gupta, chap. 7, pp. 103–122, Kluwer Academic, Dordrecht, The Netherlands.
- Arrigo, K. R., and G. L. van Dijken (2011), Secular trends in Arctic Ocean net primary production, *Journal of Geophysical Research*, *116*, C09,011, doi:10.1029/2011JC007151.
- Arrigo, K. R., G. van Dijken, and S. Pabi (2008), Impact of a shrinking Arctic ice cover on marine primary production, *Geophysical Research Letters*, *35*, L19,603, doi:10.1029/2008GL035028.
- Arrigo, K. R., D. K. Perovich, R. S. Pickart, Z. W. Brown, G. L. van Dijken, K. E. Lowry, M. M. Mills, M. A. Palmer, W. M. Balch, F. Bahr, N. R. Bates, C. Benitez-Nelson, B. Bowler, E. Brownlee, J. K. Ehn, K. E. Frey, R. Garley, S. R. Laney, L. Lubelczyk, J. Mathis, A. Matsuoka, B. G. Mitchell, G. W. K. Moore, E. Ortega-Retuerta, S. Pal, C. M. Polashenski, R. A. Reynolds, B. Schieber, H. M. Sosik, M. Stephens, and J. H. Swift (2012), Massive Phytoplankton Blooms Under Arctic Sea Ice, *Science*, *336*, 1408.
- Asahi, H., and K. Takahashi (2007), A 9-year time-series of planktonic foraminifer fluxes and environmental change in the Bering sea and the central subarctic Pacific Ocean, 1990–1999, *Progress in Oceanography*, *72*, 343–363, doi:10.1016/j.pocean.2006.03.021.
- Aurahs, R., G. W. Grimm, V. Hemleben, C. Hemleben, and M. Kucera (2009), Geographical distribution of cryptic genetic types in the planktonic foraminifer *Globigerinoides ruber*, *Molecular Ecology*, *18*, 1692–1706, doi:10.1111/j.1365-294X.2009.04136.x.
- Aurahs, R., Y. Treis, K. Darling, and M. Kucera (2011), A revised taxonomic and phylogenetic concept for the planktonic foraminifer species *Globigerinoides ruber* based on molecular and morphometric evidence, *Marine Micropaleontology*, *79*, 1–14, doi:10.1016/j.marmicro.2010.12.001.

- Barash, M. S., and I. G. Yushina (1999), Reconstruction of the Quaternary North Atlantic paleohydrological variability by means of planktic foraminifera data (method of factor analysis and spline interpolation), in *German-Russian Cooperation: Biogeographic and biostratigraphic investigations on selected sediment cores from the Eurasian continental margin and marginal seas to analyze the Late Quaternary climatic variability*, edited by R. F. Spielhagen, M. S. Barash, G. I. Ivanov, and T. J., 306 ed., pp. 5–45, Alfred Wegener Institute for Polar and Marine Research, Bremerhaven.
- Bard, E. (1988), Correction of accelerator mass spectrometry ^{14}C ages measured in planktonic foraminifera: Paleoceanographic implications, *Paleoceanography*, 3(6), 635–645.
- Bard, E., F. Rostek, J.-L. Turon, and S. Gendreau (2000), Hydrological Impact of Heinrich Events in the Subtropical Northeast Atlantic, *Science*, 289, 1321–1324.
- Bauch, D., J. Carstens, and G. Wefer (1997), Oxygen isotope composition of living *Neogloboquadrina pachyderma* (sin.) in the Arctic Ocean, *Earth and Planetary Science Letters*, 146, 47–58, doi:10.1016/S0012-821X(96)00211-7.
- Bauch, D., K. Darling, J. Simstich, H. A. Bauch, H. Erlenkeuser, and D. Kroon (2003), Palaeoceanographic implications of genetic variation in living North Atlantic *Neogloboquadrina pachyderma*, *Nature*, 424, 299–302, doi:10.1038/nature01791.1.
- Bauch, H. A., H. Erlenkeuser, R. F. Spielhagen, U. Struck, J. Matthiessen, J. Thiede, and J. Heinemeier (2001), A multiproxy reconstruction of the evolution of deep and surface waters in the subarctic Nordic seas over the last 30,000 yr, *Quaternary Science Reviews*, 20, 659–678.
- Bé, A. W. H. (1960), Some observations on Arctic planktonic foraminifera, *Contrib. Cushman Found. Foram. Res.*, 11, 64–68.
- Bé, A. W. H. (1969), Planktonic Foraminifera, in *Antarctic Map Folio Series 11: Distribution of Selected Groups of Marine Invertebrates in Waters South of 35° S Latitude*, pp. 9–12, American Geographical Society.
- Bé, A. W. H. (1977), An ecological, zoogeographic and taxonomic review of recent planktonic Foraminifera, in *Oceanic micropaleontology*, edited by A. T. S. Ramsay, pp. 1–100, Academic Press, London.
- Bé, A. W. H., and W. H. Hamlin (1967), Ecology of Recent Planktonic Foraminifera: Part 3: Distribution in the North Atlantic during the Summer of 1962, *Micropaleontology*, 13(1), 87–106.
- Bé, A. W. H., and W. H. Hutson (1977), Ecology of Planktonic Foraminifera and Biogeographic Patterns of Life and Fossil Assemblages in the Indian Ocean, *Micropaleontology*, 23(4), 369–414, doi:10.2307/1485406.
- Bé, A. W. H., and D. S. Tolderlund (1971), Distribution and ecology of planktonic foraminifera in surface waters of the Atlantic and Indian Oceans, in *The Micropaleontology of Oceans*, edited by B. Funnell and W. Riedel, pp. 105–150, Cambridge University Press, London.
- Beckmann, W., A. Auras, and C. Hemleben (1987), Cyclonic cold-core eddy in the eastern North Atlantic. III. Zooplankton, *Marine Ecology - Progress Series*, 39, 165–173, doi:10.3354/meps039165.
- Bergami, C., L. Capotondi, L. Langone, F. Giglio, and M. Ravaioli (2009), Distribution of living planktonic foraminifera in the Ross Sea and the Pacific sector of the Southern Ocean (Antarctica), *Marine Micropaleontology*, 73, 37–48, doi:10.1016/j.marmicro.2009.06.007.
- Bijma, J., W. W. Faber Jr., and C. Hemleben (1990a), Temperature and salinity limits for growth and survival of some planktonic foraminifers in laboratory cultures, *Journal of Foraminiferal Research*, 20(2), 95–116.
- Bijma, J., J. Erez, and C. Hemleben (1990b), Lunar and semi-lunar reproductive cycles in some spinose planktonic foraminifers, *Journal of Foraminiferal Research*, 20(2), 117–127.
- Bird, C., K. F. Darling, A. D. Russell, C. V. Davis, J. Fehrenbacher, A. Free, M. Wyman, and B. T. Ngwenya (2017), Cyanobacterial endobionts within a major marine planktonic calcifier (*Globigerina bulloides*, Foraminifera) revealed by 16S rRNA metabarcoding, *Biogeosciences*, 14, 901–920, doi:10.5194/bg-14-901-2017.
- Bishop, J. K., and W. B. Rossow (1991), Spatial and Temporal Variability of Global Surface Solar Irradiance, *Journal of Geophysical Research*, 96(C9), 16,839–16,858.

- Boltovskoy, E. (1971), Planktonic foraminiferal assemblages of the epipelagic zone and their thanatocoenoses, in *The Micropaleontology of Oceans*, edited by B. M. Funnell and W. R. Riedel, pp. 277–288, Cambridge University Press, London.
- Boltovskoy, E., D. Boltovskoy, N. Correa, and F. Brandini (1996), Planktic foraminifera from the southwestern Atlantic (30°–60°S): species-specific patterns in the upper 50m, *Marine Micropaleontology*, 28, 53–72, doi:10.1016/0377-8398(95)00076-3.
- Bond, G., H. Heinrich, W. Broecker, L. Labeyrie, J. McManus, J. Andrews, S. Huon, R. Jantschik, S. Clasen, C. Simet, K. Tedesco, M. Klas, G. Bonani, and S. Ivy (1992), Evidence for massive discharges of icebergs into the North Atlantic ocean during the last glacial period, *Nature*, 360, 245–249.
- Born, A., and K. H. Nisancioglu (2012), Melting of Northern Greenland during the last interglaciation, *The Cryosphere*, 6, 1239–1250, doi:10.5194/tc-6-1239-2012.
- Braconnot, P., B. Otto-Bliesner, S. Harrison, S. Joussaume, J.-Y. Peterchmitt, A. Abe-Ouchi, M. Crucifix, E. Driesschaert, T. Fichefet, C. D. Hewitt, M. Kageyama, A. Kitoh, A. Laîné, M.-F. Loutre, O. Marti, U. Merkel, G. Ramstein, P. Valdes, S. L. Weber, Y. Yu, and Y. Zhao (2007a), Results of PMIP2 coupled simulations of the Mid-Holocene and Last Glacial Maximum – Part 1: experiments and large-scale features, *Climate of the Past*, 3, 261–277, doi:10.5194/cp-3-261-2007.
- Braconnot, P., B. Otto-Bliesner, S. Harrison, S. Joussaume, J.-Y. Peterchmitt, A. Abe-Ouchi, M. Crucifix, E. Driesschaert, T. Fichefet, C. D. Hewitt, M. Kageyama, A. Kitoh, M.-F. Loutre, O. Marti, U. Merkel, G. Ramstein, P. Valdes, L. Weber, Y. Yu, and Y. Zhao (2007b), Results of PMIP2 coupled simulations of the Mid-Holocene and Last Glacial Maximum – Part 2: feedbacks with emphasis on the location of the ITCZ and mid- and high latitudes heat budget, *Climate of the Past*, 3, 279–296, doi:10.5194/cp-3-279-2007.
- Bradshaw, J. S. (1959), Ecology of living foraminifera in the North and Equatorial Pacific Ocean, *Cushman Foundation for Foraminiferal Research: Contributions*, 10, 25–64.
- Broecker, W. S. (1994), Massive iceberg discharges as triggers for global climate change, *Nature*, 372, 421–424.
- Cacho, I., J. O. Grimalt, C. Pelejero, M. Canals, F. J. Sierro, J. A. Flores, and N. Shackleton (1999), Dansgaard-Oeschger and Heinrich event imprints in Alboran Sea paleotemperatures, *Paleoceanography*, 14(6), 698–705.
- Caron, D. A., A. W. H. Bé, and O. R. Anderson (1982), Effects of variations in light intensity on life processes of the planktonic foraminifer *Globigerinoides sacculifer* in laboratory culture, *Journal of the Marine Biological Association of the United Kingdom*, 62(2), 435–451, doi:10.1017/S0025315400057374.
- Caron, D. A., W. W. Faber, and A. W. H. Bé (1987), Effects of temperature and salinity on the growth and survival of the planktonic foraminifer *Globigerinoides sacculifer*, *Journal of the Marine Biological Association of the United Kingdom*, 67(2), 323–341, doi:10.1017/S0025315400026643.
- Carstens, J., and G. Wefer (1992), Recent distribution of planktonic foraminifera in the Nansen Basin, Arctic Ocean, *Deep-Sea Research*, 39(Suppl. 2), S507–S524.
- Carstens, J., D. Hebbeln, and G. Wefer (1997), Distribution of planktic foraminifera at the ice margin in the Arctic (Fram Strait), *Marine Micropaleontology*, 29, 257–269, doi:10.1016/S0377-8398(96)00014-X.
- Chappell, J. (2002), Sea level changes forced ice breakouts in the Last Glacial cycle: new results from coral terraces, *Quaternary Science Reviews*, 21, 1229–1240, doi:10.1016/S0277-3791(01)00141-X.
- Charbit, S., D. Paillard, and G. Ramstein (2008), Amount of CO₂ emissions irreversibly leading to the total melting of Greenland, *Geophysical Research Letters*, 35, L12503, doi:10.1029/2008GL033472.
- CLIMAP Project Members (1976), The Surface of the Ice-Age Earth, *Science*, 191(4232), 1131–1137.
- CLIMAP Project Members (1981), Seasonal reconstructions of the Earth's surface at the last glacial maximum, *Geological Society of America, Map and Chart Series*, 36, 1–18.

REFERENCES

- Colebrook, J. M. (1979), Continuous Plankton Records: Seasonal Cycles of Phytoplankton and Copepods in the North Atlantic Ocean and the North Sea, *Marine Biology*, *51*, 23–32, doi:10.1016/0011-7471(66)90628-0.
- Colebrook, J. M. (1982), Continuous plankton records: seasonal variations in the distribution and abundance of plankton in the North Atlantic Ocean and the North Sea, *Journal of Plankton Research*, *4*(3), 435–462.
- Collins, W. D., C. M. Bitz, M. L. Blackmon, G. B. Bonan, C. S. Bretherton, J. A. Carton, P. Chang, S. C. Doney, J. J. Hack, T. B. Henderson, J. T. Kiehl, W. G. Large, D. S. McKenna, B. D. Santer, and R. D. Smith (2006), The Community Climate System Model Version 3 (CCSM3), *Journal of Climate*, *19*, 2122–2143.
- Conkright, M. E., S. Levitus, T. O'Brien, T. P. Boyer, C. Stephens, D. Johnson, L. Stathoplos, O. Baranova, J. Antonov, R. Gelfeld, J. Burney, J. Rochester, and C. Forgy (1999), World Ocean Database 1998 CD-ROM Data Set Documentation, *Tech. rep.*, Silver Spring, MD.
- Cortijo, E., L. Labeyrie, L. Vidal, M. Vautravers, M. Chapman, J.-C. Duplessy, M. Elliot, M. Arnold, J.-L. Turon, and G. Auffret (1997), Changes in sea surface hydrology associated with Heinrich event 4 in the North Atlantic Ocean between 40° and 60°N, *Earth and Planetary Science Letters*, *146*, 29–45, doi:10.1016/S0012-821X(96)00217-8.
- Craig, A. P., M. Vertenstein, and R. Jacob (2012), A New Flexible Coupler for Earth System Modeling developed for CCSM4 and CESM1, *International Journal of High Performance Computing Applications*, *26*, 31–42, doi:10.1177/1094342011428141.
- Crosta, X., and N. Koç (2007), Diatoms: From Micropaleontology to Isotope Geochemistry, in *Proxies in Late Cenozoic Paleooceanography*, vol. 1, edited by C. Hillaire-Marcel and A. de Vernal, chap. 8, pp. 327–369, Elsevier, Amsterdam, doi:10.1016/S1572-5480(07)01013-5.
- Curry, W. B., D. R. Ostermann, M. V. S. Gupta, and V. Ittekkot (1992), Foraminiferal production and monsoonal upwelling in the Arabian Sea: evidence from sediment traps, *Geological Society, London, Special Publications*, *64*, 93–106, doi:10.1144/GSL.SP.1992.064.01.06.
- Danabasoglu, G., S. C. Bates, B. P. Briegleb, S. R. Jayne, M. Jochum, W. G. Large, S. Peacock, and S. G. Yeager (2012), The CCSM4 Ocean Component, *Journal of Climate*, *25*, 1361–1389, doi:10.1175/JCLI-D-11-00091.1.
- Darling, K. F., and C. M. Wade (2008), The genetic diversity of planktic foraminifera and the global distribution of ribosomal RNA genotypes, *Marine Micropaleontology*, *67*, 216–238, doi:10.1016/j.marmicro.2008.01.009.
- Darling, K. F., C. M. Wade, I. A. Stewart, D. Kroon, R. Dingle, and A. J. L. Brown (2000), Molecular evidence for genetic mixing of Arctic and Antarctic subpolar populations of planktonic foraminifers, *Nature*, *405*, 43–47, doi:10.1038/35011002.
- Darling, K. F., M. Kucera, C. M. Wade, P. von Langen, and D. Pak (2003), Seasonal distribution of genetic types of planktonic foraminifer morphospecies in the Santa Barbara Channel and its paleoceanographic implications, *Paleoceanography*, *18*(2), 1032, doi:10.1029/2001PA000723.
- Darling, K. F., M. Kucera, C. J. Pudsey, and C. M. Wade (2004), Molecular evidence links cryptic diversification in polar planktonic protists to Quaternary climate dynamics, *PNAS*, *101*(20), 7657–7662.
- Darling, K. F., M. Kucera, D. Kroon, and C. M. Wade (2006), A resolution for the coiling direction paradox in *Neogloboquadrina pachyderma*, *Paleoceanography*, *21*, PA2011, doi:10.1029/2005PA001189.
- Darling, K. F., M. Kucera, and C. M. Wade (2007), Global molecular phylogeography reveals persistent Arctic circumpolar isolation in a marine planktonic protist, *PNAS*, *104*(12), 5002–5007, doi:10.1073/pnas.0700520104.
- de Abreu, L., N. J. Shackleton, J. Schönfeld, M. Hall, and M. Chapman (2003), Millennial-scale oceanic climate variability off the Western Iberian margin during the last two glacial periods, *Marine Geology*, *196*, 1–20, doi:10.1016/S0025-3227(03)00046-X.
- de Vargas, C., R. Norris, L. Zaninetti, S. W. Gibb, and J. Pawlowski (1999), Molecular evidence of cryptic speciation in planktonic foraminifers and their relation to oceanic provinces., *Proc. Natl. Acad. Sci., USA*, *96*, 2864–2868, doi:10.1073/pnas.96.6.2864.

- de Vernal, A., C. Hillaire-Marcel, J.-L. Turon, and J. Matthiessen (2000), Reconstruction of sea-surface temperature, salinity, and sea-ice cover in the northern North Atlantic during the last glacial maximum based on dinocyst assemblages, *Can. J. Earth Sci.*, *37*, 725–750.
- de Vernal, A., F. Eynaud, M. Henry, C. Hillaire-Marcel, L. Londeix, S. Mangin, J. Matthiessen, F. Marret, T. Radi, A. Rochon, S. Solignac, and J.-L. Turon (2005), Reconstruction of sea-surface conditions at middle to high latitudes of the Northern Hemisphere during the Last Glacial Maximum (LGM) based on dinoflagellate cyst assemblages, *Quaternary Science Reviews*, *24*, 897–924, doi:10.1016/j.quascirev.2004.06.014.
- Deschamps, P., N. Durand, E. Bard, B. Hamelin, G. Camoin, A. L. Thomas, G. M. Henderson, J. Okuno, and Y. Yokoyama (2012), Ice-sheet collapse and sea-level rise at the Bølling warming 14,600 years ago, *Nature*, *483*, 559–564, doi:10.1038/nature10902.
- Deuser, W. G., and E. H. Ross (1989), Seasonally abundant planktonic foraminifera of the Sargasso Sea; succession, deep-water fluxes, isotopic compositions, and paleoceanographic implications, *Journal of Foraminiferal Research*, *19*, 268–293.
- Deuser, W. G., E. H. Ross, C. Hemleben, and M. Spindler (1981), Seasonal changes in species composition, numbers, mass, size, and isotopic composition of planktonic foraminifera settling into the deep Sargasso Sea, *Palaeogeography, Palaeoclimatology, Palaeoecology*, *33*, 103–127, doi:10.1016/0031-0182(81)90034-1.
- Dieckmann, G. S., M. Spindler, M. A. Lange, S. F. Ackley, and H. Eicken (1991), Antarctic sea ice: A habitat for the foraminifer *Neogloboquadrina pachyderma*, *Journal of Foraminiferal Research*, *21*(2), 182–189, doi:10.2113/gsjfr.21.2.182.
- Doney, S. C., D. M. Glover, and R. G. Najjar (1996), A new coupled, one-dimensional biological-physical model for the upper ocean: Applications to the JGOFS Bermuda Atlantic Time-series Study (BATS) site, *Deep Sea Research Part II: Topical Studies in Oceanography*, *43*(2-3), 591–624, doi:10.1016/0967-0645(95)00104-2.
- Doney, S. C., K. Lindsay, I. Fung, and J. John (2006), Natural Variability in a Stable, 1000-Yr Global Coupled Climate-Carbon Cycle Simulation, *Journal of Climate*, *19*, 3033–3054, doi:10.1175/JCLI3783.1.
- Donner, B., and G. Wefer (1994), Flux and stable isotope composition of *Neogloboquadrina pachyderma* and other planktonic foraminifers in the Southern Ocean (Atlantic sector), *Deep-Sea Research I*, *41*(11/12), 1733–1743.
- Dowsett, H. J., M. M. Robinson, A. M. Haywood, D. J. Hill, A. M. Dolan, D. K. Stoll, W.-L. Chan, A. Abe-Ouchi, M. A. Chandler, N. A. Rosenbloom, B. L. Otto-Bliesner, F. J. Bragg, D. J. Lunt, K. M. Foley, and C. R. Riesselman (2012), Assessing confidence in Pliocene sea surface temperatures to evaluate predictive models, *Nature Climate Change*, *2*, 365–371, doi:10.1038/nclimate1455.
- Dreger, D. L. (1999), Decadal-to-centennial-scale sediment records of ice advance on the Barents shelf and meltwater discharge into the northeastern Norwegian Sea over the last 40 kyr, Dissertation, Christian-Albrechts-Universität Kiel, Germany.
- Driesschaert, E., T. Fichfet, H. Goosse, P. Huybrechts, I. Janssens, A. Mouchet, G. Munhoven, V. Brovkin, and S. L. Weber (2007), Modeling the influence of Greenland ice sheet melting on the Atlantic meridional overturning circulation during the next millennia, *Geophysical Research Letters*, *34*, L10707, doi:10.1029/2007GL029516.
- Duplessy, J.-C., L. Labeyrie, A. Juillet-Leclerc, F. Maitre, J. Duprat, and M. Sarnthein (1991), Surface salinity reconstruction of the North Atlantic Ocean during the last glacial maximum, *Oceanologica Acta*, *14*(4), 311–324.
- Dutton, A., and K. Lambeck (2012), Ice Volume and Sea Level During the Last Interglacial, *Science*, *337*(6091), 216–219, doi:10.1126/science.1205749.
- Dutton, A., A. E. Carlson, A. J. Long, G. A. Milne, P. U. Clark, R. DeConto, B. P. Horton, S. Rahmstorf, and M. E. Raymo (2015), Sea-level rise due to polar ice-sheet mass loss during past warm periods, *Science*, *349*(6244), aaa4019, doi:10.1126/science.aaa4019.
- Eguchi, N. O., H. Kawahata, and A. Taira (1999), Seasonal Response of Planktonic Foraminifera to Surface Ocean Condition: Sediment Trap Results from the Central North Pacific Ocean, *Journal of Oceanography*, *55*, 681–691.

- Eguchi, N. O., H. Ujiie, H. Kawahata, and A. Taira (2003), Seasonal variations in planktonic foraminifera at three sediment traps in the Subarctic, Transition and Subtropical zones of the central North Pacific Ocean, *Marine Micropaleontology*, *48*, 149–163, doi:10.1016/S0377-8398(03)00020-3.
- Erez, J. (1983), Calcification Rates, Photosynthesis and Light in Planktonic Foraminifera, in *Biom mineralization and Biological Metal Accumulation: Biological and Geological Perspectives Papers presented at the Fourth International Symposium on Biom mineralization, Renesse, The Netherlands, June 2–5, 1982*, edited by P. Westbroek and E. W. de Jong, pp. 307–312, Springer Netherlands, Dordrecht, The Netherlands, doi:10.1007/978-94-009-7944-4_29.
- Ewert, H., A. Groh, and R. Dietrich (2012), Volume and mass changes of the Greenland ice sheet inferred from ICESat and GRACE, *Journal of Geodynamics*, *59–60*, 111–123, doi:10.1016/j.jog.2011.06.003.
- Eynaud, F., L. de Abreu, A. Voelker, J. Schönfeld, E. Salgueiro, J.-L. Turon, A. Penaud, S. Toucanne, F. Naughton, M. F. Sánchez Goñi, and I. Cacho (2009), Position of the Polar Front along the western Iberian margin during key cold episodes of the last 45 ka, *Geochemistry, Geophysics, Geosystems*, *10*(7), Q07U05, doi:10.1029/2009GC002398.
- Fairbanks, R. G. (1989), A 17,000-year glacio-eustatic sea level record: influence of glacial melting rates on the Younger Dryas event and deep-ocean circulation, *Nature*, *342*, 637–642, doi:10.1038/342637a0.
- Fairbanks, R. G., and P. H. Wiebe (1980), Foraminifera and Chlorophyll Maximum: Vertical Distribution, Seasonal Succession, and Paleoceanographic Significance, *Science*, *209*(4464), 1524–1526.
- Fairbanks, R. G., P. H. Wiebe, and A. W. H. Bé (1980), Vertical Distribution and Isotopic Composition of Living Planktonic Foraminifera in the Western North Atlantic, *Science*, *207*, 61–63.
- Fairbanks, R. G., M. Sverdrup, R. Free, P. H. Wiebe, and A. W. H. Bé (1982), Vertical distribution and isotopic fractionation of living planktonic foraminifera from the Panama Basin, *Nature*, *298*, 841–844.
- Fettweis, X., B. Franco, M. Tedesco, J. H. van Angelen, J. T. M. Lenaerts, M. R. van den Broeke, and H. Gallée (2013), Estimating the Greenland ice sheet surface mass balance contribution to future sea level rise using the regional atmospheric climate model MAR, *The Cryosphere*, *7*, 469–489, doi:10.5194/tcd-6-3101-2012.
- Field, D. B. (2004), Variability in vertical distributions of planktonic foraminifera in the California Current: Relationships to vertical ocean structure, *Paleoceanography*, *19*, PA2014, doi:10.1029/2003PA000970.
- Field, D. B., T. R. Baumgartner, C. D. Charles, V. Ferreira-Bartrina, and M. D. Ohman (2006), Planktonic Foraminifera of the California Current Reflect 20th-Century Warming, *Science*, *311*, 63–66, doi:10.1021/jp053848o.20.
- Fischer, G., and G. Wefer (1996), Long-term observation of particle fluxes in the eastern Atlantic: seasonality, changes of flux with depth and comparison with the sediment record, in *The South Atlantic: Present and Past Circulation*, edited by G. Wefer, W. H. Berger, G. Siedler, and D. Webb, pp. 325–344, Springer, Berlin, Heidelberg, New York.
- Fraile, I., M. Schulz, S. Mulitza, and M. Kucera (2008), Predicting the global distribution of planktonic foraminifera using a dynamic ecosystem model, *Biogeosciences*, *5*, 891–911.
- Fraile, I., S. Mulitza, and M. Schulz (2009a), Modeling planktonic foraminiferal seasonality: Implications for sea-surface temperature reconstructions, *Marine Micropaleontology*, *72*, 1–9, doi:10.1016/j.marmicro.2009.01.003.
- Fraile, I., M. Schulz, S. Mulitza, U. Merkel, M. Prange, and A. Paul (2009b), Modeling the seasonal distribution of planktonic foraminifera during the Last Glacial Maximum, *Paleoceanography*, *24*, PA2216, doi:10.1029/2008PA001686.
- Franke, J., A. Paul, and M. Schulz (2008), Modeling variations of marine reservoir ages during the last 45 000 years, *Climate of the Past*, *4*, 125–136.
- Friedland, K. D., N. R. Record, R. G. Asch, T. Kristiansen, V. S. Saba, K. F. Drinkwater, S. Henson, R. T. Leaf, R. E. Morse, D. G. Johns, S. I. Large, S. S. Hjøllø, J. A. Nye, M. A. Alexander, and R. Ji (2016), Seasonal phytoplankton blooms in the North Atlantic linked to the overwintering strategies of copepods, *Elementa: Science of the Anthropocene*, *4*, 000,099, doi:10.12952/journal.elementa.000099.

- Ganssen, G. M., and D. Kroon (2000), The isotopic signature of planktonic foraminifera from NE Atlantic surface sediments: implications for the reconstruction of past oceanic conditions, *Journal of the Geological Society, London*, *157*, 693–699, doi:10.1144/jgs.157.3.693.
- Garcia, H. E., R. A. Locarnini, T. P. Boyer, J. I. Antonov, M. M. Zweng, O. K. Baranova, and D. R. Johnson (2010), *World Ocean Atlas 2009, Volume 4: Nutrients (phosphate, nitrate, silicate)*, 398 pp., U.S. Government Printing Office, Washington, D.C., doi:10.1182/blood-2011-06-357442.
- Gastrich, M. D. (1987), Ultrastructure of a new intracellular symbiotic alga found within planktonic foraminifera, *Journal of Phycology*, *23*(4), 623–632, doi:10.1111/j.1529-8817.1987.tb04215.x.
- Gastrich, M. D., and R. Bartha (1988), Primary productivity in the planktonic foraminifer *Globigerinoides ruber* (D'Orbigny), *Journal of Foraminiferal Research*, *18*, 137–142.
- Geider, R. J., H. L. MacIntyre, and T. M. Kana (1998), A dynamic regulatory model of phytoplanktonic acclimation to light, nutrients, and temperature, *Limnol. Oceanography*, *43*(4), 679–694.
- Gent, P. R., F. O. Bryan, G. Danabasoglu, S. C. Doney, W. R. Holland, W. G. Large, and J. C. McWilliams (1998), The NCAR Climate System Model Global Ocean Component, *Journal of Climate*, *11*, 1287–1306.
- Giraudeau, J. (1993), Planktonic foraminiferal assemblages in surface sediments from the south western African continental margin, *Marine Geology*, *110*, 47–62, doi:10.1016/0025-3227(93)90104-4.
- González, C., and L. M. Dupont (2009), Tropical salt marsh succession as sea-level indicator during Heinrich events, *Quaternary Science Reviews*, *28*, 939–946, doi:10.1016/j.quascirev.2008.12.023.
- Greve, R. (2000), On the Response of the Greenland Ice Sheet to Greenhouse Climate Change, *Climatic Change*, *46*, 289–303, doi:10.1023/A:1005647226590.
- Griffies, S. M., A. Biastoch, C. Böning, F. Bryan, G. Danabasoglu, E. P. Chassignet, M. H. England, R. Gerdes, H. Haak, R. W. Hallberg, W. Hazeleger, J. Jungclaus, W. G. Large, G. Madec, A. Pirani, B. L. Samuels, M. Scheinert, A. S. Gupta, C. A. Severijns, H. L. Simmons, A. M. Treguier, M. Winton, S. Yeager, and J. Yin (2009), Coordinated Ocean-ice Reference Experiments (COREs), *Ocean Modelling*, *26*(1-2), 1–46, doi:10.1016/j.ocemod.2008.08.007.
- Hall, J. M., and L.-H. Chan (2004), Ba/Ca in *Neogloboquadrina pachyderma* as an indicator of deglacial meltwater discharge into the western Arctic Ocean, *Paleoceanography*, *19*, PA1017, doi:10.1029/2003PA000910.
- Hayes, A., E. J. Rohling, S. De Rijk, D. Kroon, and W. J. Zachariasse (1999), Mediterranean planktonic foraminiferal faunas during the last glacial cycle, *Marine Geology*, *153*, 239–252.
- Hayes, A., M. Kucera, N. Kallel, L. Scaffi, and E. J. Rohling (2005), Glacial Mediterranean sea surface temperatures based on planktonic foraminiferal assemblages, *Quaternary Science Reviews*, *24*, 999–1016, doi:10.1016/j.quascirev.2004.02.018.
- Haywood, A. M., D. J. Hill, A. M. Dolan, B. L. Otto-Bliesner, F. Bragg, W.-L. Chan, M. A. Chandler, C. Contoux, H. J. Dowsett, A. Jost, Y. Kamae, G. Lohmann, D. J. Lunt, A. Abe-Ouchi, S. J. Pickering, G. Ramstein, N. A. Rosenbloom, U. Salzmann, L. Sohl, C. Stepanek, H. Ueda, Q. Yan, and Z. Zhang (2013), Large-scale features of Pliocene climate: results from the Pliocene Model Intercomparison Project, *Climate of the Past*, *9*, 191–209, doi:10.5194/cp-9-191-2013.
- Hemleben, C., M. Spindler, and O. R. Anderson (1989), *Modern Planktonic Foraminifera*, Springer, New York.
- Hemming, S. R. (2004), Heinrich Events: Massive Late Pleistocene detritus layers of the North Atlantic and their global climate imprint, *Review of Geophysics*, *42*, RG1005, doi:10.1029/2003RG000128.1.INTRODUCTION.
- Hilbrecht, H. (1996), Extant planktonic foraminifera and the physical environment in the Atlantic and Indian Oceans, in *Mitteilungen aus dem Geologischen Institut der Eidgen. Technischen Hochschule und der Universität Zürich*, Neue Folge No. 300, p. 93, Zürich.
- Hillaire-Marcel, C., and A. de Vernal (2008), Stable isotope clue to episodic sea ice formation in the glacial North Atlantic, *Earth and Planetary Science Letters*, *268*, 143–150, doi:10.1016/j.epsl.2008.01.012.

- Hillaire-Marcel, C., A. de Vernal, G. Bilodeau, and G. Wu (1994), Isotope stratigraphy, sedimentation rates, deep circulation, and carbonate events in the Labrador Sea during the last ~200 ka, *Canadian Journal of Earth Sciences*, 31(1), 63–89, doi:10.1139/e94-007.
- Holland, M. M., D. A. Bailey, B. P. Briegleb, B. Light, and E. Hunke (2012), Improved Sea Ice Shortwave Radiation Physics in CCSM4: The Impact of Melt Ponds and Aerosols on Arctic Sea Ice, *Journal of Climate*, 25, 1413–1430, doi:10.1175/JCLI-D-11-00078.1.
- Huber, M., and R. Knutti (2012), Anthropogenic and natural warming inferred from changes in Earth's energy balance, *Nature Geoscience*, 5, 31–36, doi:10.1038/NGEO1327.
- Hüls, M. (2000), Millennial-scale SST variability as inferred from planktonic foraminiferal census counts in the western subtropical Atlantic, Dissertation, Christian-Albrechts-Universität Kiel, Germany.
- Hüls, M., and R. Zahn (2000), Millennial-scale sea surface temperature variability in the western tropical North Atlantic from planktonic foraminiferal census counts, *Paleoceanography*, 15(6), 659–678.
- Hunke, E. C., and W. H. Lipscomb (2008), CICE: The Los Alamos Sea Ice Model, Documentation and Software User's Manual, Version 4.0, *Tech. rep.*, Los Alamos National Laboratory.
- Hurrell, J. W., M. M. Holland, P. R. Gent, S. Ghan, J. E. Kay, P. J. Kushner, J.-F. Lamarque, W. G. Large, D. Lawrence, K. Lindsay, W. H. Lipscomb, M. C. Long, N. Mahowald, D. R. Marsh, R. B. Neale, P. Rasch, S. Vavrus, M. Vertenstein, D. Bader, W. D. Collins, J. J. Hack, J. Kiehl, and S. Marshall (2013), The Community Earth System Model: A framework for collaborative research, *Bulletin of the American Meteorological Society*, 94, 1339–1360, doi:10.1175/BAMS-D-12-00121.1.
- Husum, K., and M. Hald (2012), Arctic planktic foraminiferal assemblages: Implications for subsurface temperature reconstructions, *Marine Micropaleontology*, 96-97, 38–47, doi:10.1016/j.marmicro.2012.07.001.
- Intergovernmental Panel on Climate Change (IPCC) (2013), *Climate Change 2013: The Physical Science Basis. Working Group I Contribution to the Fifth Assessment Report of the Intergovernmental Panel on Climate Change*, 1535 pp., Cambridge University Press, Cambridge, U.K. and New York, NY, USA.
- Iwasaki, S., K. Kimoto, A. Kuroyanagi, and H. Kawahata (2017), Horizontal and vertical distributions of planktic foraminifera in the subarctic Pacific, *Marine Micropaleontology*, 130, 1–14, doi:10.1016/j.marmicro.2016.12.001.
- Jensen, L. Ø., E. A. Mousing, and K. Richardson (2017), Using species distribution modelling to predict future distributions of phytoplankton: Case study using species important for the biological pump, *Marine Ecology*, 38, e12,427, doi:10.1111/maec.12427.
- Jensen, S. (1998), Planktische Foraminiferen im Europäischen Nordmeer: Verbreitung und Vertikalfuß sowie ihre Entwicklung während der letzten 15000 Jahre, *Berichte Sonderforschungsbereich 313, Univ. Kiel*, 75, 1–105.
- Ji, R., M. Edwards, D. L. Mackas, J. A. Runge, and A. C. Thomas (2010), Marine plankton phenology and life history in a changing climate: current research and future directions, *Journal of Plankton Research*, 32(10), 1355–1368, doi:10.1093/plankt/fbq062.
- Jodłowska, S., and S. Śliwińska (2014), Effects of light intensity and temperature on the photosynthetic irradiance response curves and chlorophyll fluorescence in three picocyanobacterial strains of *Synechococcus*, *Photosynthetica*, 52(2), 223–232, doi:10.1007/s11099-014-0024-y.
- Jonkers, L., and M. Kučera (2015), Global analysis of seasonality in the shell flux of extant planktonic Foraminifera, *Biogeosciences*, 12, 2207–2226, doi:10.5194/bg-12-2207-2015.
- Jonkers, L., and M. Kučera (2017), Quantifying the effect of seasonal and vertical habitat tracking on planktonic foraminifera proxies, *Climate of the Past*, 13, 573–586, doi:10.5194/cp-13-573-2017.
- Jonkers, L., G.-J. A. Brummer, F. J. C. Peeters, H. M. van Aken, and M. F. De Jong (2010), Seasonal stratification, shell flux, and oxygen isotope dynamics of left-coiling *N. pachyderma* and *T. quinqueloba* in the western subpolar North Atlantic, *Paleoceanography*, 25, PA2204, doi:10.1029/2009PA001849.

- Jonkers, L., S. van Heuven, R. Zahn, and F. J. C. Peeters (2013), Seasonal patterns of shell flux, $\delta^{18}\text{O}$ and $\delta^{13}\text{C}$ of small and large *N. pachyderma* (s) and *G. bulloides* in the subpolar North Atlantic, *Paleoceanography*, *28*, 164–174, doi:10.1002/palo.20018.
- Jørgensen, B. B., J. Erez, N. P. Revsbech, and Y. Cohen (1985), Symbiotic photosynthesis in a planktonic foraminiferan, *Globigerinoides sacculifer* (Brady), studied with microelectrodes, *Limnology and Oceanography*, *30*(6), 1253–1267, doi:10.4319/lo.1985.30.6.1253.
- Jung, S. J. A. (1996), Wassermassenaustausch zwischen NE-Atlantik und Nordmeer während der letzten 300.000/80.000 Jahre im Abbild stabiler O- und C-Isotope, Dissertation, Christian-Albrechts-Universität Kiel, Deutschland.
- Kandiano, E. S. (2003), Dynamics of the Ocean Surface in the Polar and Subpolar North Atlantic over the last 500 000 Years, Dissertation, Christian-Albrechts-Universität, Kiel.
- Keigwin, L. D., and G. A. Jones (1995), The marine record of deglaciation from the continental margin off Nova Scotia, *Paleoceanography*, *10*(6), 973–985.
- Kemle-von Mücke, S., and H. Oberhänsli (1999), The Distribution of Living Planktic Foraminifera in Relation to Southeast Atlantic Oceanography, in *Use of Proxies in Paleoceanography*, pp. 91–115, Springer, Berlin, Heidelberg.
- Key, R. M., A. Kozyr, C. L. Sabine, K. Lee, R. Wanninkhof, J. L. Bullister, R. A. Feely, F. J. Millero, C. Mordy, and T.-H. Peng (2004), A global ocean carbon climatology: Results from Global Data Analysis Project (GLODAP), *Global Biogeochemical Cycles*, *18*, GB4031, doi:10.1029/2004GB002247.
- Kiefer, T. (1998), Productivity and temperatures in the subtropical North Atlantic: Cyclic and abrupt changes during the Late Quaternary, Dissertation, Christian-Albrechts-Universität Kiel, Germany.
- Kienast, S. S., T. Friedrich, N. Dubois, P. S. Hill, A. Timmermann, A. C. Mix, and M. Kienast (2013), Near collapse of the meridional SST gradient in the eastern equatorial Pacific during Heinrich Stadial 1, *Paleoceanography*, *28*, 663–674, doi:10.1002/2013PA002499.
- Kincaid, E., R. C. Thunell, J. Le, C. B. Lange, A. L. Weinheimer, and F. M. H. Reid (2000), Planktonic foraminiferal fluxes in the Santa Barbara Basin: response to seasonal and interannual hydrographic changes, *Deep-Sea Research Part II*, *47*, 1157–1176, doi:10.1016/S0967-0645(99)00140-X.
- King, A. L., and W. R. Howard (2001), Seasonality of foraminiferal flux in sediment traps at Chatham rise, SW Pacific: Implications for paleotemperature estimates, *Deep-Sea Research Part I*, *48*, 1687–1708, doi:10.1016/S0967-0637(00)00106-0.
- Kjeldsen, K. K., N. J. Korsgaard, A. A. Bjørk, S. A. Khan, J. E. Box, S. Funder, N. K. Larsen, J. L. Bamber, W. Colgan, M. van den Broeke, M.-L. Siggaard-Andersen, C. Nuth, A. Schomacker, C. S. Andresen, E. Willerslev, and K. H. Kjær (2015), Spatial and temporal distribution of mass loss from the Greenland Ice Sheet since AD 1900, *Nature*, *528*, 396–400, doi:10.1038/nature16183.
- Knies, J., and C. Vogt (2003), Freshwater pulses in the eastern Arctic Ocean during Saalian and Early Weichselian ice-sheet collapse, *Quaternary Research*, *60*, 243–251, doi:10.1016/j.yqres.2003.07.008.
- Kohfeld, K. E., R. G. Fairbanks, S. L. Smith, and I. D. Walsh (1996), *Neogloboquadrina pachyderma* (sinistral coiling) as paleoceanographic tracers in polar oceans: Evidence from Northeast Water Polynya plankton tows, sediment traps, and surface sediments, *Paleoceanography*, *11*(6), 679–699.
- Kopp, R. E., F. J. Simons, J. X. Mitrovica, A. C. Maloof, and M. Oppenheimer (2009), Probabilistic assessment of sea level during the last interglacial stage, *Nature*, *462*, 863–867, doi:10.1038/nature08686.
- Kopp, R. E., F. J. Simons, J. X. Mitrovica, A. C. Maloof, and M. Oppenheimer (2013), A probabilistic assessment of sea level variations within the last interglacial stage, *Geophysical Journal International*, *193*, 711–716, doi:10.1093/gji/ggt029.
- Kretschmer, K., M. Kucera, and M. Schulz (2016), Modeling the distribution and seasonality of *Neogloboquadrina pachyderma* in the North Atlantic Ocean during Heinrich Stadial 1, *Paleoceanography*, *31*, 1–25, doi:10.1002/2015PA002819.

- Kretschmer, K., L. Jonkers, M. Kucera, and M. Schulz (2017), Modeling seasonal and vertical habitats of planktonic foraminifera on a global scale, submitted to *Biogeosciences*.
- Krishnamurthy, A., J. K. Moore, C. S. Zender, and C. Luo (2007), Effects of atmospheric inorganic nitrogen deposition on ocean biogeochemistry, *Journal of Geophysical Research*, *112*, G02019, doi:10.1029/2006JG000334.
- Kucera, M. (2007), Planktonic Foraminifera as Tracers of Past Oceanic Environments, in *Proxies in Late Cenozoic Palaeoceanography*, edited by C. Hillaire-Marcel and A. de Vernal, chap. 6, pp. 213–262, Elsevier, Amsterdam, doi:10.1016/S1572-5480(07)01011-1.
- Kucera, M., and K. F. Darling (2002), Cryptic species of planktonic foraminifera: their effect on palaeoceanographic reconstructions, *Philosophical Transactions of the Royal Society of London Series A*, *360*(1793), 695–718.
- Kucera, M., M. Weinelt, T. Kiefer, U. Pflaumann, A. Hayes, M. Weinelt, M.-T. Chen, A. C. Mix, T. T. Barrows, E. Cortijo, J. Duprat, S. Juggins, and C. Waelbroeck (2005), Reconstruction of sea-surface temperatures from assemblages of planktonic foraminifera: multi-technique approach based on geographically constrained calibration data sets and its application to glacial Atlantic and Pacific Oceans, *Quaternary Science Reviews*, *24*, 951–998, doi:10.1016/j.quascirev.2004.07.014.
- Kuroyanagi, A., and H. Kawahata (2004), Vertical distribution of living planktonic foraminifera in the seas around Japan, *Marine Micropaleontology*, *53*, 173–196, doi:10.1016/j.marmicro.2004.06.001.
- Kuroyanagi, A., H. Kawahata, H. Nishi, and M. C. Honda (2002), Seasonal changes in planktonic foraminifera in the north-western North Pacific Ocean: sediment trap experiments from subarctic and subtropical gyres, *Deep-Sea Research Part II*, *49*, 5627–5645, doi:10.1016/S0967-0645(02)00202-3.
- Labeyrie, L., L. Vidal, E. Cortijo, M. Paterne, M. Arnold, J. C. Duplessy, M. Vautravers, M. Labracherie, J. Duprat, J. L. Turon, F. Grousset, and T. van Weering (1995), Surface and deep hydrology of the Northern Atlantic Ocean during the past 150 000 years, *Philosophical Transactions of the Royal Society of London Series B*, *348*(1324), 255–264.
- Lambeck, K., T. M. Esat, and E.-K. Potter (2002), Links between climate and sea levels for the past three million years, *Nature*, *419*, 199–206, doi:10.1038/nature01089.
- Lambeck, K., M. Anzidei, F. Antonioli, A. Benini, and A. Esposito (2004), Sea level in Roman time in the Central Mediterranean and implications for recent change, *Earth and Planetary Science Letters*, *224*, 563–575, doi:10.1016/j.epsl.2004.05.031.
- Lambeck, K., C. D. Woodroffe, F. Antonioli, M. Anzidei, W. R. Gehrels, J. Laborel, and A. J. Wright (2010), Paleoenvironmental Records, Geophysical Modeling, and Reconstruction of Sea-Level Trends and Variability on Centennial and Longer Timescales, in *Understanding Sea-Level Rise and Variability*, edited by J. A. Church, P. L. Woodworth, T. Aarup, and W. S. Wilson, pp. 61–121, Wiley-Blackwell, Hoboken, NJ, USA.
- Large, W. G., and S. G. Yeager (2004), Diurnal to Decadal Global Forcing For Ocean and Sea-Ice Models: The Data Sets and Flux Climatologies, *Tech. Rep. May*, NCAR Technical Note NCAR/TN-460+STR.
- Large, W. G., and S. G. Yeager (2009), The global climatology of an interannually varying air–sea flux data set, *Climate Dynamics*, *33*(2-3), 341–364, doi:10.1007/s00382-008-0441-3.
- Lassen, M. K., K. D. Nielsen, K. Richardson, K. Garde, and L. Schlüter (2010), The effects of temperature increases on a temperate phytoplankton community — A mesocosm climate change scenario, *Journal of Experimental Marine Biology and Ecology*, *383*, 79–88, doi:10.1016/j.jembe.2009.10.014.
- Lebreiro, S., J. Moreno, I. McCave, and P. Weaver (1996), Evidence for Heinrich layers off Portugal (Tore Seamount: 39°N, 12°W), *Marine Geology*, *131*, 47–56.
- Leorri, E., A. Cearreta, and G. Milne (2012), Field observations and modelling of Holocene sea-level changes in the southern Bay of Biscay: implication for understanding current rates of relative sea-level change and vertical land motion along the Atlantic coast of SW Europe, *Quaternary Science Reviews*, *42*, 59–73, doi:10.1016/j.quascirev.2012.03.014.

- Leu, E., J. E. Sørensen, D. O. Hessen, S. Falk-Petersen, and J. Berge (2011), Consequences of changing sea-ice cover for primary and secondary producers in the European Arctic shelf seas: Timing, quantity, and quality, *Progress in Oceanography*, *90*, 18–32, doi:10.1016/j.pocean.2011.02.004.
- Lindsay, K., G. B. Bonan, S. C. Doney, F. M. Hoffman, D. M. Lawrence, M. C. Long, N. M. Mahowald, J. K. Moore, J. T. Randerson, and P. E. Thornton (2014), Preindustrial-Control and Twentieth-Century Carbon Cycle Experiments with the Earth System Model CESM1(BGC), *Journal of Climate*, *27*, 8981–9005, doi:10.1175/JCLI-D-12-00565.1.
- Liu, Z., B. L. Otto-Bliesner, F. He, E. C. Brady, R. Tomas, P. U. Clark, A. E. Carlson, J. Lynch-Stieglitz, W. Curry, E. Brook, D. Erickson, R. Jacob, J. Kutzbach, and J. Cheng (2009), Transient simulation of last deglaciation with a new mechanism for Bølling-Allerød warming, *Science*, *325*, 310–314, doi:10.1126/science.1171041.
- Lombard, F., L. Labeyrie, E. Michel, L. Bopp, E. Cortijo, S. Retailleau, H. Howa, and F. Jorissen (2011), Modelling planktic foraminifer growth and distribution using an ecophysiological multi-species approach, *Biogeosciences*, *8*, 853–873, doi:10.5194/bg-8-853-2011.
- Lubinski, D. J., L. Polyak, and S. L. Forman (2001), Freshwater and Atlantic water inflows to the deep northern Barents and Kara seas since ca 13 ¹⁴C ka: foraminifera and stable isotopes, *Quaternary Science Reviews*, *20*, 1851–1879, doi:10.1016/S0277-3791(01)00016-6.
- Luo, C., N. M. Mahowald, and J. del Corral (2003), Sensitivity study of meteorological parameters on mineral aerosol mobilization, transport, and distribution, *Journal of Geophysical Research*, *108*(D15), 4447, doi:10.1029/2003JD003483.
- Mackas, D. L., W. Greve, M. Edwards, S. Chiba, K. Tadokoro, D. Eloire, M. G. Mazzocchi, S. Batten, A. J. Richardson, C. Johnson, E. Head, A. Conversi, and T. Peluso (2012), Changing zooplankton seasonality in a changing ocean: Comparing time series of zooplankton phenology, *Progress in Oceanography*, *97-100*, 31–62, doi:10.1016/j.pocean.2011.11.005.
- Mahowald, N., K. Kohfeld, M. Hansson, Y. Balkanski, S. P. Harrison, I. C. Prentice, M. Schulz, and H. Rodhe (1999), Dust sources and deposition during the last glacial maximum and current climate: A comparison of model results with paleodata from ice cores and marine sediments, *Journal of Geophysical Research*, *104*(D13), 15,895–15,916, doi:10.1029/1999JD900084.
- Mann, K. H., and J. R. N. Lazier (1996), *Dynamics of Marine Ecosystems: Biological-Physical Interactions in the Oceans*, 2nd ed., 394 pp., Blackwell Publishing Ltd.
- Maslin, M. A., N. J. Shackleton, and U. Pflaumann (1995), Surface water temperature, salinity, and density changes in the northeast Atlantic during the last 45,000 years: Heinrich events, deep water formation, and climatic rebounds, *Paleoceanography*, *10*(3), 527–544.
- McManus, J. F., G. C. Bond, W. S. Broecker, S. Johnsen, L. Labeyrie, and S. Higgins (1994), High-resolution climate records from the North Atlantic during the last interglacial, *Nature*, *371*, 326–329, doi:10.1038/371326a0.
- McManus, J. F., D. W. Oppo, and J. L. Cullen (1999), A 0.5-Million-Year Record of Millennial-Scale Climate Variability in the North Atlantic, *Science*, *283*, 971–975, doi:10.1126/science.283.5404.971.
- McManus, J. F., R. Francois, J.-M. Gherardi, L. D. Keigwin, and S. Brown-Leger (2004), Collapse and rapid resumption of Atlantic meridional circulation linked to deglacial climate changes, *Nature*, *428*, 834–837, doi:10.1038/nature02494.
- Merkel, U., M. Prange, and M. Schulz (2010), ENSO variability and teleconnections during glacial climates, *Quaternary Science Reviews*, *29*, 86–100, doi:10.1016/j.quascirev.2009.11.006.
- Miller, K. G., J. D. Wright, J. V. Browning, A. Kulpecz, M. Kominz, T. R. Naish, B. S. Cramer, Y. Rosenthal, W. R. Peltier, and S. Sosdian (2012), High tide of the warm Pliocene: Implications of global sea level for Antarctic deglaciation, *Geology*, *40*(5), 407–410, doi:10.1130/G32869.1.
- Mix, A. C. (1986), Late Quaternary paleoceanography of the Atlantic Ocean: Foraminiferal faunal and stable-isotopic evidence, Phd thesis, Columbia University, New York, U.S.A.

- Mix, A. C. (1987), The oxygen-isotope record of glaciation, in *The Geology of North America*, chap. 6, pp. 111–135, The Geological Society of America.
- Mix, A. C., and W. F. Ruddiman (1985), Structure and timing of the last deglaciation: Oxygen-isotope evidence, *Quaternary Science Reviews*, 4, 59–108.
- Mohiuddin, M. M., A. Nishimura, Y. Tanaka, and A. Shimamoto (2002), Regional and interannual productivity of biogenic components and planktonic foraminiferal fluxes in the northwestern Pacific Basin, *Marine Micropaleontology*, 45, 57–82, doi:10.1016/S0377-8398(01)00045-7.
- Mohiuddin, M. M., A. Nishimura, Y. Tanaka, and A. Shimamoto (2004), Seasonality of biogenic particle and planktonic foraminifera fluxes: Response to hydrographic variability in the Kuroshio Extension, northwestern Pacific Ocean, *Deep-Sea Research Part I*, 51, 1659–1683, doi:10.1016/j.dsr.2004.06.002.
- Mohiuddin, M. M., A. Nishimura, and Y. Tanaka (2005), Seasonal succession, vertical distribution, and dissolution of planktonic foraminifera along the Subarctic Front: Implications for paleoceanographic reconstruction in the northwestern Pacific, *Marine Micropaleontology*, 55, 129–156, doi:10.1016/j.marmicro.2005.02.007.
- Monastersky, R. (2013), Global carbon dioxide levels near worrisome milestone, *Nature*, 497, 13–14, doi:10.1038/497013a.
- Monterey, G., and S. Levitus (1997), Seasonal variability of mixed layer depth for the world ocean, *Tech. rep.*, Washington, D.C.
- Moore, J. K., and O. Braucher (2008), Sedimentary and mineral dust sources of dissolved iron to the world ocean, *Biogeosciences*, 5, 631–656.
- Moore, J. K., S. C. Doney, J. A. Kleypas, D. M. Glover, and I. Y. Fung (2002a), An intermediate complexity marine ecosystem model for the global domain, *Deep Sea Research II*, 49, 403–462.
- Moore, J. K., S. C. Doney, D. M. Glover, and I. Y. Fung (2002b), Iron cycling and nutrient-limitation patterns in surface waters of the World Ocean, *Deep Sea Research II*, 49, 463–507.
- Moore, J. K., S. C. Doney, and K. Lindsay (2004), Upper ocean ecosystem dynamics and iron cycling in a global three-dimensional model, *Global Biogeochemical Cycles*, 18, GB4028, doi:10.1029/2004GB002220.
- Moore, J. K., S. C. Doney, K. Lindsay, N. Mahowald, and A. F. Michaels (2006), Nitrogen fixation amplifies the ocean biogeochemical response to decadal timescale variations in mineral dust deposition, *Tellus*, 58B, 560–572, doi:10.1111/j.1600-0889.2006.00209.x.
- Moore, J. K., K. Lindsay, S. C. Doney, M. C. Long, and K. Misumi (2013), Marine Ecosystem Dynamics and Biogeochemical Cycling in the Community Earth System Model [CESM1(BGC)]: Comparison of the 1990s with the 2090s under the RCP4.5 and RCP8.5 Scenarios, *Journal of Climate*, 26, 9291–9312, doi:10.1175/JCLI-D-12-00566.1.
- Morard, R., F. Quillévéré, G. Escarguel, T. de Garidel-Thoron, C. de Vargas, and M. Kucera (2013), Ecological modeling of the temperature dependence of cryptic species of planktonic Foraminifera in the Southern Hemisphere, *Palaeogeography, Palaeoclimatology, Palaeoecology*, 391, 13–33, doi:10.1016/j.palaeo.2013.05.011.
- Morey, A. E., A. C. Mix, and N. G. Piasis (2005), Planktonic foraminiferal assemblages preserved in surface sediments correspond to multiple environment variables, *Quaternary Science Reviews*, 24, 925–950, doi:10.1016/j.quascirev.2003.09.011.
- Mortyn, P. G., and C. D. Charles (2003), Planktonic foraminiferal depth habitat and $\delta^{18}\text{O}$ calibrations: Plankton tow results from the Atlantic sector of the Southern Ocean, *Paleoceanography*, 18(2), 1037, doi:10.1029/2001PA000637.
- Mulitza, S., T. Wolff, J. Pätzold, W. Hale, and G. Wefer (1998), Temperature sensitivity of planktic foraminifera and its influence on the oxygen isotope record, *Marine Micropaleontology*, 33, 223–240.
- Murray, J. (1897), On the distribution of the pelagic foraminifera at the surface and on the floor of the ocean, *Natural Science*, 11, 17–27.

- Naidu, P. D., and B. A. Malmgren (1996), A high-resolution record of late Quaternary upwelling along the Oman Margin, Arabian Sea based on planktonic foraminifera, *Paleoceanography*, *11*(1), 129–140.
- NEEM community members (2013), Eemian interglacial reconstructed from a Greenland folded ice core, *Nature*, *493*, 489–494, doi:10.1038/nature11789.
- Northcote, L. C., and H. L. Neil (2005), Seasonal variations in foraminiferal flux in the Southern Ocean, Campbell Plateau, New Zealand, *Marine Micropaleontology*, *56*, 122–137, doi:10.1016/j.marmicro.2005.05.001.
- O'Neil, J. R., R. N. Clayton, and T. K. Mayeda (1969), Oxygen Isotope Fractionation in Divalent Metal Carbonates, *The Journal of Chemical Physics*, *51*(12), 5547–5558, doi:10.1063/1.1671982.
- Ortiz, J. D., A. C. Mix, and R. W. Collier (1995), Environmental control of living symbiotic and asymbiotic foraminifera of the California Current, *Paleoceanography*, *10*(6), 987–1009.
- Otto-Bliesner, B. L., N. Rosenbloom, E. J. Stone, N. P. McKay, D. J. Lunt, E. C. Brady, and J. T. Overpeck (2013), How warm was the last interglacial? New model-data comparisons, *Phil Trans R Soc A*, *371*, 20130097, doi:10.1098/rsta.2013.0097.
- Pados, T., and R. F. Spielhagen (2014), Species distribution and depth habitat of recent planktic foraminifera in Fram Strait, Arctic Ocean, *Polar Research*, *33*, 22483, doi:10.3402/polar.v33.22483.
- Pagani, M., Z. Liu, J. LaRiviere, and A. C. Ravelo (2010), High Earth-system climate sensitivity determined from Pliocene carbon dioxide concentrations, *Nature Geoscience*, *3*, 27–30, doi:10.1038/ngeo724.
- Parsons, T. R., M. Takahashi, and B. Hargrave (1984), *Biological Oceanographic Processes*, 3rd ed., Pergamon Press, Oxford.
- Pearson, P. N. (2012), Oxygen Isotopes in Foraminifera: Overview and Historical Review, *The Paleontological Society Papers*, *18*, 1–38.
- Peeters, F. J. C., and G.-J. A. Brummer (2002), The seasonal and vertical distribution of living planktic foraminifera in the NW Arabian Sea, *Geological Society, London, Special Publications*, *195*, 463–497, doi:10.1144/GSL.SP.2002.195.01.26.
- Peltier, W. R. (2005), On the hemispheric origins of meltwater pulse 1a, *Quaternary Science Reviews*, *24*, 1655–1671, doi:10.1016/j.quascirev.2004.06.023.
- Pérez-Folgado, M., F. Sierro, J. Flores, I. Cacho, J. Grimalt, R. Zahn, and N. Shackleton (2003), Western Mediterranean planktonic foraminifera events and millennial climatic variability during the last 70 kyr, *Marine Micropaleontology*, *48*, 49–70, doi:10.1016/S0377-8398(02)00160-3.
- Pflaumann, U., J. Duprat, C. Pujol, and L. D. Labeyrie (1996), SIMMAX: A modern analog technique to deduce Atlantic sea surface temperatures from planktonic foraminifera in deep-sea sediments, *Paleoceanography*, *11*(1), 15–35.
- Pflaumann, U., M. Sarnthein, M. Chapman, L. de Abreu, B. Funnell, M. Huels, T. Kiefer, M. Maslin, H. Schulz, J. Swallow, S. van Kreveland, M. Vautravers, E. Vogelsang, and M. Weinelt (2003), Glacial North Atlantic: Sea-surface conditions reconstructed by GLAMAP 2000, *Paleoceanography*, *18*(3), 1065, doi:10.1029/2002PA000774.
- Prell, W. L., A. Martin, J. L. Cullen, and M. Trend (1999), The Brown University Foraminiferal Data Base, *IGBP PAGES/World Data Center-A for Paleoclimatology, Data Contribution Series # 1999-027*, NOAA/NGDC Paleoclimatology Program, Boulder CO, USA.
- Quiquet, A., C. Ritz, H. J. Punge, and D. Salas y Méliá (2013), Greenland ice sheet contribution to sea level rise during the last interglacial period: a modelling study driven and constrained by ice core data, *Climate of the Past*, *9*, 353–366, doi:10.5194/cp-9-353-2013.
- Rasmussen, S. O., M. Bigler, S. P. Blockley, T. Blunier, S. L. Buchardt, H. B. Clausen, I. Cvijanovic, D. Dahl-Jensen, S. J. Johnsen, H. Fischer, V. Gkinis, M. Guillevic, W. Z. Hoek, J. J. Lowe, J. B. Pedro, T. Popp, I. K. Seierstad, J. P. Steffensen, A. M. Svensson, P. Vallelonga, B. M. Vinther, M. J. C. Walker, J. J. Wheatley, and M. Winstrup (2014), A stratigraphic framework for abrupt climatic changes during the Last Glacial period based on three synchronized Greenland ice-core records: refining and extending the INTIMATE event stratigraphy, *Quaternary Science Reviews*, *106*, 14–28, doi:10.1016/j.quascirev.2014.09.007.

- Ravelo, A. C., and C. Hillaire-Marcel (2007), The use of oxygen and carbon isotopes of foraminifera in paleoceanography, in *Proxies in Late Cenozoic Paleoceanography*, edited by C. Hillaire-Marcel and A. de Vernal, chap. 18, pp. 735–764, Elsevier, Amsterdam.
- Rebotim, A., A. H. L. Voelker, L. Jonkers, J. J. Waniek, H. Meggers, R. Schiebel, I. Fraile, M. Schulz, and M. Kucera (2017), Factors controlling the depth habitat of planktonic foraminifera in the subtropical eastern North Atlantic, *Biogeosciences*, *14*, 827–859, doi:10.5194/bg-14-827-2017.
- Reimer, P. J., M. G. L. Baillie, E. Bard, A. Bayliss, J. W. Beck, C. J. H. Bertrand, P. G. Blackwell, C. E. Buck, G. S. Burr, K. B. Cutler, P. E. Damon, R. L. Edwards, R. G. Fairbanks, M. Friedrich, T. P. Guilderson, A. G. Hogg, K. A. Hughen, B. Kromer, G. McCormac, S. Manning, C. Bronk Ramsey, R. W. Reimer, S. Remmele, J. R. Southon, M. Stuiver, S. Talamo, F. W. Taylor, J. van der Plicht, and C. E. Weyhenmeyer (2004), INTCAL04 terrestrial radiocarbon age calibration, 0–26 cal kyr BP, *Radiocarbon*, *46*(3), 1029–1058.
- Reimer, P. J., E. Bard, A. Bayliss, J. W. Beck, P. G. Blackwell, C. Bronk Ramsey, C. E. Buck, H. Cheng, R. L. Edwards, M. Friedrich, P. M. Grootes, T. P. Guilderson, H. Hafliðason, I. Hajdas, C. Hatté, T. J. Heaton, D. L. Hoffmann, A. G. Hogg, K. A. Hughen, K. F. Kaiser, B. Kromer, S. W. Manning, M. Niu, R. W. Reimer, D. A. Richards, E. M. Scott, J. R. Southon, R. A. Staff, C. S. Turney, and J. van der Plicht (2013), INTCAL13 and MARINE13 radiocarbon age calibration curves 0–50,000 years cal BP, *Radiocarbon*, *55*(4), 1869–1887.
- Richardson, A. (2008), In hot water: zooplankton and climate change, *ICES Journal of Marine Science*, *65*, 279–295, doi:10.1093/icesjms/fsn028.
- Ridley, J., J. M. Gregory, P. Huybrechts, and J. Lowe (2010), Thresholds for irreversible decline of the Greenland ice sheet, *Climate Dynamics*, *35*, 1049–1057, doi:10.1007/s00382-009-0646-0.
- Ridley, J. K., P. Huybrechts, J. M. Gregory, and J. A. Lowe (2005), Elimination of the Greenland Ice Sheet in a High CO₂ Climate, *Journal of Climate*, *18*, 3409–3427, doi:10.1175/JCLI3482.1.
- Rippert, N., D. Nürnberg, J. Raddatz, E. Maier, E. Hathorne, J. Bijma, and R. Tiedemann (2016), Constraining foraminiferal calcification depths in the western Pacific warm pool, *Marine Micropaleontology*, *128*, 14–27, doi:10.1016/j.marmicro.2016.08.004.
- Robinson, A., R. Calov, and A. Ganopolski (2011), Greenland ice sheet model parameters constrained using simulations of the Eemian Interglacial, *Climate of the Past*, *7*, 381–396, doi:10.5194/cp-7-381-2011.
- Robinson, A., R. Calov, and A. Ganopolski (2012), Multistability and critical thresholds of the Greenland ice sheet, *Nature Climate Change*, *2*, 429–432, doi:10.1038/nclimate1449.
- Roche, D., D. Paillard, and E. Cortijo (2004), Constraints on the duration and freshwater release of Heinrich event 4 through isotope modelling, *Nature*, *432*, 379–382, doi:10.1038/nature03040.1.
- Rohling, E. J., K. Grant, C. Hemleben, M. Kucera, A. P. Roberts, I. Schmeltzer, H. Schulz, M. Siccha, M. Siddall, and G. Trommer (2008), New constraints on the timing of sea level fluctuations during early to middle marine isotope stage 3, *Paleoceanography*, *23*, PA3219, doi:10.1029/2008PA001617.
- Rosow, W. B., and R. A. Schiffer (1991), ISCCP Cloud Data Products, *Bulletin of the American Meteorological Society*, *72*(1), 2–20.
- Roy, T., F. Lombard, L. Bopp, and M. Gehlen (2015), Projected impacts of climate change and ocean acidification on the global biogeography of planktonic Foraminifera, *Biogeosciences*, *12*, 2873–2889, doi:10.5194/bg-12-2873-2015.
- Ruddiman, W. F. (1977), Late Quaternary deposition of ice-rafted sand in the subpolar North Atlantic (lat 40° to 65°N), *Geological Society of America Bulletin*, *88*, 1813–1827, doi:10.1130/0016-7606(1977)88<1813>
- Salgueiro, E., A. H. L. Voelker, L. de Abreu, F. Abrantes, H. Meggers, and G. Wefer (2010), Temperature and productivity changes off the western Iberian margin during the last 150 ky, *Quaternary Science Reviews*, *29*, 680–695, doi:10.1016/j.quascirev.2009.11.013.

- Salmon, K. H., P. Anand, P. F. Sexton, and M. Conte (2015), Upper ocean mixing controls the seasonality of planktonic foraminifer fluxes and associated strength of the carbonate pump in the oligotrophic North Atlantic, *Biogeosciences*, *12*, 223–235, doi:10.5194/bg-12-223-2015.
- Sanchez Goñi, M. F., and S. P. Harrison (2010), Millennial-scale climate variability and vegetation changes during the Last Glacial: Concepts and terminology, *Quaternary Science Reviews*, *29*, 2823–2827, doi:10.1016/j.quascirev.2009.11.014.
- Santer, B. D., J. F. Painter, C. Bonfils, C. A. Mears, S. Solomon, T. M. L. Wigley, P. J. Gleckler, G. A. Schmidt, C. Doutriaux, N. P. Gillett, K. E. Taylor, P. W. Thorne, and F. J. Wentz (2013), Human and natural influences on the changing thermal structure of the atmosphere, *Proceedings of the National Academy of Sciences*, *110*, 17,235–17,240, doi:10.1073/pnas.1305332110.
- Sarnthein, M., K. Winn, J.-C. Duplessy, and M. R. Fontugne (1988), Global variations of surface ocean productivity in low and mid latitudes: Influence on CO₂ reservoirs of the deep ocean and atmosphere during the last 21,000 years, *Paleoceanography*, *3*(3), 361–399.
- Sarnthein, M., K. Winn, S. Jung, J.-C. Duplessy, L. Labeyrie, H. Erlenkeuser, and G. Ganssen (1994), Changes in east Atlantic deepwater circulation over the last 30,000 years: Eight time slice reconstructions, *Paleoceanography*, *9*(2), 209–267.
- Sarnthein, M., E. Jansen, M. Weinelt, M. Arnold, J. C. Duplessy, H. Erlenkeuser, A. Flatøy, G. Johannessen, T. Johannessen, S. Jung, N. Koc, L. Labeyrie, M. Maslin, U. Pflaumann, and H. Schulz (1995), Variations in Atlantic surface ocean paleoceanography, 50°–80°N: A time-slice record of the last 30,000 years, *Paleoceanography*, *10*(6), 1063–1094.
- Sarnthein, M., K. Stattegger, D. Dreger, H. Erlenkeuser, P. Grootes, B. J. Haupt, S. Jung, T. Kiefer, W. Kuhnt, U. Pflaumann, C. Schäfer-Neth, H. Schulz, M. Schulz, D. Seidov, J. Simstich, S. van Kreveld, E. Vogelsang, A. Völker, and M. Weinelt (2001), Fundamental Modes and Abrupt Changes in North Atlantic Circulation and Climate over the last 60 ky - Concepts, Reconstruction and Numerical Modeling, in *The Northern North Atlantic: A Changing Environment*, edited by P. Schäfer, W. Ritzrau, M. Schlüter, and J. Thiede, pp. 365–410, Springer, Berlin.
- Sarnthein, M., U. Pflaumann, and M. Weinelt (2003), Past extent of sea ice in the northern North Atlantic inferred from foraminiferal paleotemperature estimates, *Paleoceanography*, *18*(2), 1047, doi:10.1029/2002PA000771.
- Sarnthein, M., P. M. Grootes, J. P. Kennett, and M.-J. Nadeau (2007), ¹⁴C Reservoir Ages Show Deglacial Changes in Ocean Currents and Carbon Cycle, in *Ocean Circulation: Mechanisms and Impacts, Geophysical Monograph Series 173*, edited by A. Schmittner, J. Chiang, and S. Hemming, pp. 175–197, American Geophysical Union, Washington, D.C.
- Sasgen, I., M. van den Broeke, J. L. Bamber, E. Rignot, L. Sandberg Sørensen, B. Wouters, Z. Martinec, I. Velicogna, and S. B. Simonsen (2012), Timing and origin of recent regional ice-mass loss in Greenland, *Earth and Planetary Science Letters*, *333–334*, 293–303, doi:10.1016/j.epsl.2012.03.033.
- Sautter, L. R., and R. C. Thunell (1989), Seasonal succession of planktonic foraminifera, results from a four-year time-series sediment trap experiment in the Northeast Pacific, *Journal of Foraminiferal Research*, *19*, 253–267, doi:10.2113/gsjfr.19.4.253.
- Sautter, L. R., and R. C. Thunell (1991), Planktonic foraminiferal response to upwelling and seasonal hydrographic conditions: sediment trap results from San Pedro Basin, Southern California Bight, *Journal of Foraminiferal Research*, *21*(4), 347–363, doi:10.2113/gsjfr.21.4.347.
- Schiebel, R. (2002), Planktic foraminiferal sedimentation and the marine calcite budget, *Global Biogeochem. Cycles*, *16*(4), 1065, doi:10.1029/2001gb001459.
- Schiebel, R., and C. Hemleben (2005), Modern planktic foraminifera, *Paläontologische Zeitschrift*, *79*(1), 135–148, doi:10.1007/BF03021758.
- Schiebel, R., and C. Hemleben (2017), *Planktic Foraminifers in the Modern Ocean*, Springer, Berlin, Heidelberg.
- Schiebel, R., J. Waniek, M. Bork, and C. Hemleben (2001), Planktic foraminiferal production stimulated by chlorophyll redistribution and entrainment of nutrients, *Deep-Sea Research Part I: Oceanographic Research Papers*, *48*, 721–740.

- Schiebel, R., J. Waniek, A. Zeltner, and M. Alves (2002), Impact of the Azores Front on the distribution of planktic foraminifers, shelled gastropods, and coccolithophorids, *Deep-Sea Research Part II*, *49*, 4035–4050.
- Schönfeld, J., R. Zahn, and L. de Abreu (2003), Surface and deep water response to rapid climate changes at the Western Iberian Margin, *Global and Planetary Change*, *36*, 237–264, doi:10.1016/S0921-8181(02)00197-2.
- Schröder-Ritzrau, A., H. Andrulheit, S. Jensen, C. Samtleben, P. Schäfer, J. Matthiessen, H. C. Hass, A. Kohly, and J. Thiede (2001), Distribution, Export and Alteration of Fossilizable Plankton in the Nordic Seas, in *The Northern North Atlantic: A Changing Environment*, edited by P. Schäfer, W. Ritzrau, M. Schlüter, and J. Thiede, pp. 81–104, Springer, Berlin.
- Schulz, H. (1995), Sea-Surface Temperatures 10,000 years B.P. - Consequences of the Early Holocene Insolation Maximum, Dissertation, Christian-Albrechts-Universität Kiel, Germany.
- Seears, H. A., K. F. Darling, and C. M. Wade (2012), Ecological partitioning and diversity in tropical planktonic foraminifera, *BMC Evolutionary Biology*, *12*, 54, doi:10.1186/1471-2148-12-54.
- Seki, O., G. L. Foster, D. N. Schmidt, A. Mackensen, K. Kawamura, and R. D. Pancost (2010), Alkenone and boron-based Pliocene pCO₂ records, *Earth and Planetary Science Letters*, *292*, 201–211, doi:10.1016/j.epsl.2010.01.037.
- Shackleton, N. J. (1974), Attainment of isotopic equilibrium between ocean water and the benthonic foraminifera genus *Uvigerina*: Isotopic changes in the ocean during the last glacial, *Colloques Internationaux du C.N.R.S.*, *219*, 203–209.
- Shepherd, A., E. R. Ivins, G. A. V. R. Barletta, M. J. Bentley, S. Bettadpur, K. H. Briggs, D. H. Bromwich, R. Forsberg, N. Galin, M. Horwath, S. Jacobs, I. Joughin, M. A. King, J. T. M. Lenaerts, J. Li, S. R. M. Ligtenberg, A. Luckman, S. B. Luthcke, M. McMillan, R. Meister, G. Milne, J. Mouginot, A. Muir, J. P. Nicolas, J. Paden, A. J. Payne, H. Pritchard, E. Rignot, H. Rott, L. Sandberg Sørensen, T. A. Scambos, B. Scheuchl, E. J. O. Schrama, B. Smith, A. V. Sundal, J. H. van Angelen, W. J. van de Berg, M. R. van den Broeke, D. G. Vaughan, I. Velicogna, J. Wahr, P. L. Whitehouse, D. J. Wingham, D. Yi, D. Young, and H. J. Zwally (2012), A Reconciled Estimate of Ice-Sheet Mass Balance, *Science*, *338*, 1183–1189, doi:10.1126/science.1228102.
- Sherman, E., J. K. Moore, F. Primeau, and D. Tanouye (2016), Temperature influence on phytoplankton community growth rates, *Global Biogeochem. Cycles*, *30*, 550–559, doi:10.1002/2015GB005272. Received.
- Shields, C. A., D. A. Bailey, G. Danabasoglu, M. Jochum, J. T. Kiehl, S. Levis, and S. Park (2012), The Low-Resolution CCSM4, *Journal of Climate*, *25*, 3993–4014, doi:10.1175/JCLI-D-11-00260.1.
- Siddall, M., E. J. Rohling, W. G. Thompson, and C. Waelbroeck (2008), Marine Isotope Stage 3 sea level fluctuations: data synthesis and new outlook, *Reviews of Geophysics*, *46*, RG4003, doi:10.1029/2007RG000226.1.
- Simstich, J., M. Sarnthein, and H. Erlenkeuser (2003), Paired $\delta^{18}\text{O}$ signals of *Neogloboquadrina pachyderma* (s) and *Turborotalita quinqueloba* show thermal stratification structure in Nordic Seas, *Marine Micropaleontology*, *48*, 107–125, doi:10.1016/S0377-8398(02)00165-2.
- Skinner, L. C., and H. Elderfield (2005), Constraining ecological and biological bias in planktonic foraminiferal Mg/Ca and $\delta^{18}\text{O}_{\text{cc}}$: A multispecies approach to proxy calibration testing, *Paleoceanography*, *20*, PA1015, doi:10.1029/2004PA001058.
- Smetacek, V. S. (1985), Role of sinking in diatom life-history cycles: ecological, evolutionary and geological significance, *Marine Biology*, *84*, 239–251.
- Smith, R., P. Jones, B. Briegleb, F. Bryan, G. Danabasoglu, J. Dennis, J. Dukowicz, C. Eden, B. Fox-Kemper, P. Gent, M. Hecht, S. Jayne, M. Jochum, W. Large, K. Lindsay, M. Maltrud, N. Norton, S. Peacock, M. Vertenstein, and S. Yeager (2010), The Parallel Ocean Program (POP) reference manual: Ocean component of the Community Climate System Model (CCSM) and Community Earth System Model (CESM), *Tech. rep.*, Los Alamos National Laboratory.
- Spero, H. J. (1987), Symbiosis in the planktonic foraminifer, *Orbulina universa*, and the isolation of its symbiotic dinoflagellate, *Gymnodinium béii* sp. nov., *Journal of Phycology*, *23*, 307–317.
- Spero, H. J., and S. L. Parker (1985), Photosynthesis in the symbiotic planktonic foraminifer *Orbulina universa*, and its potential contribution to oceanic primary productivity, *Journal of Foraminiferal Research*, *15*(4), 273–281.

- Spezzaferri, S., M. Kucera, P. N. Pearson, B. S. Wade, S. Rappo, C. R. Poole, R. Morard, and C. Stalder (2015), Fossil and Genetic Evidence for the Polyphyletic Nature of the Planktonic Foraminifera "*Globigerinoides*", and Description of the New Genus *Trilobatus*, *PLoS ONE*, *10*(5), 1–20, doi:10.1371/journal.pone.0128108.
- Spielhagen, R. F., K.-H. Baumann, H. Erlenkeuser, N. R. Nowaczyk, N. Nørgaard-Pedersen, C. Vogt, and D. Weiel (2004), Arctic Ocean deep-sea record of northern Eurasian ice sheet history, *Quaternary Science Reviews*, *23*, 1455–1483, doi:10.1016/j.quascirev.2003.12.015.
- Spielhagen, R. F., K. Werner, S. Aagaard Sørensen, K. Zamelczyk, E. Kandiano, G. Budeus, K. Husum, T. M. Marchitto, and M. Hald (2011), Enhanced Modern Heat Transfer to the Arctic by Warm Atlantic Water, *Science*, *331*(6016), 450–453.
- Spindler, M., and G. S. Dieckmann (1986), Distribution and Abundance of the Planktic Foraminifer *Neogloboquadrina pachyderma* in Sea Ice of the Weddell Sea (Antarctica), *Polar Biology*, *5*, 185–191.
- Spindler, M., and C. Hemleben (1980), Symbionts in planktonic foraminifera (Protozoa), in *Endocytobiology, Endosymbiosis and Cell Biology*, edited by W. Schwemmler and H. E. A. Schenk, 1 ed., pp. 133–140, Berlin, New York.
- Stanford, J. D., E. J. Rohling, S. E. Hunter, A. P. Roberts, S. O. Rasmussen, E. Bard, J. McManus, and R. G. Fairbanks (2006), Timing of meltwater pulse 1a and climate responses to meltwater injections, *Paleoceanography*, *21*, PA4103, doi:10.1029/2006PA001340.
- Stanford, J. D., E. J. Rohling, S. Bacon, A. P. Roberts, F. E. Grousset, and M. Bolshaw (2011), A new concept for the paleoceanographic evolution of Heinrich event 1 in the North Atlantic, *Quaternary Science Reviews*, *30*, 1047–1066, doi:10.1016/j.quascirev.2011.02.003.
- Stangeew, E. (2001), Distribution and Isotopic Composition of Living Planktonic Foraminifera *N. pachyderma* (sinistral) and *T. quinqueloba* in the High Latitude North Atlantic, Ph.D. thesis, Christian-Albrechts-Universität zu Kiel.
- Stehman, C. P. (1972), Planktonic Foraminifera in Baffin Bay, Davis Strait and the Labrador Sea, *Maritime Sediments*, *8*(1), 13–19.
- Steinacher, M., F. Joos, T. L. Frölicher, L. Bopp, P. Cadule, V. Cocco, S. C. Doney, M. Gehlen, K. Lindsay, J. K. Moore, B. Schneider, and J. Segsneider (2010), Projected 21st century decrease in marine productivity: a multi-model analysis, *Biogeosciences*, *7*, 979–1005.
- Steinberg, D. K., and M. R. Landry (2017), Zooplankton and the Ocean Carbon Cycle, *Annual Review of Marine Science*, *9*, 413–444, doi:10.1146/annurev-marine-010814-015924.
- Stewart, I. A., K. F. Darling, D. Kroon, C. M. Wade, and S. R. Troelstra (2001), Genotypic variability in subarctic Atlantic planktic foraminifera, *Marine Micropaleontology*, *43*, 143–153, doi:10.1016/S0377-8398(01)00024-X.
- Stone, E. J., D. J. Lunt, J. D. Annan, and J. C. Hargreaves (2013), Quantification of the Greenland ice sheet contribution to Last Interglacial sea level rise, *Climate of the Past*, *9*, 621–639, doi:10.5194/cp-9-621-2013.
- Storz, D., H. Schulz, J. J. Waniek, D. E. Schulz-Bull, and M. Kučera (2009), Seasonal and interannual variability of the planktic foraminiferal flux in the vicinity of the Azores Current, *Deep-Sea Research I*, *56*, 107–124, doi:10.1016/j.dsr.2008.08.009.
- Stuiver, M., and P. J. Reimer (1993), Extended ^{14}C data base and revised CALIB 3.0 ^{14}C age calibration program, *Radiocarbon*, *35*(1), 215–230.
- Taboada, F. G., and R. Anadón (2014), Seasonality of North Atlantic phytoplankton from space: Impact of environmental forcing on a changing phenology (1998-2012), *Global Change Biology*, *20*, 698–712, doi:10.1111/gcb.12352.
- Takahashi, K., and A. W. H. Bé (1984), Planktonic foraminifera: factors controlling sinking speed, *Deep-Sea Research*, *31*(12), 1477–1500.
- Telford, R. J., C. Li, and M. Kucera (2013), Mismatch between the depth habitat of planktonic foraminifera and the calibration depth of SST transfer functions may bias reconstructions, *Climate of the Past*, *9*, 859–870, doi:10.5194/cp-9-859-2013.

- Thiede, J. (1975), Distribution of foraminifera in surface waters of a coastal upwelling area, *Nature*, *253*, 712–714, doi:10.1038/253712a0.
- Thornalley, D. J. R., I. N. McCave, and H. Elderfield (2010), Freshwater input and abrupt deglacial climate change in the North Atlantic, *Paleoceanography*, *25*, PA1201, doi:10.1029/2009PA001772.
- Ting, C. S., G. Rocoap, J. King, and S. W. Chisholm (2002), Cyanobacterial photosynthesis in the oceans: The origins and significance of divergent light-harvesting strategies, *Trends in Microbiology*, *10*(3), 134–142, doi:10.1016/S0966-842X(02)02319-3.
- Tolderlund, D. S., and A. W. H. Bé (1971), Seasonal distribution of planktonic foraminifera in the western North Atlantic, *Micropaleontology*, *17*(3), 297–329.
- Turney, C. S. M., and R. T. Jones (2010), Does the Agulhas Current amplify global temperatures during super-interglacials?, *Journal of Quaternary Science*, *25*(6), 839–843, doi:10.1002/jqs.1423.
- van den Broeke, M. R., E. M. Enderlin, I. M. Howat, P. Kuipers Munneke, B. P. Noël, W. J. van de Berg, E. van Meijgaard, and B. Wouters (2016), On the recent contribution of the Greenland ice sheet to sea level change, *The Cryosphere*, *10*, 1933–1946, doi:10.5194/tc-10-1933-2016.
- Vilks, G. (1970), Circulation of Surface Waters in Parts of the Canadian Arctic Archipelago Based on Foraminiferal Evidence, *Arctic*, *23*(2), 100–111.
- Vilks, G. (1975), Comparison of *Globorotalia pachyderma* (Ehrenberg) in the water column and sediments of the Canadian Arctic, *Journal of Foraminiferal Research*, *5*(4), 313–325.
- Vincent, E., and W. H. Berger (1981), Planktonic foraminifera and their use in Paleoceanography, in *The oceanic lithosphere. The sea*, edited by C. Emiliani, 7 ed., chap. 25, pp. 1025–1119, Harvard University Press, Cambridge, Massachusetts and London.
- Voelker, A. H. L. (1999), Dansgaard-Oeschger events in ultra-high resolution sediment records from the Nordic Seas, Dissertation, Christian-Albrechts-Universität Kiel, Germany.
- Voelker, A. H. L., and L. de Abreu (2011), A Review of Abrupt Climate Change Events in the Northeastern Atlantic Ocean (Iberian Margin): Latitudinal, Longitudinal, and Vertical Gradients, *Geophysical Monograph Series*, *193*, 15–37.
- Voelker, A. H. L., L. de Abreu, J. Schönfeld, H. Erlenkeuser, and F. Abrantes (2009), Hydrographic conditions along the western Iberian margin during marine isotope stage 2, *Geochemistry, Geophysics, Geosystems*, *10*(12), Q12U08, doi:10.1029/2009GC002605.
- Vogelsang, E. (1990), Paläo-Ozeanographie des Europäischen Nordmeeres an Hand stabiler Kohlenstoff- und Sauerstoffisotope, Dissertation, Christian-Albrechts-Universität Kiel, Deutschland.
- Vogelsang, E., M. Sarnthein, and U. Pflaumann (2001), $\delta^{18}\text{O}$ -Stratigraphy, Chronology, and Sea Surface Temperatures of Atlantic Sediment Records (GLAMAP-2000) Kiel, *Tech. Rep. 13*, Christian-Albrechts-Universität Kiel, Germany.
- Volkman, R. (2000), Planktic foraminifers in the outer Laptev Sea and the Fram Strait - modern distribution and ecology, *Journal of Foraminiferal Research*, *30*, 157–176.
- Waelbroeck, C., J.-C. Duplessy, E. Michel, L. Labeyrie, D. Paillard, and J. Duprat (2001), The timing of the last deglaciation in North Atlantic climate records, *Nature*, *412*, 724–727.
- Waelbroeck, C., S. Mulitza, H. Spero, T. Dokken, T. Kiefer, and E. Cortijo (2005), A global compilation of late Holocene planktonic foraminiferal $\delta^{18}\text{O}$: relationship between surface water temperature and $\delta^{18}\text{O}$, *Quaternary Science Reviews*, *24*, 853–868, doi:10.1016/j.quascirev.2003.10.014.
- Watkins, J. M., and A. C. Mix (1998), Testing the effects of tropical temperature, productivity, and mixed-layer depth on foraminiferal transfer functions, *Paleoceanography*, *13*(1), 96–105.

- Watkins, J. M., A. C. Mix, and J. Wilson (1996), Living planktic foraminifera: tracers of circulation and productivity regimes in the central equatorial Pacific, *Deep Sea Research II*, 43(4-6), 1257–1282.
- Watkins, J. M., A. C. Mix, and J. Wilson (1998), Living planktic foraminifera in the central tropical Pacific Ocean: Articulating the equatorial 'cold tongue' during La Niña, 1992, *Marine Micropaleontology*, 33, 157–174, doi:10.1016/S0377-8398(97)00036-4.
- Weinelt, M., E. Vogelsang, M. Kucera, U. Pflaumann, M. Sarnthein, A. Voelker, H. Erlenkeuser, and B. A. Malmgren (2003), Variability of North Atlantic heat transfer during MIS 2, *Paleoceanography*, 18(3), 1071, doi:10.1029/2002PA000772.
- Wilke, I., H. Meggers, and T. Bickert (2009), Depth habitats and seasonal distributions of recent planktic foraminifers in the Canary Islands region (29°N) based on oxygen isotopes, *Deep-Sea Research I*, 56, 89–106, doi:10.1016/j.dsr.2008.08.001.
- Wolfteich, C. M. (1994), Satellite-Derived Sea Surface Temperature, Mesoscale Variability, and Foraminiferal Production in the North Atlantic, M.Sc., Cambridge, MS.
- Xiao, W., R. Wang, L. Polyak, A. Astakhov, and X. Cheng (2014), Stable oxygen and carbon isotopes in planktonic foraminifera *Neogloboquadrina pachyderma* in the Arctic Ocean: An overview of published and new surface-sediment data, *Marine Geology*, 352, 397–408, doi:10.1016/j.margeo.2014.03.024.
- Yeager, S. G., C. A. Shields, W. G. Large, and J. J. Hack (2006), The Low-Resolution CCSM3, *Journal of Climate*, 19, 2545–2566.
- Yokoyama, M., and T. M. Esat (2011), Global climate and sea level: Enduring variability and rapid fluctuations over the past 150,000 years, *Oceanography*, 24(2), 54–69, doi:10.5670/oceanog.2011.27.COPYRIGHT.
- Yu, E.-F., R. Francois, M. P. Bacon, S. Honjo, A. P. Fleer, S. J. Manganini, M. M. Rutgers van der Loeff, and V. Ittekkot (2001), Trapping efficiency of bottom-tethered sediment traps estimated from the intercepted fluxes of ²³⁰Th and ²³⁰Pa, *Deep-Sea Research Part I*, 48, 865–889, doi:10.1016/S0967-0637(00)00067-4.
- Zachariasse, W.-J., F. J. Jorissen, C. Perissoratis, E. J. Rohling, and V. Tsapralis (1997), Late Quaternary foraminiferal changes and the nature of Sapropel S1 in Skopelos Basin, *Proceeding of the 5th Hellenic Symposium on Oceanography and Fisheries*, 1, 391–394.
- Žarić, S., B. Donner, G. Fischer, S. Mulitza, and G. Wefer (2005), Sensitivity of planktic foraminifera to sea surface temperature and export production as derived from sediment trap data, *Marine Micropaleontology*, 55, 75–105, doi:10.1016/j.marmicro.2005.01.002.
- Žarić, S., M. Schulz, and S. Mulitza (2006), Global prediction of planktic foraminiferal fluxes from hydrographic and productivity data, *Biogeosciences*, 3, 187–207.

Technical Model Description

S1.1 Coupling of PLAFOM2.0 to CESM1.2

The planktonic foraminifera model, version 2 (PLAFOM2.0) has been embedded into the ocean component of the Community Earth System Model, version 1.2.2 (CESM1.2) as a separate module. The source code of CESM1.2 can be downloaded from https://svn-ccsm-models.cgd.ucar.edu/cesm1/release_tags/cesm1_2_2. After successfully porting and validating CESM1.2 on the user's platform (see the CESM1.2 user's guide) the following files, which are provided in the electronic appendix, had to be customized and/or newly created to properly implement PLAFOM2.0:

- `plafom_parms.F90` (new)
- `plafom_mod.F90` (new)
- `ecosys_mod.F90` (changed)
- `ecosys_parms.F90` (changed)
- `passive_tracers.F90` (changed)
- `namelist_definition_pop2.xml` (changed)
- `namelist_defaults_pop2.xml` (changed)
- `build-namelist` (changed)
- `ocn.plafom.tavg.csh` (new)
- `pop2.buildexe.csh` (changed)
- `PLAFOM_IC_gx3v7_Nov2016.nc` (new)

The planktonic foraminifera model is executed as a submodel of the CESM1.2 active ocean model (i.e., the Parallel Ocean Program, version 2) with the ecosystem model being enabled. It is activated by adding the string 'plafom' to the CESM1.2 environment variable `$OCN_TRACER_MODULES` in the user's `$CASE/env_build.xml` file. Only active ocean cases using POP2 and including the CESM ocean ecosystem model can run PLAFOM2.0. When a new case is created, the user has to select a PLAFOM2.0 case by selecting a PLAFOM2.0 component set, in which the `$OCN_TRACER_MODULES` variable already includes the 'plafom' string (see `config_compsets.xml`).

The PLAFOM2.0 model code as well as the user modified files are copied into the `$CASE/SourceMods/src.pop2` directory before setting up the `$CASE`. The parameter values of PLAFOM2.0 and the corre-

sponding namelists are defined in the file `plafom_parms.F90`. Additionally, the PLAFOM2.0 namelists need to be added to the files `namelist_definition_pop2.xml`, `namelist_defaults_pop2.xml`, and `build-namelist`. To properly implement the planktonic foraminifera model into the ocean component of CESM1.2, the number of passive tracers has to be adjusted in `pop2.buildexe.csh`.

The source code of PLAFOM2.0 including the necessary equations and variables is given in `plafom_mod.F90` and has been added as a separate module to the code trunk of POP2. The input variables, needed to calculate the foraminifera carbon concentrations, are computed in the ecosystem model (`ecosystem_mod.F90`) and shared via the `passive_tracers.F90` subroutine (see Figure S1.1). The initial conditions for each planktonic foraminifera species (the initial values amount to $0.0125 \text{ mmol C/m}^3$) are read from the file `PLAFOM_IC_gx3v7_Nov2016.nc`. Depending on the component set, the forcing data for an active ocean case can be provided by the data models for atmosphere and river runoff or by the full atmosphere and land surface models.

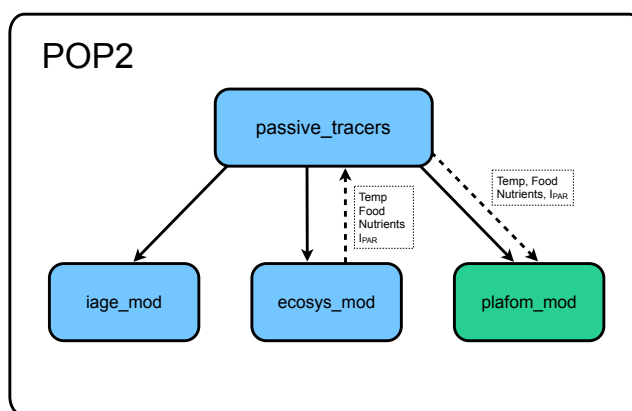


Figure S1.1: Schematic of the POP2 passive tracer modules active in the used CESM1.2 configuration, including the existing ecosystem module (`ecosys_mod`) and the new PLAFOM2.0 module (`plafom_mod`). The central `passive_tracers` module serves as driver for the tracer modules (solid arrows) and is additionally used to share those variables (i.e., temperature, food sources, nutrients, and photosynthetically active radiation) computed in the ecosystem model and needed by PLAFOM2.0 to perform the correct calculations (dashed arrows). Note that the passive tracers and ecosystem subroutines have been edited to properly implement PLAFOM2.0 to the code trunk of POP2.

The time-averaged output variables of the planktonic foraminifera model (i.e., `NPachyderma`, `NIncompta`, `GBulloides`, `GRuberW`, and `TSacculifer`) are set in the file `ocn.plafom.tavg.csh`. The desired variables are automatically added to the ocean model's output files. For instance, the monthly averaged fields are saved in a file in the format of `$CASE.pop.h.yyyy-mm.nc`.

For the simulations described here, component sets with an active ocean and active sea ice model as well as with data models for atmosphere, land, and river routing have been used. For instance, for the preindustrial-control simulation, the component set (`$COMPSET`) `G1850PLAFOM` has been chosen with a model resolution (`$RES`) of the form `T31_g37_rx1`, which refers to an atmospheric grid with a resolution of $\sim 3.75^\circ$ (T31), a 3° grid for the ocean and sea ice components (g37) as well as a 1° river routing grid (rx1). The preindustrial-control simulation was forced with the Coordinated Ocean-ice Reference Experiments Version 2 (CORE2) normal year forcing and the biogeochemical tracer fields have been initialized from data-based climatologies.

The following instructions show how to set up and run a CESM1.2-PLAFOM2.0 case in general:

```
#!/bin/csh -f
# ===== #
# 1. Create new case #
# ===== #

cd $CESMROOT/scripts
create_newcase -case $CASE \
  -compset $COMPSET \
  -res $RES \
  -mach $MACHINE

" Successfully created the case for $MACHINE "
```

```
# ===== #
# 2. Copy user changes #
# ===== #

cp $HOMEDIR/PLAFOM2.0/*.F90 $HOMEDIR/PLAFOM/*.xml $HOMEDIR/PLAFOM2.0/build-namelist \
  $HOMEDIR/PLAFOM2.0/ocn.plafom.tavg.csh $CASEDIR/SourceMods/src.pop2
cp $HOMEDIR/PLAFOM2.0/pop2.buildexe.csh $CASEDIR/Buildconf
cp $HOMEDIR/PLAFOM2.0/PLAFOM_IC_gx3v7_Nov2016.nc $DIN_LOC_ROOT
```

```
# ===== #
# 3. Set up and build case #
# ===== #

cd $CASEDIR
cesm_setup

" cesm_setup was successful "
```

```
$CASE.build

" CESM BUILDEXE SCRIPT HAS FINISHED SUCCESSFULLY "
```

```
# ===== #
# 4. Submit case #
# ===== #

xmlchange -id STOP_OPTION -val ndays/nmonths/nyears -file env_run.xml # sets run length
xmlchange -id STOP_N -val nn -file env_run.xml # sets run length
xmlchange -id REST_N -val nn -file env_run.xml # sets number of intervals to write restart files
```

```
$CASE.submit

" SUCCESSFUL TERMINATION OF CPL7-CCSM "
```

```
# ===== #
# 5. Resubmit case #
# ===== #

xmlchange -id CONTINUE_RUN -val TRUE -file env_run.xml # TRUE implies continuation run
xmlchange -id RESUBMIT -val nn -file env_run.xml # enables model to automatically resubmit a run
```

```
$CASE.submit

" SUCCESSFUL TERMINATION OF CPL7-CCSM "
```

S1.2 Model Notation, Parameters, and Equations

To ensure a smooth implementation of PLAFOM2.0, the parameters and equations used within the model code will be introduced and/or described below.

Biological Parameter Values

The following biological parameters are identical for each species and have the same values as in *Fraile et al.* (2008). The parameters given in day^{-1} have to be converted to sec^{-1} within the model code as CESM1.2

operates on time steps of seconds. Note that in the model the biological parameters have been set in the file `plafom_parms.F90` and the code name of each biological parameter is given in parentheses.

<i>g</i>	0.66	Grazing coefficient [mmol C/m ³] (<code>parm_f_grz</code>)
GGE	0.3	Gross Growth Efficiency (<code>parm_f_GGE</code>)
<i>G</i>_{max_{zo}}	2.16	Maximum foraminiferal grazing rate when grazing on zooplankton [day ⁻¹] (<code>parm_zf_umax</code>)
<i>G</i>_{max_{sp}}	1.08	Maximum foraminiferal grazing rate when grazing on small phytoplankton [day ⁻¹] (<code>parm_sf_umax</code>)
<i>G</i>_{max_{lp}}	1.08	Maximum foraminiferal grazing rate when grazing on diatoms [day ⁻¹] (<code>parm_diatf_umax</code>)
<i>G</i>_{max_{dr}}	1.08	Maximum foraminiferal grazing rate when grazing on detritus [day ⁻¹] (<code>parm_detrf_umax</code>)
<i>L</i>_{thres}	0.01	Threshold of foraminiferal concentration, where losses go to zero [mmol C/m ³] (<code>loss_thres_foram</code>)

Species-specific Parameter Values

Based on the species-specific preferred living conditions (depending on temperature, food, and/or light availability), species-specific parameters have been defined (Table S1.1), which are used within the model equations to determine the foraminifera carbon concentration. Note that the species-specific parameter values are given in the file `plafom_parms.F90` and since CESM1.2 operates on time steps of seconds the parameters given in day⁻¹ have to be converted to sec⁻¹ within the model code. The code name of each parameter is given in parentheses.

<i>T</i>_{opt}	Optimal temperature [°C] (<code>Topt</code>)
<i>σ</i>	Standard deviation of optimal temperature (<code>sigma</code>)
<i>T</i>_{thres_{min}}	Minimum tolerated temperature value [°C] (<code>T_thres_min</code>)
<i>T</i>_{thres_{max}}	Maximum tolerated temperature value [°C] (<code>T_thres_max</code>)
<i>p</i>_{zo}	Preference for grazing on zooplankton [0 – 1] (<code>f_graze_zoo</code>)
<i>p</i>_{sp}	Preference for grazing on small phytoplankton [0 – 1] (<code>f_graze_sp</code>)
<i>p</i>_{lp}	Preference for grazing on diatoms [0 – 1] (<code>f_graze_diat</code>)
<i>p</i>_{dr}	Preference for grazing on detritus [0 – 1] (<code>f_graze_detr</code>)
<i>p</i>_{zo*}	Preference for grazing on zooplankton when main food source is missing [0 – 1] (<code>f_graze_zoo2</code>)
<i>p</i>_{sp*}	Preference for grazing on small phytoplankton when main food source is missing [0 – 1] (<code>f_graze_sp2</code>)
<i>p</i>_{lp*}	Preference for grazing on diatoms when main food source is missing [0 – 1] (<code>f_graze_diat2</code>)
<i>p</i>_{dr*}	Preference for grazing on detritus when main food source is missing [0 – 1] (<code>f_graze_detr2</code>)
<i>k</i>	Parameter, which controls the influence of temperature depending on the food availability (<code>k_TC</code>)
<i>c</i>	Scaling parameter (<code>f_scale_parm</code>)
<i>P</i>_{F,0}	Maximum foraminiferal growth rate at a reference temperature [day ⁻¹] (<code>PFref</code>)
<i>α</i>_{PI}	Initial slope of the photosynthesis-light (PI) curve [m ² W ⁻¹ day ⁻¹] (<code>f_alphaPI</code>)
<i>p</i>_%	Fraction of photosynthesis potentially contributing to growth (<code>photo_frac</code>)
<i>f</i>_{mort}	Linear mortality rate [day ⁻¹] (<code>f_mort</code>)
<i>f</i>_{mort2}	Quadratic mortality rate [1/day/(mmol C/m ³)] (<code>f_mort2</code>)
<i>c</i>_{ij}	Maximum competition pressure of species <i>i</i> upon species <i>j</i> [0 – 1] (<code>c1_Np</code> , <code>c1_Ni</code> , <code>c1_Gb</code> , <code>c1_Gr</code> , <code>c1_Ts</code>)
<i>d</i>	Constant, controlling steepness of Michaelis-Menten equation (<code>steep_const_d</code>)

Model Equations and Local Variables

For each species the changes in the foraminifera carbon concentration are determined as follows:

$$\frac{dF}{dt} = (GGE \cdot TG) - ML \quad (\text{S1.1})$$

with *F* being the foraminifera carbon concentration, GGE is the portion of grazed matter that is incorporated into foraminiferal biomass, TG represents total grazing (i.e., the growth rate), and ML denotes mass loss (i.e., the mortality rate).

Table S1.1: Species-specific Model Parameters.

Species	<i>N. pachyderma</i>	<i>N. incompta</i>	<i>G. bulloides</i>	<i>G. ruber</i> (white)	<i>T. sacculifer</i>
T_{opt}	3.8 ⁺	15.0 ⁺	12.0 ⁺	23.5 ⁺	28.0 ⁺
σ	4.0 ⁺	6.0 ⁺	6.0 ⁺	4.0 ⁺	4.0 ⁺
$T_{thres_{min}}$	-	3.0	3.0	10.0	15.0 ⁺
$T_{thres_{max}}$	18.0	28.0	-	-	-
p_{zo}	0 ⁺	0 ⁺	0	0.6 ⁺	0.7 ⁺
p_{sp}	0.3 ⁺	0.2 ⁺	0	0 ⁺	0 ⁺
p_{lp}	0.7 ⁺	0.8 ⁺	0.9	0.2 ⁺	0.1 ⁺
p_{dr}	0 ⁺	0 ⁺	0.1	0.2 ⁺	0.2 ⁺
p_{zo*}	-	0 ⁺	0 ⁺	-	0.6 ⁺
p_{sp*}	-	0.4 ⁺	0.2 ⁺	-	0 ⁺
p_{lp*}	-	0.6 ⁺	0.8 ⁺	-	0.3 ⁺
p_{dr*}	-	0 ⁺	0 ⁺	-	0.1 ⁺
k	1.0 ⁺	1.2 ^{sp+}	1.25 ^{lp+}	1.0 ⁺	1.0 ⁺
c	10	15	15	10	10
$P_{F,0}$	-	-	2.6	2.6	2.6
α_{pl}	-	-	0.012	0.01	0.07
$p\%$	-	-	0.3	0.3	0.4
f_{mort}	0.06 ⁺	0.06 ⁺	0.06 ⁺	0.06 ⁺	0.06 ⁺
f_{mort2}	1.0 ⁺	4.0 ⁺	5.0 ⁺	5.0 ⁺	4.0 ⁺
$cl_{N.pachyderma,j}$	-	0.2 ⁺	0 ⁺	0 ⁺	0 ⁺
$cl_{N.incompta,j}$	-	-	0.1 ⁺	0.2	0 ⁺
$cl_{G.bulloides,j}$	-	0.8	-	0.8	0.8
$cl_{G.ruber(white),j}$	-	0.2	0.1	-	0.2
$cl_{T.sacculifer,j}$	-	0 ⁺	0.1	0.2	-
d	-	0.05 ⁺	0.5 ⁺	0.1	0.1

⁺ Denotes the same value as in *Frailé et al.* (2008).

Growth Rate

The growth rate depends on the available food and temperature sensitivity (TG_{graze}) as well as on light intensity (TG_{photo}):

$$TG = TG_{graze} + TG_{photo} \quad (S1.2)$$

The grazing rate is defined as:

$$TG_{graze} = \sum_{n=1}^4 p_n \cdot \left[G_{max_n} \cdot \alpha_{TG} \cdot F \cdot \left(\frac{C_n}{C_n + g} \right) \right]$$

$$g = \begin{cases} g & \text{if } n = \text{sp} \\ g \cdot 0.81 & \text{if } n = \text{zo, lp, dr} \end{cases}$$

$$p_n = \begin{cases} p_{n*} & \text{if } C_{lp} < 0.02 \text{ mmol C/m}^3 \\ & \text{(concerns } N. incompta \text{ and } G. bulloides) \\ & \text{or } T < 26^\circ \text{C (concerns } T. sacculifer) \\ p_n & \text{elsewhere} \end{cases}$$

where p_n , G_{max_n} , and C_n denote the species' grazing preference, the maximum foraminiferal grazing rate, and the carbon concentration when considering either zooplankton (zo), small phytoplankton (sp), diatoms (lp), or detritus (dr) as food source. p_{n*} describes the species' grazing preference when the main food source is missing and g is the grazing coefficient, which is set lower for diatoms, detritus, and zooplankton than for small phytoplankton (see *Moore et al.*, 2002a). α_{TG} is used to limit the foraminiferal growth rate

through temperature (T) and is calculated as follows:

$$\alpha_{TG} = \left\langle \frac{c}{\sigma \cdot \sqrt{2\pi}} \cdot \exp \left[-0.5 \cdot \left(\frac{T - T_{opt}}{\sigma} \right)^2 \right] \right\rangle^{\frac{1}{k}}$$

with c and k being parameters used for scaling and/or controlling the temperature influence depending on the food availability, whereas σ denotes the standard deviation of the species' optimal temperature (T_{opt}).

The photosynthetic growth rate is determined as follows:

$$TG_{photo} = P_{F, photo} \cdot F \cdot p\%$$

where $p\%$ represents the fraction of photosynthesis contributing to growth and $P_{F, photo}$ describes the foraminiferal specific rate of photosynthesis, defined as:

$$P_{F, photo} = P_{F, max} \cdot \left[1 - \exp \left(\frac{-\alpha_{PI} \cdot I_{PAR}}{P_{F, max}} \right) \right]$$

with $P_{F, max}$ being the maximum value of $P_{F, photo}$ at temperature T :

$$P_{F, max} = P_{F, 0} \cdot T_{func}$$

α_{PI} is the initial slope of the photosynthesis-light curve, I_{PAR} is the average irradiance over the mixed layer depth, $P_{F, 0}$ represents the maximum foraminiferal growth rate at a specific temperature T_0 , and T_{func} is the temperature response function used for scaling, which is defined as:

$$T_{func} = q_{10}^{\frac{T-T_0}{10}} \quad \text{with } T_0 = 30.0^\circ\text{C}, q_{10} = 1.5$$

To account for adaptation in low productivity regions, the growth of *G. ruber* (white) and *T. sacculifer* is limited to regions, where maximum nutrient (nitrate) and chlorophyll concentrations do not exceed a threshold value:

$$TG = \begin{cases} TG & \text{for } N. pachyderma, N. incompta, \text{ and } G. bulloides \\ TG \cdot Chl_m \cdot NO3_m & \text{for } G. ruber \text{ (white)} \\ TG \cdot Chl_m & \text{for } T. sacculifer \end{cases}$$

where the terms Chl_m and $NO3_m$ are used to mask high productivity areas through hyperbolic tangent functions:

$$Chl_m = 0.5 - 0.25 \cdot (\tanh [\max(Chl) \cdot 2.7 - 1.7] \cdot 2) + 0.006$$

$$NO3_m = 3 \cdot \left(0.5 - 0.25 \cdot \left(\tanh \left[\frac{\max(NO3)}{1.2} - 2 \right] \cdot 2 \right) + 0.006 \right)$$

with $\max(Chl)$ and $\max(NO3)$ denoting the maximum in the chlorophyll and/or nitrate concentration.

Mortality Rate

The mortality rate comprises of three terms representing respiration loss (ML_{resp}), predation by higher trophic levels (ML_{pred}), and competition among species (ML_{comp}):

$$ML = ML_{resp} + ML_{pred} + ML_{comp} \quad (S1.3)$$

The term for respiration loss is given by:

$$ML_{resp} = f_{mort} \cdot F_p$$

where f_{mort} describes the linear mortality rate and F_p is used to limit the planktonic foraminifera mortality at very low biomass levels and is calculated as follows:

$$F_p = \max((F - C_{thres}), 0)$$

with

$$C_{thres} = p_{loss} \cdot L_{thres}$$

$$p_{loss} = \begin{cases} 1 & \text{if } z \leq 100 \text{ m} \\ 0 & \text{if } z \geq 500 \text{ m} \\ \frac{500 - z}{400} & \text{if } z > 100 \text{ m and } z < 500 \text{ m} \end{cases}$$

C_{thres} is the threshold, at which losses go to zero depending on depth, p_{loss} determines the fraction of the grazing loss reduction at depth, and L_{thres} denotes the foraminiferal concentration threshold, at which losses go to zero.

The predation term is defined as follows:

$$ML_{pred} = f_{mort2} \cdot T_{func} \cdot F_p^2$$

where f_{mort2} represents the quadratic mortality rate.

Furthermore, competition is determined by:

$$ML_{comp} = \sum_i \left[F_p \cdot \frac{cl_{ij} \cdot F_i \cdot d}{F_i \cdot d + 0.1} \right]$$

with F_i being the concentration of the foraminiferal species exerting competition, cl_{ij} the maximum competition pressure of species i upon species j , and d the constant controlling the steepness of the Michaelis-Menten relationship for competition.

Local Variables

For overview purposes the local variables have been collectively listed in the following. Note that in the model the variable declarations occur in the module `plafom_mod.F90` and the code name of each variable is given in parentheses.

<i>F</i>	Foraminifera carbon concentration [mmol C/m ³] (<code>foram_loc</code>)
<i>TG</i>	Growth rate (i.e., total grazing) [mmol C/m ³ /day] (<code>Fgraze</code>)
<i>ML</i>	Mortality rate (i.e., mass loss) [mmol C/m ³ /day] (<code>f_loss</code>)
<i>F_p</i>	Term used to limit foraminifera mortality at low biomass [mmol C/m ³] (<code>Fprime</code>)
<i>C_{thres}</i>	Threshold, at which losses go to zero depending on depth [mmol C/m ³] (<code>C_loss_thres</code>)
<i>p_{loss}</i>	Fraction of grazing loss reduction at depth [0-1] (<code>f_loss_thres</code>)
<i>T_{func}</i>	Temperature response function [non-dim] (<code>Tfunc</code>)
<i>α_{TG}</i>	Foraminiferal growth limitation parameter [non-dim] (<code>f_alpha</code>)
<i>P_{F, photo}</i>	Foraminiferal specific rate of photosynthesis [day ⁻¹] (<code>PFphoto</code>)
<i>P_{F, max}</i>	Maximum value of <i>P_{F, photo}</i> at temperature <i>T</i> [day ⁻¹] (<code>PFmax</code>)
<i>Chl_m</i>	Term used to mask high productivity areas (<code>CHL_mask</code>)
<i>NO_{3m}</i>	Term used to mask high productivity areas (<code>NO3_mask</code>)
<i>T⁺</i>	Temperature [°C] (<code>TEMP</code>)
<i>C_{zo}⁺</i>	Zooplankton carbon concentration [mmol C/m ³] (<code>zooC</code>)
<i>C_{sp}⁺</i>	Small phytoplankton carbon concentration [mmol C/m ³] (<code>sphytoC</code>)
<i>C_{lp}⁺</i>	Large phytoplankton (i.e., diatom) carbon concentration [mmol C/m ³] (<code>lphytoC</code>)
<i>C_{dr}⁺</i>	Detrital carbon concentration [mmol C/m ³] (<code>ldetrC</code>)
<i>Chl⁺</i>	Chlorophyll concentration (<code>Chl</code>)
<i>NO₃⁺</i>	Nitrate concentration (<code>NO3</code>)
<i>I_{PAR}⁺</i>	Average irradiance over the mixed layer depth [W/m ²] (<code>PAR_avg</code>)

⁺ Determined in the ecosystem model (`ecosys_mod.F90`) and shared via the central passive tracers module (`passive_tracers.F90`) to be used in PLAFOM2.0 (`plafom_mod.F90`) (see Figure S1.1).

S1.3 Electronic Appendix

In addition to this technical model description, an electronic appendix is handed in. This appendix provides all files, which have been customized and/or newly created by the author, and which are necessary to properly run PLAFOM2.0 within CESM1.2.

Supporting Information for “Modeling the distribution and seasonality of *Neogloboquadrina pachyderma* in the North Atlantic Ocean during Heinrich Stadial 1”

Kerstin Kretschmer^{1*}, Michal Kucera¹, and Michael Schulz¹

¹MARUM-Center for Marine Environmental Sciences and Faculty of Geosciences, University of Bremen, Bremen, Germany

Contents of this file

Figure S2.1

Table S2.1

Introduction

This supporting information provides details about the parameter controlling the change in the modeled annual mean abundance pattern of *N. pachyderma* in the North Atlantic north of 30°N over the course of millennia. This information further supports and illustrates the findings of this study that changes in sea surface temperature (SST) from the Last Glacial Maximum (LGM) to Heinrich Stadial 1 (H1) to modern conditions most likely led to the shift in the distribution of *N. pachyderma* especially in the eastern North Atlantic (Figure S2.1). Therefore, we show the annual mean relative abundance of *N. pachyderma* with overlying SST contours for modern conditions, H1, and the LGM.

Additionally, the Heinrich Stadial 1 compilation of planktonic foraminiferal abundances considering the five species modeled by PLAFOM is provided (Table S2.1). The source information for each core is given in the main article in Table 2.1.

Relative abundance of *N. pachyderma* and Sea Surface Temperature

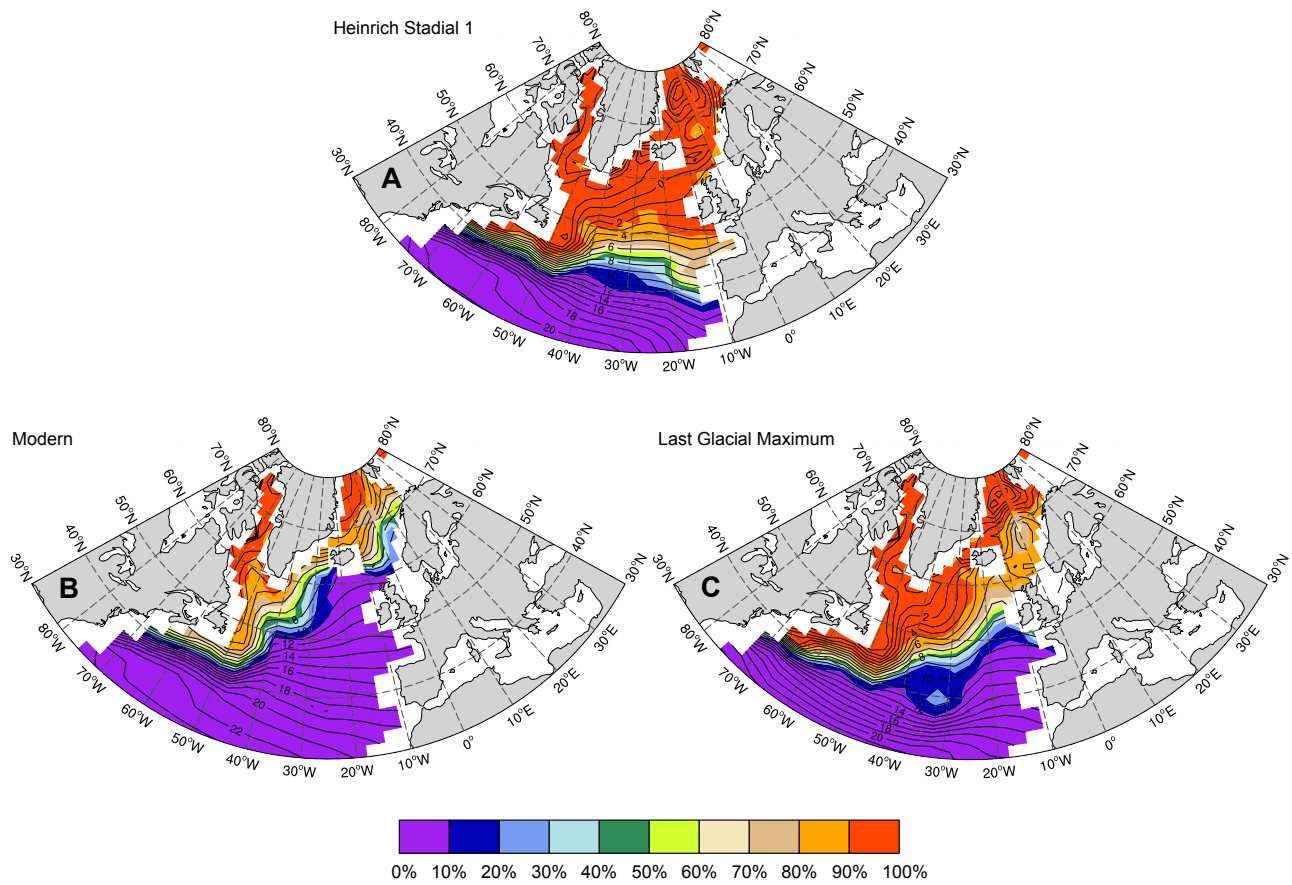


Figure S2.1: Annual mean relative abundances (% individuals) of *N. pachyderma* predicted by PLAFOM (colored contours) and annual mean sea surface temperature estimates (contour lines) for (a) Heinrich Stadial 1, (b) modern conditions, and (c) the Last Glacial Maximum. The relative abundances consider only the five foraminiferal species included in PLAFOM.

Table S2.1: Relative Abundances of Planktonic Foraminifera During Heinrich Stadial 1^a

Core	Core Details				Sample Details				Average Relative Abundance (%) ^b					Stdev. of Average Relative Abundance (±) ^b				
	Latitude (°N)	Longitude (°E)	Water Depth (m)	H1 Interval from (cm) to (cm)	Sample Size ^c	Fraction (μm) ^d	Np	Ni	Gb	Gr _w	Gs	Np	Ni	Gb	Gr _w	Gs		
GIK17730-4	72.11	7.39	2749	122.50	132.50	> 150	97.78	1.98	0.24	0.00	0.00	0.77	0.64	0.39	0.00	0.00		
PS1243-1	69.37	-6.55	2711	44.00	48.00	3	97.45	2.28	0.27	0.00	0.00	1.53	1.24	0.31	0.00	0.00		
GIK23065-2	68.50	0.83	2804	22.00	26.00	3	93.32	2.95	3.73	0.00	0.00	1.04	2.36	1.52	0.00	0.00		
GIK23071-3	67.09	2.91	1308	92.00	103.00	3	98.49	1.38	0.13	0.00	0.00	0.66	0.45	0.23	0.00	0.00		
GIK23074-1	66.67	4.91	1157	97.00	132.00	13	96.98	2.88	0.14	0.00	0.00	1.03	0.90	0.21	0.00	0.00		
L-348	63.95	-30.03	2262	31.00	83.00	4	93.04	4.17	2.78	0.00	0.00	8.29	3.80	4.92	0.00	0.00		
GIK16396-1	61.87	-11.24	1145	180.00	198.00	3	96.95	2.85	0.20	0.00	0.00	0.12	0.27	0.17	0.00	0.00		
MK-316	58.74	-27.29	2155	71.00	86.00	4	84.84	3.14	11.99	0.03	0.00	12.60	2.91	11.52	0.06	0.00		
GIK17051-3	56.16	-31.99	2295	180.00	190.00	2	85.36	4.28	10.36	0.00	0.00	7.77	0.18	7.59	0.00	0.00		
L-198	55.71	-18.90	1265	-	80.00	1	95.42	2.97	1.61	0.00	0.00	n.a.	n.a.	n.a.	n.a.	n.a.		
GIK17049-6	55.26	-26.73	3331	140.00	-	1	64.56	16.52	18.92	0.00	0.00	n.a.	n.a.	n.a.	n.a.	n.a.		
GIK23415-9	53.18	-19.15	2472	105.00	129.00	14	48.99	27.36	23.63	0.03	0.00	19.22	13.45	7.95	0.06	0.00		
GIK17045-3	52.43	-16.67	3663	66.00	70.00	3	91.79	4.05	4.16	0.00	0.00	3.70	2.65	2.28	0.00	0.00		
GIK15612-2	44.36	-26.54	3050	37.75	44.75	6	58.65	18.36	21.98	0.96	0.05	14.96	6.19	8.29	0.71	0.11		
SU92-03	43.20	-10.11	3005	61.75	87.50	8	94.71	2.87	2.33	0.09	0.00	1.63	0.65	1.67	0.19	0.00		
MD81-BC15	41.95	5.93	2500	46.00	65.00	4	2.98	22.99	74.02	0.00	0.00	1.63	15.60	15.30	0.00	0.00		
MD95-2040	40.58	-9.86	2465	206.50	299.50	31	78.95	8.29	12.12	0.64	0.00	19.08	10.78	7.63	1.17	0.00		
MD95-2041	37.83	-9.51	1123	181.50	271.50	10	51.15	10.18	37.75	0.87	0.05	9.80	6.02	6.46	0.61	0.10		
MD95-2043	36.14	-2.62	1841	710.00	800.00	9	3.16	75.50	20.76	0.57	0.00	2.68	13.27	13.27	0.52	0.00		
GIK15637-1	27.01	-18.99	3849	46.00	50.00	3	1.44	41.31	36.09	19.62	1.55	0.61	9.86	6.30	3.96	0.70		
A180-39	25.83	-19.30	3470	20.00	-	1	16.39	0.00	52.46	30.33	0.82	n.a.	n.a.	n.a.	n.a.	n.a.		
V30-51	19.87	-19.92	3409	45.00	-	1	1.71	45.30	48.21	3.59	1.20	n.a.	n.a.	n.a.	n.a.	n.a.		
V30-49	18.43	-21.08	3093	52.00	64.00	4	0.84	33.43	57.02	5.47	3.24	0.35	3.03	3.52	0.95	1.56		
M35003-4	12.09	-61.24	1299	275.00	300.00	6	0.41	1.18	10.93	63.68	23.79	0.77	1.53	5.27	4.68	5.91		
RC09-49	11.18	-58.59	1851	60.00	75.00	4	1.10	2.10	4.81	64.46	27.52	0.77	0.79	1.55	6.72	4.27		
V25-75	8.58	-53.17	2743	90.00	100.00	3	0.62	1.63	6.15	59.71	31.89	0.44	0.36	1.08	0.97	2.40		
V30-36	5.35	-27.32	4245	28.00	32.00	3	0.29	7.49	3.41	39.51	49.29	0.25	2.46	0.18	3.36	4.48		
V27-178	5.10	-26.65	4327	32.00	-	1	0.00	1.03	0.00	45.88	53.09	n.a.	n.a.	n.a.	n.a.	n.a.		
V25-60	3.28	-34.83	3749	37.50	41.00	2	0.25	3.43	3.82	54.73	37.78	0.35	0.17	1.67	3.72	2.23		
RC13-189	1.86	-30.00	3233	38.00	52.00	7	0.22	14.94	8.48	45.15	31.20	0.29	4.93	3.89	7.37	3.28		
V25-59	1.37	-33.48	3824	40.00	45.00	3	0.18	5.99	5.97	54.04	33.83	0.31	3.08	0.67	5.96	4.11		
RC24-1	0.56	-13.65	3850	36.00	44.00	3	0.00	40.32	6.87	29.28	23.53	0.00	2.45	2.51	3.13	1.34		
V30-41	0.22	-23.07	3874	36.50	38.50	2	0.49	41.14	11.10	27.15	20.11	0.19	6.46	0.29	2.82	3.54		
V15-168	0.20	-39.90	4219	105.00	115.00	2	0.00	1.83	1.57	41.92	54.67	0.00	0.10	0.27	7.39	7.22		

^a Planktonic foraminiferal census data for Heinrich Stadial 1 (H1) of those five species modeled by PLAFOM, i.e., *N. pachyderma* (Np), *N. incompta* (Ni), *G. bulloides* (Gb), *G. ruber* (white) (Gr_w), and *G. sacculifer* (Gs).

^b Based on the depth interval covering H1 the average relative abundance and the respective standard deviation have been calculated for each considered planktonic foraminiferal species.

^c Number of samples with counts in H1 based on the depth resolution of the respective core.

^d If the size fraction was not given (n.a.) in the original data set a size fraction > 150μm was assumed.

Supporting Information for “Modeling seasonal and vertical habitats of planktonic foraminifera on a global scale”

Kerstin Kretschmer^{1*}, Lukas Jonkers¹, Michal Kucera¹, and Michael Schulz¹

¹MARUM-Center for Marine Environmental Sciences and Faculty of Geosciences, University of Bremen, Bremen, Germany

Contents of this file

Figure S3.1 (page 131): 50-year (left panel) and 200-year (right panel) time series of the year-to-year difference (in mmol m^{-3}) of the modeled carbonate ion concentration (CO_3^{2-} ; grey), dissolved inorganic nitrate (NO_3^- ; light blue), small phytoplankton concentration (orange), zooplankton concentration (magenta), and the concentration of *N. pachyderma* (black) at the surface of the ocean, 105 m, 250 m, and 530 m water depth. Note that the left panel only shows a zoom for the latter three mentioned concentrations.

Figure S3.2 (page 132): Modeled peak timing (top row) and/or modeled peak amplitude (bottom row) vs. annual mean temperature (in $^{\circ}\text{C}$) averaged over the top 55 m of the water column for (a) *N. pachyderma*, (b) *N. incompta*, (c) *G. bulloides*, (d) *G. ruber* (white), and (e) *T. sacculifer*. The color coding corresponds to latitude. Modeled peak timing is given in months and modeled peak amplitudes have been log-transformed. Note that peak timings of each species from the southern hemisphere have been transformed to northern hemisphere equivalents by adding or subtracting 6 months. For a better visualization, the peak timing data has been offset along the ordinate axis to avoid that overlapping points plot on top of each other (this has been achieved by adding a small amount of white noise to the peak timing data). The grey shadings in the top row panels show the data density, i.e., where most of the data points occur.

Figure S3.3 (pages 133-143): Comparison of export planktonic foraminiferal shell fluxes in sediment traps (in $\log_{10}[\#\text{ m}^{-2}\text{ day}^{-1}]$; grey triangles) with the residuals (i.e., the deviation from the mean) of the volume integrated modeled biomass (in $\text{mmol C m}^{-3} \times 10^{-4}$; light blue squares). The respective location of each sediment trap is given in Table S3.1.

Figure S3.4 (pages 144-155): Comparison of the vertical distribution of live specimens in plankton tows (in $\#\text{ m}^{-3}$; grey bars) with modeled concentrations over depth (in mmol C m^{-3} ; light blue profiles). Dashed dark grey and blue lines indicate average living depth (in m) and vertical dispersion calculated for the plankton

tows ($ALD_{\text{tow}} \pm VD_{\text{tow}}$) and PLAFOM2.0 ($ALD_{\text{mod}} \pm VD_{\text{mod}}$), respectively. The respective location of each plankton tow sample is given in Table S3.2.

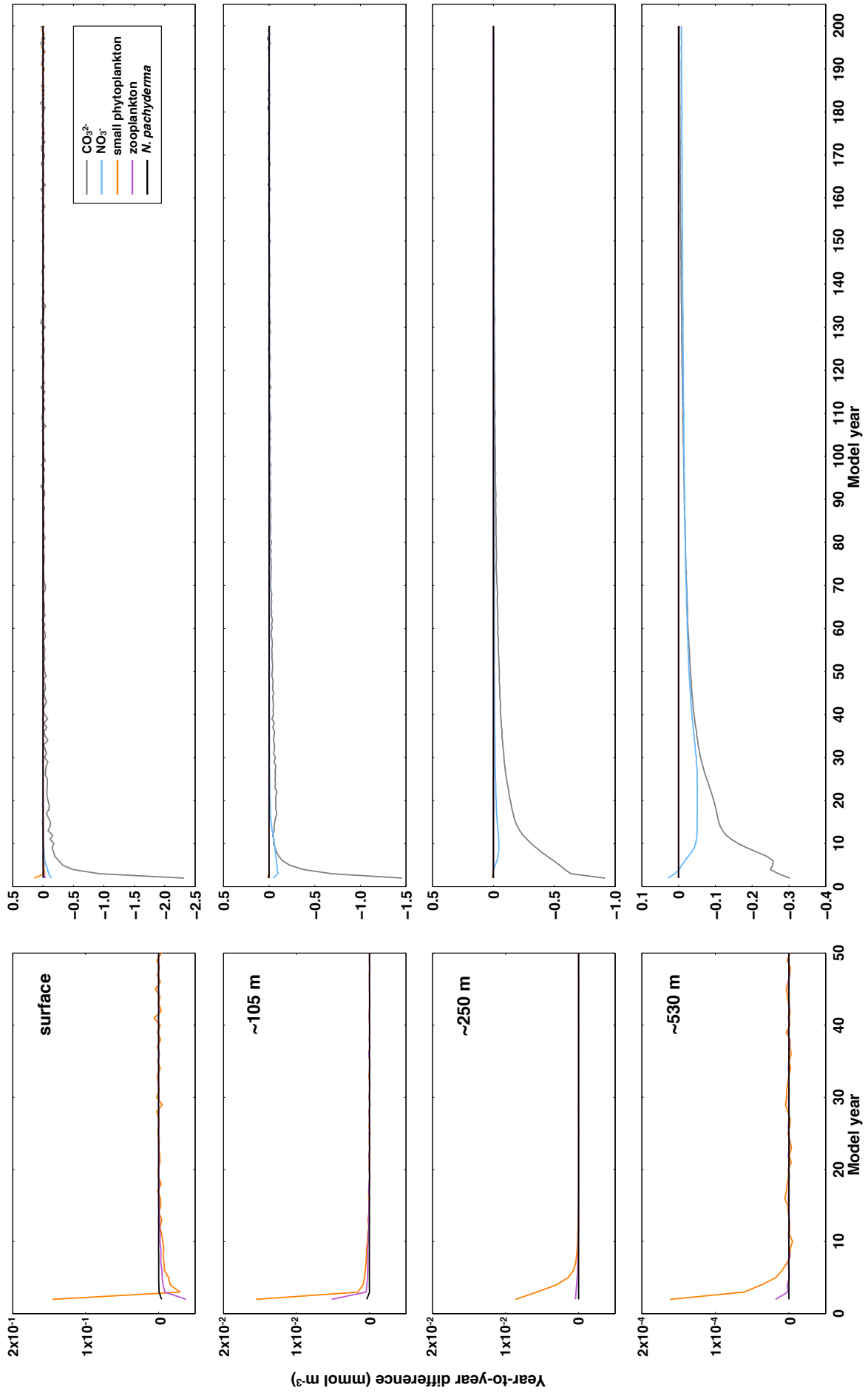
Table S3.1 (page 156): Information on sediment trap data.

Table S3.2 (pages 157-159): Information on plankton tow data.

Table S3.3 (pages 160-161): (a) Peak season (i.e., season of maximum production) and (b) peak amplitude (i.e., maximum in production divided by the annual mean) for each planktonic foraminiferal species at the locations of the sediment traps shown in Figure 3.1b in the main text. Empty cells indicate absence of species in either the sediment trap data or the model output.

Table S3.4 (page 162): Average living depths for each planktonic foraminiferal species at the locations of the plankton tows shown in Figure 3.1b in the main text. Empty cells indicate if species has been absent in either the plankton tow data or the model output.

Figure S3.1



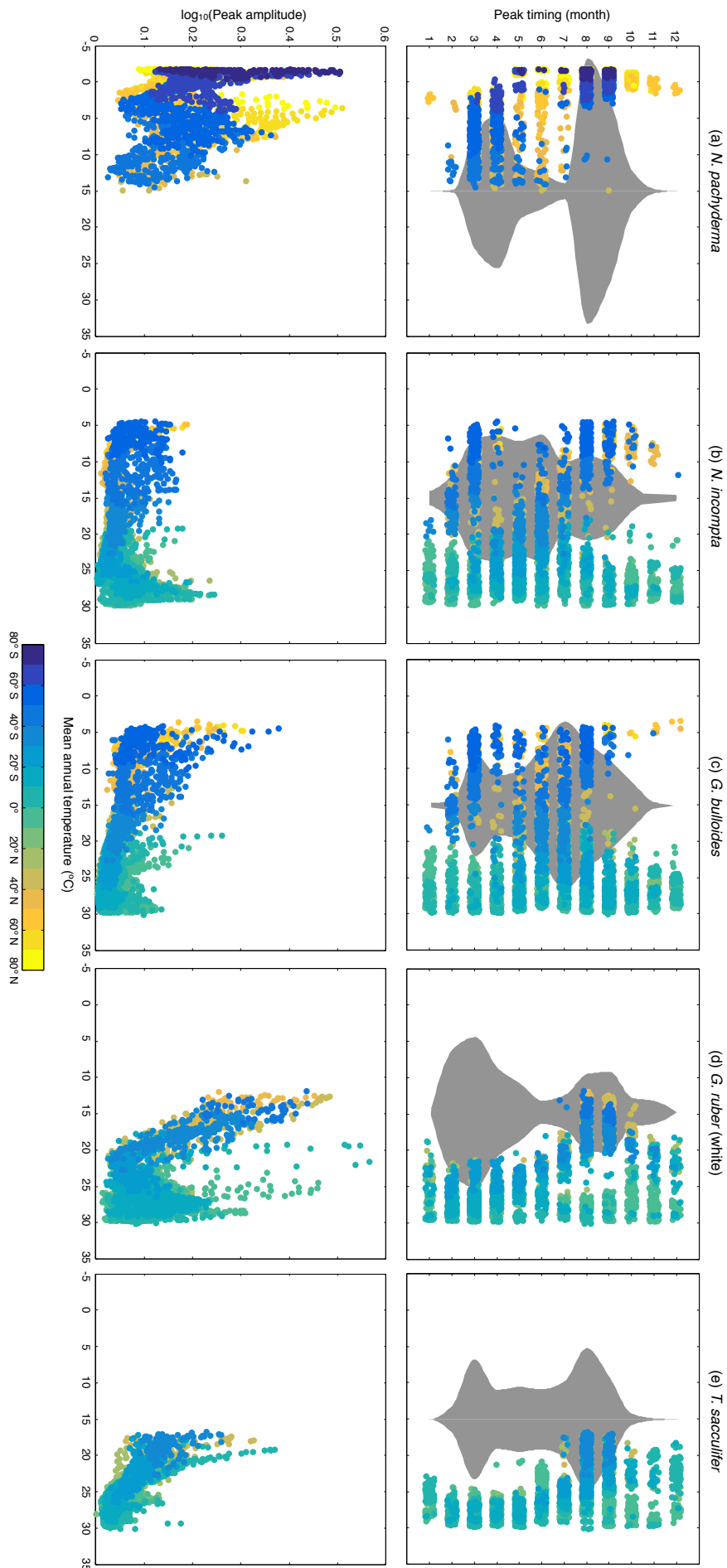
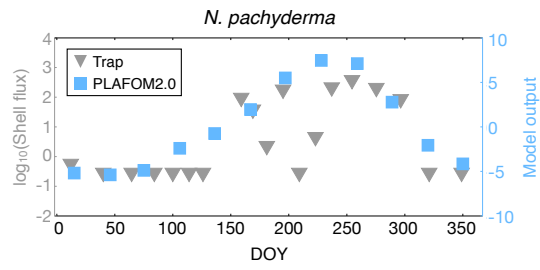


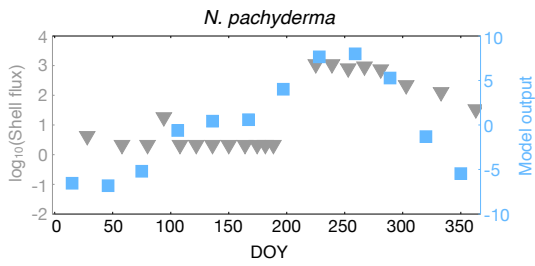
Figure S3.2

Figure S3.3

Site GS2



Site OG5



Site NB6/7

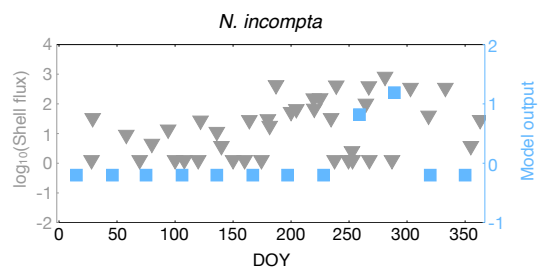
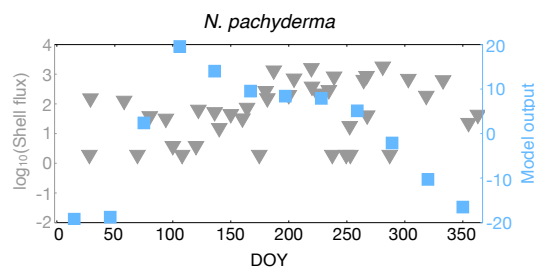
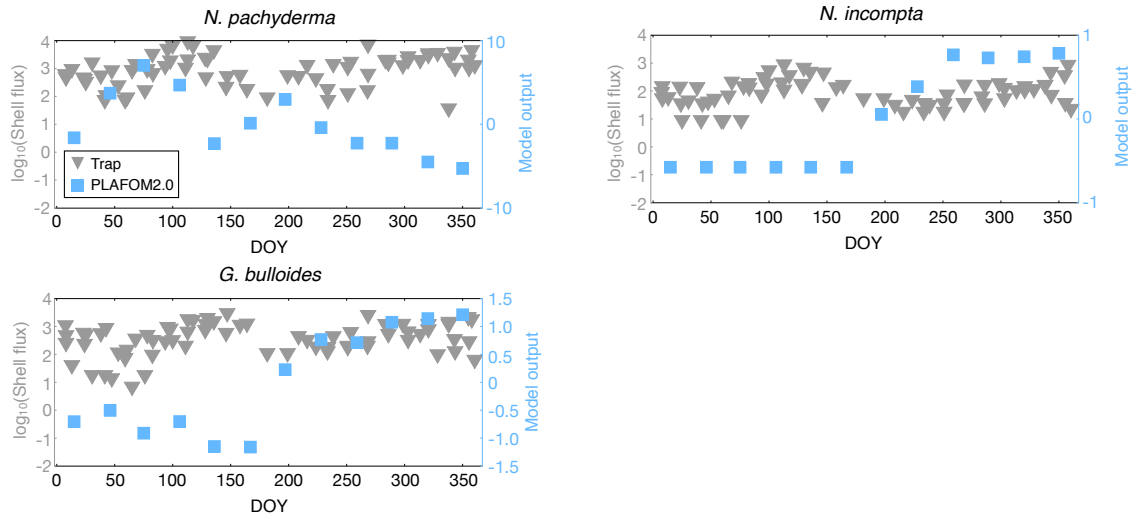
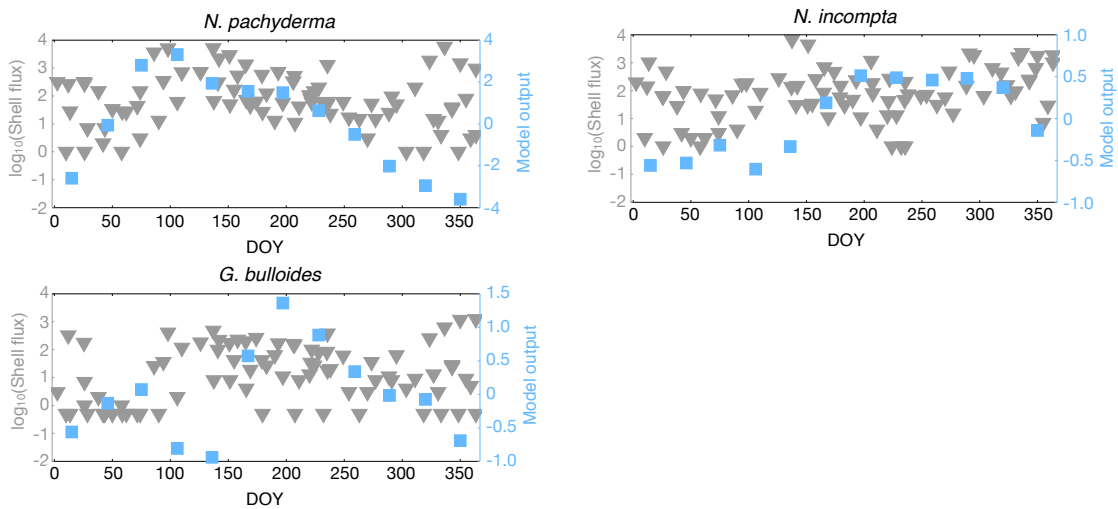


Figure S3.3 (cont.)

Site PAC50



Site PAPA



Site SA

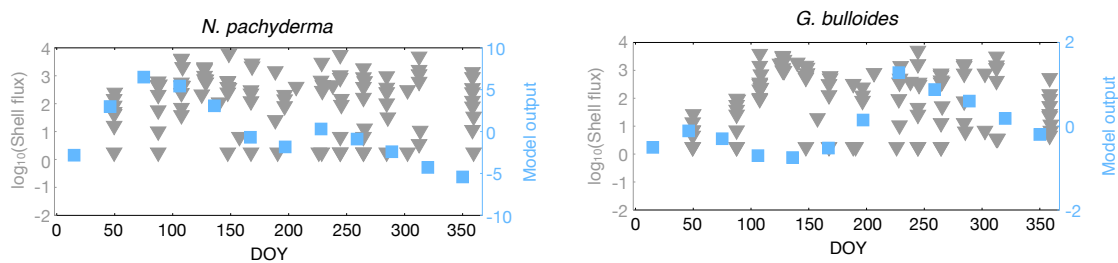
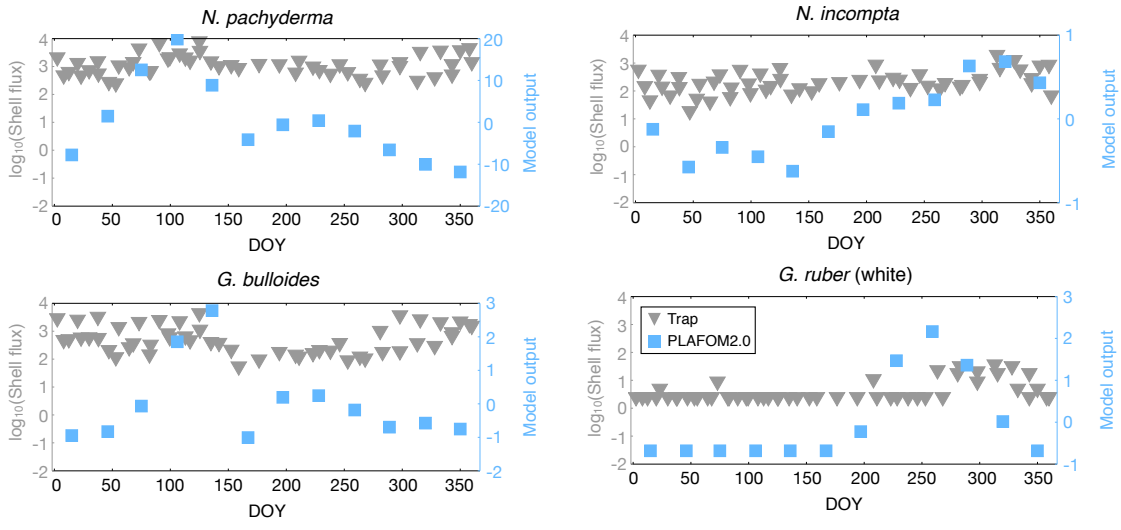


Figure S3.3 (cont.)

Site KNOT



Site WCT6

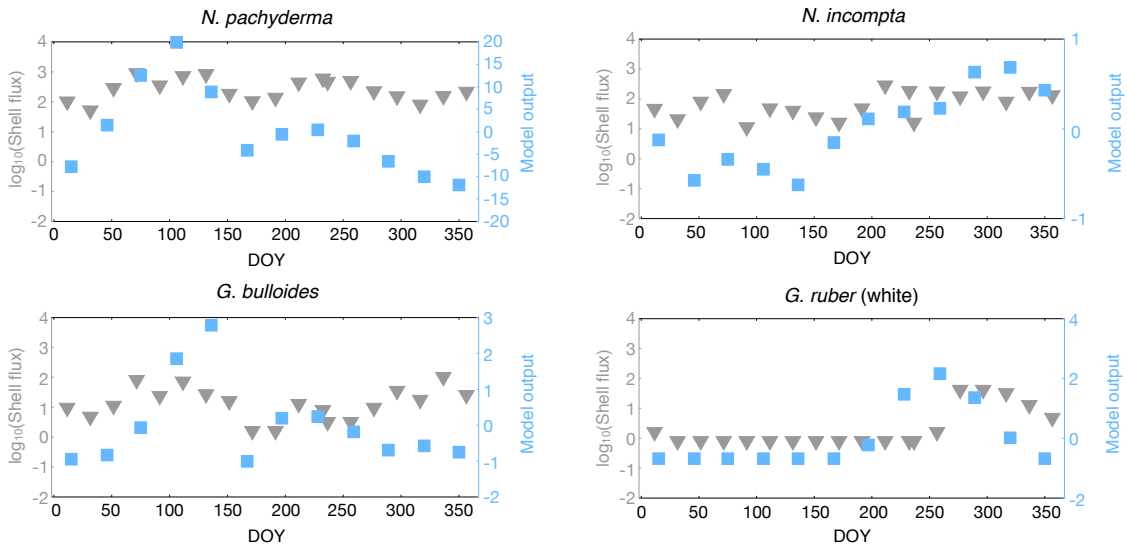
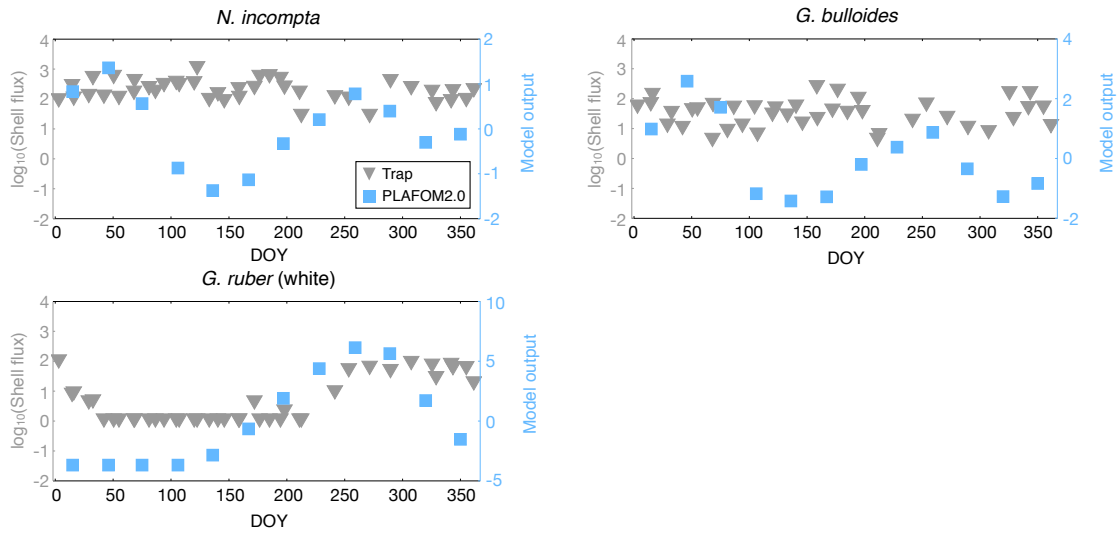
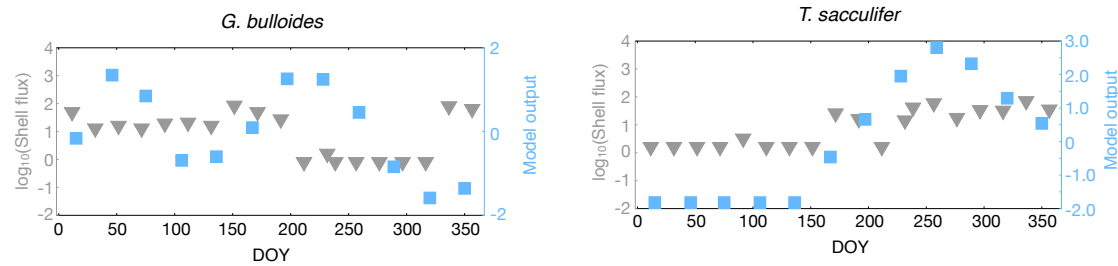


Figure S3.3 (cont.)

Site WCT2



Site WCT7



Site WCT1

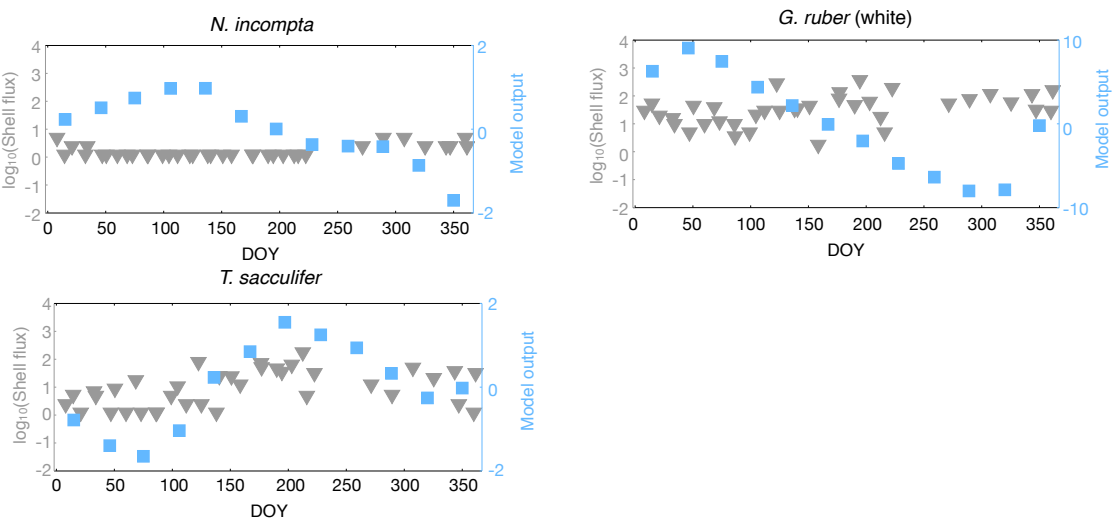
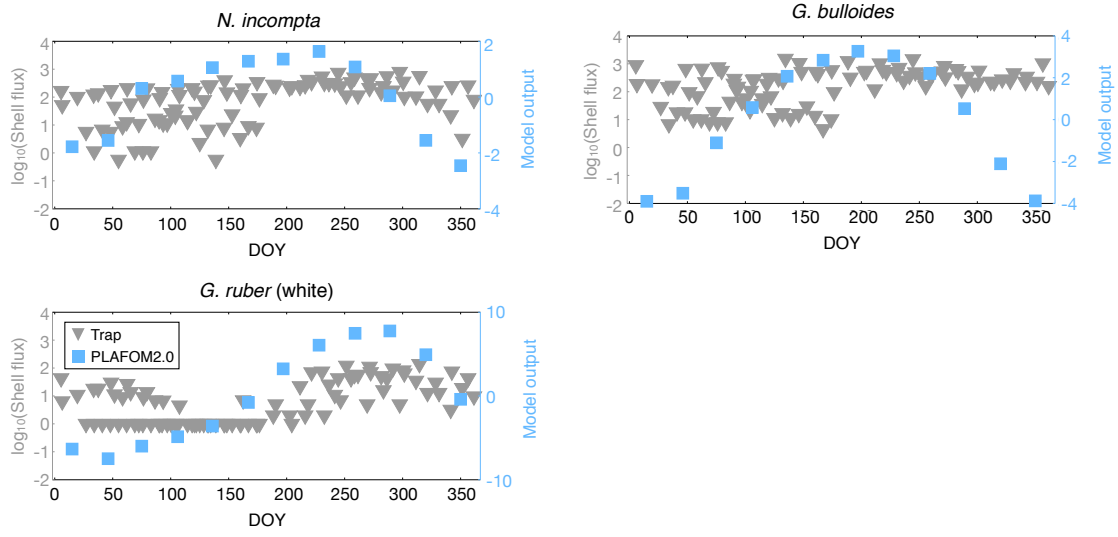


Figure S3.3 (cont.)

Site SBB



Site SPB

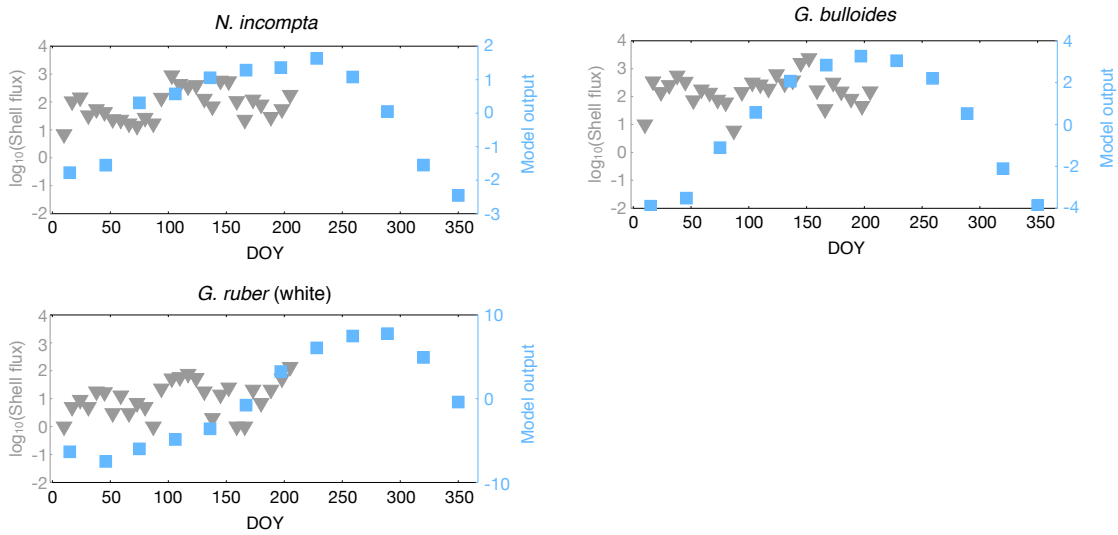
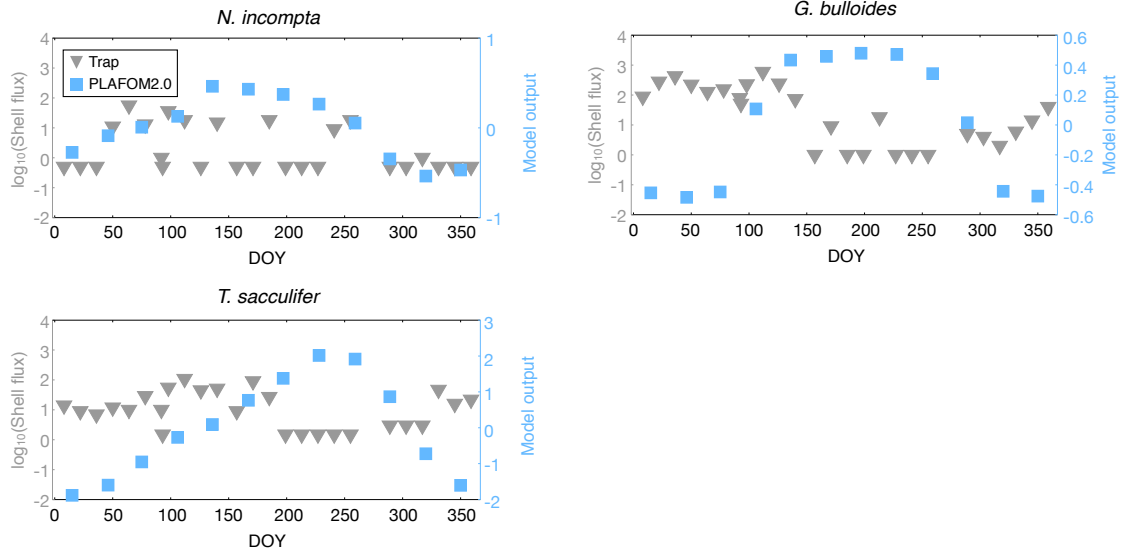


Figure S3.3 (cont.)

Site JGOF34



Site L1

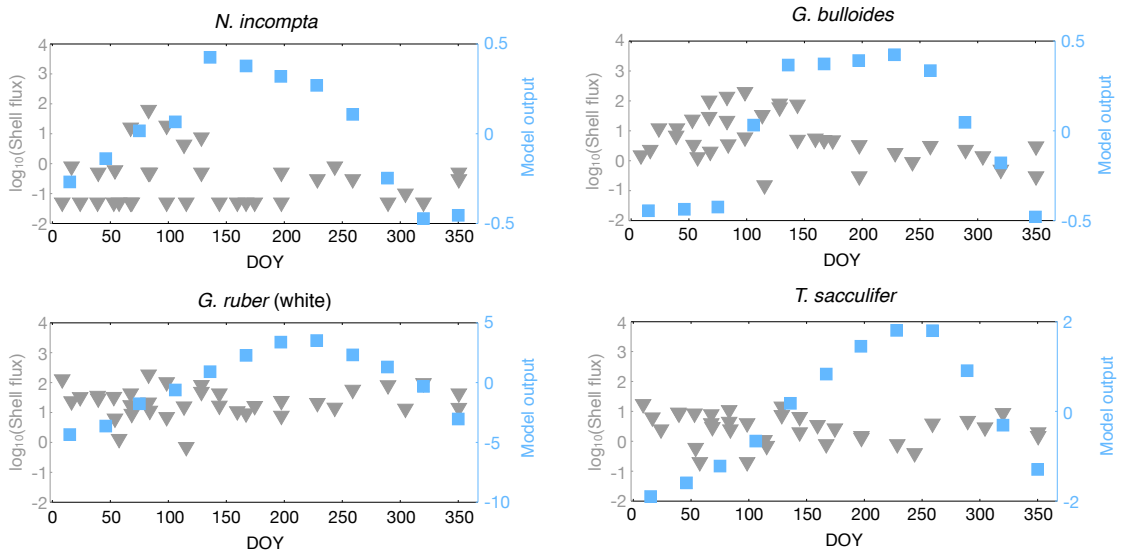
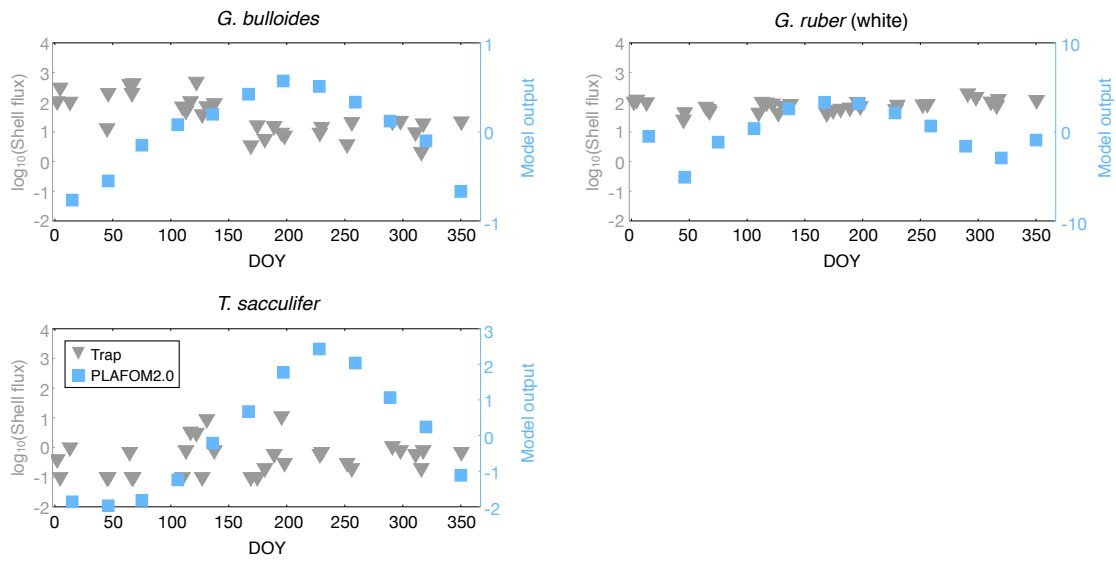


Figure S3.3 (cont.)

Site BATS



Site WAST

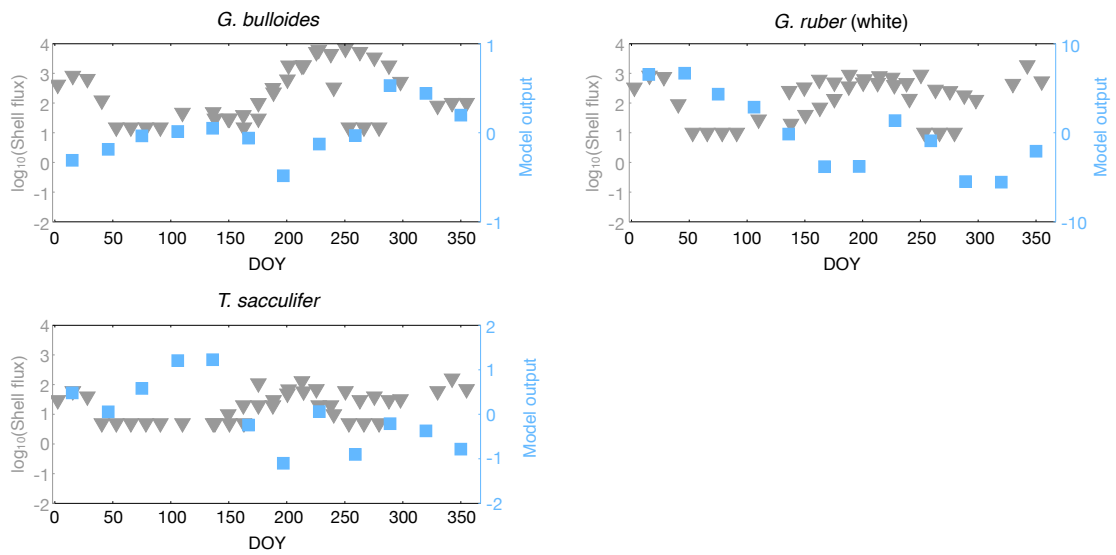
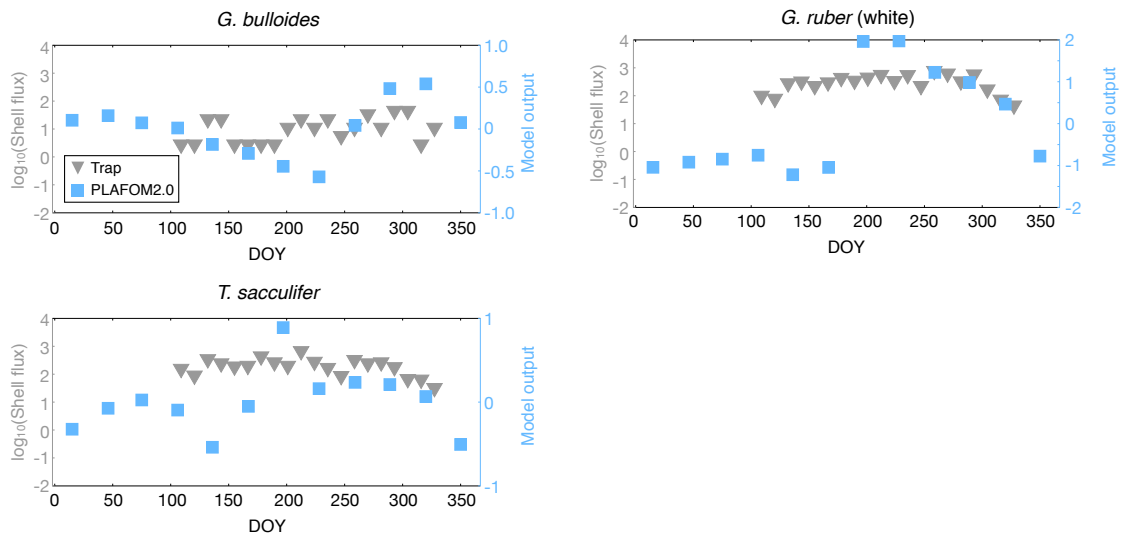


Figure S3.3 (cont.)

Site EA1



Site EA2

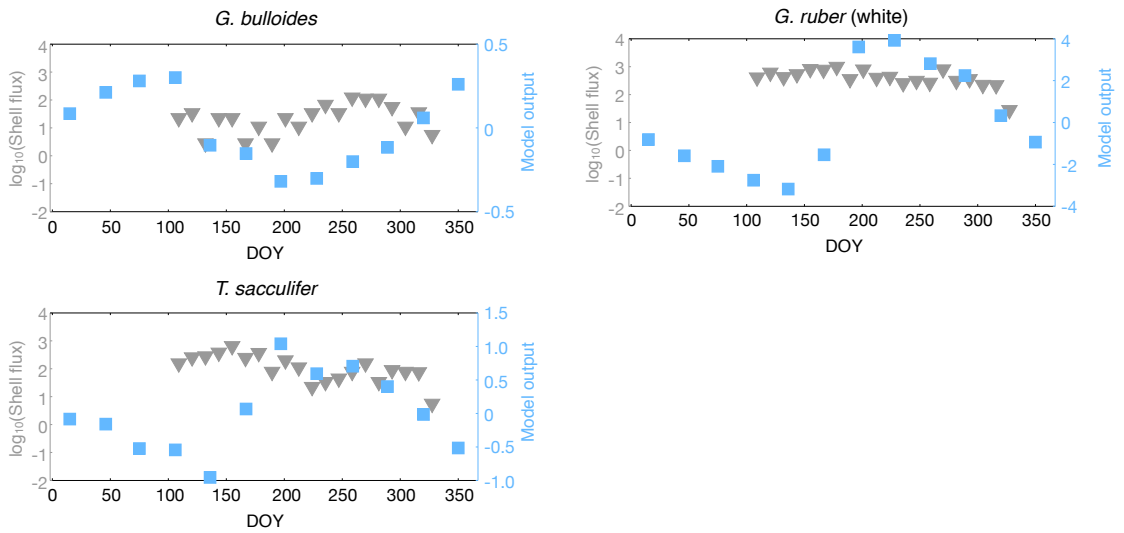
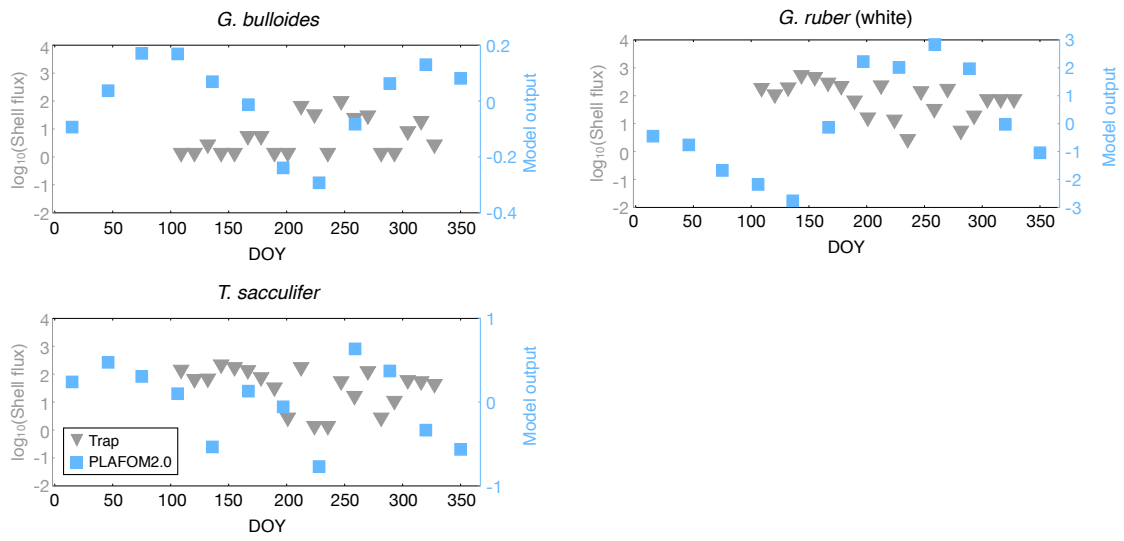
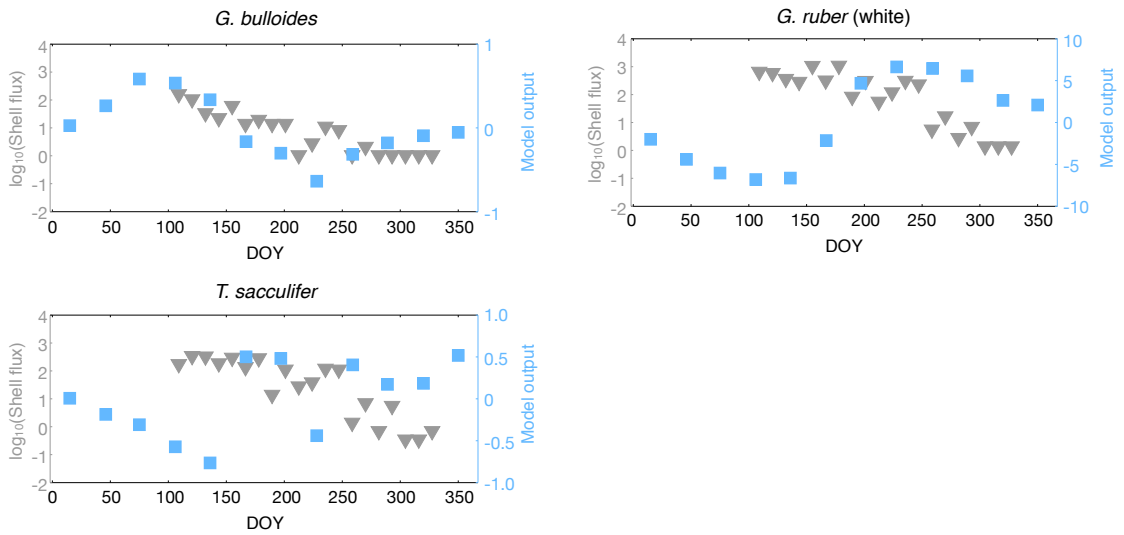


Figure S3.3 (cont.)

Site EA3



Site EA4



Site WA1

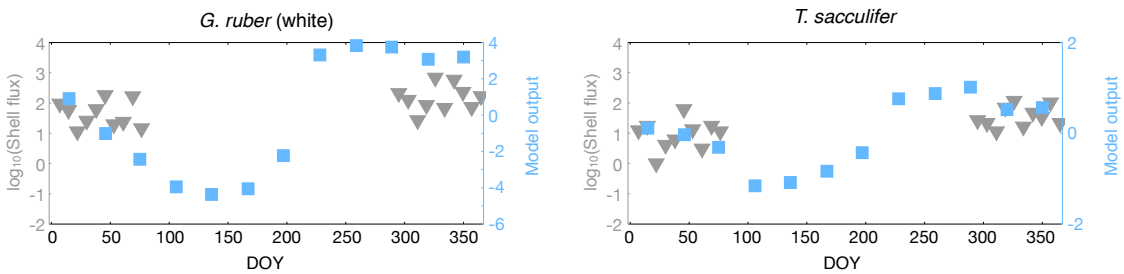
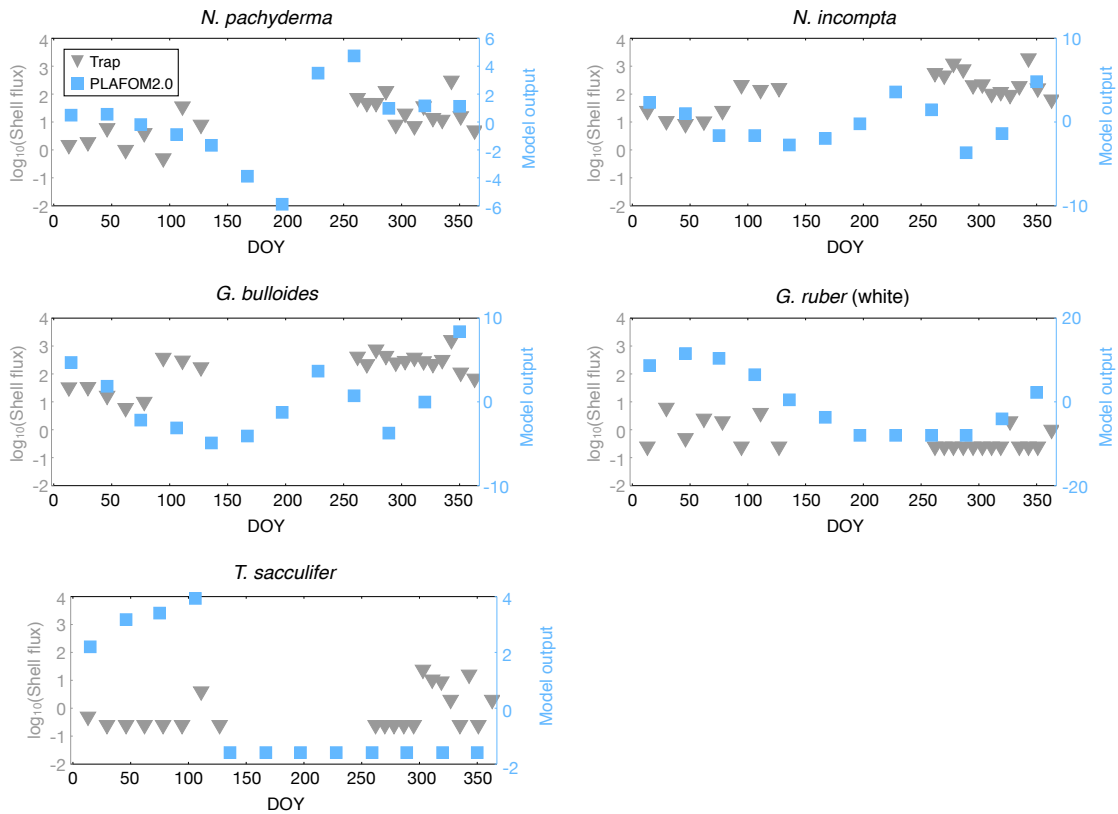


Figure S3.3 (cont.)

Site NCR



Site SCR

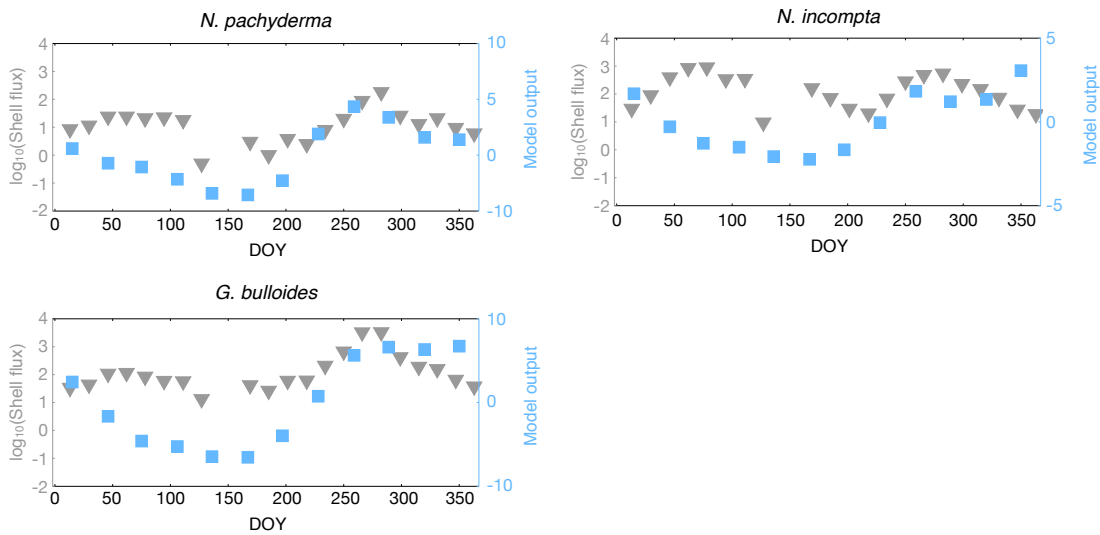
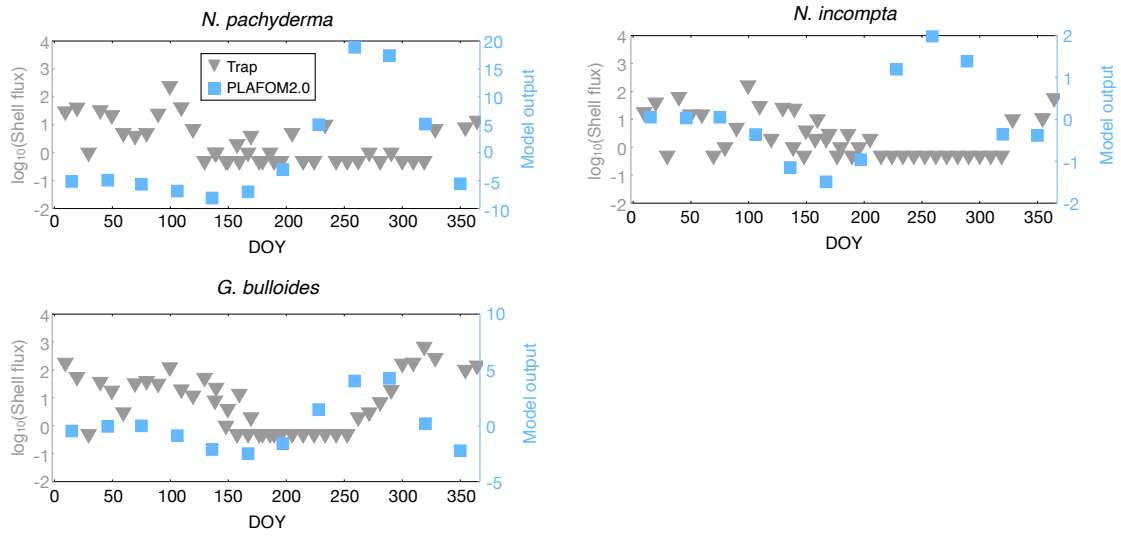


Figure S3.3 (cont.)

Site CP



Site WS34

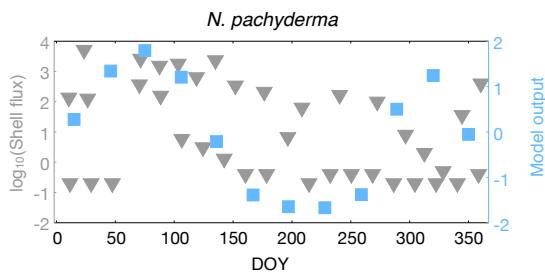
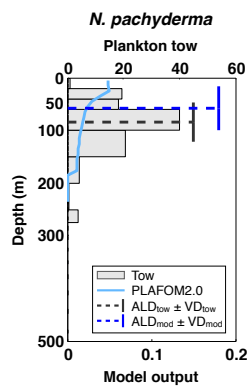
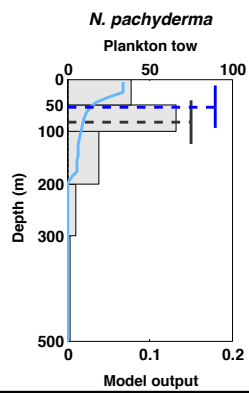


Figure S3.4

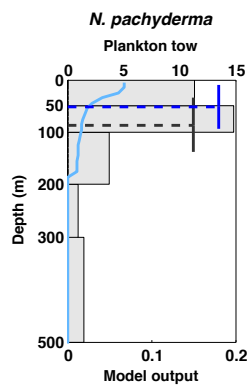
Station 93-36



Station PS78-25



Station PS78-44



Station PS78-75

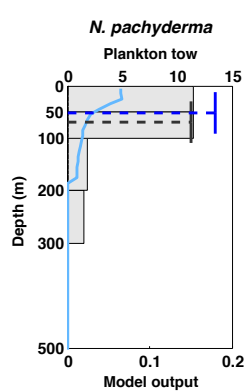
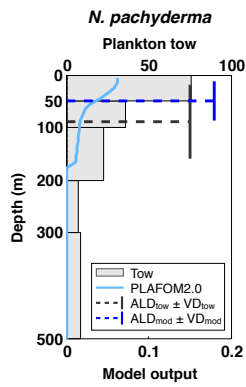
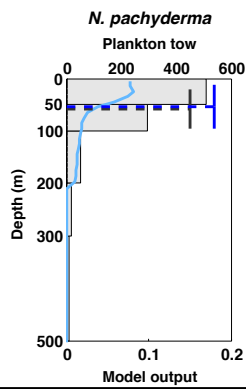


Figure S3.4 (cont.)

Station PS55-025



Station PS55-043



Station PS55-063

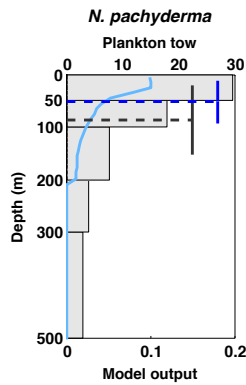
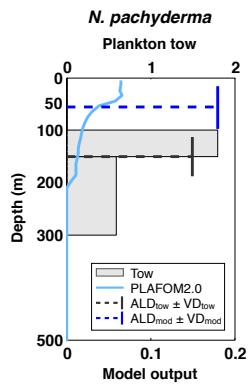
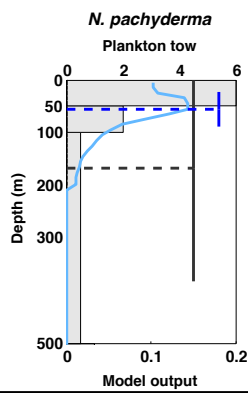


Figure S3.4 (cont.)

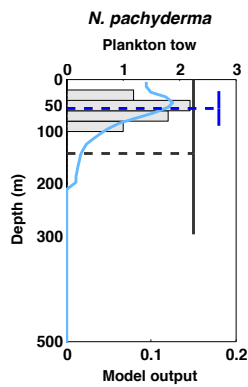
Station MN116



Station MN2



Station MN323



Station MN314

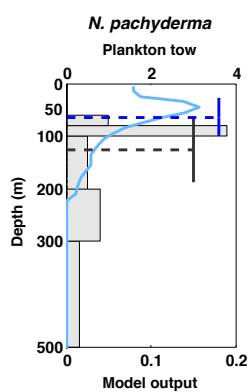
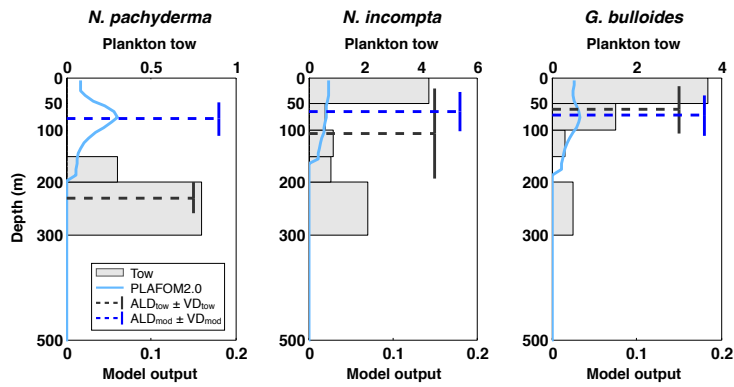
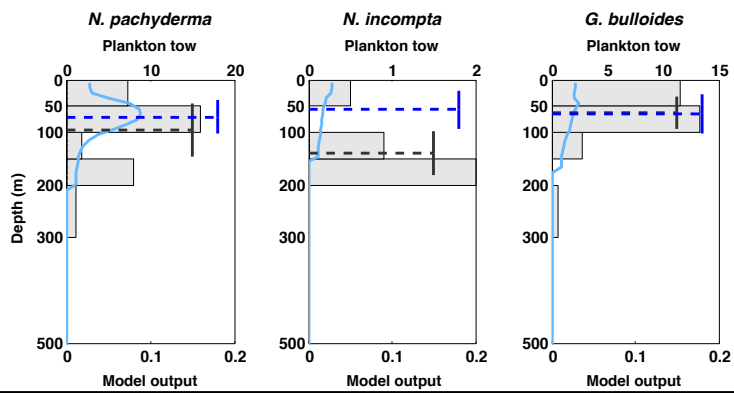


Figure S3.4 (cont.)

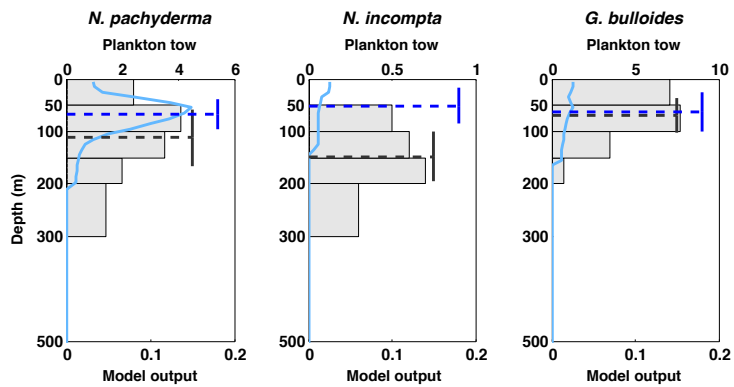
Station PAPA



Station 101



Station 79



Station KNOT

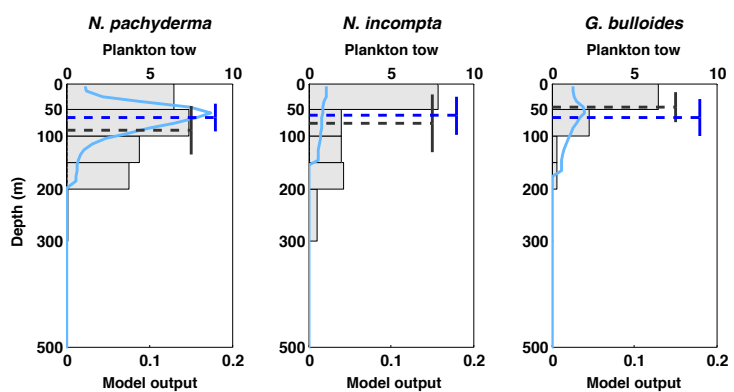
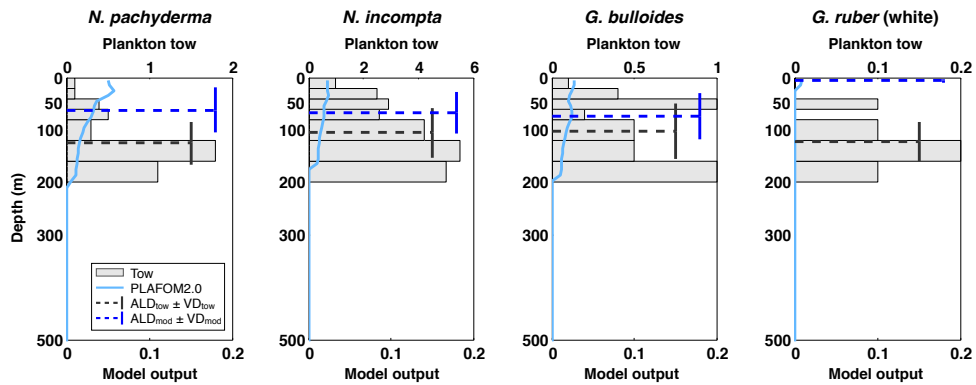
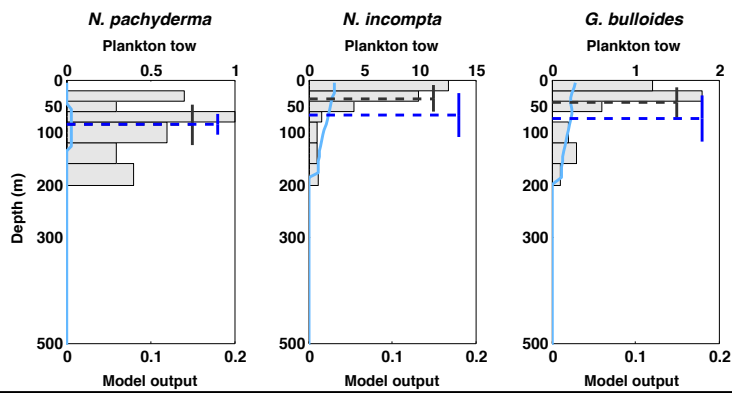


Figure S3.4 (cont.)

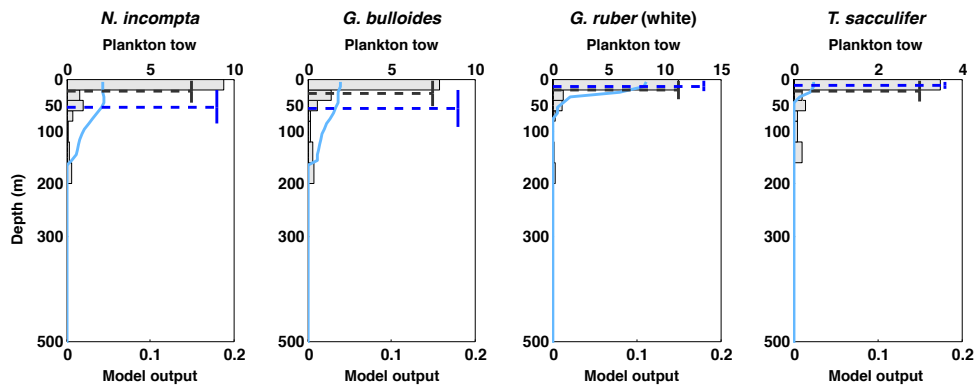
Station #B



Station #b



Station #A



Station #E

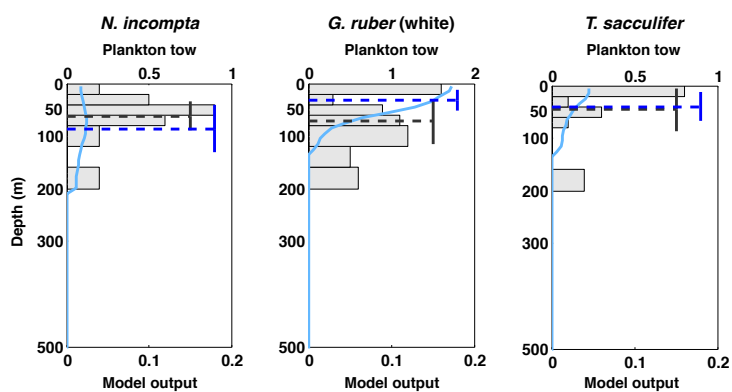
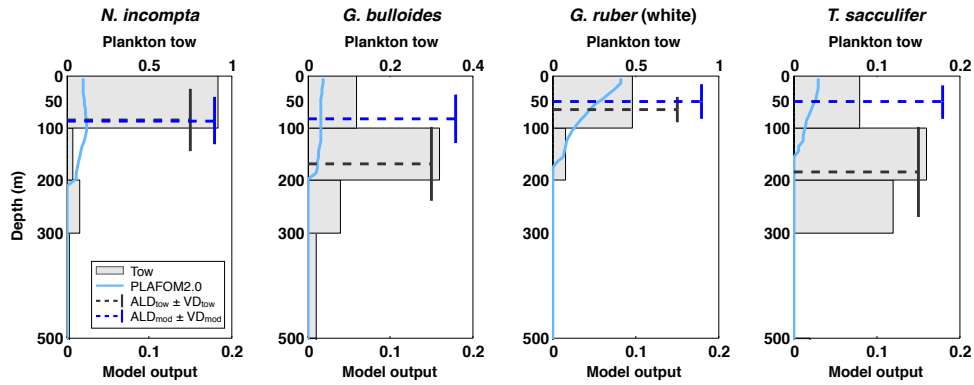
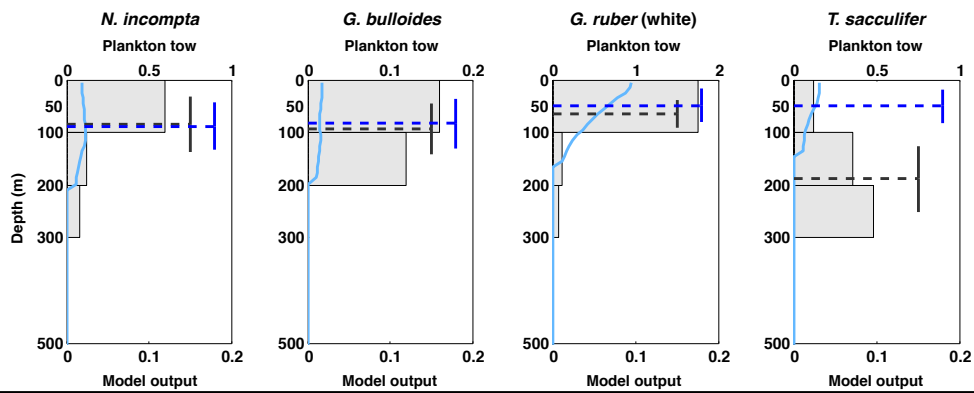


Figure S3.4 (cont.)

Station POS383-165



Station POS383-175



Station POS247-1389

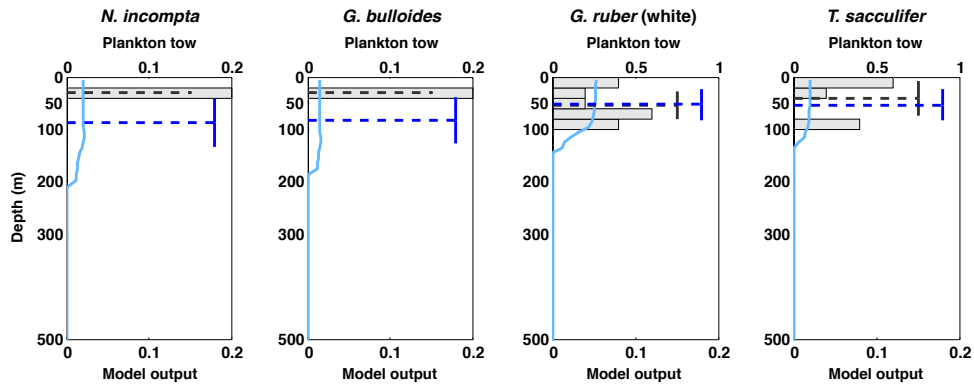
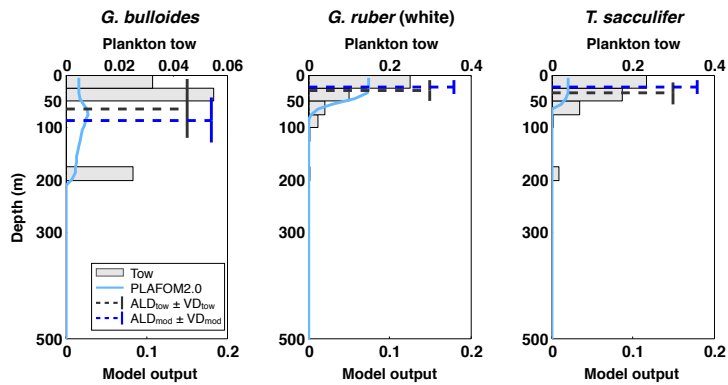
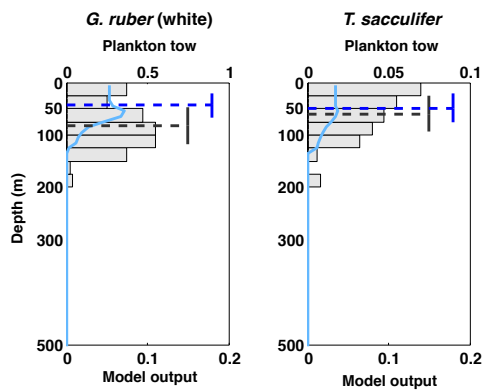


Figure S3.4 (cont.)

Station MOC1-38



Station MOC1-28



Station MOC1-23

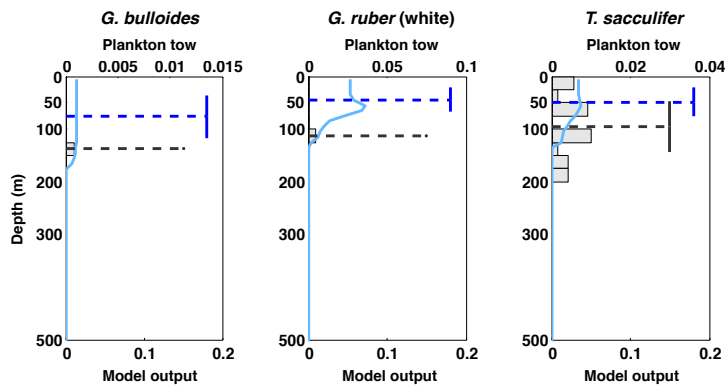
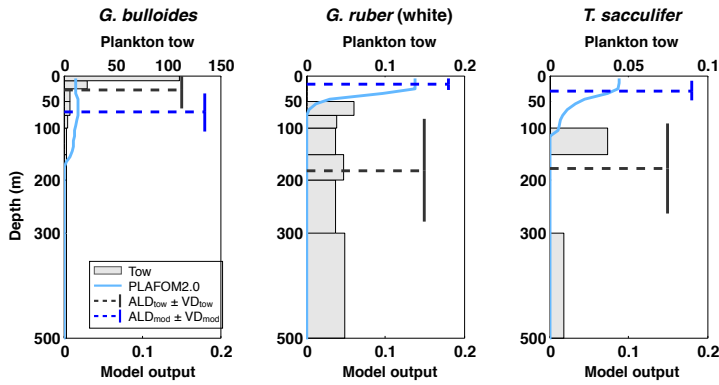
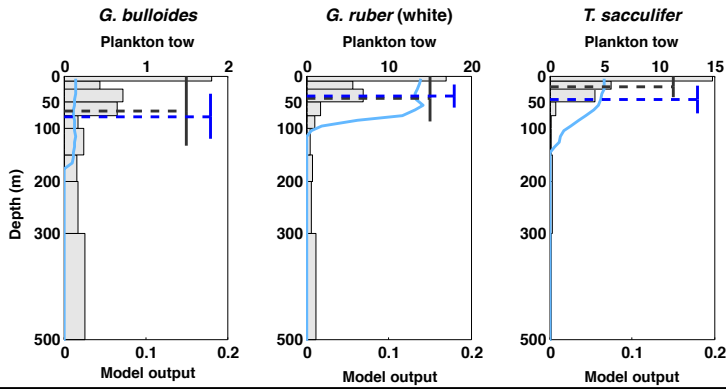


Figure S3.4 (cont.)

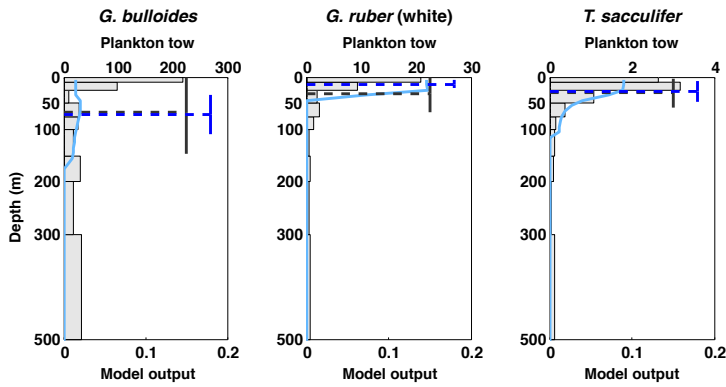
Station 310



Station 920



Station 313



Station 917

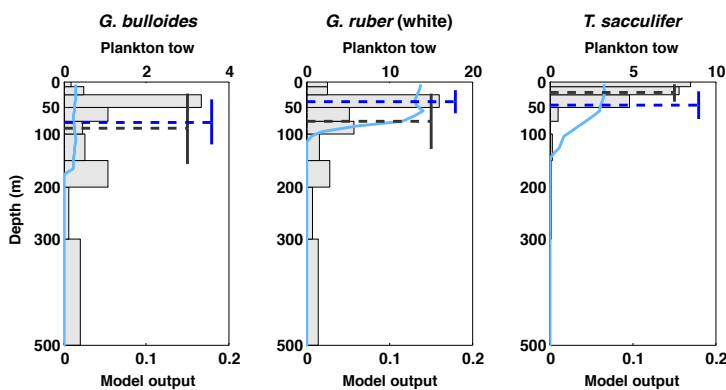
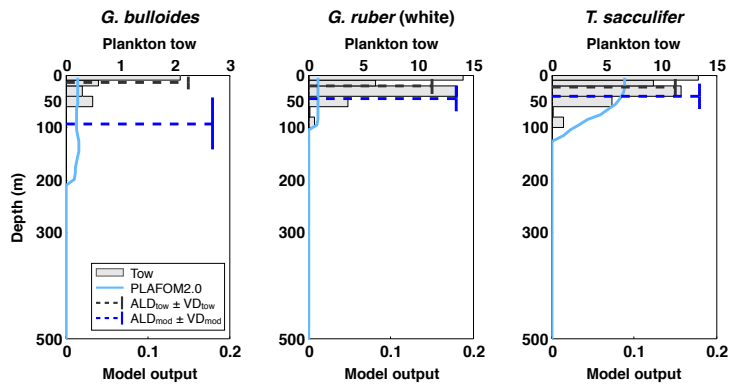
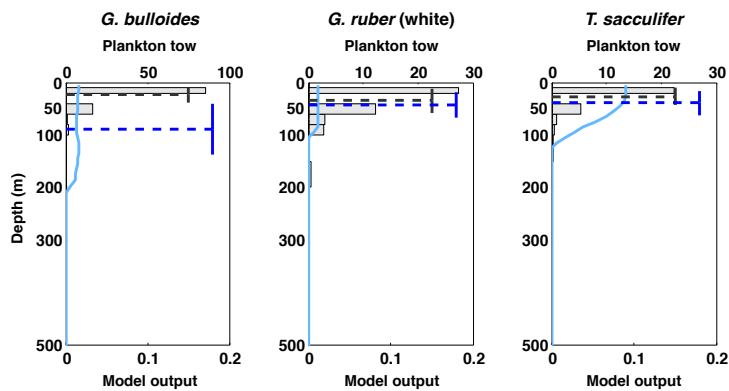


Figure S3.4 (cont.)

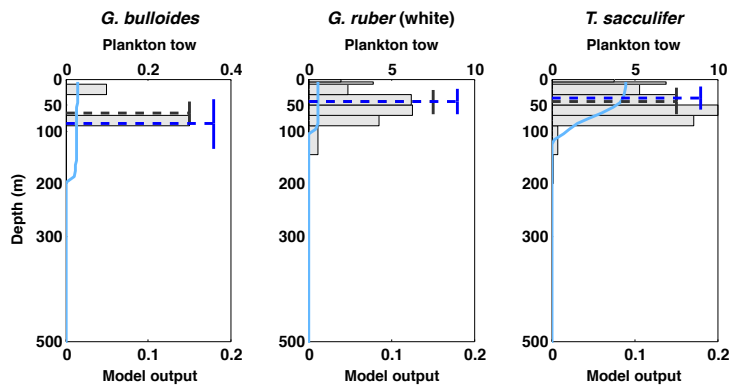
Station MOC63



Station MOC65



Station MOC12



Station MOC66

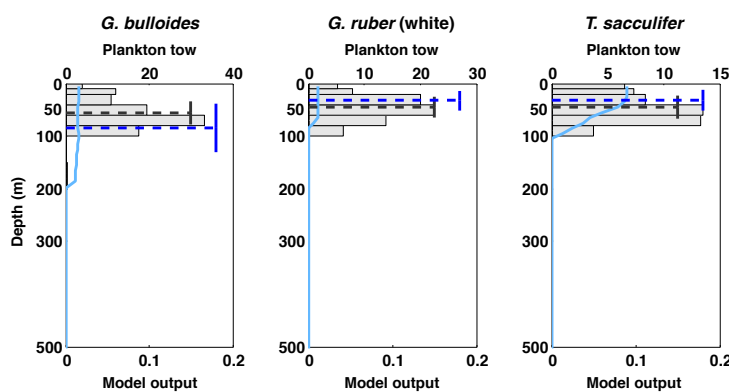
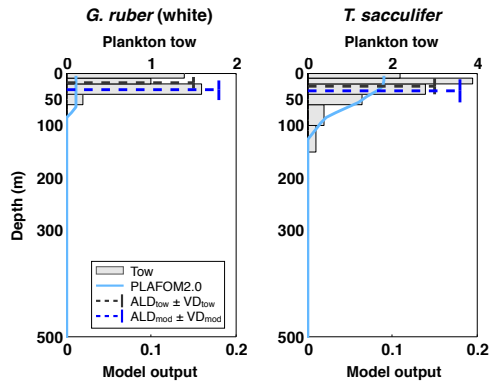
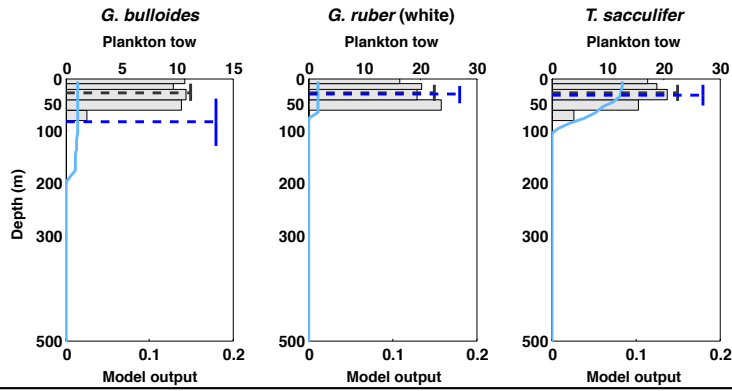


Figure S3.4 (cont.)

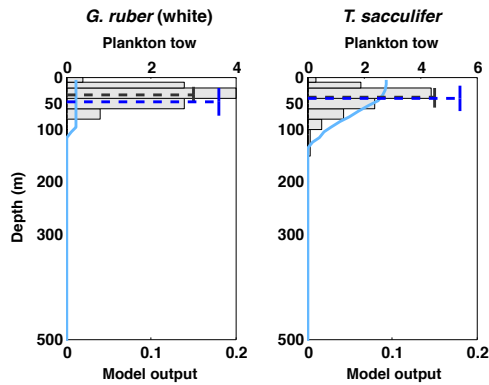
Station MOC15



Station MOC69



Station MOC20



Station MOC71

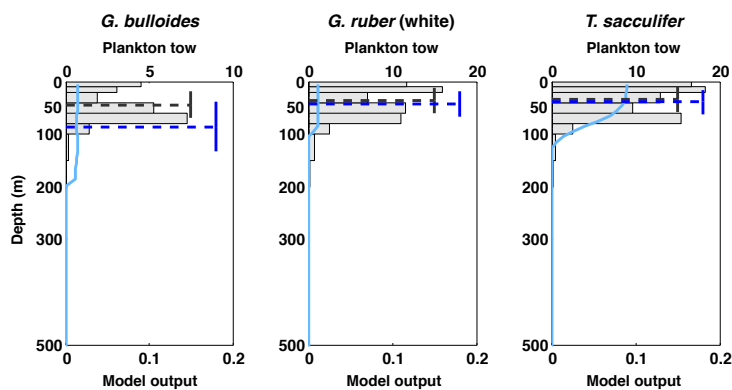
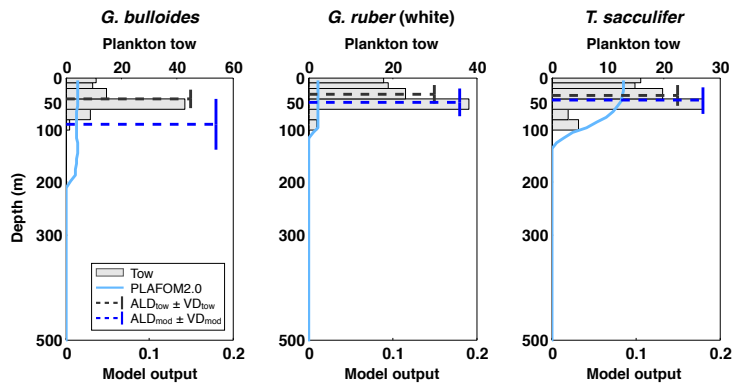
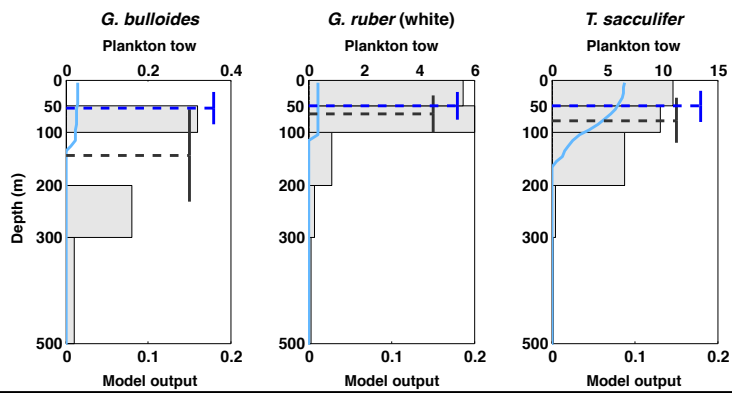


Figure S3.4 (cont.)

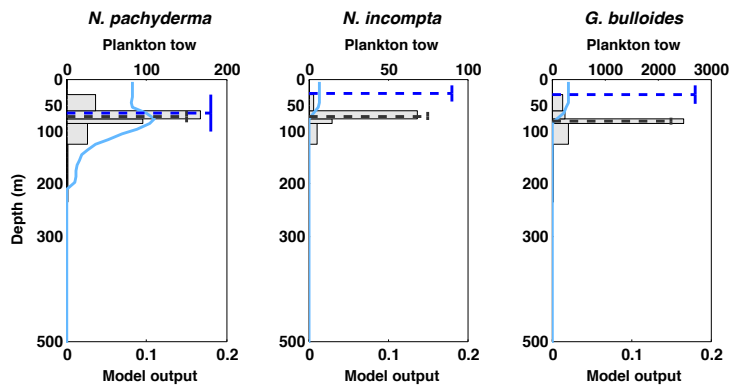
Station MOC72



Station SO225-21-3



Station TNO57-16



Station TNO57-13

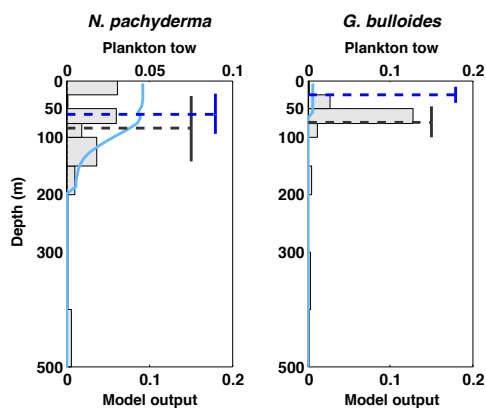
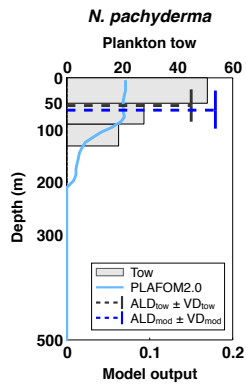
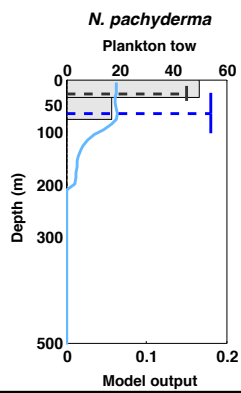


Figure S3.4 (cont.)

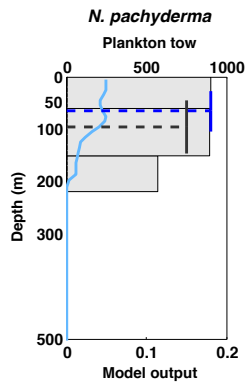
Station AN98-O



Station AN99-O



Station AN00-O



Station AN01-O

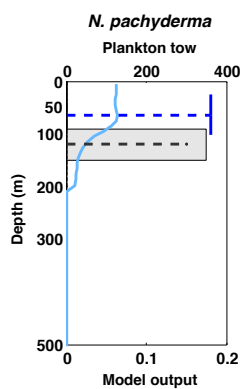


Table S3.1

#	Site	Latitude (°N)	Longitude (°E)	Water Depth (m)	Trap Depth (m)	Deployment Time ^a	Duration (days)	Species	Fraction (μ m)	Source
1	GS2	75.00	0.00	3720	300	03/06/1994 to 11/05/1995	342	Np	63-500	Jensen (1998)
2	OG5	72.40	-7.70	2624	500	06/08/1991 to 10/07/1992	339	Np	63-500	Jensen (1998)
3	NB6/7	69.69	0.47	3273	500	06/08/1991 to 02/10/1993	780	Np, Ni	63-500	Jensen (1998)
4	PAC50	50.01	165.03	5570	3260	01/12/1997 to 10/06/2001	1091	Np, Ni, Gb	>125	Kuroyanagi et al. (2002)
5	PAPA	50.00	-145.00	4240	3800	23/09/1982 to 30/08/1986	1122	Np, Ni, Gb	>125	Sautter and Thunell (1989)
6	SA	49.00	-174.00	5406	4812	23/08/1990 to 03/08/1999	2702	Np, Gb	>125	Asahi and Takahashi (2007)
7	KNOT	43.97	155.06	5370	2957	01/12/1997 to 12/05/2000	799	Np, Ni, Gb, Gr	>125	Kuroyanagi et al. (2002)
8	WCT6	42.00	155.34	5578	1091	15/08/1999 to 31/08/2000	382	Np, Ni, Gb, Gr	>125	Mohiuddin et al. (2005)
9	WCT2	39.00	147.00	5356-5322	1371; 1586	19/11/1997 to 10/08/1999	608	Ni, Gb, Gr	>125	Mohiuddin et al. (2002)
10	WCT7	36.68	154.94	5578	5034	19/08/1999 to 29/08/2000	376	Gb, Ts	>125	Mohiuddin et al. (2004)
11	WCT1	25.00	136.99	4905-5308	917; 1388	07/12/1997 to 12/08/1999	560	Ni, Gr, Ts	>125	Mohiuddin et al. (2002)
12	SBB	34.23	-120.03	650	590; 470	12/08/1993 to 26/06/1999	1015	Ni, Gb, Gr	>125	Kincaid et al. (2000) Darling et al. (2003)
13	SPB	33.55	-118.50	880	500	07/01/1988 to 26/07/1988	199	Ni, Gb, Gr	>125	Sautter and Thunell (1991)
14	JGOF534	34.00	-21.00	n.a.	2000	03/04/1989 to 16/04/1990	378	Ni, Gb, Ts	>150	Wolfteich (1994)
15	L1	33.00	-22.00	5300	3000	24/02/2002 to 01/04/2004	764	Ni, Gb, Gr, Ts	>125	Storz et al. (2009)
16	BATS	32.08	-64.25	4200	3200	06/04/1978 to 17/05/1984	1848	Gb, Gr, Ts	>125	Deuser et al. (1981) Deuser and Ross (1989)
17	WAST	16.32	60.47	4016	3026	10/05/1986 to 21/10/1987	506	Gb, Gr, Ts	>150	Curry et al. (1992)
18	EA1	3.17	-11.25	4524	984	13/04/1991 to 29/11/1991	230	Gb, Gr, Ts	>150	Fischer and Wefer (1996)
19	EA2	1.78	-11.25	4399	953	13/04/1991 to 29/11/1991	230	Gb, Gr, Ts	>150	Fischer and Wefer (1996)
20	EA3	0.08	-10.77	4141	1097	13/04/1991 to 29/11/1991	230	Gb, Gr, Ts	>150	Fischer and Wefer (1996)
21	EA4	-2.19	-10.09	3906	1068	13/04/1991 to 29/11/1991	230	Gb, Gr, Ts	>150	Fischer and Wefer (1996)
22	WA1	-4.00	-25.57	5530	652	17/10/1992 to 21/03/1993	155	Gr, Ts	>150	Fischer and Wefer (1996)
23	NCR	-42.70	178.63	1500	1000	14/09/1996 to 15/05/1997	243	Np, Ni, Gb, Gr, Ts	>150	King and Howard (2001)
24	SCR	-44.62	178.62	1500	1000	09/06/1996 to 15/05/1997	340	Np, Ni, Gb, Gr, Ts	>150	King and Howard (2001)
25	CP	-52.62	174.15	n.a.	442; 362	14/05/1998 to 13/07/1999	368	Np, Ni, Gb	>150	Northcote and Neil (2005)
26	WS34	-64.90	-2.60	5053	360	16/01/1988 to 26/02/1990	745	Np	>125	Donner and Wefer (1994)

^a Dates are formatted as day/month/year.

Np – *N. pachyderma*; Ni – *N. incompta*; Gb – *G. bulloides*; Gr – *G. ruber* (white); Ts – *T. sacculifer*
n.a. – not available (i.e., not given in data set)

Table S3.2

#	Station	Latitude (°N)	Longitude (°E)	Water Depth (m)	Depth Intervals	Date (season)	Species	Fraction (μ m)	Source
1	93-36	80.36	-10.14	n.a.	0-20, 20-40, 40-60, 60-100, 100-150, 150-200, 200-250, 250-275	27/07/1993 (summer)	Np	n.a.	<i>Kohfeld et al. (1996)</i>
2	PS78-25	78.83	7.00	1465	0-50, 50-100, 100-200, 200-300, 300-500	26/06/2011 (summer)	Np, Ni, Gb	100-250	<i>Pados and Spielhagen (2014)</i>
3	PS78-44	78.83	0.08	2636	0-50, 50-100, 100-200, 200-300, 300-500	29/06/2011 (summer)	Np, Ni, Gb	100-250	<i>Pados and Spielhagen (2014)</i>
4	PS78-75	78.83	-3.92	1978	0-50, 50-100, 100-200, 200-300, 300-500	04/07/2011 (summer)	Np, Ni, Gb	100-250	<i>Pados and Spielhagen (2014)</i>
5	PS55-025	75.00	-10.58	3084	0-50, 50-100, 100-200, 200-300, 300-500	11/07/1999 (summer)	Np, Ni, Gb	125-250	<i>Stangeew (2001)</i>
6	PS55-043	75.00	0.36	3789	0-50, 50-100, 100-200, 200-300, 300-500	14/07/1999 (summer)	Np, Ni, Gb	125-250	<i>Stangeew (2001)</i>
7	PS55-063	75.00	10.65	2542	0-50, 50-100, 100-200, 200-300, 300-500	16/07/1999 (summer)	Np, Ni, Gb	125-250	<i>Stangeew (2001)</i>
8	MN116	75.00	-7.31	3393	0-50, 50-100, 100-150, 150-300	21/08/1994 (summer)	Np	125-250	<i>Simstich et al. (2003)</i>
9	MN2	70.00	3.40	3261	0-50, 50-100, 100-500, 500-1000, 1000-2000	10/07/1994 (summer)	Np	125-250	<i>Simstich et al. (2003)</i>
10	MN323	69.69	0.47	3290	0-20, 20-40, 40-60, 60-80, 80-100, 100-200, 200-300, 300-500, 500-700, 700-1000, 1000-1500, 1500-2000, 2000-2500	07/07/1992 (summer)	Np	125-250	<i>Simstich et al. (2003)</i>
11	MN314	67.54	5.58	1438	0-20, 20-40, 40-60, 60-80, 80-100, 100-200, 200-300, 300-500, 500-700	28/06/1992 (summer)	Np	125-250	<i>Simstich et al. (2003)</i>
12	PAPA	49.98	-144.97	4253	0-50, 50-100, 100-150, 150-200, 200-300	16/08/2015 (summer)	Np, Ni, Gb	>100	<i>Iwasaki et al. (2017)</i>
13	101	47.00	-174.95	5790	0-50, 50-100, 100-150, 150-200, 200-300	05/08/2015 (summer)	Np, Ni, Gb	>100	<i>Iwasaki et al. (2017)</i>
14	79	46.98	166.73	5957	0-50, 50-100, 100-150, 150-200, 200-300	31/07/2015 (summer)	Np, Ni, Gb	>100	<i>Iwasaki et al. (2017)</i>
15	KNOT	44.08	154.98	5335	0-50, 50-100, 100-150, 150-200, 200-300	25/07/2015 (summer)	Np, Ni, Gb	>100	<i>Iwasaki et al. (2017)</i>
16	#B	41.57	141.90	1000	0-20, 20-40, 40-60, 60-80, 80-120, 120-160, 160-200	03/06/2002 (summer)	Np, Ni, Gb, Gr, Ts	125-1000	<i>Kuroyanagi and Kawahata (2004)</i>
17	#b	41.15	143.38	2077	0-20, 20-40, 40-60, 60-80, 80-120, 120-160, 160-200	04/06/2002 (summer)	Np, Ni, Gb, Gr, Ts	125-1000	<i>Kuroyanagi and Kawahata (2004)</i>
18	#A	36.02	141.78	2220	0-20, 20-40, 40-60, 60-80, 80-120, 120-160, 160-200	25/05/2002 (spring)	Np, Ni, Gb, Gr, Ts	125-1000	<i>Kuroyanagi and Kawahata (2004)</i>
19	#E	32.17	133.88	2660	0-20, 20-40, 40-60, 60-80, 80-120, 120-160, 160-200	27/05/2002 (spring)	Np, Ni, Gb, Gr, Ts	125-1000	<i>Kuroyanagi and Kawahata (2004)</i>
20	POS383-165	34.00	-22.00	5288	0-100, 100-200, 200-300, 300-500, 500-700	23/04/2009 (spring)	Np, Ni, Gb, Gr, Ts	>100	<i>Rebotim et al. (2017)</i>

Continued on next page

Table S3.2 (cont.)

#	Station	Latitude (°N)	Longitude (°E)	Water Depth (m)	Depth Intervals	Date (season)	Species	Fraction (μ m)	Source
21	POS383-175	33.15	-22.00	5232	0-100, 100-200, 200-300 300-500, 500-700	26/04/2009 (spring)	Np, Ni, Gb, Gr, Ts	>100	<i>Rebotim et al. (2017)</i>
22	POS247-1389	33.08	-22.00	5226	0-20, 20-40, 40-60, 60-80 80-100, 100-200, 200-300, 300-500, 500-700	24/01/1999 (winter)	Np, Ni, Gb, Gr, Ts	>100	<i>Rebotim et al. (2017)</i>
23	MOC1-38	38.92	-67.90	n.a.	0-25, 25-50, 50-75, 75-100, 100-125, 125-150, 150-175, 175-200	11/1975 (fall)	Gb, Gr, Ts	n.a.	<i>Fairbanks et al. (1980)</i>
24	MOC1-28	33.91	-71.78	n.a.	0-25, 25-50, 50-75, 75-100, 100-125, 125-150, 150-175, 175-200	11/1975 (fall)	Gr, Ts	n.a.	<i>Fairbanks et al. (1980)</i>
25	MOC1-23	32.73	-71.16	n.a.	0-25, 25-50, 50-75, 75-100, 100-125, 125-150, 150-175, 175-200	11/1975 (fall)	Gr, Ts	n.a.	<i>Fairbanks et al. (1980)</i>
26	310	16.02	52.73	n.a.	0-10, 10-25, 25-50, 50-75, 75-100, 100-150, 150-200, 200-300, 300-500	20/08/1992 (summer)	Np, Gb, Gr, Ts	>125	<i>Peeters and Brummer (2002)</i>
27	920	16.09	52.70	n.a.	0-10, 10-25, 25-50, 50-75, 75-100, 100-150, 150-200, 200-300, 300-500	27/02/1993 (winter)	Np, Gb, Gr, Ts	>125	<i>Peeters and Brummer (2002)</i>
28	313	15.91	53.02	n.a.	0-10, 10-25, 25-50, 50-75, 75-100, 100-150, 150-200, 200-300, 300-500	21/08/1992 (summer)	Np, Gb, Gr, Ts	>125	<i>Peeters and Brummer (2002)</i>
29	917	15.89	52.97	n.a.	0-10, 10-25, 25-50, 50-75, 75-100, 100-150, 150-200, 200-300, 300-500	25/02/1993 (winter)	Np, Gb, Gr, Ts	>125	<i>Peeters and Brummer (2002)</i>
30	MOC63	2.92	-140.20	n.a.	0-10, 10-20, 20-40, 40-60, 60-80, 80-100, 100-150, 150-200	22/08/1992 (summer)	Gb, Gr, Ts	>150	<i>Watkins et al. (1998)</i>
31	MOC65	2.05	-141.49	n.a.	10-20, 40-60, 60-80, 80-100, 100-150, 150-200	26/08/1992 (summer)	Gb, Gr, Ts	>150	<i>Watkins et al. (1998)</i>
32	MOC12	2.01	-139.88	n.a.	0-5, 5-10, 10-30, 30-50, 50-70, 70-90, 90-145, 145-200	17/02/1992 (winter)	Gb, Gr, Ts	>150	<i>Watkins et al. (1996)</i>
33	MOC66	1.13	-140.01	n.a.	0-10, 10-20, 20-40, 40-60, 60-80, 80-100, 100-150, 150-200	27/08/1992 (summer)	Gb, Gr, Ts	>150	<i>Watkins et al. (1998)</i>
34	MOC15	0.00	-140.07	n.a.	0-10, 10-20, 20-40, 40-60, 60-100, 100-150	23/02/1992 (winter)	Gr, Ts	>150	<i>Watkins et al. (1996)</i>
35	MOC69	-1.05	-139.97	n.a.	0-10, 10-20, 20-40, 40-60, 60-80, 100-150, 150-200	01/09/1992 (fall)	Gb, Gr, Ts	>150	<i>Watkins et al. (1998)</i>
36	MOC20	-2.02	-140.16	n.a.	0-10, 10-20, 20-40, 40-60, 60-80, 80-100, 100-150, 150-200	29/02/1992 (winter)	Gr, Ts	>150	<i>Watkins et al. (1996)</i>
37	MOC71	-2.33	-140.32	n.a.	0-10, 10-20, 20-40, 40-60, 60-80, 80-100, 100-150, 150-200	04/09/1992 (fall)	Gb, Gr, Ts	>150	<i>Watkins et al. (1998)</i>
38	MOC72	-3.21	-140.25	n.a.	0-10, 10-20, 20-40, 40-60, 60-80, 80-100, 100-150, 150-200	06/09/1992 (fall)	Gb, Gr, Ts	>150	<i>Watkins et al. (1998)</i>
39	SO225-21-3	-3.05	-165.06	5188	0-50, 50-100, 100-200, 200-300, 300-500	08/12/2012 (winter)	Gb, Gr, Ts	>150	<i>Rippert et al. (2016)</i>

Continued on next page

Table S3.2 (cont.)

#	Station	Latitude (°N)	Longitude (°E)	Water Depth (m)	Depth Intervals	Date (season)	Species	Fraction (μm)	Source
40	TNO57-16	-50.12	5.75	3761	0-30, 30-60, 60-75, 75-85, 85-125, 125-235, 235-300, 300-440	24/02/1996 (winter)	Np, Ni, Gb	>150	<i>Mortyn and Charles</i> (2003)
41	TNO57-13	-53.18	5.13	2851	0-25, 25-50, 50-75, 75-100, 100-150, 150-200, 200-300, 300-400, 400-500	21/02/1996 (winter)	Np, Ni, Gb	>150	<i>Mortyn and Charles</i> (2003)
42	AN98/O	-63.25	177.25	4100	0-50, 50-90, 90-130	20/01/1998 (winter)	Np, Ni, Gb	>100	<i>Bergami et al.</i> (2009)
43	AN99/O	-63.40	178.05	4074	0-35, 35-70	09/01/1999 (winter)	Np, Ni, Gb	>100	<i>Bergami et al.</i> (2009)
44	AN00/O	-63.53	178.38	3548	0-60, 60-150, 150-220	11/01/2000 (winter)	Np, Ni, Gb	>100	<i>Bergami et al.</i> (2009)
45	AN01/O	-63.43	178.10	3964	0-90, 90-150	09/01/2001 (winter)	Np, Ni, Gb	>100	<i>Bergami et al.</i> (2009)

Np – *N. pachyderma*; Ni – *N. incompta*; Gb – *G. bulloides*; Gr – *G. ruber* (white); Ts – *T. sacculifer*
n.a. – not available (i.e., not given in data set)
Here the season refers to those of the Northern Hemisphere.

Table S3.3a

Province	Sediment Trap Details				<i>N. pachyderma</i>		<i>N. incompta</i>		<i>G. bulloides</i>		<i>G. ruber</i> (white)		<i>T. sacculifer</i>	
	Site	Latitude (°N)	Longitude (°E)	Trap	PLAFOM2.0	Trap	PLAFOM2.0	Trap	PLAFOM2.0	Trap	PLAFOM2.0	Trap	PLAFOM2.0	
Polar	G52	75.00	0.00	Jun-Sep	Jul-Sep	-	-	-	-	-	-	-	-	
	OG5	72.40	-7.70	Aug-Sep	Aug-Sep	-	-	-	-	-	-	-	-	
	NB6/7	69.69	-0.47	Jun-Nov	Mar-Jul	Jul-Nov	Sep-Oct	-	-	-	-	-	-	
Subpolar	PAC50	50.01	155.03	Mar-May	Feb-Apr	Mar-May	Sep-Dec	Apr-Jun	Oct-Dec	-	-	-	-	
	PAPA	50.00	-145.00	Mar-May	Mar-May	Apr-Jun	Jul-Nov	Apr-Jun	Jun-Aug	-	-	-	-	
	SA	49.00	-174.00	Nov-Dec	Mar-May	-	-	Nov-Dec	Jun-Aug	-	-	-	-	
				Apr-Jul	Feb-May	-	-	Apr-May	Aug-Oct	-	-	-	-	
Transitional	KNOT	43.97	155.06	Mar-May	Mar-May	none	Oct-Dec	Mar-May	Apr-May	Sep-Nov	Aug-Oct	-	-	
	WCT6	42.00	155.34	Mar-May	Mar-Apr	Jun-Oct	Oct-Dec	Mar-May	Apr-May	Sep-Nov	Aug-Sep	-	-	
	WCT2	39.00	147.00	-	-	none	Jan-Mar	none	Jan-Mar	Sep-Dec	Aug-Oct	-	-	
	WCT7	36.68	154.94	-	-	-	Aug-Oct	May-Jun	Aug-Sep	Feb-Mar	Jul-Aug	Aug-Dec	Jul-Nov	
Subtropics	SBB	34.23	-120.03	-	-	Aug-Oct	May-Sep	Jun-Aug	May-Sep	Jul-Nov	Jul-Nov	-	-	
	JGOFSS34	34.00	-21.00	-	-	Feb-Apr	May-Aug	Mar-May	May-Sep	-	-	Apr-Jun	Jun-Oct	
	SPB	33.55	-118.50	-	-	Mar-May	May-Sep	May-Jun	May-Sep	Apr-Jul	Jul-Nov	-	-	
	L1	33.00	-22.00	-	-	Mar-May	May-Aug	Mar-May	May-Sep	Mar-May	Jun-Sep	Mar-May	Jun-Oct	
	BATS	32.08	-64.25	-	-	Feb-Apr	-	Jan-May	Jun-Sep	none	May-Jul	May-Jul	Jun-Oct	
WCT1	25.00	136.99	-	-	none	Mar-May	Jan-May	Jun-Aug	Jun-Aug	Jan-Apr	Jun-Aug	Jun-Sep		
Tropics	WAST	16.32	60.47	-	-	-	-	Jan-Feb	Oct-Dec	Dec-Feb	Jan-Apr	Jun-Sep	Mar-May	
	EA1	3.17	-11.25	-	-	-	-	Jul-Oct	Oct-Nov	May-Aug	Aug-Sep	Jun-Sep	Mar-May	
	EA2	1.78	-11.25	-	-	-	-	Sep-Nov	Feb-Apr	none	Jul-Oct	none	Jun-Aug	
	EA3	0.08	-10.77	-	-	-	-	Jul-Oct	Nov-Dec	none	Jul-Oct	May-Jul	Jun-Oct	
	EA4	-2.19	-10.09	-	-	-	-	Jul-Sep	Mar-Apr	May-Jun	Jul-Oct	May-Jun	Jan-Mar	
WAI	-4.00	-25.57	-	-	-	-	Apr-May	Oct-Dec	Apr-Aug	Jul-Oct	Apr-Aug	Sep-Oct		
Transitional	NCR	-42.70	178.63	Sep-Dec	Aug-Sep	Sep-Oct	Aug-Sep	Apr-May	Jul-Sep	none	Jan-Apr	Oct-Dec	Jan-Apr	
	SCR	-44.62	178.62	Sep-Oct	Aug-Oct	Feb-Apr	Sep-Oct	Sep-Oct	Dec-Feb	-	-	-	-	
Subpolar	CP	-52.62	174.15	Mar-May	Aug-Nov	Mar-May	Aug-Oct	Nov-May	Aug-Oct	-	-	-	-	
	WS34	-64.90	-2.60	Mar-May	Feb-Apr	-	-	-	-	-	-	-	-	

Table S3.3b

Province	Sediment Trap Details			<i>N. pachyderma</i>		<i>N. incompta</i>		<i>G. bulloides</i>		<i>G. ruber</i> (white)		<i>T. sacculifer</i>	
	Site	Latitude (°N)	Longitude (°E)	Trap	PLAFOM2.0	Trap	PLAFOM2.0	Trap	PLAFOM2.0	Trap	PLAFOM2.0	Trap	PLAFOM2.0
Polar	GS2	75.00	0.00	0.78	0.21	-	-	-	-	-	-	-	-
	OG5	72.40	-7.70	0.64	0.17	-	-	-	-	-	-	-	-
	NB6/7	69.69	-0.47	0.80	0.23	0.95	0.84	-	-	-	-	-	-
Sub-polar	PAC50	50.01	165.03	0.75	0.12	0.77	0.37	0.66	0.22	-	-	-	-
	PAPA	50.00	-145.00	1.07	0.11	1.20	0.04	1.10	0.07	-	-	-	-
	SA	49.00	-174.00	0.95	0.15	-	-	0.94	0.08	-	-	-	-
Transitional	KNOT	43.97	155.06	0.69	0.28	0.79	0.07	0.66	0.14	0.76	0.62	-	-
	WCT6	42.00	155.34	0.42	0.28	0.47	0.07	0.62	0.14	0.73	0.62	-	-
	WCT2	39.00	147.00	-	-	0.64	0.06	0.69	0.11	0.74	0.43	-	-
	WCT7	36.68	154.94	-	-	-	-	0.55	0.08	-	-	0.57	0.40
Subtropics	SBB	34.23	-120.03	-	-	0.68	0.03	0.67	0.06	0.87	0.16	-	-
	JGOF34	34.00	-21.00	-	-	0.85	0.02	0.76	0.03	-	-	0.69	0.12
	SPB	33.55	-118.50	-	-	0.73	0.03	0.85	0.06	0.77	0.16	-	-
	L1	33.00	-22.00	-	-	1.28	0.02	0.91	0.03	0.70	0.08	0.59	0.11
	BATS	32.08	-64.25	-	-	-	-	0.72	0.05	0.37	0.09	0.96	0.13
	WCT1	25.00	136.99	-	-	0.42	0.08	-	-	0.77	0.14	0.88	0.06
	WAST	16.32	60.47	-	-	-	-	0.77	0.04	0.70	0.11	0.66	0.03
Tropics	EA1	3.17	-11.25	-	-	-	-	0.48	0.04	0.36	0.08	0.47	0.03
	EA2	1.78	-11.25	-	-	-	-	0.52	0.02	0.33	0.12	0.59	0.04
	EA3	0.08	-10.77	-	-	-	-	0.81	0.01	0.57	0.07	0.47	0.02
	EA4	-2.19	-10.09	-	-	-	-	0.83	0.04	0.60	0.12	0.50	0.02
	WA1	-4.00	-25.57	-	-	-	-	-	-	0.67	0.09	0.58	0.04
Transitional	NCR	-42.70	178.63	0.91	0.26	0.78	0.07	0.73	0.12	0.77	0.39	0.85	0.54
	SCR	-44.62	178.62	0.87	0.12	0.57	0.06	0.89	0.10	-	-	-	-
Sub-polar	CP	-52.62	174.15	1.29	0.28	1.12	0.11	1.10	0.15	-	-	-	-
Polar	WS34	-64.90	-2.60	1.12	0.13	-	-	-	-	-	-	-	-

Table S3.4

Province	Plankton Tow Details				<i>N. pachyderma</i>		<i>N. incompta</i>		<i>G. bulloides</i>		<i>G. ruber</i> (white)		<i>T. sacculifer</i>	
	Site	Latitude (°N)	Longitude (°E)	Tow ^a (m)	PLAFOM2.0 ^a (m)	Tow ^a (m)	PLAFOM2.0 ^a (m)	Tow ^a (m)	PLAFOM2.0 ^a (m)	Tow ^a (m)	PLAFOM2.0 ^a (m)	Tow ^a (m)	PLAFOM2.0 ^a (m)	
Polar	P93-36	80.36	-10.14	85±35	55±40	-	-	-	-	-	-	-	-	
	P578-25	78.83	0.08	80±40	55±40	-	-	-	-	-	-	-	-	
	P578-44	78.83	7.00	85±55	50±40	-	-	-	-	-	-	-	-	
	P578-75	78.83	-3.92	70±40	50±40	-	-	-	-	-	-	-	-	
	PS55-025	75.00	-10.58	90±70	50±35	-	-	-	-	-	-	-	-	
	PS55-043	75.00	0.36	60±40	55±40	-	-	-	-	-	-	-	-	
	PS55-063	75.00	10.65	85±65	50±40	-	-	-	-	-	-	-	-	
	MN116	75.00	-7.31	150±40	55±40	-	-	-	-	-	-	-	-	
	MN2	70.00	3.40	170±215	55±35	-	-	-	-	-	-	-	-	
	MN323	69.69	0.47	140±155	55±35	-	-	-	-	-	-	-	-	
	MN314	67.54	5.58	125±60	65±35	-	-	-	-	-	-	-	-	
	Sub-polar	PAPA	49.98	-144.97	230±30	80±35	105±85	65±35	60±45	70±40	-	-	-	-
101		47.00	-174.95	95±50	70±30	140±40	55±35	65±30	65±40	-	-	-	-	
79		46.98	166.73	110±55	65±30	150±50	50±35	70±35	65±35	-	-	-	-	
Transitional	KNOT	44.08	154.98	90±45	65±25	75±55	60±35	45±30	65±35	-	-	-	-	
	#B	41.57	141.90	125±40	60±45	105±45	65±40	100±55	75±45	122±40	5±5	-	-	
	#b	41.15	143.38	85±40	85±20	35±25	65±40	40±30	75±45	-	-	-	-	
	MOC1-38	38.92	-67.90	-	-	65±25	65±40	65±55	85±45	30±20	25±15	35±20	25±15	
	#A	36.02	141.78	-	-	25±20	55±30	25±25	55±35	20±20	15±10	25±20	10±10	
Subtropics	POS383-165	34.00	-22.00	-	-	85±60	85±45	170±70	85±45	65±25	50±35	185±85	50±30	
	MOC1-28	33.91	-71.78	-	-	85±55	90±45	95±50	85±45	80±35	45±25	60±35	50±30	
	POS383-175	33.15	-22.00	-	-	30±0	85±45	30±0	85±45	65±25	50±30	190±65	50±30	
	POS247-1389	33.08	-22.00	-	-	-	85±45	140±0	75±40	55±25	55±30	40±35	55±30	
	MOC1-23	32.73	-71.16	-	-	-	-	140±0	75±40	115±0	45±25	95±50	45±30	
	#E	32.17	133.88	-	-	60±30	85±45	-	-	70±45	30±20	45±40	40±30	
	910	16.09	52.70	-	-	-	-	65±65	75±45	40±45	40±20	20±20	45±25	
	310	16.02	52.73	-	-	-	-	30±35	70±35	180±100	15±10	180±85	30±20	
	313	15.91	53.02	-	-	-	-	70±80	70±35	30±35	15±10	30±30	30±20	
	917	15.89	52.97	-	-	-	-	90±65	75±45	20±15	40±20	20±15	45±25	
	MOC63	2.92	-140.20	-	-	-	-	15±10	95±50	20±15	45±25	25±15	40±25	
	MOC65	2.05	-141.49	-	-	-	-	25±15	90±50	35±25	45±25	25±15	40±25	
MOC12	2.01	-139.88	-	-	-	-	65±25	85±45	45±25	45±25	45±25	35±20		
MOC66	1.13	-140.01	-	-	-	-	55±25	85±45	45±20	35±20	45±25	35±20		
MOC15	0.00	-140.07	-	-	-	-	-	85±45	20±10	35±20	25±15	35±20		
MOC69	-1.05	-139.97	-	-	-	-	25±15	-	25±15	30±15	25±15	35±20		
MOC20	-2.02	-140.16	-	-	-	-	-	85±45	35±15	50±25	40±20	40±25		
MOC71	-2.33	-140.32	-	-	-	-	45±25	85±45	35±25	45±25	35±25	40±25		
SO225-21-3	-3.05	-165.06	-	-	-	-	145±90	55±30	65±35	50±25	75±45	50±30		
MOC72	-3.21	-140.25	-	-	-	-	40±20	90±50	35±15	50±25	35±20	45±25		
Sub-polar	TNO57-16	-50.12	5.75	70±10	65±35	70±10	25±15	80±5	30±15	-	-	-	-	
	TNO57-13	-53.18	5.13	85±60	60±35	-	-	75±25	25±15	-	-	-	-	
Polar	AN98-O	-63.25	177.25	55±30	60±35	-	-	-	-	-	-	-	-	
	AN99-O	-63.40	178.05	25±15	65±40	-	-	-	-	-	-	-	-	
	AN01-O	-63.43	178.10	120±0	65±40	-	-	-	-	-	-	-	-	
	AN00-O	-63.53	178.38	95±50	65±40	-	-	-	-	-	-	-	-	

^aALD±VD (in m) of the planktonic foraminiferal species calculated after *Rebotim et al.* (2017) for the plankton tow samples and for PLAFOM2.0 (obtained at the nearest model grid points of the given plankton tow locations). Note that the values have been rounded to the nearest 5 m.

Supplement **S4**

Supporting Information for “Response of marine zooplankton to global warming: insights from modeling planktonic foraminifera species distribution”

Kerstin Kretschmer^{1*}, Lukas Jonkers¹, Michal Kucera¹, Pepijn Bakker¹, and Michael Schulz¹

¹MARUM-Center for Marine Environmental Sciences and Faculty of Geosciences, University of Bremen, Bremen, Germany

Contents of this file

Figure S4.1

Figure S4.2

Figure S4.3

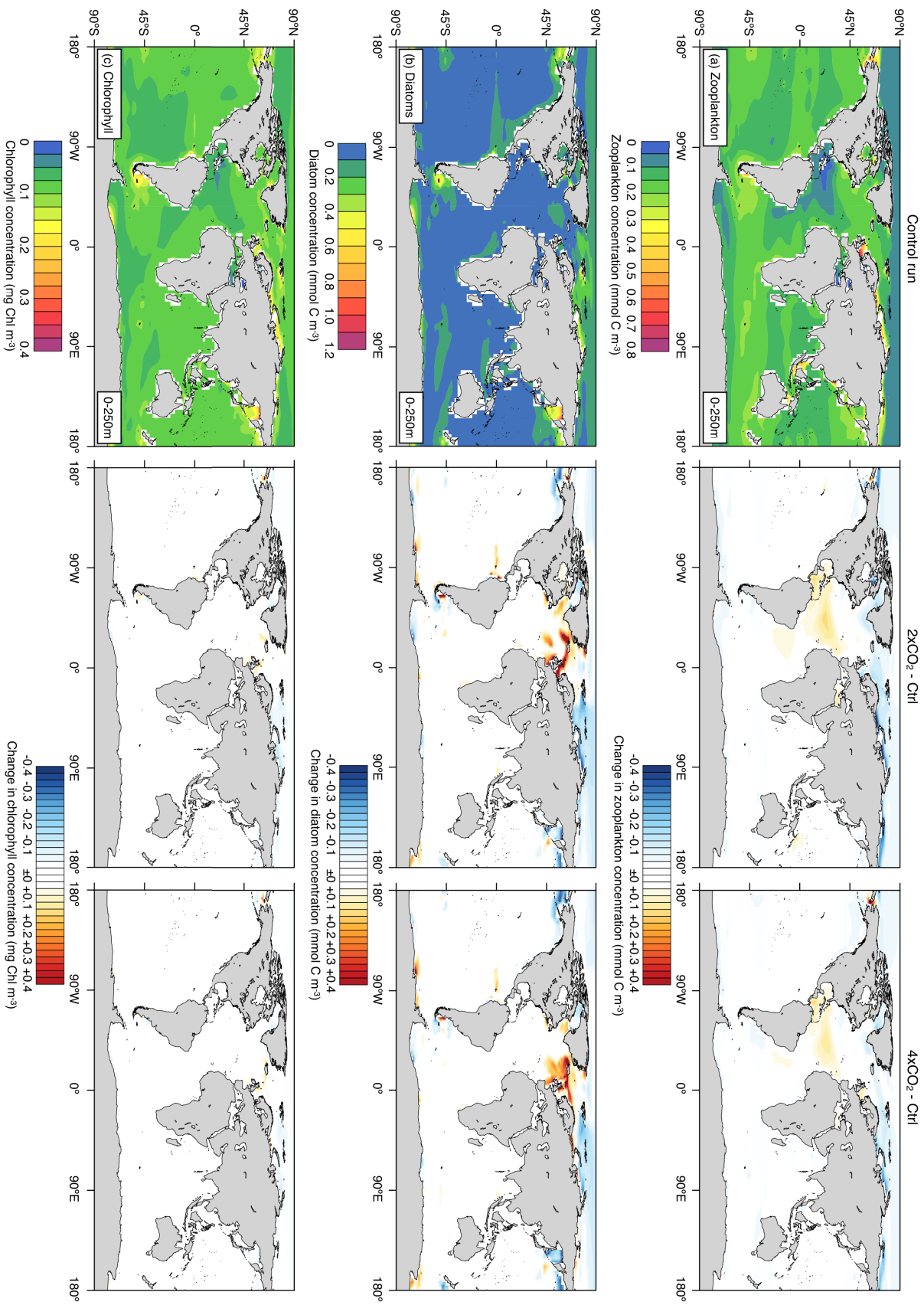


Figure S4.1: Depth integrated (0 – 250 m) annual mean (a) zooplankton (in mmol C/m³), (b) diatom (in mmol C/m³), and (c) chlorophyll (in mg/m³) concentrations for the control simulation (left column) as well as of the changes in the concentrations (middle column: 2xCO₂-Control; right column: 4xCO₂-Control).

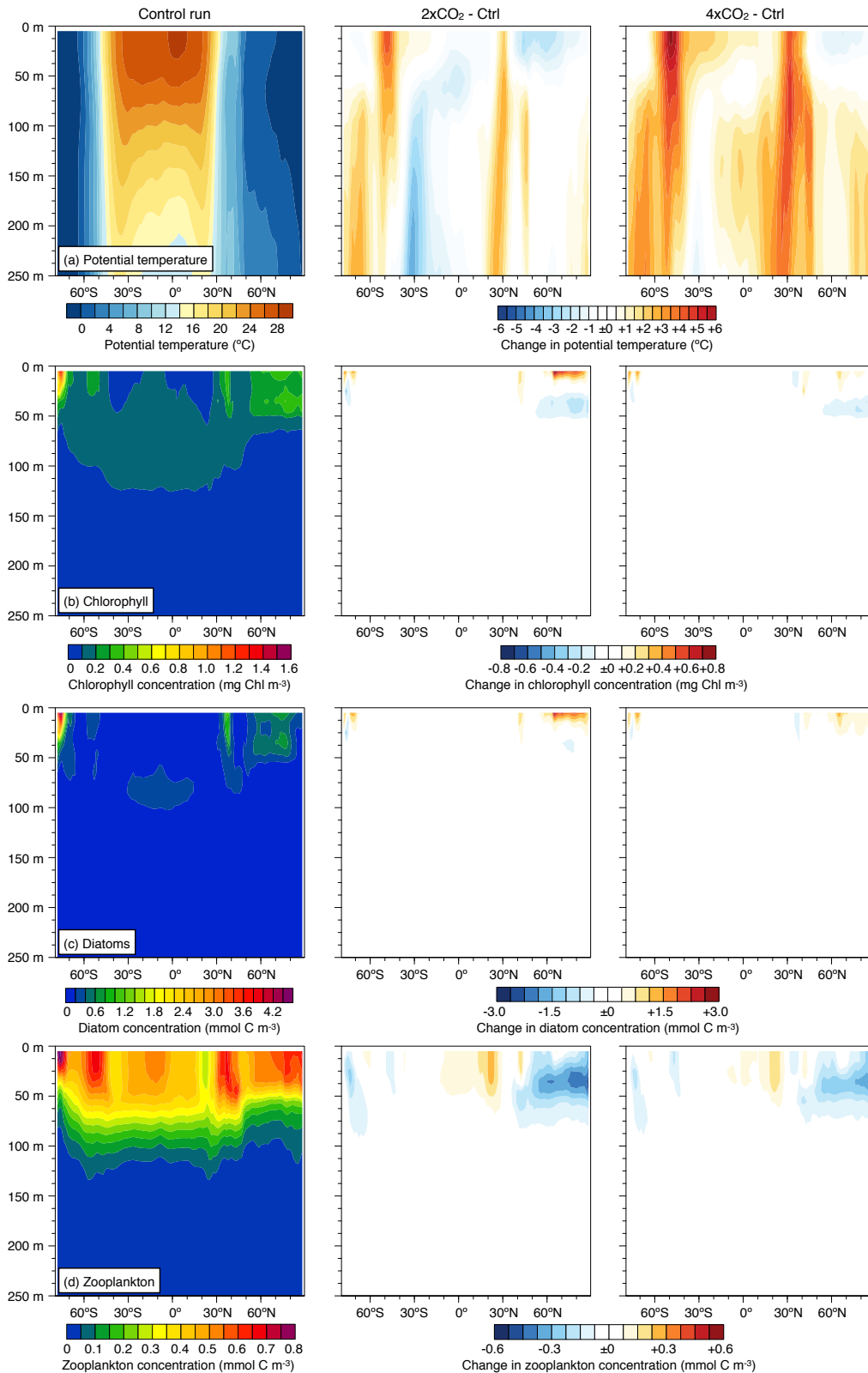


Figure S4.2: Zonal average of the modeled annual mean (a) potential temperature (in °C), (b) chlorophyll (in mg/m³), (c) diatom (in mmol C/m³), and (d) zooplankton (in mmol C/m³) concentrations over the top 250 m for the control simulation (left column) as well as of the changes in the annual mean potential temperature and the (food) concentrations (middle column: 2xCO₂-Control; right column: 4xCO₂-Control).

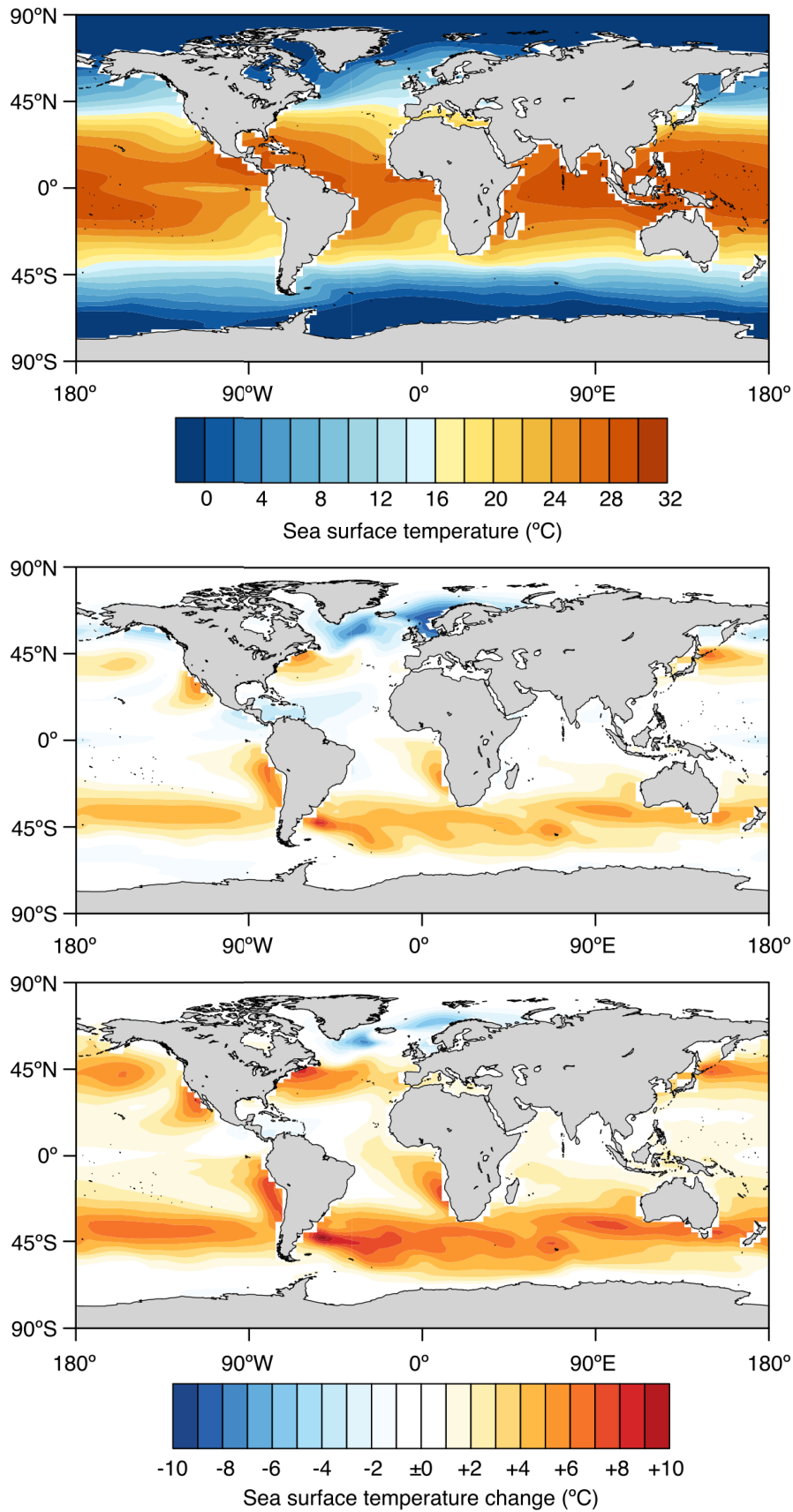


Figure S4.3: (a) Sea surface temperature (in °C) for the control run and the change in sea surface temperature (in °C) considering a doubling (b) or a quadrupling (c) of atmospheric CO₂ relative to the control run.

Acknowledgments

First of all, I would like to thank Prof. Dr. Michael Schulz and Prof. Dr. Michal Kucera for their support, guidance, and trust in me during the last years. Thank you for the long discussions and your helpful advice during our meetings. I also would like to thank Prof. Dr. Michael Schulz and Prof. Dr. Dr. h.c. Gerold Wefer for reviewing this thesis.

It was a great experience to be part of the International Research Training Group ArcTrain. Therefore, I would like to thank ArcTrain for giving me the opportunity to visit several conferences, to attend the field trip to the Torngat Mountains, to join the Floating University on RV Polarstern, and to conduct a research stay in Montréal. A special thanks goes to my fellow ArcTrain PhD students in Germany and Canada for the great experiences we shared.

Furthermore, I want to thank my colleagues for their support and encouragement throughout the last years. Andreas, thank you for your patience and for always having an open ear no matter what had happened. Jeroen and Lukas, I really enjoyed our fruitful discussions and am really grateful for all your help. Barbara, thank you for your moral support and your encouraging words.

I would also like to thank my family and my parents for their endless support throughout my life. I especially want to thank my dad, who never lost faith in me and encouraged me to never give up. Thank you!

A special thanks goes to my friends near and far for all the adventures we shared throughout the last years. Cara, I really enjoyed our Skype meetings and the great discussions we had regarding our “beloved” BEC – without your advice I would not have gotten this far. I also would like to thank Andrea, Rike, Henriette, Linde, Tilia, Annegret, Becky, and Alex. Thank you for the dinner invitations, movie nights, sewing evenings, endless coffee breaks, several running events (“Run DAKL Run!!!”), the great conversations we had at work or anywhere else, and and and. Thank you for all your help!

Sandra, I am so grateful for all the lovely moments we spent together. I deeply enjoyed our sharing of thoughts over coffee and especially cake. Thank you that I can always rely on you. I also want to thank Piet for always cheering me up. :)

Last but not least, I would like to thank Henrike, Julian, and Robert. I am really grateful for the last ten years, for the many memorable moments, and for the tears and laughter we shared. Thank you for your endless support throughout our studies and during the hardest time of my life. I am glad that you have taken me on some of my greatest adventures all over the world and I look forward to many more to come.

Without my family and especially my friends, this work would have never been possible. Thank you for joining me during this challenging and exciting period of my life!

